The Thesis Committee for Matthew Daniel Ledvina
Certifies that this is the approved version of the following thesis:

Fluid Inclusion Constraints on the Hydrothermal Processes Responsible for Cu-Au Mineralization in the Ertsberg East Skarn System, Papua, Indonesia

APPROVED BY
SUPERVISING COMMITTEE:

Supervisor:

James Richard Kyle

Mark Cloos

Brent Elliott

Fluid Inclusion Constraints on the Hydrothermal Processes Responsible for Cu-Au Mineralization in the Ertsberg East Skarn System, Papua, Indonesia

by

Matthew Daniel Ledvina, B.S.

Thesis

Presented to the Faculty of the Graduate School of

The University of Texas at Austin

in Partial Fulfillment

of the Requirements

for the Degree of

Master of Science in Geological Sciences

The University of Texas at Austin

May 2017

Dedication

This thesis is dedicated to my family. Thank you for all you have done to support me.

Acknowledgements

I would like to thank Dr. Kyle, Dr. Cloos, and Dr. Elliott for their involvement in this project. They take a great deal of pride in their work and strive to produce high quality results with a drive that I admire. They set an example of what it means to work hard for something that you believe in and I will take away a plethora of life lessons from my time under their guidance and supervision. Thank you.

A thank you to Clyde Leys who provided insight and support during fieldwork as well as valuable feedback and research questions that provoked meaningful research focused on application in the field. I had the pleasure of a short visit to Papua and I can say with certainty that the geologists involved in the Ertsberg-Grasberg district are some of the finest I have come across. You set a very high standard for quality geology, which I hope to compliment with this small study. This project would not have been possible in any capacity without the financial and logistical support of PT Freeport Indonesia. I was wildly fortunate to have an industry leading company back this project.

Thank you to those working in Dr. Kyle's lab as undergraduate researchers and specifically Daniel Young for his dedication to producing high quality data and a JGB poster.

Elizabeth Cleland deserves a great deal of praise for her knowledge and guidance with fluid inclusion work and LA-ICP-MS data. Without her, this thesis would be

significantly lower quality and I would still be lost with a pile of unanalyzed samples and FI microthermometry set-up in need of some love.

Dr. Bodnar provided the use of his facilities at Virginia Tech as well as invaluable advice regarding the analysis of fluid inclusions and how to present the data. I wish I would have come to him sooner as it may have prevented me from prematurely graying and gaining the grad school 25. Luca Fedele was a magician with the LA-ICP-MS at Virginia Tech and I appreciated his devotion to quality data and Serie A.

I owe many thanks to my friends and family that constantly reminded me that there is always light at the end of the tunnel. Joe and Steve have taken me on some great adventures and helped me remember to relax. The Tosa Droogs were a source of inspiration and continue to challenge my understanding of the world around me. Stef, Christine, Mackenzie, Nate, and Kylie, thank you for putting up with my cheerful office demeanor, I know it could be a bit overwhelming at times. Godspeed Mackenzie, Nate and Kylie, I hope to see you all walk across the finish line someday as well.

Finally, I would like to thank my folks, Dan and Sue Ledvina, my Aunt Marianne, Uncle John, Uncle Dave, and my grandparents for understanding that I could not make it home as often and I would have liked throughout the duration of this project. I am glad that you have always been supportive of my choices in life. Thank you for being loving parents, aunts, uncles, and grandparents.

Abstract

Fluid Inclusion Constraints on the Hydrothermal Processes Responsible for Cu-Au Mineralization in the Ertsberg East Skarn System, Papua, Indonesia

Matthew Daniel Ledvina, M.S. Geo Sci.

The University of Texas at Austin, 2017

Supervisor: James Richard Kyle

The Ertsberg East Skarn System (EESS) is a 3-Gt orebody at 0.59% Cu and 0.49 ppm Au that extends from the surface at 4200m at least to 1800m elevation. Skarn-hosted Cu-Au ores are localized in Upper Cretaceous siliciclastic to Lower Paleogene carbonate strata along the steeply dipping contact with the 3-Ma Ertsberg Diorite that locally hosts stockwork ores. Petrography, quartz SEM-Cathodoluminesence (SEM-CL), fluid inclusion microthermometry, and fluid inclusion LA-ICP-MS were used to characterize vein formation and fluid conditions in the ore-forming system.

Five vein-hosting lithologies and five stages of vein formation were defined petrographically, and 41 SEM-CL transects from 17 quartz vein samples were used to identify eight recurring quartz CL textures that vary by elevation and host lithology. The CL texture paragenesis reveals quartz-sulfide vein architecture rife with brittle deformation features and evidence of repeated opening and mineralization of fractures.

Brittle deformation increased with depth in diorite-hosted veins and was most prevalent in skarn-hosted veins.

Fluid inclusion petrography of 16 samples, in-situ micro-thermometry of 107 fluid inclusions in eight samples, and LA-ICP-MS of 99 inclusions revealed four types of inclusions consistent with Cu-Au porphyry systems. Type 1 inclusions are 4-11% salinity, 40-70 vol% vapor bubble, homogenize between 332-396 °C and can contain chalcopyrite daughter crystals. Type 2a inclusions are 27-51% salinity, 10-30 vol% vapor bubble, homogenize between 280-420 °C and contain halite. Type 2a inclusions may also contain sylvite, anhydrite, chalcopyrite, magnetite, and hematite. Type 2b inclusions are 1-12% salinity, 65-90 vol% vapor bubble, homogenize between 340-392 °C and typically do not contain daughter minerals. Type 3 inclusions at ambient conditions are 2-23% salinity, 15-50 vol% vapor bubble, homogenize between 283-403°C and may contain opaque minerals. LA-ICP-MS analysis indicate that EESS fluid inclusions have high Na, K, and Ca, and support mineralization by Cu, Fe, Mn, Pb and Zn-rich brine derived from phase separation of a primary magmatic fluid. All fluid inclusion types were observed over the 1.7 km of elevation sampled – nearly 4x the vertical extent documented for other porphyry systems. The upper limit of the phase separation zone is present at ~2500 m, which corresponds with deepest known Cu-Au concentrations. These data support fault-controlled fluid migration and a lack of lithologic control on Cu-Au mineralization in veins.

Table of Contents

List of Tables

List of Figures

Chapter 1: Introduction

1.1 Introduction

As a concluding remark to a review of porphyry systems, Sillitoe (2010) posed the question of how single phase magmatic fluids exit magma chambers and how far these fluids travel before un-mixing into vapor and brine. This study examines this question in the natural laboratory of the Ertsberg East Skarn System (EESS), a supergiant porphyry-skarn orebody consisting of vertically extensive ore-grade Cu-Au mineralization. A deep magmatic source from which multiple-pulses of single phase metal-bearing aqueous fluid ascended along structural pathways near the steeply dipping contact of diorite and altered sedimentary wall rocks. Critical density fluid inclusions that record the single-phase parent fluid are present over at least a 2 km extent of mineralization presumed to be above the source cupola. This observation, in concert with EESS vein quartz cathodoluminescence textures recording vein growth, suggests that pulses of single phase fluid traveled a minimum of 2 km after being released from the source of melt and the location of phase separation changed over duration of hydrothermal mineralization of the EESS.

1.2 EESS Discovery and Mining History

The EESS is located in the Ertsberg-Grasberg District of south-central Papua, Indonesia. The Ertsberg-Grasberg District comprises a series of world class Cu-Au porphyry and skarn deposits clustered in a 100 km^2 area of the New Guinea Central Fold Belt in the Sudirman Range (*Figure 1*).

The Ertsberg-Grasberg District has a storied history that began with Jean Jacques Dozy's Royal Dutch Shell backed expedition in 1936 to summit the Sudirman Range (Dozy, 1939). Dozy took careful notes of the island's geology, with particular emphasis on the "Ertsberg" (*Dutch*: ore mountain) – a distinct exposure rich in chalcopyrite and bornite that he discovered. Dozy noted the Ertsberg and associated intrusion (the Ertsberg intrusion) and related skarn occurrences in his report to Royal Dutch Shell, but the report (Dozy, 1939) was overlooked with the onset of WWII.

In the early 1960s, Freeport Sulphur Company sent Forbes Wilson to explore the mineral occurrence Dozy had described. Freeport was granted mineral rights to the 100 km^2 Ertsberg District in 1967 with the signing of the Contract of Work (COW), an agreement with the Indonesian government. Development began in 1971. Open pit mining of the Gunung Bijih, the original discovery in the Ertsberg-Grasberg, began in 1969 (Wilson, 1981). The nearby Gunung Bijih Timur (GBT) skarn was discovered along the contact between Ertsberg Diorite and wallrock in the mid-1970s and put into production in 1981 as a block cave mine (Leys et al., 2012). Further exploration identified ore grade mineralization extending more than 1.5 km below the GBT discovery (Leys et al., 2012). The entire vertically extensive orebody became known as the Ertsberg East Skarn System (EESS) and mining continues to this day.

The Ertsberg-Grasberg district can be divided into two main mineralized zones: porphyry and skarn mineralization centered on the Grasberg Igneous Complex and skarn-dominated mineralization around the Ertsberg Intrusion (*Figure 1*). The Grasberg Cu-Au-Mo porphyry system and the associated Kucing Liar skarn has produced and in reserve 2.8 billion tonnes of ore at 1.05% Cu and 1.04 ppm Au with a 1.7 billion tonne resource at 0.64% Cu and 0.59 ppm Au (Leys at al., 2012). The Ertsberg skarn, EESS, Big Gossan, and Dom skarn contain 1.1 billion tonnes of ore at a grade of 1.01% Cu and

0.70 ppm Au with a 729 million tonne resources at 0.60% Cu and 0.52 ppm Au (Leys et al., 2012).

Today, the Ertsberg-Grasberg District is operated by PT-Freeport Indonesia in a joint venture between Freeport-McMoRan, Rio Tinto plc, and the Indonesia Government. In 2015, Freeport produced 752 million pounds of recoverable copper and 1.232 million ounces of recoverable gold from its Indonesian operations (FCX, 2015). These metals were sourced from active operations at the Grasberg open pit, Deep Ore Zone underground mine, and the Deep Mill Level Zone underground mine (FCX, 2015). Production of the Deep Mill Level Zone began in 2015 and will become increasing important in future district production, with current reserves of 460 Mt at 0.89% Cu and 0.74g/t Au (FCX, 2015). The onset of production from the Grasberg Block Cave (slated to begin in 2018) is designed to produce ~240,000 tonnes of ore per day (FCX, 2014).

Four decades of open pit mining since production began on the Ertsberg skarn has largely exhausted the shallow resources. This has intensified exploration efforts to discover deep orebodies and to understand the favorable conditions under which they formed, to extend the life of one of Earth's great mineral districts.

1.3 Regional Geologic Setting

The Cu-Au orebodies of the Ertsberg-Grasberg District is a product of favorable tectonic setting, host lithology, and magmatic activity that produced focused metal-bearing aqueous fluids. Mineralization is associated with emplacement of Pliocene quartz monzodiorite to granodiorite intrusions into a deformed Late Mesozoic and Cenozoic sequence of siliciclastic platform and carbonate shelf facies (Leys et al., 2012). These strata are present in the Yellow Valley syncline, which records the uplift associated

with the arc-continent collision between the Australian and Pacific plates that began ca. 12Ma (Hill et al. 2002; Sapiie and Cloos, 2004). Collisional delamination occurred during this period, which thickened the crust and resulted in the emplacement of lithospheric mantle-derived magmas into the crust with the subsequent switch to a strike-slip margin ca. 4Ma (Cloos & Housh, 2008). Cu-Au-rich fluids collected at the top of the magama chamber and periodically ascended to shallow levels forming giant Cu-Au orebodies in shallow intrusions and wallrocks (Cloos, 2001; Gandler, 2006).

1.4 GEOLOGY OF THE ERTSBERG-EAST SKARN SYSTEM

The EESS provides the opportunity to study the world's most vertically extensive skarn-hosted Cu-Au deposit to constrain the controls for the formation of this mineralizing system and determining its genetic relationship to the associated pluton that is locally mineralized. The EESS is a zone of calc-silicate alteration that extends outward from the northeastern edge of the Ertsberg Intrusion (*Figure 2)*. The orebody extends 200-600m outward from the intrusion-skarn contact, 1.5km laterally, and from the surface elevation of 4300m to below 2600m (Gandler, 2006; Leys et al., 2012; *Figure 3*). The EESS formed in a 3 km-thick Late Mesozoic to Late Cenozoic sedimentary sequence (Gandler, 2006). The siliciclastic Kembelangan Group of alternating fine-grained sandstone and shales is overlain by the New Guinea Carbonate Group of fossiliferous and magnesian carbonates (Quarles van Ufford, 1996). These units locally dip steeply north-northeast in the southern limb of the Yellow Valley Syncline.

The EESS is divided into four ore zones to distinguish specific block cave mining operations: the Gunung Bijih Timur, the Intermediate Ore Zone, the Deep Ore Zone (base at 2900 m), and the Deep Mill Level Zone (base at 2500 m) which is currently under

exploration and development (FCX, 2015). The DMLZ spans the Cretaceous-Paleocene contact between the Kembelangan Shale and Waripi Formation. It can be divided into forsterite-diopside skarn, anhydrite unit, massive sulfide, magnetite skarn, calc-silicate hornfels, marble and hydrothermal carbonate, endoskarn, and diorite (Hughes and Wiwoho, 2005; Gandler, 2006).

Three faults adjacent to the EESS appear to define the skarn's extent and control mineralization. Two NE-trending tear faults offset bedding enough to define the eastern and western boundaries of the Ertsberg East orebody. The Ertsberg intrusion propagated along the WNW-trending Ertsberg No. 2 fault (*Figures 2, 3*)– a steeply dipping reactivated fault near the intrusion-skarn contact that served as a possible conduit for mineralizing fluids (Sapiie and Cloos, 2004; Leys et al., 2012). The Ertsberg Intrusion has a surface area of 2km by 1km and is composed of clinopyroxene-dominated equigranular diorite and biotite-clinopyroxene-equigranular diorite (Leys et al., 2012; Freihauf et al., 2005; McMahon, 1994b). Leys et al. (2012) identified intrusion-hosted potassic alteration up to 600m inboard of the intrusion margins, postulating that this may be evidence that mineralizing fluids ascended through the Ertsberg Intrusion.

1.5 HYDROTHERMAL FLUIDS IN THE EESS

This investigation relies heavily of the use of scanned luminescence imaging and fluid inclusion analysis to describe vein textures in the EESS and to constrain the fluids responsible for mineralization. Previous work done by Gandler (2006) outlined potential fluid pathways and 1.) Transport of hydrothermal fluids in the fractured rind of the Ertsberg Diorite or along the diorite-skarn contact. 2.) Propogation of hydrothermal fluids along a fault. 3.) Skarn formation focused along different structural pathways, which

might include the transport of hydrothermal fluids through the permeable unreactive siliciclastic units underlying the Waripi or fluid transport along interconnected fracture networks.

1.5.1 Quartz Cathodoluminescence

Cathodoluminescence (CL) imaging is a technique that reveals textures in quartz based on the energy emitted as visible light when electrons bombard a quartz crystal. Optical cathodoluminescence has been used in provenance analysis of quartz grains in sediments since the 1970s (Zinkernagel, 1978). More recent studies utilizing the higher resolving power of the scanning electron microscope have adapted cathodoluminescence to the study of ore deposits. Penniston-Dorland (2001) and Baline (2007) analyzed the textures of hydrothermal quartz veining in the Grasberg Igneous Complex to reconstruct the evolution of quartz precipitation in the system and correlate the data to trace element variation. Rusk et al. (2006) and Müller et al. (2010) identified correlations between luminescence intensity and trace element concentrations of quartz in stockwork veining at the Butte porphyry Cu deposit and Mongolian porphyry-style deposits, respectively.

1.5.2 Fluid Inclusion Record

Earlier fluid inclusion petrography was done on vein quartz in the Ertsberg Stockwork Zone by Gibbins (2006). She categorized inclusions based on the liquid-vapor ratio and the composition of daughter salts. Fluid inclusions are described in the classification scheme devised by Nash (1976). Gibbins (2006) examined inclusions in each of the five specific veins types: Stage II Quartz-magnetite, Stage III Biotite-anhydrite-biotite, Stage V Bornite-quartz-green sericite, Stage VI Pyrite-quartz-white

sericite. The study found that the potassic alteration veins (Stage II and III) were consistent with the pressure, temperature, and salinity (P-T-X) of a fluid exolving from an intermediate magma at ~700°C and 5-10wt% NaCl. The presence of Cu-sulfide daughter salts in Stage II was interpreted to indicate that the fluid was near saturation with Cu, whereas the absence of Cu-sulfide daughter salts in Stage III indicates that Cu precipitation had begun. Stage V contained evidence of boiling fluids with >26.3wt% NaCl and some precipitation of Cu. Stage VI veins are known to be ore stage, but contained Type I inclusions suggesting that fluids were low salinity. Gibbins (2006) did not conduct any fluid inclusion microthermometry analyses but used fluid inclusion types to estimate temperature and salinity for each quartz-bearing vein type present in the Ertsberg Stockwork Zone.

Rubin (1996) studied fluid inclusion hosted in monticellite, forsterite, garnet, and quartz from 10 samples from the upper part of EESS (~3550 to 3700 m elevation) and from the DOZ (2950 to 3100 m elevation). Halite-bearing fluid inclusions trapped in early quartz had T_h between 294-436 °C with 35-58.5wt% $NaCl_{equiv}$. Two-phase fluid inclusions in late quartz had T_h ranging from 228 to 360°C with 9-23wt% $NaCl_{equiv}$.

Harrison (1999) examined fluid inclusions in quartz stockwork in the upper Grasberg Intrusive Complex (3000-4000 m elevation) in relation to associated alteration. Inclusions associated with potassic alteration had the highest T_h, ranging from 521 to >700°C, with salinities ranging from 56 to 84wt% NaCl equivalent. Fluid inclusions in quartz veins in phyllically altered hosts had lower T_h and salinities. Baline (2007) did a CL-guided microthermomety study of fluid inclusions in quartz veins in the Deep Grasberg to catalogue the inclusion types present to elevations of ~2500 m. She obtained inclusion homogenization temperatures between 225°C and >700°C with a bimodal distribution averaging 368°C with a standard deviation of 58°C and 598°C with a

standard deviation of 107°C. The moderate temperature fluid inclusions had average salinity of 44 wt.% NaCl equivalent and the higher temperature inclusions had an average of 51 wt. % NaCl equivalent.

1.6 Study Objectives

The overarching purpose of this study is to characterize mineralizing fluid pathway(s) within the EESS and to constrain the nature of the mineralizing system. This is broadly accomplished with two complementary research directions, which both contribute to our understanding of EESS mineralization. First, a study of vein character in the EESS, with emphasis on vein growth textures that provide paragenetic context to the structural and mineralogical formation of veins. The objective of this portion of the study is to describe and map vein types and quartz textures in EESS. Secondly, a study of the fluid inclusions in the EESS, with a focus on describing the Cu-bearing magmatic-hydrothermal fluid responsible for EESS mineralization.

Research was focused on quartz veining and fluid inclusions present in quartz. Although quartz is not itself an ore mineral, there is a clear association between vein quartz and younger Cu-sulfide minerals. The intended outcome of this project is to describe the magmatic-hydrothermal fluids that mineralized veins in the EESS and understand what controlled vein formation during mineralization of the EESS.

To develop a model, samples were selected to capture the vertical and lateral extent of the EESS, supplemented by samples from Rubin (1996) and Gandler (2006) to extend the study into the higher reaches of the EESS, which are no longer preserved in the PTFI core repository. Veins hosted in diorite tend to have less complex vein morphologies and simpler mineral assemblages than wall-rock-hosted veins, so this study

focused on those samples. However, skarn-hosted quartz veins were used as a means of comparing veining characteristics with diorite-hosted veins.

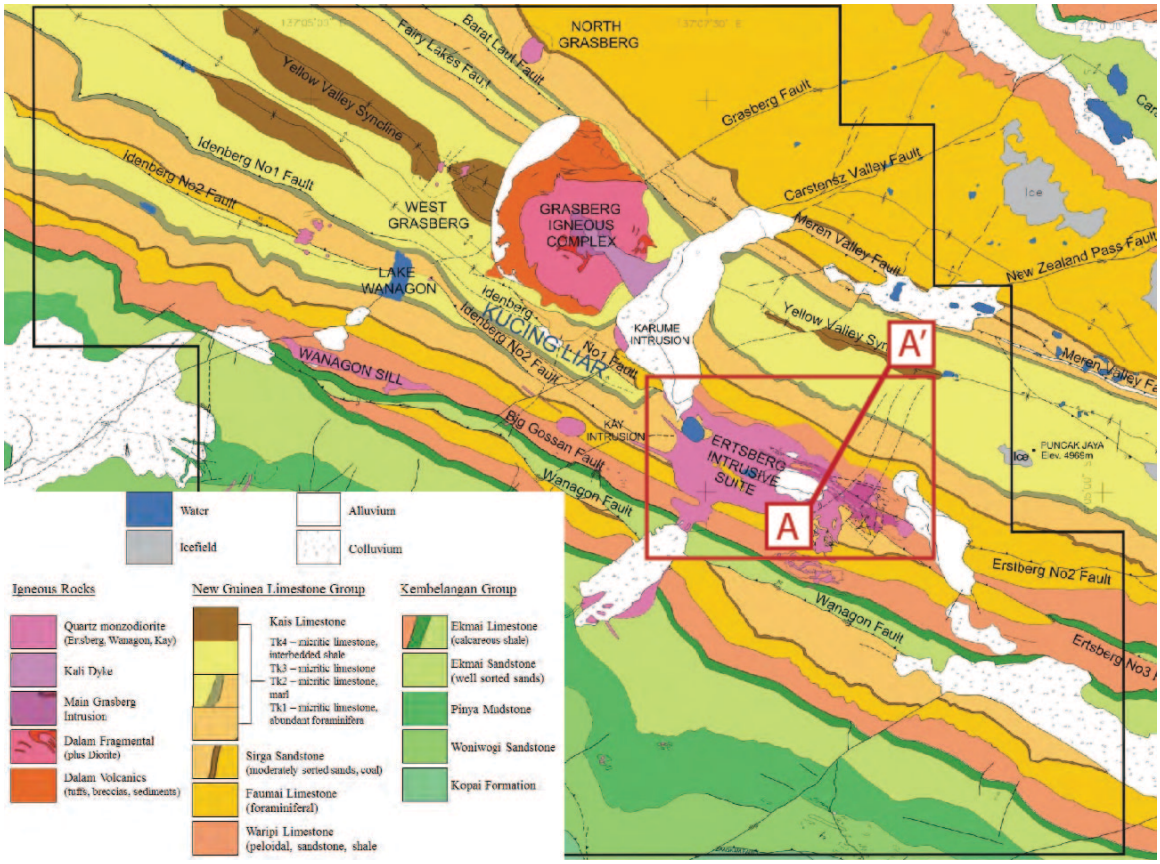

Figure 1: Ertsberg-Grasberg District Geologic Map.

The EESS is located on the NE flank of the Ertsberg Intrusive Suite, along the contact with the sedimentary strata. (Leys et al. (2012).

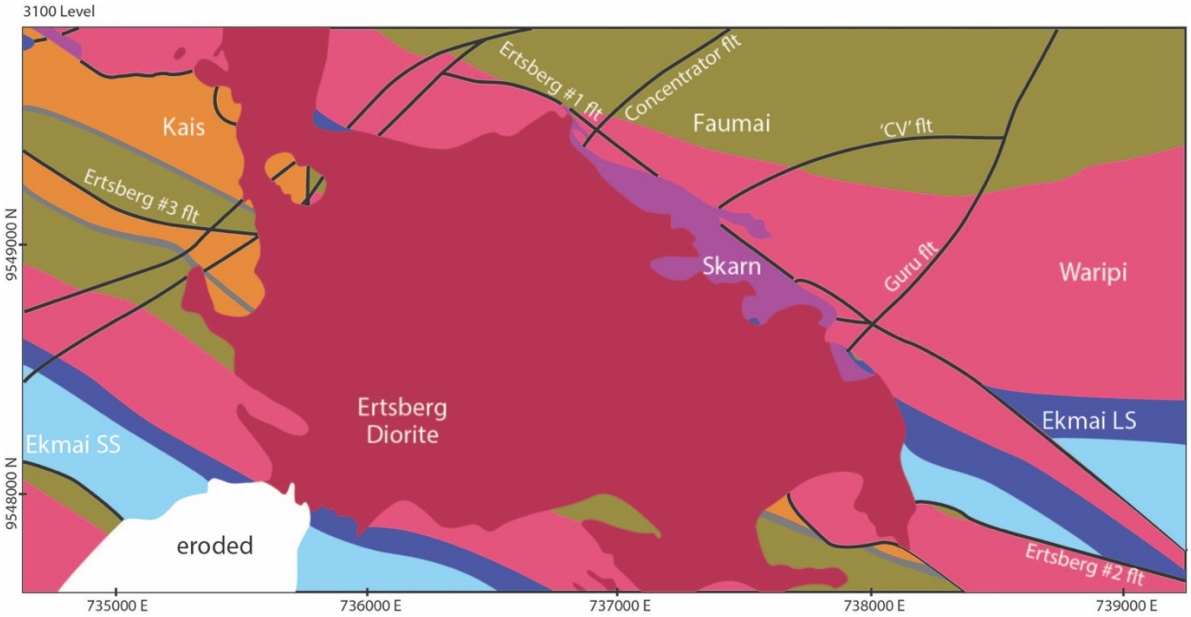

Figure 2: Map view of EESS at 3100 m elevation.

Plan view map of the 3100 m level of the EESS displaying the location of major faults and skarn mineralization at the contact between Ertsberg Diorite and Waripi skarn. Modified from Leys et al. (2012).

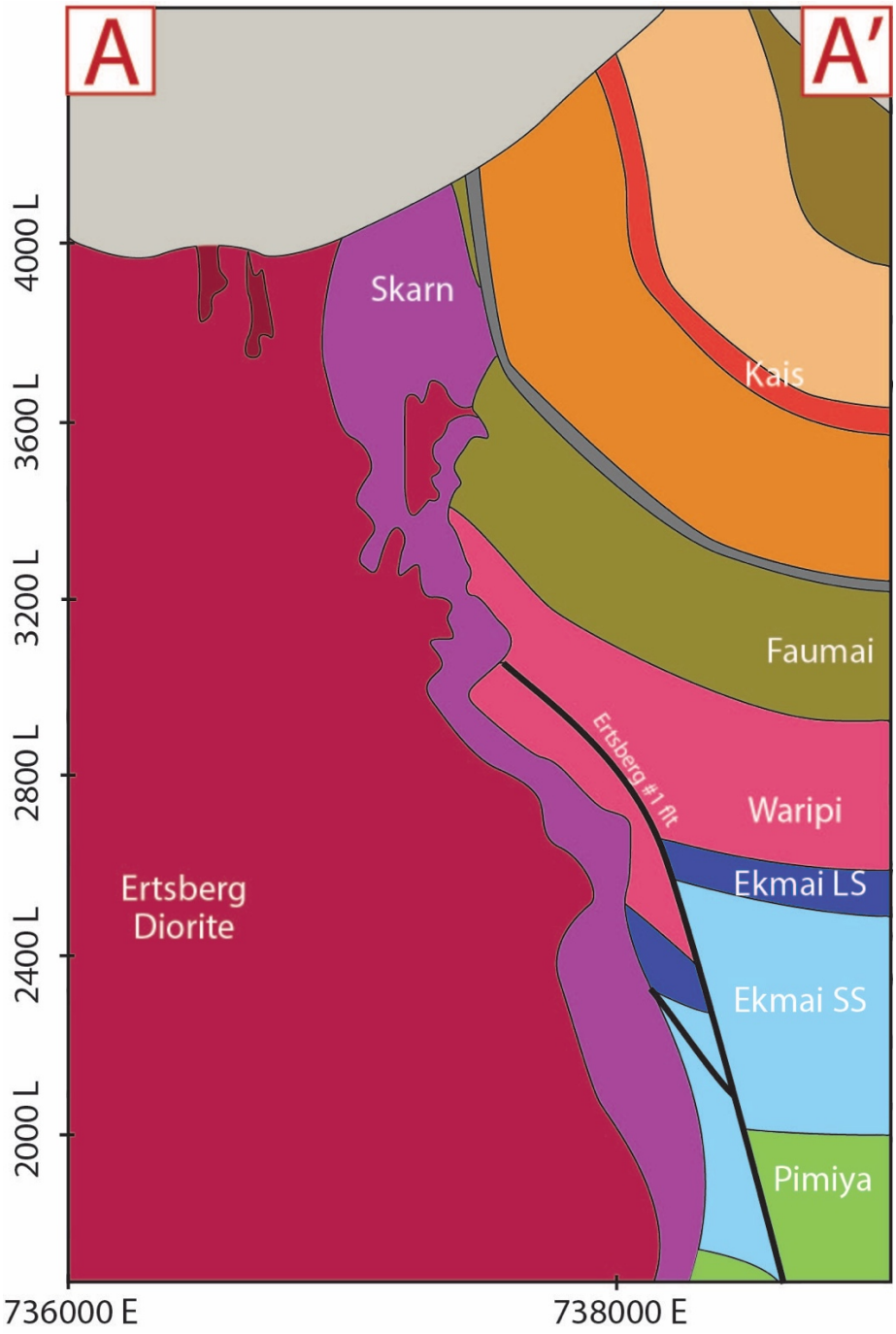

Figure 3: Cross Section of the EESS.

Cross section from A-A' (figure 1) highlighting the development of skarn along the contact between Ertsberg Diorite and sedimentary strata. The Ertsberg #1 fault runs parallel to mineralization in this cross section. Leys et al. (2012).

Chapter 2: Veining

2.1 Introduction

Seventeen well characterized EESS samples were studied in detail with one or more of the following techniques (SEM-CL, Fluid Inclusion Microthermometry, and LA-ICP-MS). Samples were chosen from core intervals available at the PTFI core facility in Papua, Indonesia, and an attempt was made to choose samples that accurately represent the large scale variability in the EESS. Samples that had ~0.75cm qz veins (the ideal size for SEM-CL transects), minimal anhydrite or carbonate minerals (minerals that pose challenges during SEM-CL imaging), and captured a large range of elevations along a transect perpendicular to the diorite-skarn contact. Because of the expectation of a mineralizing system that involved fluids rising from depth and responding to reduced P-T conditions, the emphasis was placed on samples from lower elevations that might allow key transitions to be assessed. Previous work by Gandler (2006) and Gibbins (2006) suggested that porphyry alteration designations (potassic, propylitic, phyllic) were not strong indicators of vein mineralogy. Therefore, sampling for this study was focused on capturing variation in quartz textures and fluid characteristics by elevation and by broadly comparing skarn-hosted veins with diorite-hosted veins.

2.2 Host Lithology and Alteration

Gandler (2006) divided the hydrothermally altered and mineralized units of the DMLZ between 2900m and 2600m into eight groups. The upper portion of the stratigraphic section, dominated by altered Waripi abutting against Ertsberg Intrusion, was designated as diorite, endoskarn, forsterite-diopside skarn, magnetite skarn, anhydrite unit, marble and hydrothermal carbonate, or massive sulfide. Stratigraphically

below the Waripi, the Ekmai was designated hornfels. This study followed Gandler's nomenclature, aided by drill core reports, to describe five vein-hosting lithologies: Diorite, Endoskarn, Forsterite-Diopside skarn, Hornfels, and Magnetite Skarn (*Figure 4*). However, as samples from this study extend well below 2600m elevation, the addition of a sandstone unit is necessary to describe a unit believed to be the lower Ekmai. Furthermore, samples lacking calc-silicate alteration have been organized in accordance with traditional porphyry Cu mineralization styles: potassic, propylitic, and phyllic (Table 1). Gibbins (2006) identified three alteration zones within the Ertsberg Stockwork: propylitic, potassic, and endoskarn. Phyllic alteration is also common although it is restricted to vein halos; likewise, Gibbins (2006) does not describe pervasive phyllic alteration of wall-rock.

The majority of potassically altered samples studied do not have orthoclase (after albite) present, the reaction commonly used to distinguish the potassic core from the periphery. Rather, potassically altered samples contain hydrothermal biotite (likely after clinopyroxene) are the common manifestation of the potassic periphery as defined by Gibbins (2006). Hydrothermal biotite veins up to 1 cm wide are also present in the EESS.

Endoskarn, calc-silicate replacement of igneous rocks (Einaudi et al., 1981), is characterized by garnet, epidote, and diopside. Gibbins (2006) associated this alteration type with regions of highest hydrothermal fluid flow within the Ertsberg Diorite, as that study did not explore mineralogy of skarn facies except for the exoskarn.

Phyllic alteration is the most prevalent alteration type within the EESS samples studied petrographically. As phyllic alteration is associated with highly acidic fluids, it is not surprising that phyllic alteration is common along veins transporting a fluid responsible for precipitating sulfide. This halo-limited (as opposed to pervasive) phyllic

alteration may give some indication of the extent of penetration of mineralizing fluids into the adjacent wall rock – perhaps phyllic alteration represents zones that served as feeders for sulfide-depositing fluids (although fractures transporting acidic fluids were filled with sulfides during the time of alteration). This idea is consistent with findings presented later that sulfide deposition tends to post-date quartz vein formation, commonly filling pores within the rock (perhaps pores in the selvage/halo left by dissolved minerals).

2.3 VEINS

For the EESS, there is not a strong association between vein mineralogy and alteration type, as Gibbins (2006) noted even for veins in the Ertsberg Stockwork Zone. Quartz veins in skarn and hornfels, which post-date calc-silicate alteration, do not have unique mineral assemblages specific to skarn alteration type, a conclusion that is supported by the more extensive studies of Rubin (1996) who concluded that rheology and volume change during skarn formation are controls on veining. This lack of correlation is the basis for this study's focus on determining fluid chemistry based on fluid inclusion contents and mapping the vertical and lateral variation in quartz textures as a means of understanding fluid pathways.

2.3.1 Diorite-Hosted Veins

Gibbins (2006) divides 22 veins types into seven stages of mineralization, which are categorized by vein and selvage mineral assemblages (*Figure 5*). These vein types and ore stages capture the complexity of EESS mineralization, but it may not take into account that there is overwhelming evidence for fractures being opened and mineralized,

re-opened and overprinted with later mineralization from a later pulse of fluid (*Figure 6*). CL images show two distinct quartz generations account for deposition of quartz in the veins studied: an early completely zoned, but sulfide-barren quartz and a later CL-dark quartz associated with sulfide deposition. CL textures in these two quartz generations supports the vein re-opening model and suggests that we see large scale (and quite likely, smaller scale, high frequency) variations in the physical and chemical conditions affecting mineral precipitation that collectively forms a vein. Therefore, we have chosen to view veins in a more traditional porphyry vein nomenclature, building on the A, B, D vein notation (Sillitoe, 2010).

By nature of the study, only quartz-bearing veins were studied in detail, but sample selection was focused on capturing a range of elevations, host lithologies, and alteration types within the EESS (*Figures 7, 8*). Veins studied consistently display early quartz, followed by open space filling sulfide phases and late open space filling sulfates and carbonates (Table 3). Quartz crystals in quartz-chalcopyrite veins and early quartz along the margins of more complex veins tends to be coarser (0.5-5mm diameter) than younger quartz and lacks a consistent orientation of quartz crystals. Quartz textures within a vein may transition from coarse, poorly oriented crystals to comb quartz toward the center of the vein (*Figure 9*). Sulfides occur in the center of the vein, filling open space or along fractures and grain boundaries in the pre-existing vein quartz. Cu-sulfides predate or are contemporaneous with pyrite. Pyrite veinlets and quartz-pyrite veins commonly cross-cut earlier quartz veins. These veins and veinlets occur in wall-rock, but can often form the younger portions of mineralogically complex veins, effectively becoming "nested" within quartz-mineralized fractures (veins) (*Figure 10*). This results in veins with complex mineral assemblages, which can more simply be categorized as aggregates of multiple mineralization events, which have been captured in a fracture that

has been opened and mineralized, then re-opened and mineralized again. This study has attempted to distill complex vein mineral assemblages described in Gibbins (2006) down to multiple independent events of fracture opening and mineralization as opposed to describing "vein-types" which implies that the minerals present were deposited synchronously.

2.3.2 Skarn-Hosted Veins

EESS skarn mineralogy varies in accordance with protolith, the thermal gradient around the Ertsberg Intrusion after emplacement, and the degree to which metasomatic fluids caused retrograde alteration (Rubin, 1996). Skarn samples were chosen in an attempt to capture quartz veining in each common skarn facies as well as represent a variety of elevations within the ore zone. Quartz veins have similar mineralogy to those found in diorite, although some samples have late calcite that is roughly coeval with anhydrite formation (Table 4). Calc-silicate minerals such as garnet and forsterite can occur in veins, although these minerals predate vein quartz. Interstitial pore spaces in calc-silicates are commonly filled with quartz. This relationship may suggest that early hydrothermal quartz effectively coats fractures and seals off the host-rock, limiting wall rock reaction with later hydrothermal fluids that are not in equilibrium with the host rock. A similar effect in diorite-hosted samples may explain why phyllic alteration can be very minimal along some sulfide-bearing quartz veins.

2.3.3 Geometry and mineralogy of Ore-stage veins

Ore-stage quartz veins in the EESS do not neatly fall into the porphyry vein categorizations of Sillitoe (2010). They have straight, parallel walls like B veins,

suggesting that they form in diorite (and skarn) that is brittle. However, these veins are the primary chalcopyrite-bearing veins in the system, generally with only minor molybenite, which tends to be the case with A-veins (Sillitoe, 2010). Therefore, these veins share defining characteristics of both A and B veins. Ore stage veins are followed by pyrite-quartz veins that closely resemble D-veins, which is consistent with other porphyry systems.

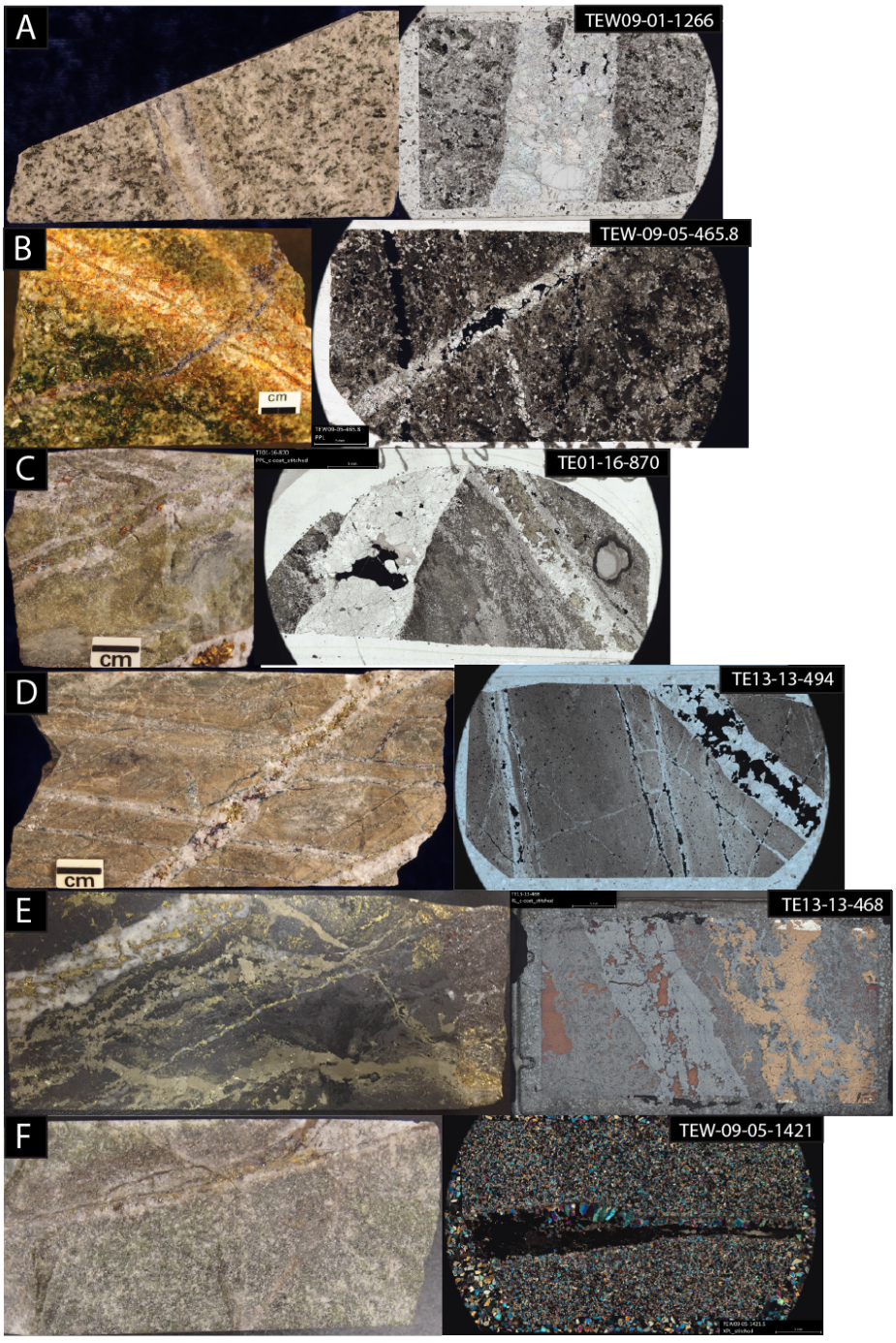

Figure 4: EESS lithologies that host quartz veins

A) Diorite with mafics altered to chlorite B) Endoskarn C) Forsterite-diopside skarn D) Hornfels E) Magnetite skarn F) Quartzite

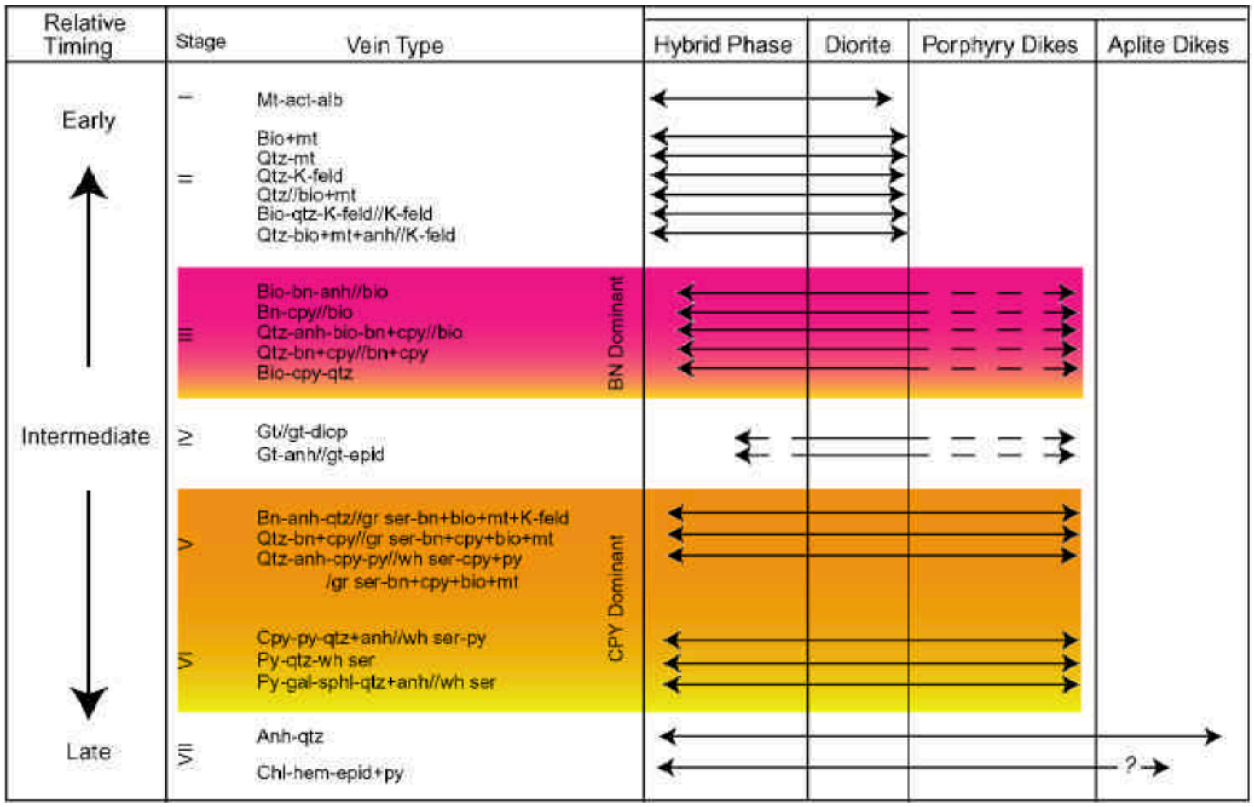

Figure 5: Ertsberg stockwork vein classification from Gibbins (2006)

This vein classification captures the complexity of veining in the EESS by describing 22 vein types and dividing them into seven stages of mineralization.

Table 1: EESS diorite hosted vein paragenesis from this study:

	Stages of Mineral Precipitation in Diorite-hosted Samples					
Mineralogy	Mafic	Ore I	Calc-silicate	Ore II	D	Late
magnetite	xxxxxxxxx					
biotite	xxxxxxxxx			xxxxxxxxx		
quartz	xxxxxxxxx	xxxxxxxxx		xxxxxxxxx	xxxxxxxxx	
apatite	xxxxxxxxx					
chalcopyrite		xxxxxxxxx		xxxxxxxxx	xxxxxxxxx	
garnet			xxxxxxxxx			
diopside						
epidote						
tremolite			xxxxxxxxx			
forsterite						
molybdenite				xxxxxxxxx		
orthoclase						
pyrite					xxxxxxxxx	
sericite						
pyrrhotite					xxxxxxxxx	
sphalerite					xxxxxxxxx	
chlorite						xxxxxxxxx
hematite						xxxxxxxxx
anhydrite						xxxxxxxxx
barite						xxxxxxxxx
carbonate						xxxxxxxxx
rutile						xxxxxxxxx

XXXXXXXXX	Vein Mineral
	Selvage/Halo Mineral
Mafic Stage	Magnetite veinlets and biotite veins with potassic alteration assemblage
Ore Stage I/II	Cu-sulfide and quartz veins with transition from potassic alteration assemblage to phyllic alteration assemblage
Calc-silicate	Garnet, diopside, and epidote veining and alteration
D-veining	assemblage and accessory low temperature base-metal sulfides
Late	Sulfates, carbonates, oxides and propylitic assemblage

Timing relationships of diorite-hosted vein minerals were used to identify six stages of mineralization in the EESS based on Sillitoe (2010) porphyry vein classifications. Mafic minerals form in veinlets and selvages cross-cut by all later mineralization. Quartz and chalcopyrite, with rare molybdenite and K-feldspar occur in veins with similar characteristics to classic A and B style veins (Sillitoe, 2010). Early quartz-chalcopyrite veins (Ore I) are occasional cross-cut with veins of calc-silicate minerals that have similar mineral assemblages to Endo-skarn. Later quartz-chalcopyrite veins (Ore II) have rare molybdenite and common orthoclase selvages. Quartz-pyrite-sericite veins cross-cut all four of these veins types. A number of phases consistent with more oxidized fluids form late veins and fill voids in earlier veins and have been grouped as Late stage.

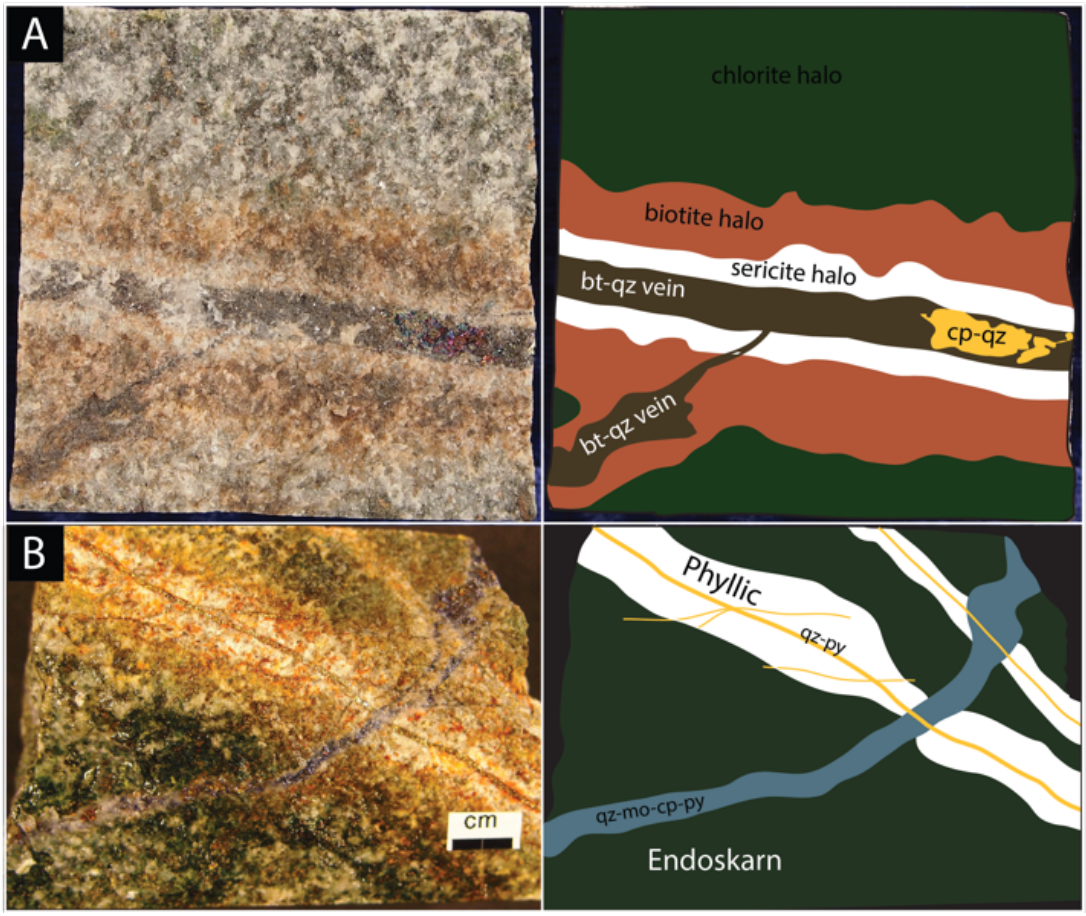

Figure 6: Alteration types in diorite.

A) Example of phyllic alteration (plagioclase altered to sericite) juxtaposed onto potassic alteration (hornblende altered to biotite) along a bt-qz vein hosted in diorite with mafic minerals altered to chlorite. In this case, pervasive alteration of plagioclase to sericite has taken place adjacent to the vein with moderate amounts of biotite preserved within this texture. The intense sericite alteration transitions to biotite alteration of mafic minerals in diorite away from the vein. This likely fits with the vein mineralogy itself, where we see early quartz and hydrothermal biotite that may correspond with the mafic alteration to biotite in the wallrock. Paragenetically later sulfide deposition in the center of the vein, which may correspond with the sericite halo immediately outside of the vein. In this case, little to no orthoclase is observed and the pink color commonly seen in hand sample is attributed to fine grained secondary biotite (which likely has a brown/red hue due to Fe^{3+} content) after mafics. B) Endoskarn-hosted qz-mo-co-py vein lacking a halo cross-cut by qz-py vein with well defined sericite (after plagioclase) halo. The early qz-mo-cp-py vein is representative of ore-stage veining and qz-py vein with sericitic halo would be grouped as a D-vein.

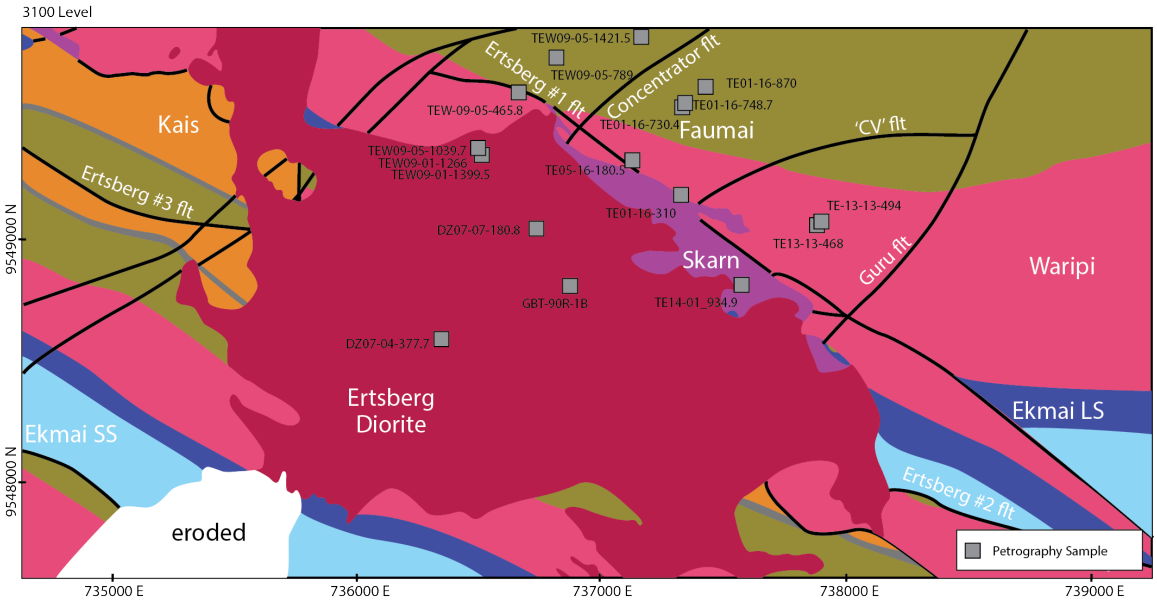

Figure 7: Geologic map of the 3100-m level of the EESS showing projected locations of petrography samples.

See Appendix A for exact sample locations. Because of the dip of the intrusive contact and skarn zones, lower elevation samples plotting from the contact are actually in the skarn zone. Modified from Leys (2012).

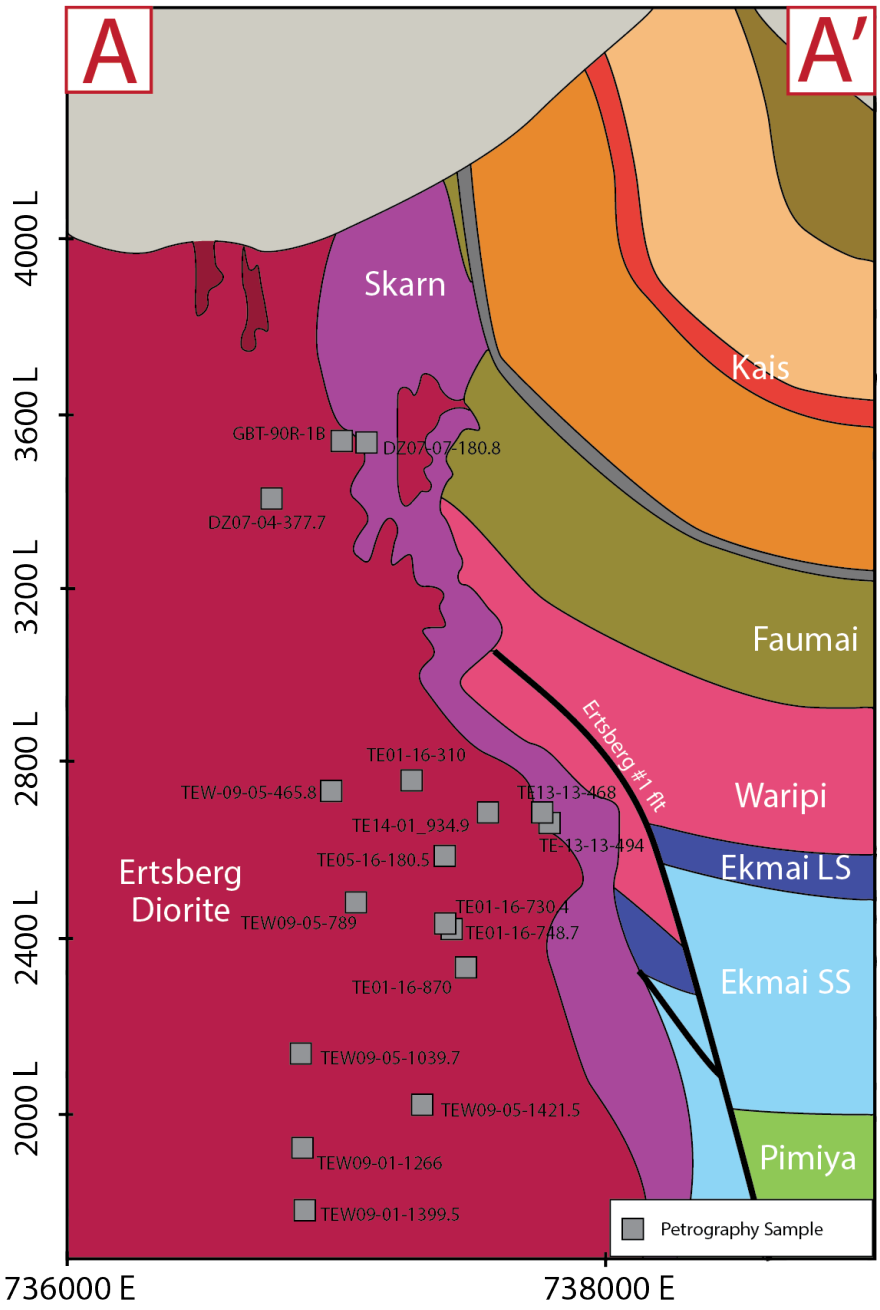

Figure 8: Geologic cross section of the EESS showing projected petrography sample locations.

Sample locations project into the diorite along the A-A' cross-section, although they are distributed lithologically distributed amogst skarn and diorite. See Appendix A for exact locations. Modified from Leys (2012).

Table 2: Diorite-hosted sample mineral assemblages.

Sample	Host Lithology	Altertation Type	Wallrock Minerals			Selvage Mineralogy			Vein Mineralogy		
			Major	Min	Trace	Major	Min	Trace	Major	Min	Trace
DZ07-07-180.8	Diorite	potassic?	qz, plg	bt, cp					qz, plag, cp, an		
GBT-90R-1B	Diorite	phyllic/ potassic	qz, plag, (ser?)	mt, (bt?)		ser, qz, cp			qz, cp	bt?	
TE01-16-310	Diorite	phyllic	ser, qz, py						qz, an	py, barite	
TE01-16-180.5	Diorite	phyllic				ser, qz, bt (hydrot	cp, py		qz	py, cp, an	
TE14-01_934.9	Diorite	phyllic	ser, qz, py	cp		ser, qz	py		qz, py	an, cp	mt
TEW09-01-1266	Diorite	propylitic/ phyllic	ser, plag, qz,	chl (after hbl)	mt	ser, qz		an, mt, cp	qz, an		
TEW09-01-1399.5	Diorite	phyllic/potassic	ser (after plg), bt (after hbl), qz		py, cp	ser ,qz			qz, an		py
TEW09-05-1039.7	Diorite	potassic	plg, qz,	bt (after hbl),		ser, qz,	bt (after hbl)		qz, an		mo, mt, cp
DZ07-04-377.7	Diorite	phyllic/ potassic	ser, qz, plg, bt (after hbl)	mt					qz		an
TEW09-05-789	Diorite	potassic	bt, py, qz	ser	cp				qz, cp, py		an
TE01-16-730.4	Diorite	phyllic/ potassic	ser, qz, py	cp	an		bt		qz,		cp, py, an

Major Min	> 5%
Minor Min	1-5%
Trace	<1%

Mineralogy was determined exclusively through the use of optical petrography.

Table 3: Skarn-hosted sample mineral assemblages.

Sample (Image)	Proto-lith	Alteration Type	Wallrock Minerals			Selvage/Halo Mineralogy			Vein Mineralogy		
			Major	Minor	Trace	Major	Minor	Trace	Major	Minor	Trace
TE01-16-748.7	ls	Hornfels	qz, tremolite	ep, apatite	cp, hm				qz, py, an		
TE01-16-870	ls	Foresterite-diopside Skarn	qz, fo	tremolite, diopside	py, cp				qz, gar (green), fo, py	carb	cp
TE13-13-468	do-ss	Magnetite Skarn	mt, qz, py, cp						qz, cp	an	
TE-13-13-494	do-ss	Hornfels	qz, tremolite/ actinolyte, ep	chl	bt				qz, py, cp	an	
TEW09-05-1421.5	ss	Potassic	qz, chl, py		cp	qz, bt, cp	py, chl		qz, cp, py, carb, mt	hm, mo, po	bt, rutile
TEW-09-05-465.8	Diorite	Endoskarn	plag, qz		mo, mt	ser, qz	garnet (red), diopside, bt		qz, cp, mo		hm, an

Major Min	> 5%
Minor Min	1-5%
Trace	<1%

Mineralogy was determined exclusively through the use of optical petrography.

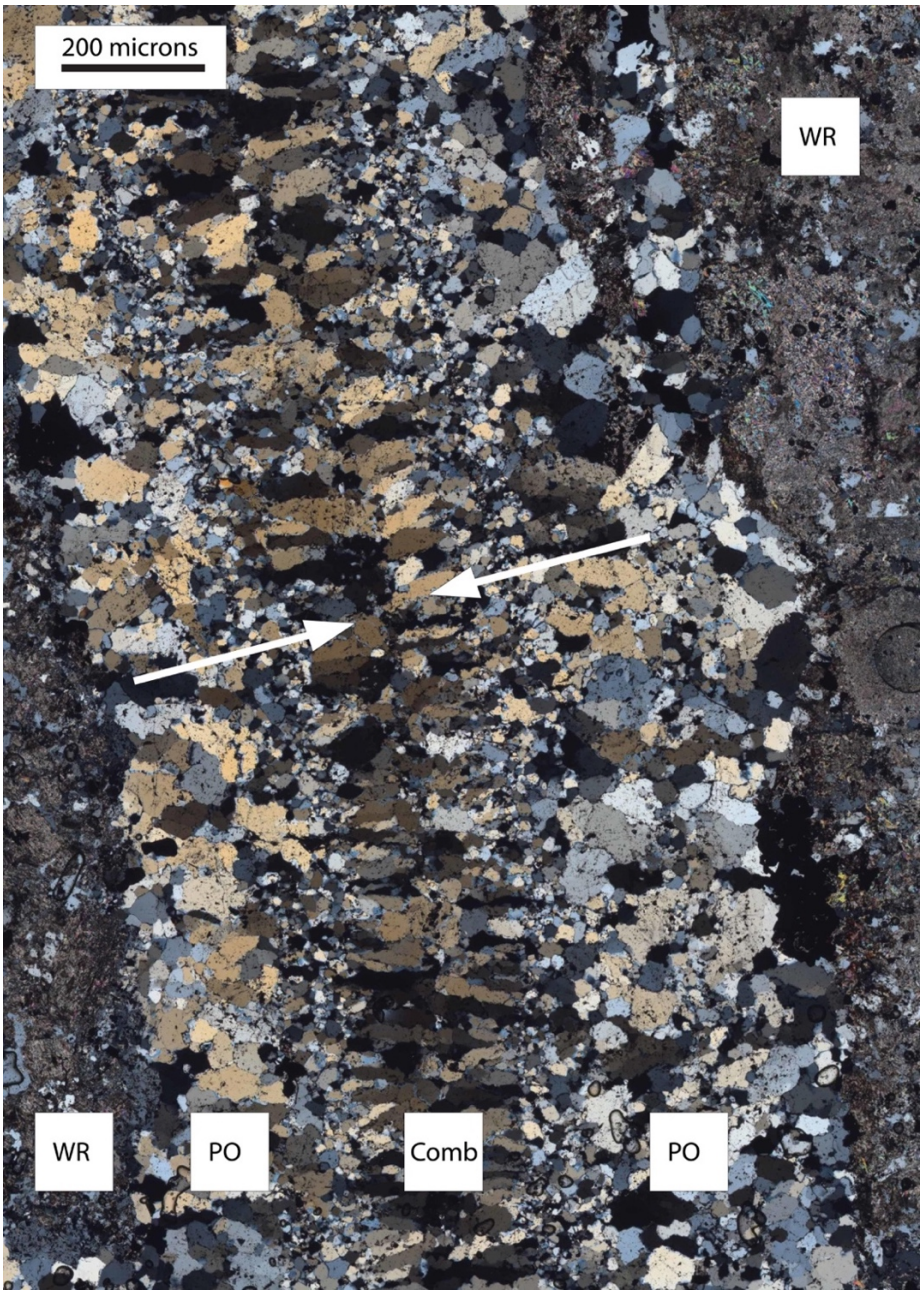

Figure 9: Quartz crystals aligning perpendicular to vein walls.

XPL photomicrograph of quartz crystals becoming increasingly parallel oriented. Crystals oriented toward the center of the vein overtake crystals at lower angles to the vein walls such that a consistent orientation and comb texture is realized near the center of the vein. Arrows indicate the direction of crystal growth. WR = Wall Rock; PO = Poorly Oriented quartz; Comb = Comb quartz

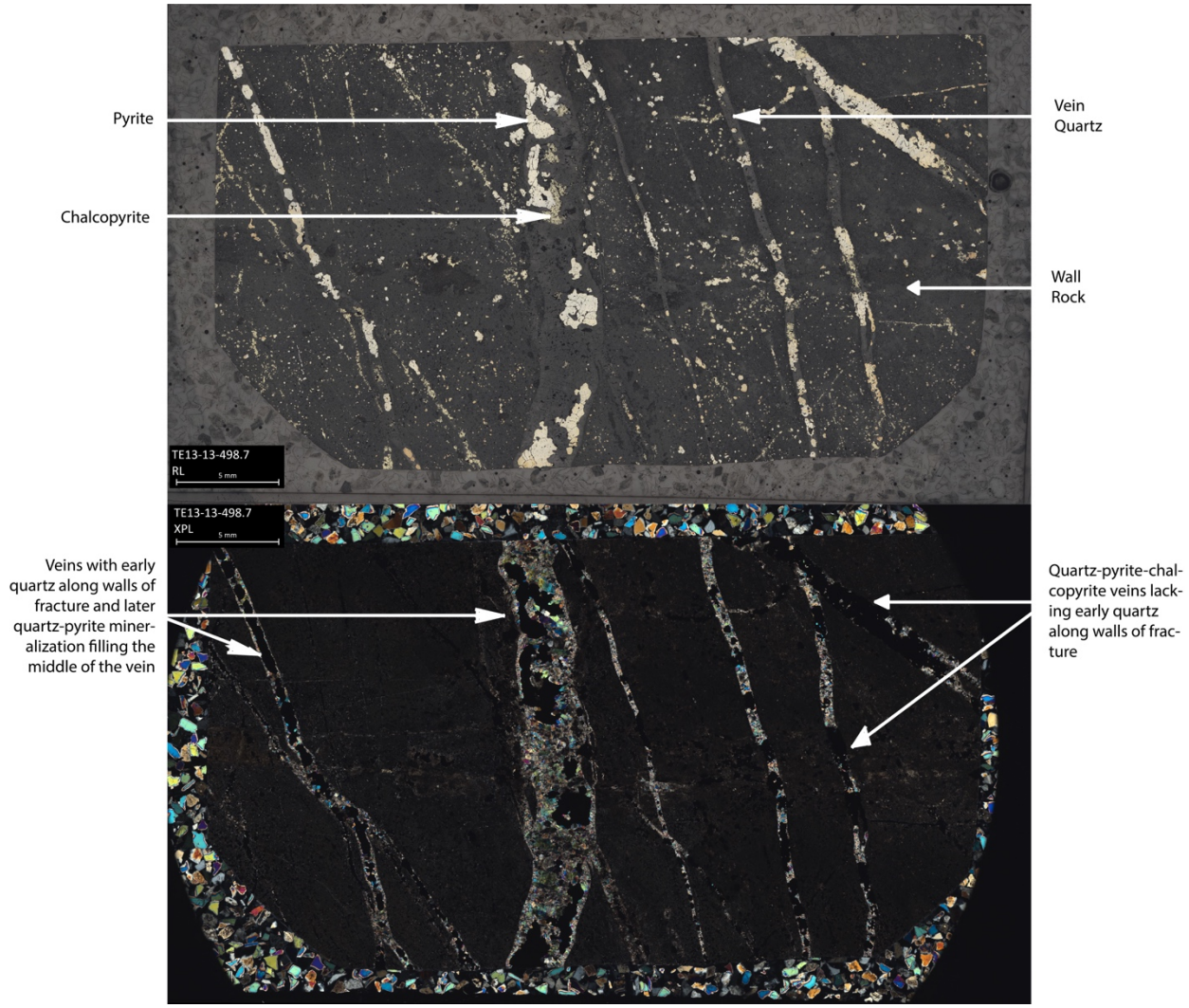

Figure 10: Quartz-pyrite-chalcopyrite veins nested within earlier quartz vein.

Two photomicrographs of the same thin section, sample TE-13-13-498.7, showing two variations on quartz-pyrite-chalcopyrite veins. Veins on the right have quartz, pyrite, and chalcopyrite deposited at the same time, while those on the left have an early generation of quartz that predates any sulfide deposition. This is an example where quartz may have mineralized in fractures, sealing them. Subsequently those quartz veins re-opened to be mineralized by later quartz-pyrite-chalcopyrite veins. Top image was taken under reflected light. Bottom images was taken under crossed nicols.

Chapter 3: Vein Quartz Luminescence Textures

3.1 Introduction

The Scanning Electron Microscope – Cathodoluminescence (SEM-CL) imaging study explores variation in vein quartz CL textures by elevation, host lithology, and vein/halo mineralogy. Samples were selected to cover the range of lithologies and elevations which contain quartz veins in the EESS (*Figures 11, 12*). Individual SEM-CL images, typically 30-60, are taken along vein-perpendicular transects and stitched into composite panoramas (*Figure 13*). CL imaging of EESS quartz reveals euhedral oscillatory zonation, rounded/embayed cores, CL-dark fracture fill and late CL-black quartz – textures consistent with porphyry-style veining as described by Rusk (2012). Multiple generations of quartz overgrowths on quartz breccia clasts, CL-bright quartz after CL-dark quartz in fractured porphyry style veins, and symmetrically banded CL in veins implies that fractures were repeatedly reopened and healed while the hydrothermal system was active. Colloform-banded quartz is found in skarn-hosted and quartzite-hosted samples at all elevations, and sector-zoned quartz occurs in diorite-hosted quartz samples above 3500 m. These textures have been interpreted to represent quartz growth from low temperature (< 300 °C) fluids (Rusk, 2012).

3.2 SEM-Cathodoluminescence Methodology

Eighteen samples were scanned with the SEM-CL to create ~40 panoramic images of quartz vein transects. To achieve the highest quality SEM-CL images, systematic sample preparation techniques were developed to avoid imaging problems that plagued early CL imaging trials.

1. Doubly polished sections (30-100 μm) were checked for polish quality using a petrographic microscope. Samples with major pitting of quartz or sulfide were

polished further to avoid charging issues that can arise from an highly irregular surface.

2. Sections were soaked in 10% NaCl solution for ~24 hours to remove anhydrite, a highly luminescent mineral that overwhelms the CL-detector with light and causes bright streaks on images. Sections were then polished on a vibratory polisher using a colloidal silica solution for 2-6 hours (softer samples will become pitted if left on the polisher for too long).
3. Sections were carbon coated to a thickness of ~30 μm.
4. Copper tape and carbon paint were used to ground the sample and discourage a static electric charge from building up on the surface of the sample during CL imaging.
5. Samples were imaged at the University of Texas at Austin, Jackson School of Geosciences using a Philips/FEI XL30 with tungsten filament at 10-15 kV, ~12 μm working distance, spot size 5-6, 150x – 180x. CL detector was set at 500-720 PMT volts depending on luminescence intensity of the sample.

   Images were taken at ~180x and stitched together using photo editing software (e.g. Photoshop CS6).

3.3 SEM-CATHODOLUMINESENCE TEXTURES

For each quartz vein transect, textures were tallied if present (Table 5). A textural paragenesis was then generated for each transect based on cross-cutting relationships. Textures and paragenesis were compared with sample elevation and host lithology to elucidate the factors impacting the distribution of quartz CL textures. All samples had Euhedral Banded Quartz (EBQ), followed or cross-cut by dark CL quartz, and very late

CL-black quartz associated with sulfides in micro-fractures. These three textures serve as temporal markers in the development of a quartz veins and are useful for relating the timing of other, less common textures within the veins.

1. Euhedral Bands with Bright Cores

Concentric bands of contrasting brightness that extend perpendicular to crystal face (*Figure 14A, 14E, 14H*). Bands have gradational boundaries and there is a tendency for bands to darken away from the center of an individual quartz crystal. Commonly this texture is centered on highly luminescent cores that do not display flat luminesce to very low contrast banding. (30/37 images, 16/17 samples)

2. Dark Sector Zoned Euhedral Banding

Concentric bands of contrasting brightness that extend perpendicular to crystal face (*Figure 14A, 14E, 14H*). Bands have gradational boundaries and there is a tendency for bands to darken away from the center of an individual quartz crystal. Commonly this texture is centered on highly luminescent cores that do not display flat luminesce to very low contrast banding. (10/37 images, 6/17 samples)

3. Sulfide-Associated Dark Luminescence

Quartz deposited immediately predating sulfides tends to be CL-dark (*Figure 15A-15I*). This may be due to Fe-quenching of CL-activators (Penniston-Dorland, 2001) or due to depletion of CL-activators like Ti (Rusk, 2006; Rusk et al. 2008). (30/37 images, 17/17 samples)

4. Late CL-black microfractures

Micro-fractures exhibiting a CL-black luminescence, or lack of luminescence (*Figure 16A, 16B*). Fluid inclusions that homogenize to liquid (type 3) commonly occur along the fracture plane associated with CL-black luminescence. CL-black micro-fractures have been observed to cross-cut all other othe quartz textures and may be coeval with or post-date sulfide deposition. (30/37 images, 17/17 samples)

5. Colloform banding

Repeating rounded growth bands intermittently occur in small sets between euhedral or sector zoned bands in high elevation diorite hosted samples and skarn/sandstone hosted samples (*Figure 14C*). Colloform banding accounts for <5% of CL-texture area in veins when present in samples. These bands are interpreted to be a lower temperature texture and do not appear to be associated with ore formation (Rusk, 2012). (5/37 images, 3/17 samples)

6. Uniform CL

CL of a single intensity throughout a major portion of a quartz crystal or group of quartz crystals (*Figure 14B*). Uniform CL commonly occurs at the core of crystals and gives way to euhedral banding in the younging direction of the crystal. (16/37 images, 8/17 samples)

7. Cemented Fragments

Angular to sub-angular quartz fragments cemented with CL-dark quartz (*Figure 14D, Figure 16B*). This textures is highly variable and may include fragments of quartz

that contain This texture is most common in samples hosted in a sedimentary protolith and is presumed to record a healed micro-breccia. (6/37 images, 4/17 samples)

In addition to the textures listed above, linear features commonly are observed within CL images of quartz crystals. The two most common features, dissolution surfaces and overgrowth surfaces are described below as a guide to future studies to better constrain the origin and significance of these features. Classifying these surfaces in each sample is subjective, so they were not included in the CL texture tally.

Dissolution Surfaces

Typically, a smooth curvilinear surface within a texture or dividing two textures (*Figure 14G-14H*). These surfaces are interpreted to form during periods of quartz dissolution as explained by the quartz solubility diagram (Rusk and Reed, 2002; Rusk, 2006). Conchoidal fractures of quartz crystals may have similar appearance to a dissolution surface, particularly if moving fluids removed loose quartz fragments. Additional criteria are necessary to confidently distinguish between dissolution surfaces and fracture surfaces preserved in EESS quartz veins.

Overgrowth Surfaces

Abrupt changes in quartz crystal orientation within a continuous growth pattern, commonly observed in euhedral banded quartz (*Figure 14H*). The change in pattern orientation is interpreted to be the result of a nearby crystal overtaking the growth of the quartz crystal studied. The boundary at this change in texture should be geometric and oriented with the older crystal growth.

3.4 CL Texture Groups

In general, the earliest quartz in a vein is brightest and the latest quartz is darkest. However, CL-brightness and CL-darkness are subjective measures that were not possible to quantify with the instruments used in this study. Therefore, the CL textures were tallied and the CL texture paragenesis was recorded for each panorama (*Table 5*). Quartz CL textures were then divided into three texture groups based on the relative timing of CL textures derived from cross-cutting relationships (*Table 5*).

Texture Group 1 (TG1) consists of early bright quartz textures that volumetrically account for the majority of vein quartz in the EESS. Texture Group 2 (TG2) is made up of darker quartz textures that immediately pre-date or are contemporaneous with deposition of Cu-Fe-sulfides and pyrite. TG2 can be the only textures in veins with sulfides, but commonly TG2 will cross-cut or coat veins of TG1. In this second scenario, TG1 is effectively a "framework" on which TG2 and sulfides are deposited. TG3 is comprised of brittle deformation features that overprint TG1 and TG2.

Texture Group 1: Quartz framework

Euhedral banded quartz, commonly with bright cores of broad euhedral bands in low contrast to one another, or simply flat luminescence (*Figure 14*). Individual bands within the euhedral banded quartz do not have sharp boundaries, but instead grade into the adjacent band of contrasting luminescence. In some cases, fracture filling bright quartz will cross-cut euhedral banded quartz in linear zones on comparable brightness to the host quartz and may even develop a similar euhedral banded texture. Dissolution surfaces and overgrowth (which mark changes in crystallographic orientation) are commonly observed in this texture group. Dissolution surfaces commonly cap TG1

quartz. Sulfides found in this fracture group appear to have precipitated in cavities connected by micro-fractures or in places where asymmetrical fracturing of the vein (away from the center-line) occurred. Colloform texture is rare, but occurs contemporaneous with other TG1 textures.

Texture Group 2: Quartz associated with Cu-Fe-sulfides and pyrite

Texture Group 2 (TG2) is characterized by CL-dark quartz, which occurs paragenetically after TG1 and prior to sulfide deposition (*Figure 15*). TG2 occurs as overgrowths on TG1, as cross-cutting veins, and and as stand-alone quartz or quartz-sulfide veins. The transition between TG1 and TG2 can be gradational or sharp when TG2 overgrows TG1, but where TG2 cross-cuts TG1, a smooth, a rounded contact is usually present. Cross-cutting veins may contain euhedral quartz grains that grow toward the center of the fracture, or anhedral quartz coating the walls of the fracture. Sector-zoned euhedral quartz is present in TG2 at high elevations and has not been observed in deep portions of the EESS. A uniform CL texture and mottle CL texture also occur in TG2.

Texture Group 3: Quartz textures associated with brittle deformation

Texture group 3 (TG3) includes CL-black fractures and cemented angular fragments. CL-black fractures occur in nearly every sample as planar CL-black features lacking internal textures that cross-cut all other quartz textures (*Figure 16*). Cemented angular fragments are zones of fragmented TG1, TG2, and sulfide that are cemented with CL-dark or CL-black quartz. Cemented angular fragments may also incorporate carbonates, sulfates, and oxides. It can be difficult to distinguish CL-black fractures from

veinlets of TG2 due to similarity in the CL intensity of TG2 and CL-black fractures. TG3 occurs along healed fractures that host two-phase fluid and these fractures have been observed in conjunction with sulfide mineralization. As Diamond (2014) noted, the larger black blotches that are intersected by CL-black fractures are commonly associated with decrepitated fluid inclusions.

3.5 Variation in Vein Quartz CL Texture by Elevation and Lithology

The review of quartz CL textures allows an interpretation of the spatial and temporal distribution of these features in the EESS based on the samples studied.

1. Sector zoning is only observed above 2586 m and only occurs in diorite-hosted samples. However, in some cases, CL-dark quartz was observed to be of the same generation as sector-zoned quartz. Euhedral banded late dark (D-vein) quartz is present in samples extending to low elevations – the deeper in the system, the fewer imperfections quartz has. Distinguishing between EBQ from TG1 and TG2 is difficult. TG1 EBQ is CL-brighter and tends to gradationally darken in the younging direction of the quartz crystals, while D-vein EBQ bands oscillate between CL-darker hues and darkening does not occur in the younging direction. TG2 EBQ has a sharply defined euhedral banded texture that has significantly darker bands with distinct contacts compared to early euhedrally banded quartz of TG1. The transition between early euhedral quartz and late CL-dark quartz of TG2 may occur simply as overgrowths, along fractures and pore spaces in the quartz, or following a dissolution surface. Euhedral growth zoning is most common is lower temperature deposits and subordinate to higher temperature textures in porphyry system (Rusk, 2012), yet euhedral growth zones of

oscillating CL intensity are the most common texture in the EESS, suggesting that the EESS is somewhat lower temperature than other porphyry systems.

2. The cemented fragment texture only occurred in veins in a sedimentary protolith (skarn or quartzite) – the cause for this is unknown but may suggest that skarn is more prone to brittle deformation, or that the samples studied lay along a fault zone.
3. The deepest samples (1750-2100m) tend to have the most complex textural patterns (*Figure 17*). This relationship can be explained if the system underwent thermal collapse and these zones experienced the longest lived quartz deposition. Alternatively, these samples might be associated with a structure or sheeted vein system. However, the vein density of a sheeted vein system has not been identified in the deeper parts of the EESS system at this time.
4. The deepest samples also have the most euhedral banding cross-cutting each other, which if the euhedral banding represents the highest T/earliest quartz, these deep zones of the system have fractures that were re-opened many times.
5. Skarn-hosted veins have more cross-cutting generations of euhedral quartz and more varied textures, which often do not neatly fall into a classification scheme (*Figure 18*). This may in part have to do with the more varied mineral assemblages and rheological properties of the exoskarn in which these veins formed.

3.6 Paragenesis of CL Textures

Virtually 100% of samples displayed the paragenetic sequence: Euhedral Banded Quartz (1) followed by CL-dark quartz (3) followed by CL-black micro-fractures (4)

(*Table 5*). The most complex samples show the basic paragenetic components 1>3>4 (*Table 5*) repeated multiple times. For example: 1>1>3>4>1>2/3>4.

The repeating sequence of textures is consistent with a process of fluid maturation during and after quartz crystallization. One possibility is that a fluid high in luminescence activators (ie. Ti, Al, Ge) precipitates bright euhedral banded quartz and associated CL-bright features (x-cutting bright quartz, bright flat/textureless cores). Somehow, as quartz continues to precipitate, luminescence goes down. This fluid may become exhausted of these activator elements or enriched in luminescence-quenching elements before quartz-deposition is complete, or the rate of precipitation may outpace the incorporation of luminescence activators in the quartz, leading to darker CL response as crystals grow. This depleted fluid may reside in existing fractures or may be drawn into new fractures and precipitate CL-dark quartz. This may coincide with the fluid approaching sulfide saturation, since chalcopyrite and pyrite are present in veins adjacent to CL-dark quartz. Following sulfide deposition and alteration of host rock selvages, CL-black quartz may form by a similar mechanism, as a lower salinity fluid is left over. If that low salinity fluid is drawn into micro-fractures, it may reduce the luminescence along those microfractures, possibly by allowing luminescence activating elements to diffuse from the quartz lattice.

3.7 Fracturing Evidence in Quartz Revealed by SEM-CL

The general model for EESS quartz veins is of early bright euhedral quartz propping open fractures to allow later fluid passage and providing a zone for additional fracturing within quartz and wallrock for later sulfide depositing fluids to travel along. A dark generation of quartz precedes the sulfides and the sulfides are deposited on top of

that dark quartz or within veins of the dark quartz. Figure 14G is a rare example where the EBQ, CL-dark and CL-black sequence is capped with a dissolution surface and followed by additional CL-dark and CL-black quartz. This is evidence that the primary texture sequence can repeat within a vein. Furthermore, within the EBQ texture, couplets of light to dark CL bands are repeated many times. Both examples suggest that cyclic CL-bright to CL-dark or CL-black patterns are present in EESS vein quartz and suggest high frequency chances in P-T-X conditions. Such observations support a model where fracturing and resultant pressure decrease is occurring repeatedly during mineralization.

Considerable textural evidence has been documented for veins that have repeatedly opened and been sealed by quartz. Some of these veins opened asymmetrically and include fragments of wallrock within EBQ (*Figure 13*). Other samples record early quartz precipitation producing symmetrical veins with repeated patterns of light to dark quartz that likely coincides with each time the vein is opening and silica-rich fluids are drawn into the vein (*Figure 19*). Quartz veins do not always contain sulfides (*Figure 13*), but when sulfides are present, the sulfides form along the youngest surfaces of quartz – CL-dark quartz – and can form along CL-dark quartz-lined veinlets that cross-cut earlier EBQ (*Figure 19*).

Examples where sulfides and pyrite appear to be deposited within TG1 quartz have small amounts of dark TG2 quartz alongside the sulfides and CL-dark (not CL-black) micro-fractures linking the sulfides. These CL-dark micro-fractures are evidence that sulfide-depositing fluids permeated along fractures and deposited TG2 and sulfides where voids were present.

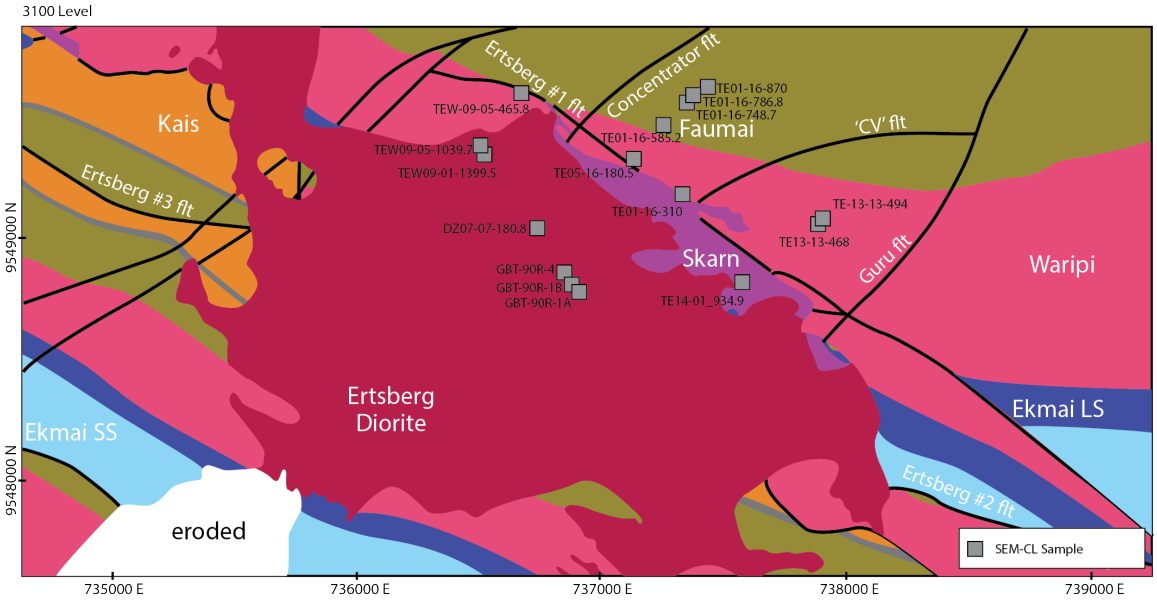

Figure 11: Map view of SEM-CL sample locations projected on the 3100m level geologic map.

See Appendix A for exact sample locations. Modified from Leys et al. (2012).

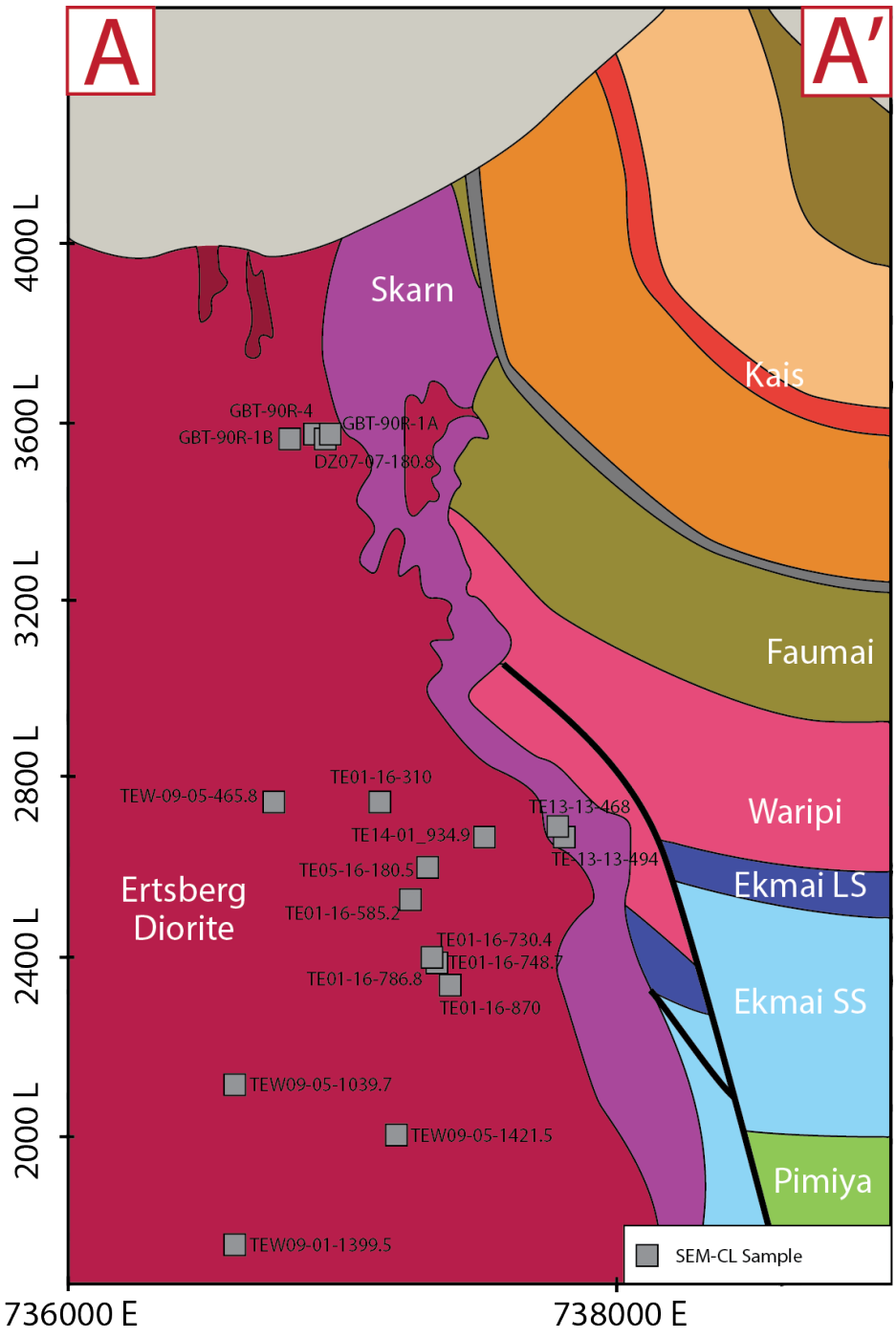

Figure 12: Geologic cross section of the EESS showing projected SEM-CL sample locations.

See Appendix A for exact sample locations. Modified from Leys et al. (2012).

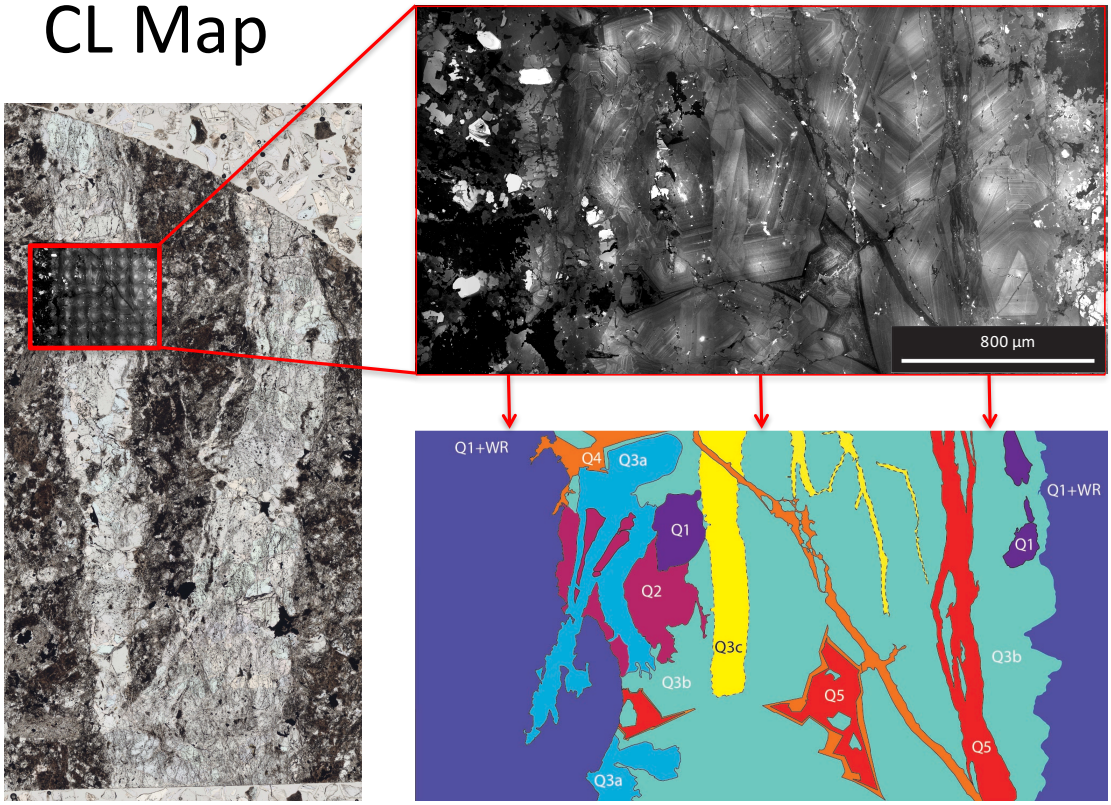

Figure 13: Diorite-hosted Quartz Vein showing at least 5 stages of reopening and quartz precipitation.

Quartz veins in diorite host (left) with composite of CL images along a vein transect (upper right) and a sketch of the quartz generations to emphasize. cross-cutting relationships. Quartz vein has been re-opened and mineralized with quartz at least five times. This vein is a good example of a vein which has opened asymmetrically and may have incorporated wall rock quartz in with Q1 vein quartz. Re-opening and mineralization of veins suggest that many episodes of fracturing and fluid input occurred in the EESS, which supports a model of EESS mineralization along prominent structural features.

Table 4: Summary of CL textures and paragenesis.

Sample (Image)	Host Lithology/ Protolith	Texture							Texture Paragenesis
		1-Euhedral Bands	2-Sector Zoned Bands	3-Sulfide Associated Dark-CL	4-Late CL-black microfractures	5-Colloform banding	6-Uniform CL	7-Cemented Fragments	
DZ07-07-180.8 (1)	Diorite	X		X	X		X		6>1>3>4
GBT-90R-1B (1)	Diorite		X		X	X			2>5>2>4
GBT-90R-1B (2)	Diorite		X		X	X			2>5>2>4
GBT-90R-1B (3)	Diorite		X		X	X			2>5>2>4
GBT-91R-1A (1)	?	X		X			X		1/6>3>4
GBT-91R-1A (2)	?	X		X	X		X		1/6>3>4
GBT-91R-1A (3)	?	X		X	X		X		6>1>3>4
GBT-91R-4 (1)	Diorite	X		X			X		6>1>3
GBT-91R-4 (2)	Diorite	X		X	X				1>3>4
TE01-16-310 (1)	Diorite	X		X	X				1>3>4
TE01-16-585.2 (1)	Diorite	X		X	X		X		1/6>3>4
TE01-16-748.7 (1)	ls	X	X	X	X			X	7/1>2/1>3>4
TE01-16-786.8 (1)	ls	X		X	X			X	1>3/7>4
TE01-16-786.8 (2)	ls	X		X	X				1>3>4
TE01-16-786.8 (3)	ls	X		X	X		X		1>3>4>6
TE01-16-786.8 (4)	ls						X		6
TE01-16-786.8 (5)	ls						X		6
TE01-16-870 (1)	ls	X		X	X				1>3>4
TE01-16-180.5 (1)	Diorite	X		X	X				1>3>4
TE01-16-180.5 (2)	Diorite	X	X	X	?		X		6/1>2/3>4?
TE01-16-180.5 (3)	Diorite	X	X	X	X				1>2/3>4
TE01-16-180.5 (4)	Diorite	X		X			X		1/6>3>4?
TE01-16-180.5 (5)	Diorite			X	X		X		6>3?>4?
TE13-13-468 (1)	do-ss	X	X		X	?		X	1/2>5?>4
TE13-13-468 (2)	do-ss	X		X	X	X		X	1>5>3>4
TE-13-13-494 (1)	do-ss	X		X	X				1>3>4
TE14-01_934.9 (1)	Diorite	X		X	X				1>3>4
TE14-01_934.9 (2)	Diorite	X		X	X		X		6>1>3>4
TE14-01_934.9 (3)	Diorite	X	X	X	X				1>3>4>2>3
TEW09-01-1399.5 (BEG)	Diorite	X	?	X	X				1>3/2?>4
TEW09-01-1399.5 (1a)	Diorite	X		X	X		X		6>1>3>4
TEW09-01-1399.5 (1)	Diorite	X		X			X		6>1>3
TEW-09-05-465.8 (1)	Diorite		X	X	X		X		1/6> 2/3>4
TEW-09-05-465.8 (2)	Diorite	X	X	X	X				1>2>2/3>4
TEW09-05-1039.7 (1)	Diorite	X			X				1>4
TEW09-05-1039.7 (2)	Diorite	X		X	X				1>3>4>2
TEW09-05-1421.5 (1)	ss	X		X	X	X			1>5>1>3>4

An “x” signifies that a given texture was present in the image. Each texture was assigned numbers (1-7) so that the order of the textures (determined by cross-cutting relationships) could be represented in the Texture Paragenesis column. Textures left of the “>” symbol occur before texures to the right of the symbol. The “/” symbol was used to indicate that two textures occurred concurrently. The sequence of 1 (euhedral banded quartz) followed by 3 (sulfide associated dark quartz) followed by 4 (Late CL-black) quartz occurred in 28/37 CL images studied.

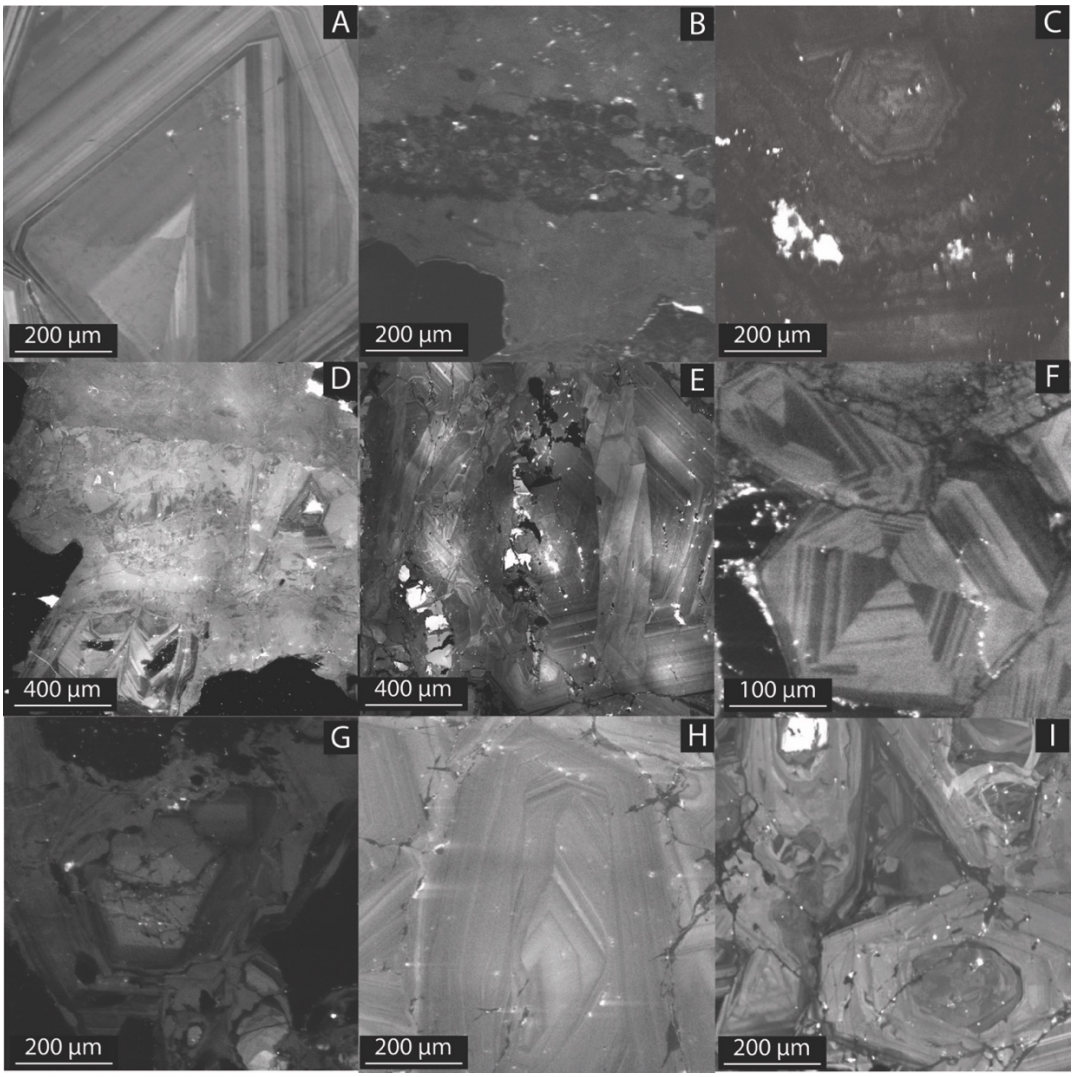

Figure 14: Quartz CL Textures – Texture Group 1, Framework.

A) Euhedral Banded quartz (EBQ) is the most common texture in EESS veins B) Uniform CL has as single CL intensity or an extremely low contrast geometric texture C) Colloform Banding is found in veins hosted by sedimentary protolith and diorite hosted samples above 3000 m D) Breccia composed of TG1 Fragments with overgrowth of euhedral banded TG1 quartz (bottom left) E) Euhedral Banded TG1 quartz cross-cut by Euhedral Banded TG1 quartz, evidence that veins were fractured during TG1 growth F) Sector Zoned quartz found in high elevation veins G) Dissolution surfaces in TG1 that truncate fractures containing type 1, type 2a, and type 2b fluids H) Overgrowth Surfaces and Dissolution Surfaces in EBQ I) Multiple dissolution surfaces present within individual quartz crystals, demonstrating the volatility of hydrothermal conditions during EESS vein formation.

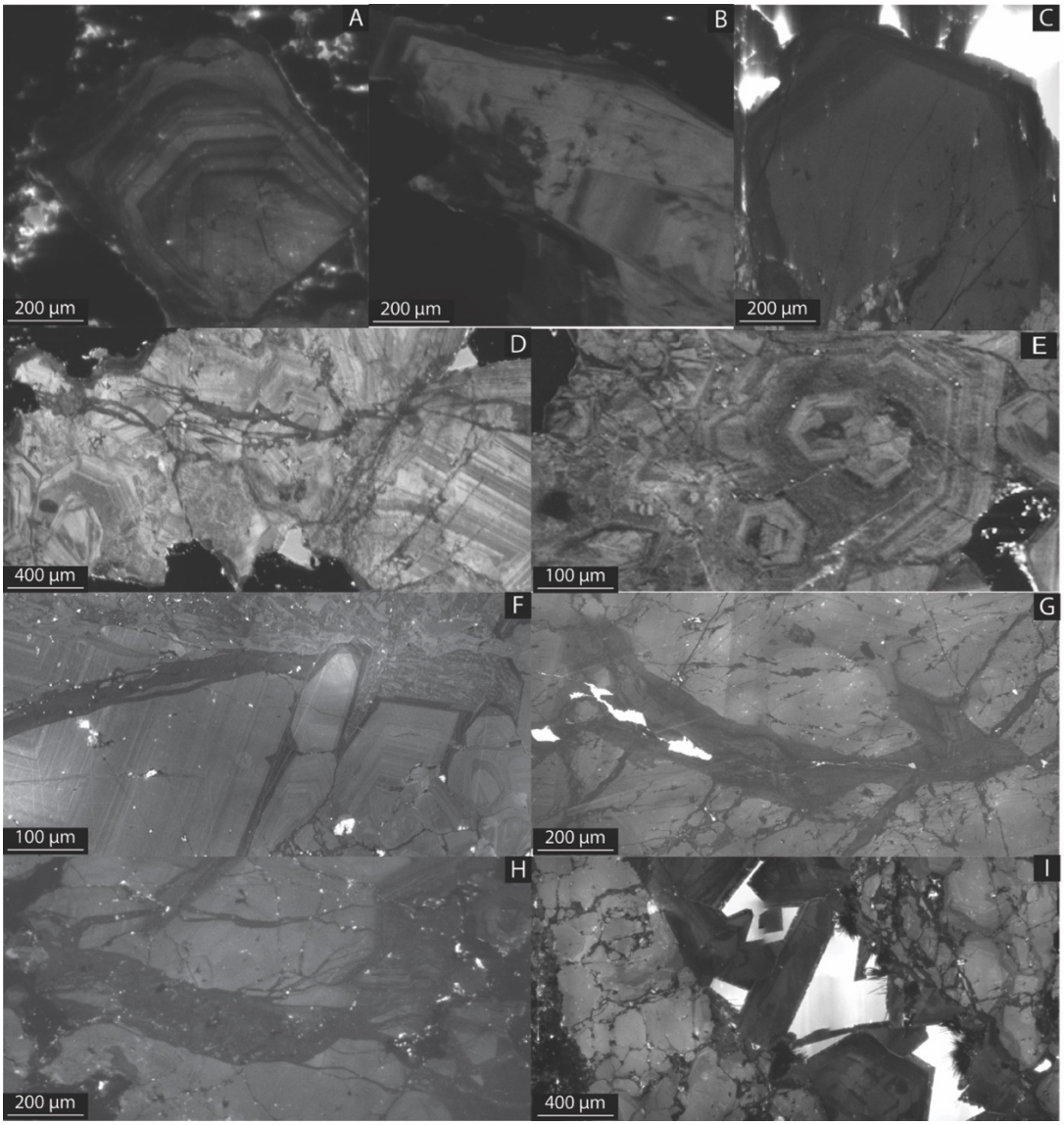

Figure 15: Quartz CL Textures – Texture Group 2, Sulfide Associated.

A-C) CL-dark rim immediately adjacent to sulfide deposition D-E) CL-dark quartz along fractures that run between sulfides F) CL-dark quartz transitioning from fracture to rim on TG1 quartz, illuminating the relationship between CL-dark quartz in fractures and CL-dark rims G) CL-dark quartz along fractures with development of CL-dark euhedral textures within the CL-dark fracture H) CL-dark quartz transitioning from veinlets to euhedral quartz around a sulfide I) CL-dark quartz with euhedral banded quartz crystals cross-cutting a TG1 vein, white is ep and vein contains sulfides post-quartz in other parts of the vein

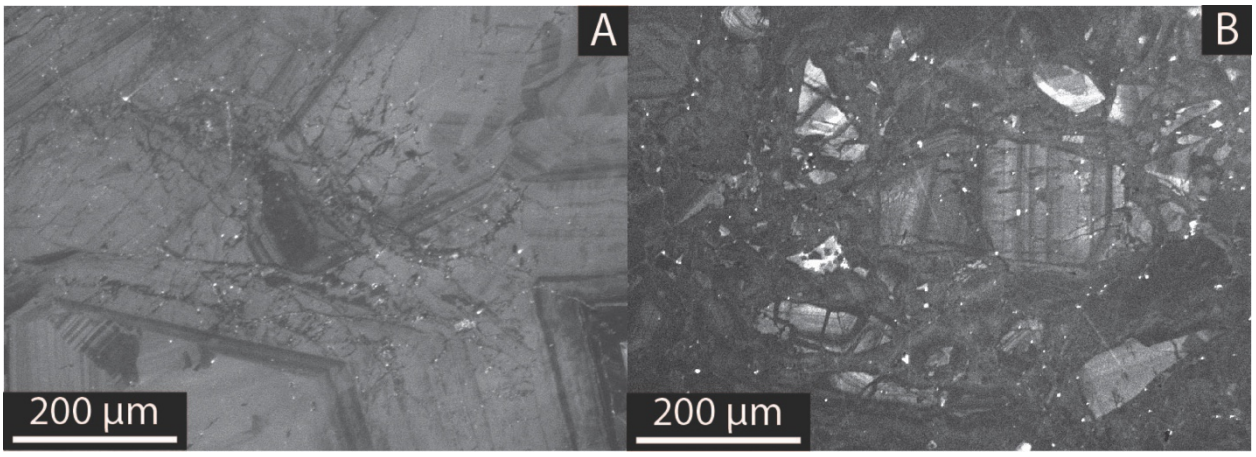

Figure 16: Quartz CL Textures – Texture Group 3, Brittle Deformation.

A) CL-black fractures pictured here cross-cutting earlier euhedral banded quartz is a nearly ubiquitous feature in EESS quartz vein CL images and is the last feature according to cross-cutting relationships. B) This example of cemented angular fragments contains quartz fragments with CL-black fractures, suggesting that the micro-breccia formation post-dates CL-black fracture formation and was thus included in TG3 as a feature that can occur very late in the development of a quartz vein.

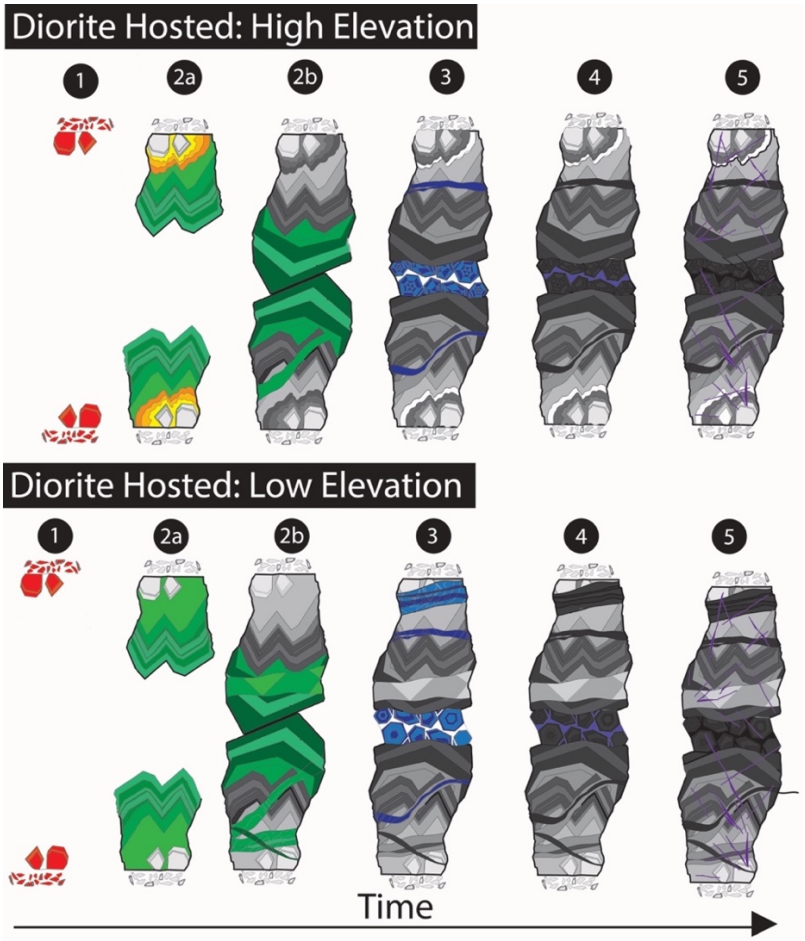

Figure 17: **Quartz vein paragenesis comparing high and low elevation veins**.

This figure is an original cartoon intended to illustrate the timing relationship of the CL textures observed in the EESS. (**1**) Early bright euhedral banded CL grows into fracture and seals wallrock pores (red hues) (**2a**) growth of quartz crystals with euhedral banded CL continues toward center of vein (green); high elevation samples may contain bands of colloform texture as well (yellow-orange hues); bands become darker in younging direction of crystal growth (**2b**) multiple mechanical closure and re-opening of vein caused fractures in early quartz which were followed by euhedral banded quartz deposition sealing the fractures; cross-cutting the early quartz; fractures are more prevalent in deep samples; an overgrowth surface is present where quartz oriented with another crystal (nucleated out of plane of view) grows on earlier 2a quartz (**3**) additional mechanical opening and closure events allow precipitation of CL-dark quartz cross-cutting earlier generations of quartz; a fracture down the center of the vein is enlarged by dissolution and filled with CL-dark euhedral quartz; in high elevation samples this quartz is sector zoned (**4**) Sulfide deposition fills open spaces (**5**) CL-black micro-fractures cross-cut all quartz generations

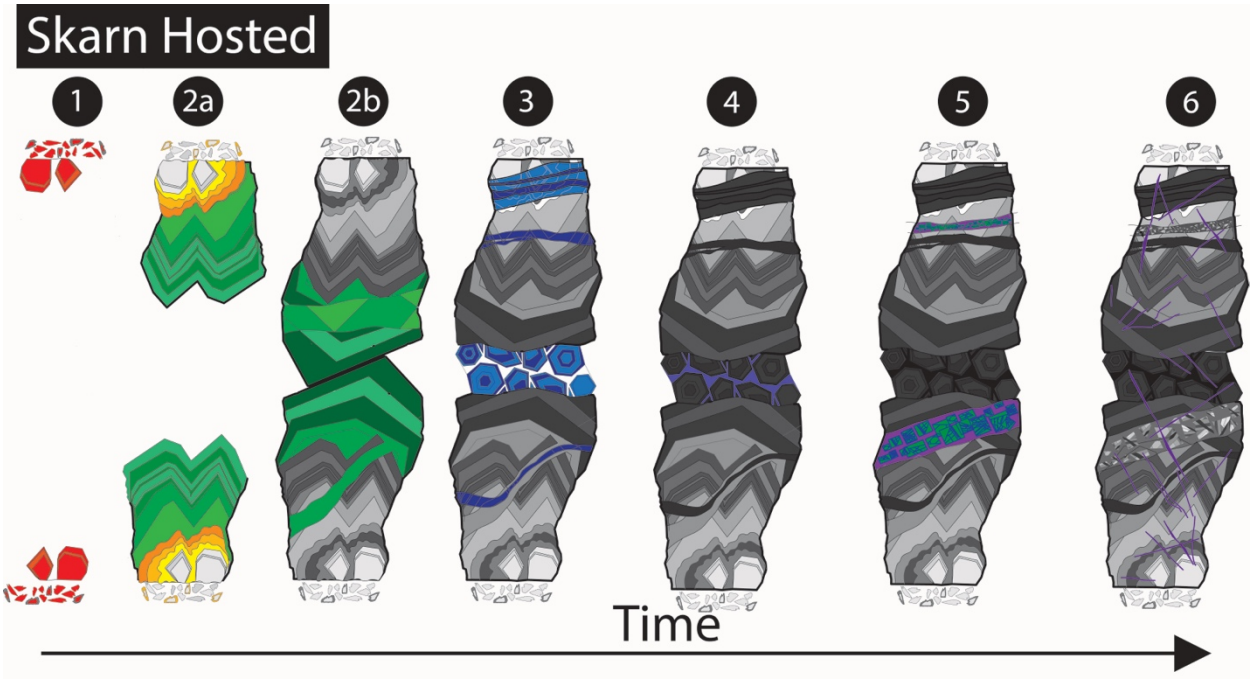

Figure 18: Quartz Vein paragenesis of skarn-hosted quartz vein.

This figure is an original cartoon intended to illustrate the timing relationship of the CL textures observed in the EESS. Skarn-hosted quartz veining is comparable to High Elevation Diorite with more mechanical opening/closing events with quartz precipitation and stage 5 contains cemented fractures that contain angular fragments of earlier quartz generations.

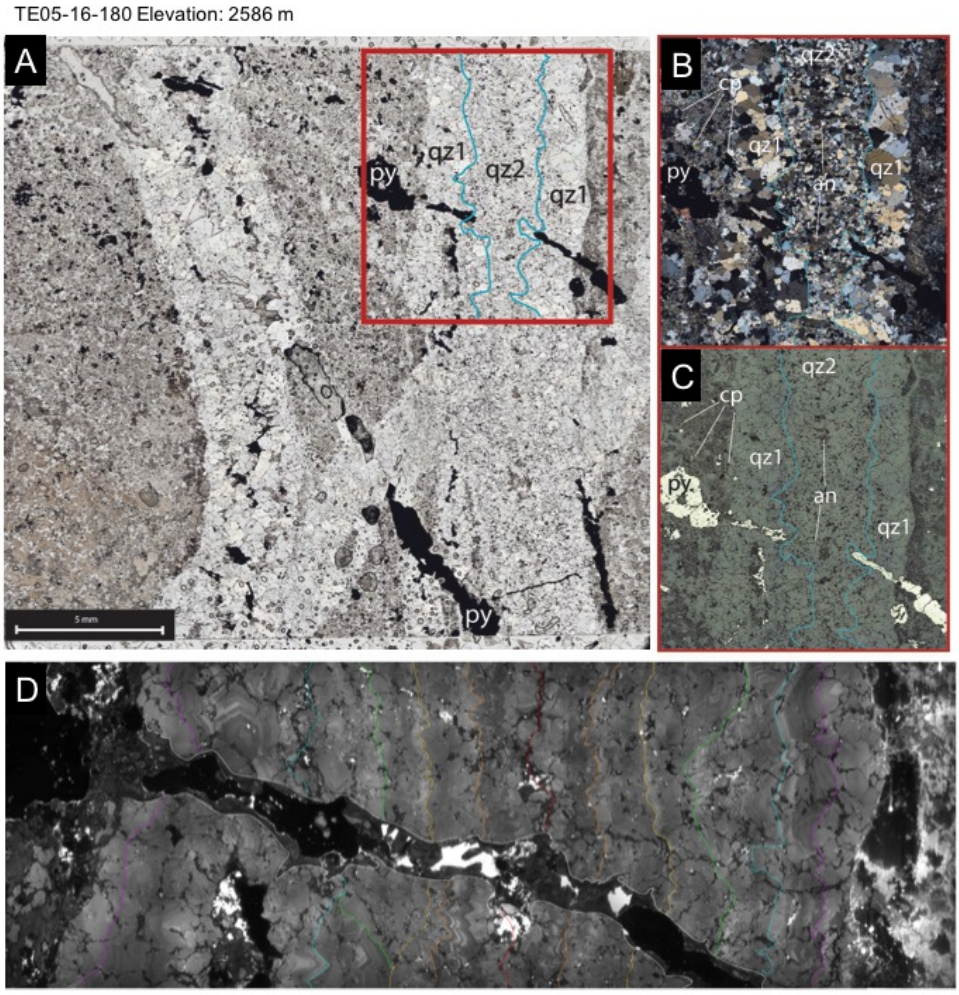

Figure 19: CL images documenting multiple opening of diorite-hosted sheeted quartz vein.

A. Photomicrograph of diorite-hosted sheeted quartz veins cross-cut by quartz-pyrite veins. The locations of images B and C is indicated with the red square **B.** Photomicrograph of quartz vein cross-cut by sheeted quartz vein, taken under crossed nicols. **C**. Photomicrograph of quartz vein cross-cut by sheeted quartz vein, taken under reflected light. **D**. SEM-CL image transect of the quartz vein in images B and C. This vein shows alternating light to dark transitions (couplets) from vein margin toward the center of the vein. The vein is roughly symmetrical and has likely re-opened along the same fracture or remained open for the majority of mineralization. The cross-cutting the sheeted quartz vein at a low angle is comprised of significantly CL-darker quartz, pyrite and epoxy. Dark CL (TG2) + sulfide cross-cutting early CL-brighter quartz (TG1) is a defining feature of EESS veins. CL-black micro-fractures (TG3) can be seen in sharp contrast to the TG1 quartz.

Chapter 4: Fluid Compositions

4.1 Introduction

Initial fluids exsolved from magma are high salinity (50% or higher) but decrease in salinity as additional crystallization decreases the volume of melt present, forcing additional water to exsolve. These initial fluids exsolved from magmas and collected in the cupolas are supercritical and typically have salinities less that 5 wt% chlorine and low Cu contents (Cloos, 2001). In porphyry systems, these magmatic fluids ascend along extension fractures and infiltrate into the overlying rock. Separation of a single intermediate phase fluid into a low density fluid and a high density fluid occurs when pressure, temperature and fluid composition are such that supercritical fluid unmixes (Roedder, 1985). These unmixing to liquid and vapor during cooling and/or pressure decrease causes Cl and Cu to partition into the high density (brine) phase (Beane and Bodnar, 1995; Cloos, 2001; Redmond et al., 2004). The parent fluid and the fluids resulting from phase separation in this environment are consistent with three of the fluid inclusion types characterized in Nash (1976) – Moderate Salinity, Vapor-Rich, and Halite-Bearing inclusions. In the EESS, fluid inclusions are trapped along healed fractures in vein quartz. As a result, EESS fluid inclusion post-date the quartz crystals in which they are trapped and timing relationships are difficult to determine for different fluid inclusion types.

Nash (1976) described four inclusion types as typical of porphyry systems: moderate salinity, gas-rich, halite-bearing and CO_2-rich. Moderate salinity and halite-bearing inclusions homogenize to liquid upon heating in the microthermometry stage (*Figure 20*). Gas-rich inclusions homogenize to vapor upon heating in the microthermometry stage (*Figure 20*). The first three types are petrographically observed in EESS. Notably, CO_2-rich inclusions were not identified – double bubbles were not

observed in this skarn. Although, some inclusions had notably dark fluid contents that raised suspicion that a fluid other than H_2O might be present. Positive ice melt temperatures were recorded in a few cases during microthermometry and the presence of CO_2-rich inclusions was confirmed with Raman spectrometry. A fifth type of fluid inclusion exists in the EESS, which was not explicitly described by Nash (1976). These inclusions are petrographically similar in appearance to moderate salinity inclusions described in Nash (1976), but were found to homogenize by critical behavior during heating runs on the microthermometry stage (*Figure 20*).

A change from single-phase to two-phase inclusion assemblages present together over some three-dimensional zone can delineate the location of phase separation in the hydrothermal system: parent fluid exsolved from magma to vapor and brine. In Bingham, Landtwing et al., (2005) showed low salinity chalcopyrite-bearing inclusions are found in the deepest portions of the porphyry system, while vapor-dominated and halite-bearing inclusions are present in upper portions of the system. The presence of all three fluid inclusion types approximates a zone of phase separation, which has been constrained to a laterally extensive region that extends vertically over ~500m of elevation.

4.2 EESS Fluid Inclusion Types in Quartz

The four fluid inclusion types identified in this study are referred to as type 1, type 2a, type 2b, and type 3 which are not to be confused with Nash's nomencalture (*Table 5*). Type 1 inclusions at ambient conditions are 2.2-6.0% salinity, 40-70 vol% vapor bubble, homogenize between 332-396 °C and can contain chalcopyrite daughter crystals. Type 2a inclusions at ambient conditions are 27.7-51.2% salinity, 10-30 vol%

vapor bubble, homogenize between 280-420 °C and contain halite. They may also contain sylvite, chalcopyrite, magnetite, anhydrite and hematite. Type 2b inclusions at ambient conditions are 1.2-11.7% salinity, 65-90 vol% vapor bubble, homogenize between 340-392 °C and typically do not contain daughter minerals, although two inclusions contained opaque minerals. Type 3 inclusions at ambient conditions are 2.4-23.0% salinity, 15-50 vol% vapor bubble, homogenize between 283-403°C and may contain opaque minerals.

These types are consistent with fluid inclusions types described by Nash 1976 and subsequent porphyry studies. The presence of type 1, type 2a and type 2b inclusions likely records a primary magmatic-hydrothermal fluid that separated into vapor and brine phases (*Figure 21*). The origins of type 3 inclusions in poorly understood. Type 3 inclusions may have trapped liquid from a condensed vapor (*Heinrich, 2004*), a high density fluid that was diluted or did not reach halite saturation, or the ion-depleted remnants of intermediate or high density fluids that reacted with wall-rock and mineralized the EESS.

Delineating the Single-Phase Field vs. Two-Phase Field in the EESS

A fluid inclusion petrographic survey was conducted to delineate the phase separation zone within the EESS and guide sample selection for microthermometry. Sixteen samples were examined for the presence of vapor-dominated inclusions, halite-bearing inclusions, and inclusions with chalcopyrite, but lacking halite. Inclusion types present in each sample were plotted by northing, easting, and elevation coordinates (*Figure 22*). Samples from 1748 m to 3581 m contain fluid inclusions from both liquid and vapor regions of the water phase diagram indicating that phase separation occurs in

the EESS system (*Figure 21*). Assemblages of fluid inclusions with a vapor bubble approximately 50 ± 20 vol% of the inclusion, which had opaque daughters minerals believed to be chalcopyrite were present from 1748 m to 3571 m (*Figure 21*). The chalcopyrite bearing inclusions lacking halite were initially interpreted to have been trapped in the single-phase field. Halite-bearing and vapor dominated inclusions were interpreted to have been trapped fluid in the two-phase field. The transition from a single-phase field to a two phase field is not apparent from the petrographic data (*Figure 22*) due to the existence of all three inclusion types throughout the vertical and lateral extent over which the EESS was sampled.

Microthermometry of vein quartz discussed in the next section confirms that fluid inclusion assemblages from both the single-phase field and the two-phase field have been measured in 1882 m (sample TEW09-01-1266, diorite-hosted), 2472 m (sample TEW-09-05-789, skarn-hosted), and 3409 m (sample DZ07-04-377.7, diorite-hosted). This delineates a zone of at least 1527 m where microthermometry confirms the presence of type 1, type 2a, and type 2b inclusions.

A ready mechanism is not apparent to account for phase separation in the EESS over a vertical range of more than 1500 m. However, type 1 assemblages were not observed between 2472 m and 3409 meters (Gibbins, 2006, and this study), suggesting that the higher elevation type 1 occurrences might not represent the same fluid system as recorded by the deeper type 1 assemblages. Perhaps the DZ07-04-377.7 assemblage was associated with early calc-silicate mineralization which Rubin (1996) demonstrated to have temperatures hotter than the 330-400 °C range established for EESS quartz fluid inclusions in this study.

Setting aside the DZ07-04-377.7 type 1 assemblage, a phase separation zone which runs from at least 1882 m to 2472 m elevation and is present in both diorite-hosted

and skarn-hosted veins. The fluid inclusion petrography indicates the presence of brine and vapor inclusions as deep as 1748 m in sample TEW09-01-1399.5 (Figure 22). Type 1 inclusions should be present below 1882 m. Therefore, co-existence of type 1, type 2a, and type 2b inclusions likely occurred from 2472 m to 1748m, an elevation range comparable to Bingham. The presence of the majority of known Cu-Au mineralization above the 2500-m elevation supports the significance of the phase separation zone.

Alternatively, the presence of type 1, type 2a, and type 2b inclusions over such a large vertical extent might be explained by varying the composition of the magmatic fluid exsolved from the magma. There is evidence that brines can exsolve directly from magmas (Cline and Bodnar, 1991, 1994). However, the presence of type 1 inclusions with chalcopyrite daughters in the EESS suggests that low salinity (~5% NaCl equiv.) fluids transporting copper were exsolved from the source magma. It follows that type 2a inclusions are the product of phase separation and originate from a fluid compositionally similar to type 1 inclusions.

25 fluid inclusion assemblages were evaluated to determine if trapping occurred in the single-phase field or the two-phase field. Trapping that occurred in the two-phase field should result in assemblages with two contrasting inclusion types – typically halite-bearing inclusions that homogenize to liquid and inclusions that homogenize to vapor. Only three assemblages consisted of well-defined co-existing fluid inclusion types (keeping in mind only halite-bearing inclusions were measured in these assemblages). These evaluations were completed using fluid inclusion photographs as the inclusions themselves had already been ablated for LA-ICP-MS. One possible explanation for the lack of two-phase field trapping is visual bias during microthermometry – assemblages with uniform fluid inclusion populations were analyzed in most cases. In the majority of cases, single crystals contain separate assemblages of vapor-dominated, halite-bearing,

and liquid. In line with Mueller et al. (2010), vapor-dominated and halite-bearing inclusion assemblages may have been present more widely.

4.3 Fluid Inclusion Relationship to CL

Petrographic studies of vein quartz CL textures were conducted to attempt to define a genetic relationship between quartz stages and fluid inclusions. Although some samples display an apparent organization of inclusion types that corresponds with CL-textures, crystal growth history, or petrographic observations (*Figure 23*), it was not possible to consistently identify these relationships in enough samples to detect a spatial pattern. The most plausible explanation for this pattern is that the majority of inclusions are trapped along fractures within quartz, which makes it difficult to determine the precise timing relationship between those inclusions and the SEM-CL patterns associated with quartz growth.

4.4 Microthermometry

Fluid inclusion assemblages were identified based on proportions of vapor bubble and liquid in the inclusion as well as the identity and volume of daughter crystals. An assemblage was deemed to exist if the homogenization temperatures of fluid inclusions measured were similar for a group of spatially associated inclusions. A total of 101 fluid inclusions representing 31 fluid inclusion assemblages from 8 samples (*Figure 24, 25*) were measured (*Figure 26*). A minimum of two inclusions were measured from each assemblage to establish the T_h and salinity ranges for each inclusion type (*Figure 27*).

JMP statistical software was used to evaluate the distribution of the data and establish the best measures of central tendency to use when representing the data in

graphic form. 29 of 31 assemblages had $\rho>0.05$ when tested for goodness of fit, indicating most assemblages have a normal distribution of data and the mean could be used as the best measure of central tendency. Summary statistics for each assemblage can be found in (Appendix F). The T_h distribution of all inclusions measured in this study of the EESS includes a total of 108 inclusions, 7 of which did not fall into assemblages.

Microthermometry data plotted as individual inclusions on a salinity vs. T_h diagram is strikingly similar to a water phase diagram (*Figure 28 and Figure 29*). The majority of data represents samples between 2400-2700m elevations, with lesser data for ~1900m and ~3600m. There does not appear to be a simple relationship between elevation and T_h, even when examining inclusions by fluid inclusion type (*Figure 30*).

Rubin (1996) studied 66 fluid inclusions trapped in monticellite, forsterite, garnet, and quartz from 10 samples from the upper part of EESS (~3550 to 3700 m elevation) and from the DOZ (2950 to 3100 m elevation). Fluid inclusions were categorized according to the number of phases observed within the fluid inclusions. Monticellite, forsterite, and garnet all contained halite-bearing inclusions. Halite-bearing inclusions in monticellite homogenized to liquid, with T_h = 489-534 °C, and salinity of 38.7-54.4 %NaCl equivalence and contained halite. Three-phase inclusions in forsterite homogenized to liquid, with T_h = 422-499 °C, and salinity of 35.5-38.0 %NaCl equivalence and contained halite. Three-phase inclusions in garnet homogenized to liquid, with T_h = 372-411 °C, and salinity of 39.4-44.5 %NaCl equivalence and contained halite. Metallic daughter minerals were not observed in any inclusions, suggesting that fluids that were responsible for skarn development were not the ore-forming fluids.

The emphasis of Rubin's study was on calc-silicate formation, and the quartz-bearing samples studied were not similar to the principal copper sulfide-bearing quartz veins that are the focus of this study. Thus, the results of the two studies are not easily

compared. Two-, three-, and four-phase inclusions were found in paragenetically early quartz. Two-phase inclusions in late quartz homogenized to liquid, with T_h =228-360 °C, and salinity of 9.2-23.0 %NaCl equivalence and contained no daughter minerals. Three-phase inclusions in early quartz homogenized to liquid, with T_h = 294-436 °C, and salinity of 34.7-39.0 %NaCl equiv and contained only halite daughter minerals. Four-phase inclusions homogenized to liquid, with T_h = 362-420 °C, and salinity of 53.7-58.5 %NaCl equivalence and contained both halite and sylvite.

In general, fluid inclusions in monticellite, forsterite, and garnet homogenized at higher temperatures and had higher salinities than inclusions in quartz. Three-phase and four-phase inclusions described by Rubin (1996) are comparable to type 2a inclusions described in this study. Two-phase inclusions which homogenized by vapor-bubble disappearance and salinities up to 23 %NaCl equivalence are most likely comparable to type 3 inclusions described in this study, as type 1 inclusions would be expected to have lower salinities and homogenize by critical behavior.

One difference in the quartz fluid inclusion data between the two studies is that Rubin (1996) reported 4-phase inclusions with higher maximum T_h and salinity than type 2a inclusions described. When inclusions were homogenized at these temperatures in during the course of this study, they could not convincingly be placed into assemblages. Maybe the high temperature four-phase inclusions described by Rubin (1996) contained daughter salts at the time of trapping and therefore do not display the consistent phase ratios expected of an assemblage.

A second difference is the report of two-phase inclusions with T_h as low as 228°C, while type 3 inclusions in this study did not have T_h below 280°C. Type 3 inclusions have been measured with salinities as low as 2.2 %NaCl equivalence, well below the 9

%NaCl equivalence reported in this study. Type 3 inclusions are the most poorly understood EESS inclusion type at present, and more work is needed to understand them.

4.5 LA-ICP-MS

4.5.1 Methods

Fluid inclusion LA-ICP-MS was carried out in February 2016 with an Agilent 7500ce ICP-MS in Dr. Robert Bodnar's lab at Virginia Polytechnic Institute and State University. The laser had been recalibrated in December 2015. Fluid inclusions that had been previously analyzed by microthermometry in the Kyle lab were ablated. Where possible, the exact fluid inclusions measured with microthermometry were used. Where this was not possible due to fluid inclusion decrepitation or location of the fluid inclusions, effort was made to ablate fluid inclusions in the same assemblage.

Fluid inclusions were ablated using small spot size to initiate quartz drilling then and switching to a large spot once a hole had begun to develop. The larger spot size was chosen to exceed the dimensions of the inclusion, such that liquid, vapor, solids, and any elements that had adsorbed onto the walls of the inclusion were ablated and measured (Heinrich et al., 1999; Heinrich et al., 2006).

For each sample, two standards were run prior to ablation of fluid inclusions and an additional two standards were run following ablation. These standards were used in the data reduction to reduce error from the equipment in accordance with the procedures described by Lee (2006). The EESS vein quartz containing the fluid inclusions was reasonable clean – mineral inclusions were occasionally ablated during fluid inclusion ablation runs, but the sharp signal produced by an inclusion is distinctly different than the longer smoother curve of an ablated fluid inclusion. Quartz generally was well behaved

during ablation with fracturing occurring in approximately 40% of samples. Note that within any assemblage there can be a very substantial difference in signal depending on the depth of inclusions and the degree to which the quartz fractured during ablation. Fluid inclusion data reduction was carried out in accordance with the methods outlined in Mutchler et al., (2008).

4.5.2 Results

Elemental results were reported in both wt% and ppm for Li, Na, Mg, K, Ca, Mn, Fe, Cu, Zn, As, Sr, Mo, Ag, Sb, Ba, Au, and Pb – the dominant cations in brines, base metal cations, pathfinder elements, and precious metals. Correlation matrices were prepared to identify elements present in each inclusion type (1, 2a, 2b, and 3) (*Appendix E*). As each ablated inclusion had elemental values that plotted below detection limits, it was necessary to choose whether to null values below detection limit or input a consistent fraction of the detection limit to indicate that non-zero amounts of those elements were likely present.

4.5.3 Elements Correlating with Cu in EESS Fluid Inclusions

The Type 1 and Type 2b inclusions show correlations of Cu content with other cations when examining the 1% and 10% of LOD tables (*Table 6, Appendix E*). Type 2a and Type 3 show very minimal correlation between Cu and other cations. There is a negative correlation between Cu in type 1 inclusions and T_h, as well as Cu in type 1 and elevation. The small number of samples successfully analyzed for type 1 and type 2b may explain why the correlations are better than with type 2a and type 3 inclusions. Cu was the focus of these correlation matrices because there were examples of visible

chalcopyrite in inclusions and it is the primary metal being mined in the EESS and therefore the most important to future exploration. Although gold is also an important metal in the EESS mining operation, concentrations were below detection limit or too close to the detection limit to arrive at meaningful conclusions.

Using a 10% limit of detection (LOD), Cu in type 1 inclusions have a moderate to strong positive correlation with Mg, Mn, Fe, Zn, Pb, and Ca. Mg and Ca are Alkaline Earths with a +2 charge (*Table 6*). Mn, Fe, and Zn are transition metals that have a 2+ or greater charge and are relatively close in ionic size to Cu. The elements Li, Na, K, As, Mo, Ag, Sb, and Au have a moderate to strong negative correlation with Cu in type 1 inclusions. Li, Na, and K are Alkali metals with a 1+ charge. Au and Ag are transition metal in the same family as Cu. Ag has a 1+ charge and Au is either 1+ or 3+. As and Sb are metalloids that are commonly associated with Au and Ag in minerals exploration for low temperature deposits. Cu has a positive correlation with 2+ cations and a negative correlation with 1+ cations in type 1 fluids. In type 2b fluids, Cu positively correlates with Mo, Fe, and Na, as also confirmed by the microthermometry-based %NaCl.

Two samples had Cu-bearing type 3 fluids: TE01-16-730.4 had one type 3 fluid inclusion with Cu and sample TEW09-05-789 had 14 type 3 fluid inclusions with Cu spread across 7 assemblages. All elements measured had low correlations for type 3 fluids. Elemental concentration diagrams were used to identify elemental groupings for type 2a inclusions (*Figures 31, 32*). Two elemental signatures can be identified in the data. The Cu-rich signature (*Figure 31*) has high levels of Cu (0.11 – 0.71 wt%) and Li (0.38-1.95 wt %, intermediate levels of Na (6.03-9.41 wt%) and Fe (0.17-1.21 wt%), and low levels of Ca (0.31-0.41 wt%), Mn (0.09-0.12 wt %), Pb (<0.01), Zn (<0.01), and K (0.25-1.16 wt%). The Fe-rich signature (*Figure 31*) has high levels of Fe (1.06-11.84 wt%), Ca (0.82-8.37), K (0.006-6.71), Mn (<0.01-0.93), Zn (<0.006-0.42), and Pb

(<0.01-0.09), with low levels of Cu (<0.01-0.06) and Li (<0.01). Note that the lithium content in these samples appears to be very high, which may be attributed to measurement error.

Comparing the elemental concentration diagrams, it appears that higher Cu-content is associated with lower Fe, Ca, K, Mn, Zn and Pb. The inverse is also true, lower Cu-content is associated with higher Fe, Ca, K, and Mn, Zn, and Pb. Na has a moderately inverse relationship to Cu, but not as much as other elements. The reason for this variation is unclear, but could be attributed to partitioning of elements between magma and exsolved water in the source batholith and exchange of cations with wall rock during mineralization. However, phase separation is another possible mechanism to explanation the trend recorded in these fluid chemistries. In phase separation, a parent fluid should have Fe, Ca, K, Mn, Zn, Pb, and Cu contents trend towards a type 2a fluid during phase separation as a low salinity (type 2b) fluid is removed. The cation concentrations trend towards the composition of a type 2a fluid until Cu precipitates out.

Perhaps, the large variation in Cu content, but relatively stable Na content supports the precipitation of Cu-minerals during phase separation. The fluids depleted in Cu (enriched in Fe, Ca, K, Mn, Zn, Pb, Na) may have already precipitated Cu-sulfides. If that depletion in Cu occurs in tandem with phase separation, Fe, Ca, K, Mn, Zn, Pb, and Na concentration will go up in the residual fluid as a vapor phase is removed.

Should the higher density fluid not reach halite saturation, you may end up with a fluid that has salinity resembling a type 3 fluid. In some cases, this fluid may continue to undergo phase separation and concentrate the residual cations until it reaches Halite saturation and the saturation points of other minerals such as sylvite or Fe-oxides. However, this may result in a salinity gradient or fluid stratification (by salinity) during mineralization. The result would be high salinity brines residing at or below the phase

separation zone and lower salinity fluids depleted in Cu residing higher in the phase separation zone.

4.6 Cu Content of Fluid Inclusions

Seven assemblages (19 inclusions) measured with microthermometry had detectable Cu in every fluid inclusion analyzed, even if opaque daughter minerals were not observed. The presence of Cu in all inclusions within an assemblage is strong evidence that the Cu measured was from the inclusion intended and not an ablated mineral inclusion in quartz or a nearby inclusion unintentionally ablated. These assemblages homogenized from 319-390 °C and had well constrained salinities for each fluid inclusion type (*Table 7*). All three inclusion types have maximum T_h 380-390 °C. These conditions provide refined constraints on the conditions of the EESS magmatic-hydrothermal system during Cu-deposition, within the broader temperature and salinity conditions defined by measurements from all fluid inclusions assemblages.

29 inclusions in total had measurable Cu. Cu-content does not show a strongly increasing or decreasing trend by elevation for any fluid inclusion type (Figure 33). More samples are needed to accurately depict Cu-content spatial variability as the deepest Cu-bearing inclusion was at 2413 m. Despite the limited sample set, the lack of a strong spatial trend for Cu-content may support a system in which the phase-separation zone has moved throughout the duration of Cu mineralization, with mineralization occurring above the phase separation zone.

4.7 RAMAN

Because of the presence of carbonate wall rocks affected by the EESS mineralizing system, the presence of CO_2 was suspected in EESS fluid inclusions.

Reconnaissance Raman spectrometry was performed at Virginia Polytechnic and State University to get a qualitative understanding of the amount of CO_2 trapped in fluid inclusions in EESS fluids. The data gathered are not intended to explore the source of the CO_2 or the percentage of CO_2 present in inclusions. This data was pursued to test the hypothesis that unaccounted for CO_2 is a source of error in this study that may contribute to misinterpretations of the data presented.

4.7.1 Methods

Three fluid inclusions from sample TEW-09-05-789 were examined. Inclusions were measured with a JY Horiba LabRam HR800, and/or electronically cooled CCD detector system using 600 gr/mm grating, Modu-Laser Stellar Pro-L 514nm/100mW laser set at 50 mW source/9 mW at sample, Labspec 5 software, Olympus 100X objective MSPlan NA 0.95 coupled to an Olympus BX-41 microscope.

One inclusion was measured from an assemblage of nearly opaque vapor-rich inclusions (*Figure 34a*). The laser was pointed at the vapor bubble for this fluid inclusion. The meniscus between liquid and vapor was at the edge of the inclusion and liquid could not be properly targeted. Two inclusions were measured from an assemblage of what appeared to be Type 3 or Type 1 inclusions (*Figures 35a, 36a*). Separate RAMAN measurements were made for both the liquid and vapor portions of the fluid inclusion to compare the compositions of the liquid and vapor. In both cases, the assemblages from which the inclusions were chosen are in the single phase field – only that single inclusion type is present in the fluid inclusion trail.

4.7.2 Results

All three inclusions had detectable amounts of CO_2 present in the vapor bubble. The measurements made with Raman do not allow quantification of the results, but enough CO_2 was present that it should be addressed in future research on EESS fluids (Figures 34b, 35b, 36b).

4.7.3 Fluid Composition

The Type 3 inclusion homogenized to liquid and did not display critical behavior. Both assemblages measured contained fluid inclusions that appear darker in transmitted light than type 2a and Type 1 inclusions. It is reasonable to believe that the inclusions measured represent a trapped magmatic fluid that would plot on the liquid side of the critical curve in P-T space. The fact that these inclusions were trapped in the single phase field supports the assumption that these fluid have not undergone phase separation.

When reviewing the Cu concentrations of type 2a inclusions, it is important to note that several contain significant Cu, ranging from 104 to 47,325 ppm. Inclusions FI125 and FI126 both have smaller vapor bubbles than most fluid inclusions that homogenize to vapor. These inclusions are likely to be representative of the primary magmatic fluid that predates Cu deposition. In this case, the fluid is vapor as opposed to critical density or liquid at the time of trapping. Inclusions 138 and 139 were noted to have odd freezing behavior and these inclusions are darker than most and not as vapor-rich as typical vapor inclusions. These factors are consistent with other vapor-rich assemblages that shared characteristics with critical density inclusions. As is the case with inclusions 25 and 26, inclusions 138 and 139 likely record a primary magmatic fluid that has not yet deposited its copper during phase separation. In this case, that fluid is simply present as a vapor instead of a critical density fluid or a liquid (Bodnar and Cline,

1991, 1994). The majority of vapor inclusions measured with LA-ICP-MS, particularly those with large vapor bubbles did not provide enough signal to provide viable data.

The origin of the CO_2 present in EESS samples is unknown. Decarbonation reactions associated with skarn formation would source CO_2 which could be trapped in vein quartz. The parent magmatic fluid may simply have been enriched in CO_2 as has been documented at Butte, but negligible carbonate alteration has been observed in the Ertsberg pluton rocks (Rusk, 2004; Rusk, 2008). The presence of CO_2 in fluid inclusions is cause for additional evaluation of EESS fluid compositions. Fluid inclusion microthermometry and the subsequent commentary was carried out on the assumption that EESS quartz contained fluid inclusions containing fluids trapped in the H_2O-NaCl field, not the H_2O-CO_2-NaCl field.

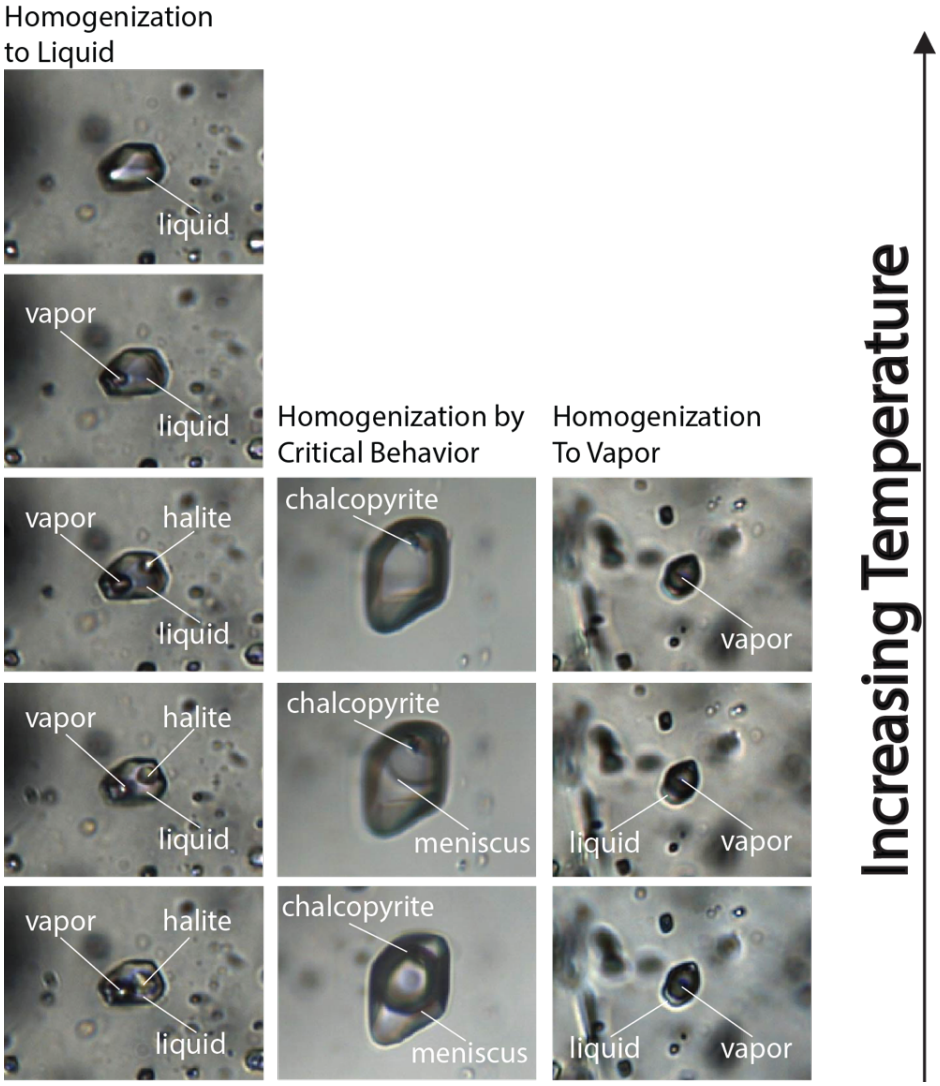

Figure 20: Homogenization behavior of EESS fluid inclusions.

Inclusions began at ambient conditions and were heated until fluid phases (and halite where present) homogenized to a single fluid. The different homogenization behaviors are displayed. In the halite bearing inclusion (left) halite disappears before the vapor bubble and the inclusion homogenizes to the liquid phase. In the vapor dominated inclusion (right) the vapor bubble expands until all liquid has homogenized to vapor. The critical behavior inclusion does not homogenize by vapor bubble disappearance or expansion, instead the meniscus of the vapor bubble fades until the fluid inclusions is a single phase. Note that some daughter minerals do not homogenize upon heating, such as the chalcopyrite in the center column.

Table 5: Characteristics of fluid inclusion types

Type	Salinity Range (% NaCl equiv.)	Homogenization behavior	Th Vapor (◦C)	Vapor Bubble (vol. %)	Daughter Minerals
1	2.2-6.0	critical behavior	332-396	40-70	No halite, chalcopyrite is common, but many type 1 inclusions lack daughters
2a	27.7-51.2	homogenized to liquid	280-420	10-30	Halite, commonly chalcopyrite, and may also contain sylvite, magnetite, anhydrite, hematite, and sphalerite
2b	1.2-11.7	homogenizes to vapor	340-392	65-90	Typically no daughter minerals observed, although two measured inclusions contain
3	2.4-23.0	homogenized to liquid	283-403	15-50	Rare opaque daughter minerals

Comparison of fluid inclusion types by their characteristics measured using fluid inclusions microthermomtry and described with thin section petrography. Fluid inclusion type 1 is low salinity with a moderate vapor bubble, homogenizes by critical behavior at 332-396 °C and may contain chalcopyrite. Fluid inclusion type 2a is high salinity with a small vapor bubble, homogenizes to liquid at 280-420 °C and contains halite ± other daughter minerals. Fluid inclusion type 2b is low salinity with a large vapor bubble, homogenizes to liquid at 340-392 °C and typically does not contain daughter minerals. Fluid inclusion type 3 is low to moderate salinity with a small vapor bubble, homogenizes to liquid at 283-403 °C and rarely contains opaque minerals.

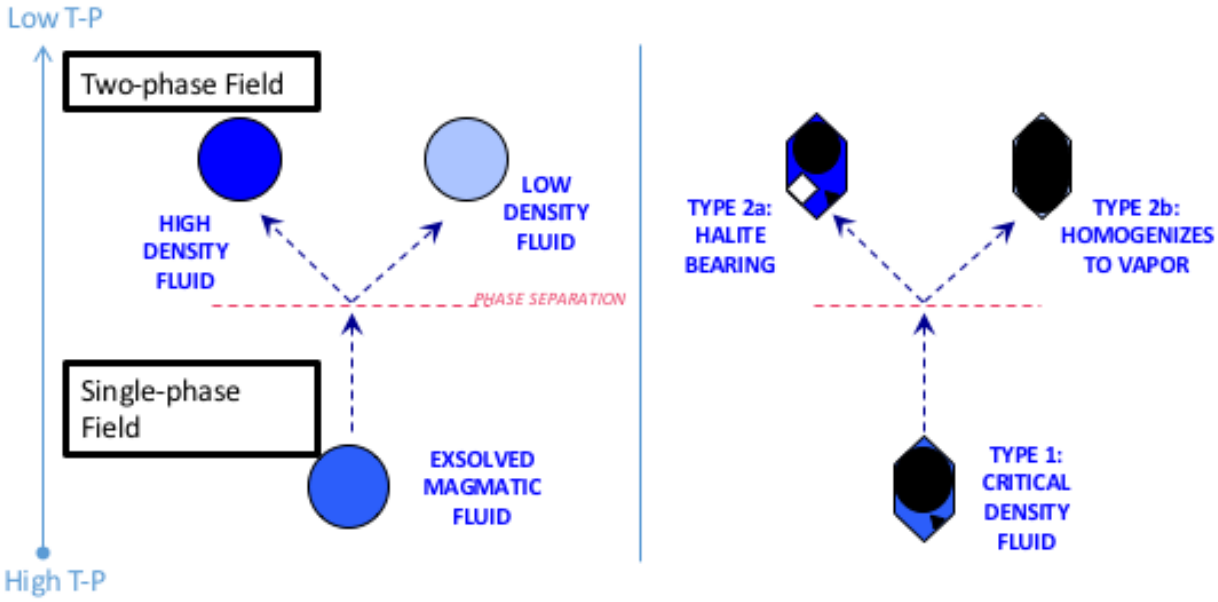

Figure 21: Conceptual diagram of phase separation in EESS and resulting fluid inclusions at ambient conditions.

A single phase fluid exsolved from magma moves to lower pressure and temperature conditions, where it phase separates into a low density fluid and a high density fluid (left). Fluids trapped in quartz crystals separate in vapor and liquid phases at ambient conditions and may precipitate daughter minerals. Aliquots of magmatic-hydrothermal fluid are represented with colored circles (left). Corresponding fluid inclusions at ambient conditions are depicted as polygons (right). Darker blues are higher salinity. Black ovals are vapor bubbles. Black triangles are the opaque mineral chalcopyrite. The white box is a halite daughter crystal. Refer to *Table 5* for descriptions of the fluid inclusion types.

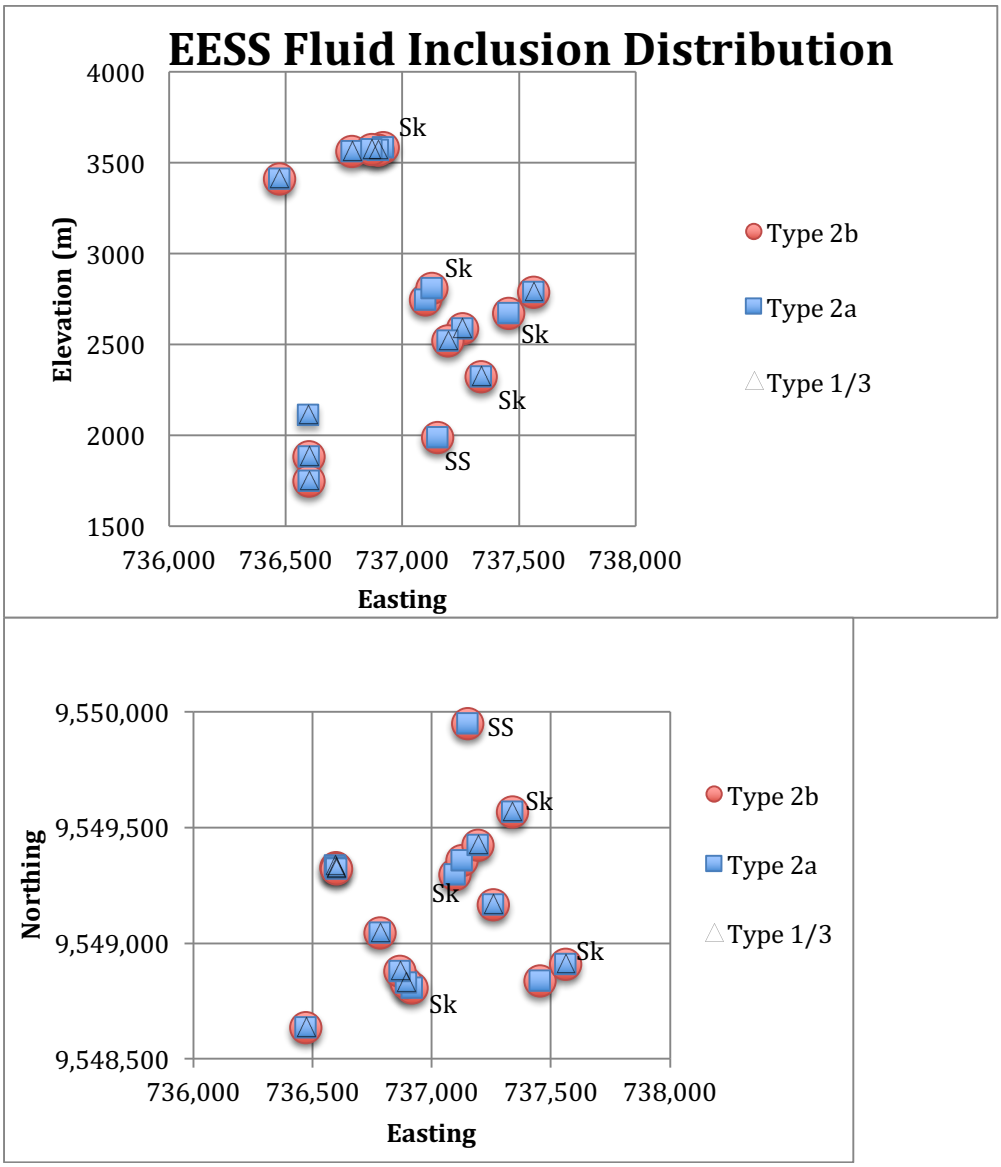

Figure 22: Distribution of fluid inclusion types in EESS.

Three fluid inclusion types were identified with petrography performed on 15 vein quartz samples. Assemblages of vapor-dominated inclusions (Type 2b), assemblages of halite-bearing fluid inclusions (Type 2a), and assemblages of opaque bearing fluid inclusions that lack halite (Type 1/3) were present. Elevation vs. Easting (top) and Northing vs. Easting (bottom) plots display the vertical and lateral zonation of fluid inclusion types. Fluid Inclusions are diorite hosted unless indicated with an "SS" for sandstone protolith or an "Sk" for skarn. All three fluid inclusion types are distributed throughout the system vertically and laterally. No apparent zonation of fluid inclusion types was identified petrographically. Microthermometry was necessary to distinguish Type 1 from Type 3.

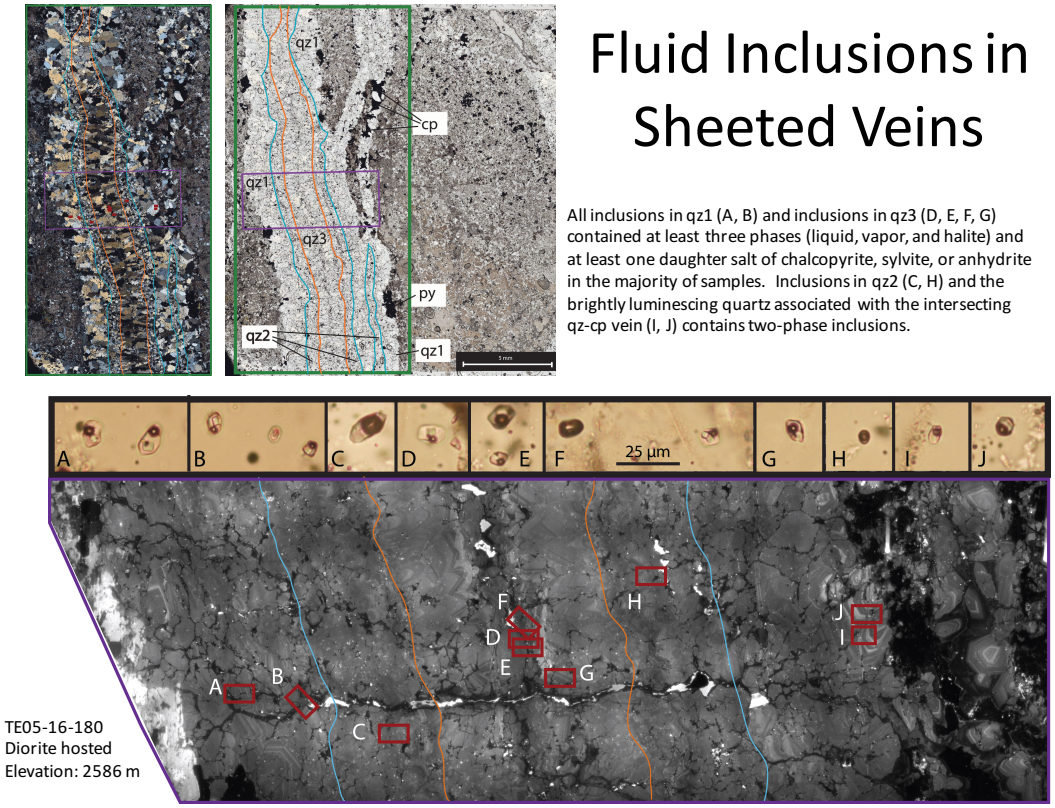

Figure 23: Fluid Inclusions variation by CL texture.

It was possible to identify a relationship between fluid inclusion type and the texture of host quartz under XPL and with SEM-CL. However, this relationship could not consistently be identified in other samples.

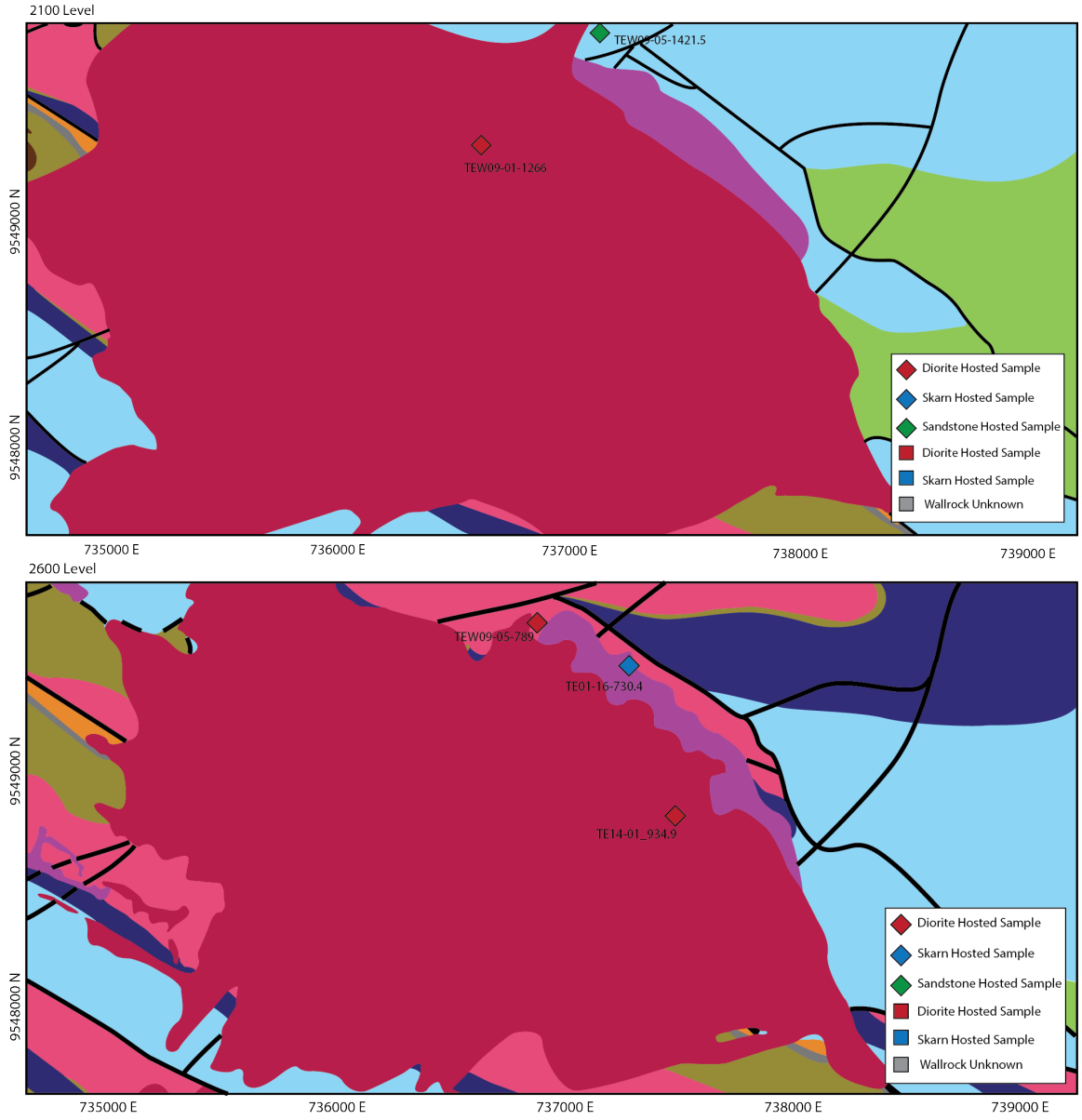
2100 Level
TEW09-05-1421.5
TEW09-01-1266
9549000 N
9548000 N
735000 E
736000 E
737000 E
738000 E
739000 E
Diorite Hosted Sample
Skarn Hosted Sample
Sandstone Hosted Sample
Diorite Hosted Sample
Skarn Hosted Sample
Wallrock Unknown
2600 Level
TEW09-05-789
TE01-16-730.4
TE14-01_934.9
9549000 N
9548000 N
735000 E
736000 E
737000 E
738000 E
739000 E
Diorite Hosted Sample
Skarn Hosted Sample
Sandstone Hosted Sample
Diorite Hosted Sample
Skarn Hosted Sample
Wallrock Unknown

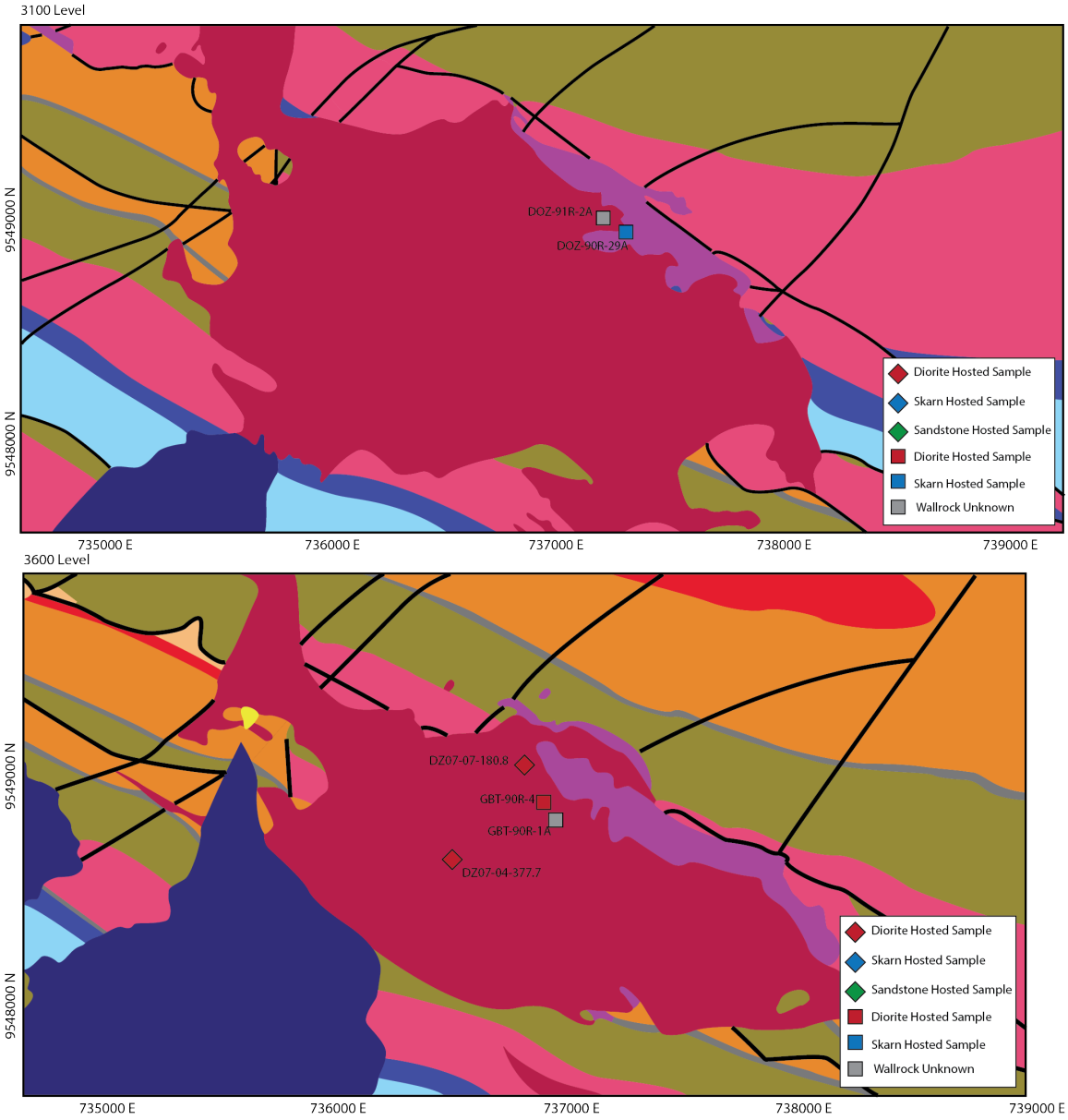

Figure 24: EESS geologic maps with location of FI samples plotted on the closest elevation of the 2100, 2600, 3100, and 3600m levels.

Modified from the COW-A Block Model provided by PTFI. For unit information, see Fig. 2.

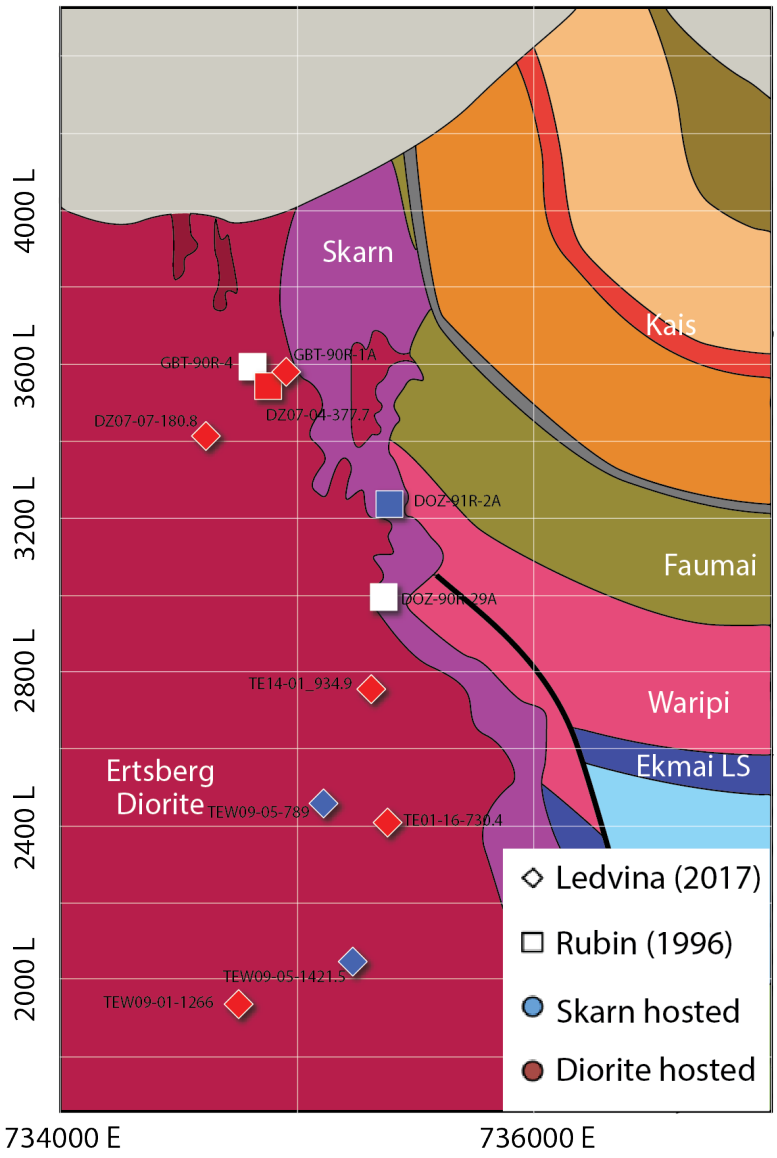

Figure 25: Cross-section view of EESS with location of FI samples plotted.

See Appendix A for exact sample locations. Note that sample are projected onto a 2-D plane, which results in some sample lithologies not matching the lithologies on the map. Modified from Leys et al. (2012).

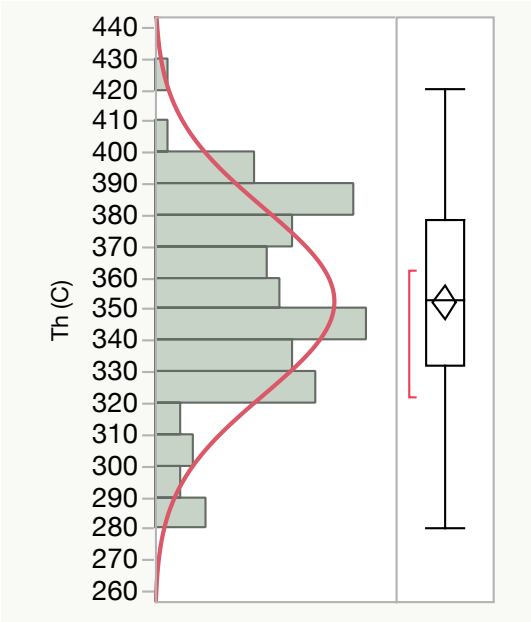

Figure 26: Statistical distribution of all fluid inclusions by T_h

n=107 (101 inclusions in 31 assemblages; 6 additional inclusions that did not form assemblages); mean= 352.3; std dev = 29.8; red bracket is shortest half (densest data). Data is normally distributed ρ=0.0568. All fluid inclusions were part of assemblages.

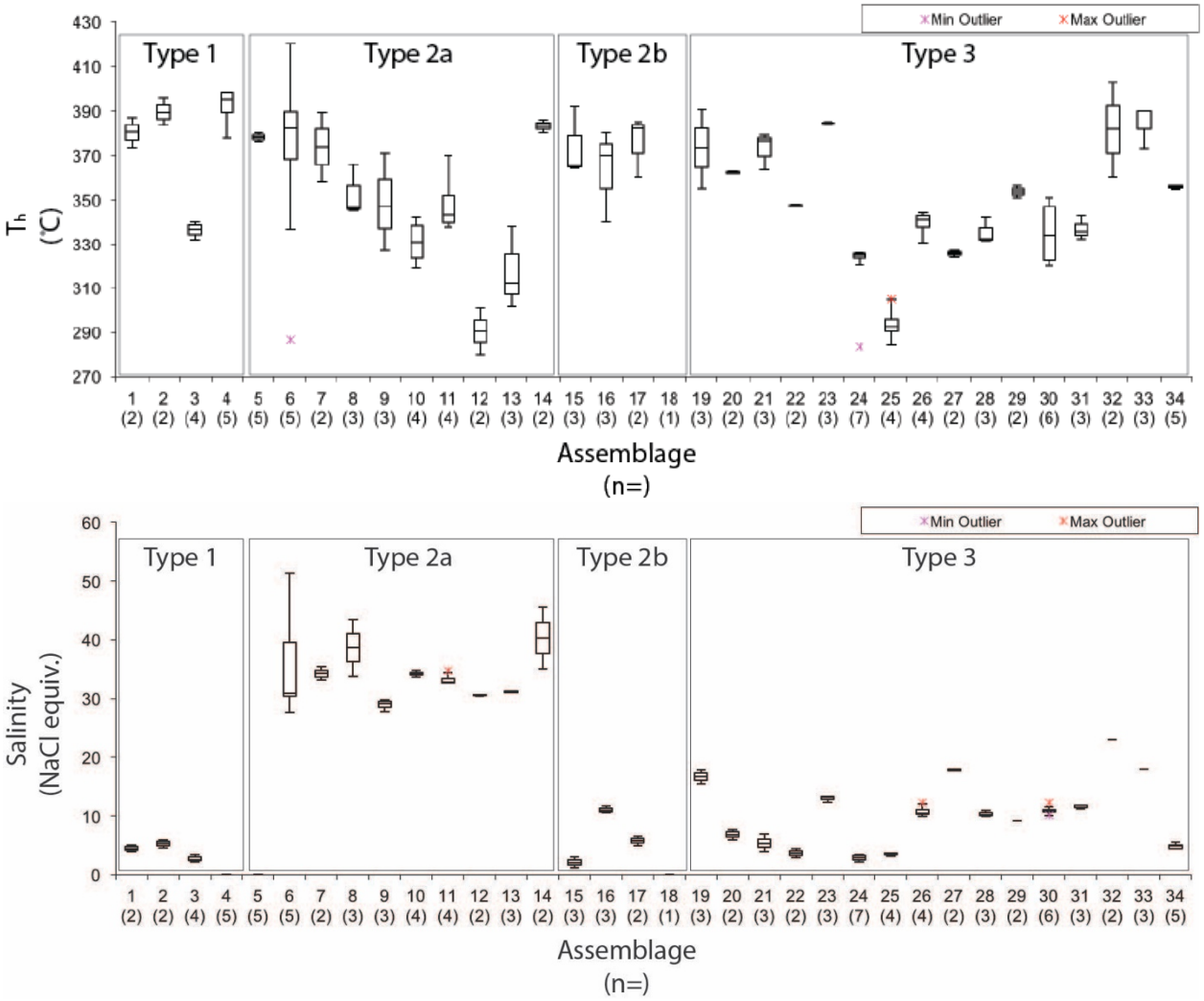

Figure 27: Box and whisker plot of homogenization temperature and salinities for fluid inclusion assemblages.

101 fluid inclusions were measured in 31 assemblages. Note that not inclusions which did not fall into assemblages were omitted from this study. The number of inclusions in each assemblage is indicated in parenthesis below the assemblage number. An assemblage size of 1 indicates that only a single inclusion was measured, but adjacent inclusions were deemed to have sufficiently similar daughter salts, vapor ratios, temperatures of homogenization, and ice melt temperatures. Type 1 and Type 2b inclusions have larger vapor bubbles and are more difficult to measure accurately so there are fewer assemblages in the data. See column "Assemblages" in Appendix C to relate each assemblage with sample and microthermometry data.

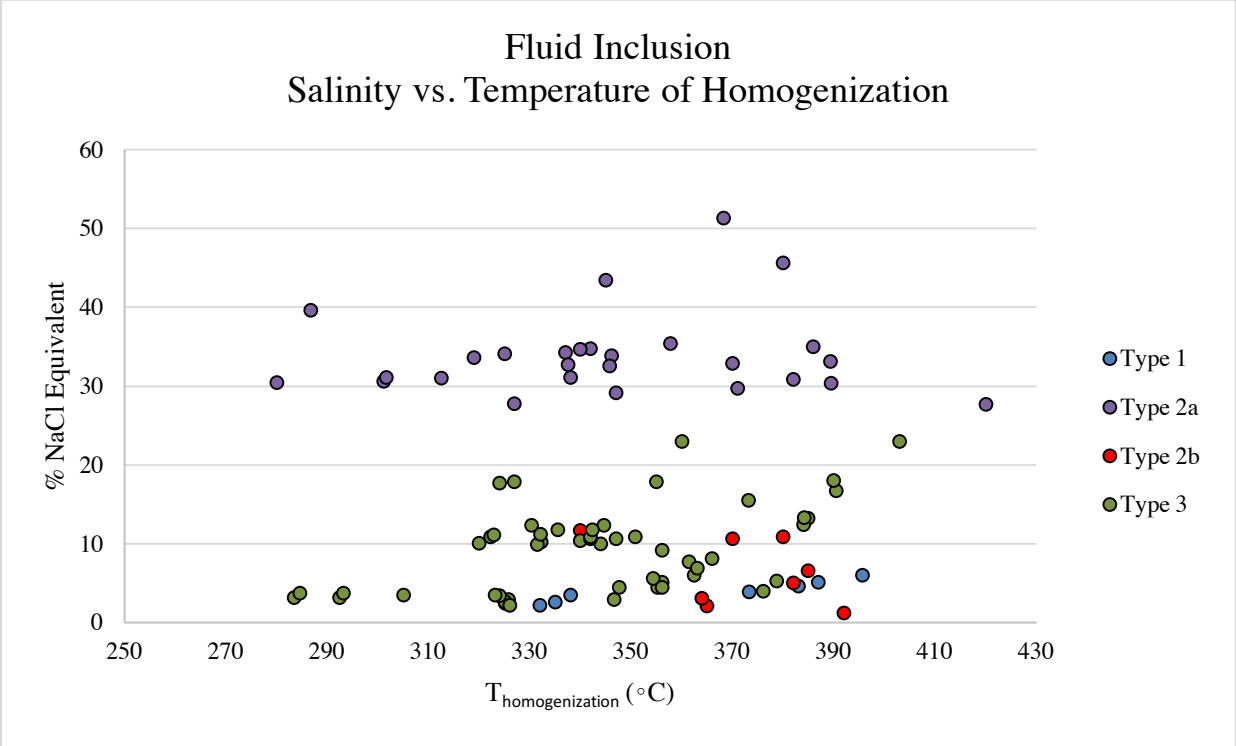

Figure 28: Fluid inclusion salinity vs. temperature of homogenization.

Plot of 107 fluid inclusions measured with microthermometry. Each point represents a single inclusion. Temperature of homogenization is directly measured for each inclusion. Salinity is expressed as %NaCl equivalence which is calculated from the temperature of last ice melt for type 1, type 2b, and type 3 inclusions. Salinity is calculated from the temperature of homogenization of halite using the SALTY program for type 2a inclusions. Inclusions are color coded by homogenization behavior to illustrate the high data quality in this study. Inclusions which homogenized by critical behavior plot with a linear positive slope that approximates the critical curve. Inclusions which homogenize to vapor plot below the critical curve.

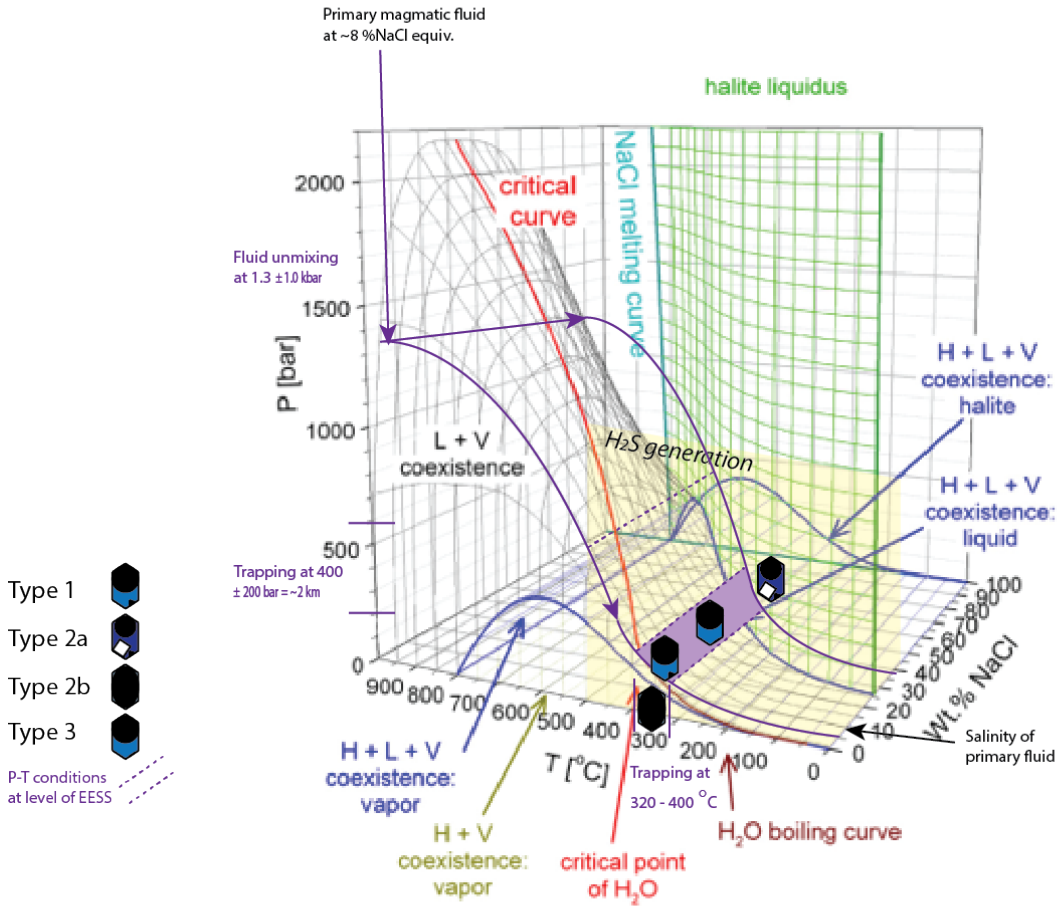

Figure 29: Fluid phase diagram

A primary magmatic fluid ~ 8 %NaCl migrates upward in the EESS. Transport of Cu cations in the primary fluid is facilitated by chlorine complexing. Unmixing of the primary fluid occurs at approximately 1kbar (Cline, 1995) and Cu is concentrated in the higher density fluid phase with Cl anions. The low density and high density fluids evolve as they migrate upwards in the EESS (decreasing P and T) and are trapped in cracked quartz at approximately 2 km depth (200 bar). Below 500 C, SO2 gas reacts with H2O to produce H2S and H2S04. H2S reacts with Cu and Fe in solution to form CuFe-sulfides: chalcopyrite and bornite. Where Cl-mediated transport of Cu cations is superimposed with H2S, Cu-sulfide ore forms.

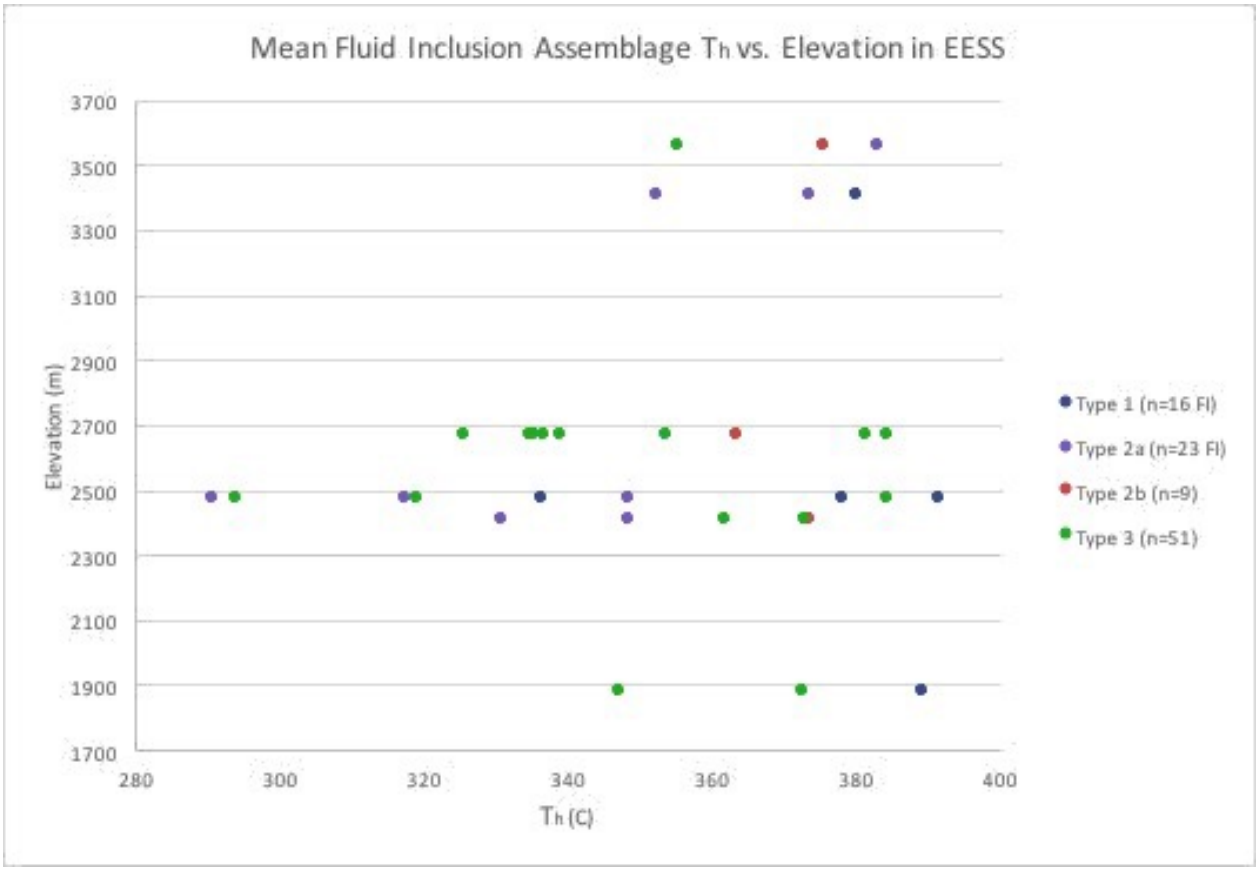

Figure 30: Elevation vs. T_h comparisons by fluid inclusion type.

Fluid inclusion assemblages were plotted by average T_h to evaluate temperature trends in EESS fluids. Individual plots of each inclusion type (top) and a composite plot of with all inclusion types (bottom) illustrate T_h variation by depth. Type 1, Type 2b, and Type 3 inclusions show little variation. Type 1 and type 2b inclusions tend to be have higher T_h than Type 2a and much higher than type 3. Type 2a inclusions show a trend of having a higher T_h at higher elevations. The deeper type 2a fluids may have been trapped at higher pressures, which would allow the quartz precipitation necessary for trapping to occur at a lower temperature than at a higher elevation (lower pressure) setting.

Table 6: Element correlation coefficients for fluid inclusion types

1% LOD						
Type	Strong Positive (>0.8)	Moderate Positive (0.5 - 0.8)	Low Positive (0.2 - 0.5)	Low Negative (-0.2 - -0.5	Moderate Negative (-0.5 - -0.8)	Very Negative (<-0.8)
1	Mg, Ca, Mn, Fe, Zn, Sr, Pb			K, Ag, Ba	Na, As, Mo, Sb, Au	Li
2a			Li, Na	Ca, Mn, Fe, Sr, Pb		
2b	Mo	wt% NaCl, Na, Fe, As	Li, Mg, K, Ag, Au	Ca, Sr, Sb	Zn	
3						
10% LOD						
Type	Strong Positive (>0.8)	Moderate Positive (0.5 - 0.8)	Low Positive (0.2 - 0.5)	Low Negative (-0.2 - -0.5	Moderate Negative (-0.5 - -0.8)	Very Negative (<-0.8)
1	Mg, Mn, Fe, Zn, Pb	Ca		Sr	Li, Na, K, As, Mo, Ag, Sb	Au
2a			Li, Na, Mg, Au	Mn, Fe, Sr, Pb		
2b	Mo	wt% NaCl, Na, Fe, As	Li, Mg, K, Ag, Au	Ca, Sr	Zn	
3				K, Ba		
Ignoring detection limit: Null values for below LOD						
Type	Strong Positive (>0.8)	Moderate Positive (0.5 - 0.8)	Low Positive (0.2 - 0.5)	Low Negative (-0.2 - -0.5	Moderate Negative (-0.5 - -0.8)	Very Negative (<-0.8)
1						
2a	Mo	Zn, As, Ag	Na	Ca, Fe, Zn, Ba		
2b	Mo	wt% NaCl, Na, Fe, As			Zn	
3	As, Sb			Li, K, Ca, Mn, Fe, Zn, Pb	Ba	

Three correlation coefficient plots are shows. A 1% limit of detection (LOD) and a 10% limit of detection (LOD) were used to compare the effect on correlation coefficients if elements are very low concentration (1%) or of moderate concentration (10%). Increasing to 50% LOD or another large percentage results in anomalously high correlation coefficients for elements below LOD. The null case in which we ignore elements below LOD was included for statistical thoroughness. The correlation matrices on which this table is based are presented in Appendix E.

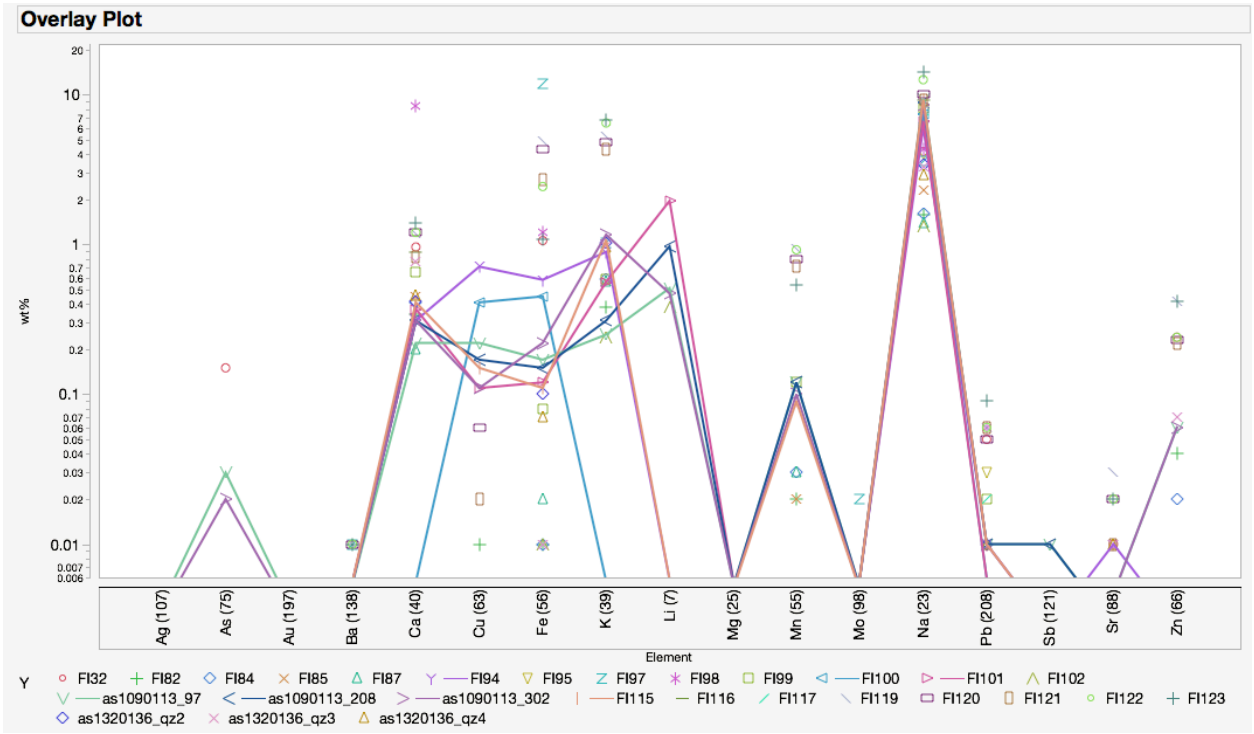

Figure 31: Type 3 signature for high Cu inclusions:

Seven inclusions distributed across four assemblages display Cu content greater than 0.1 wt%. These inclusions contained fluids with Fe content between 0.17 and 1.21wt%, Mn 0.09-0.12 wt%, Na 6.03-9.41 wt%, K 0.25-1.16 wt%, and Ca 0.31-0.41wt%

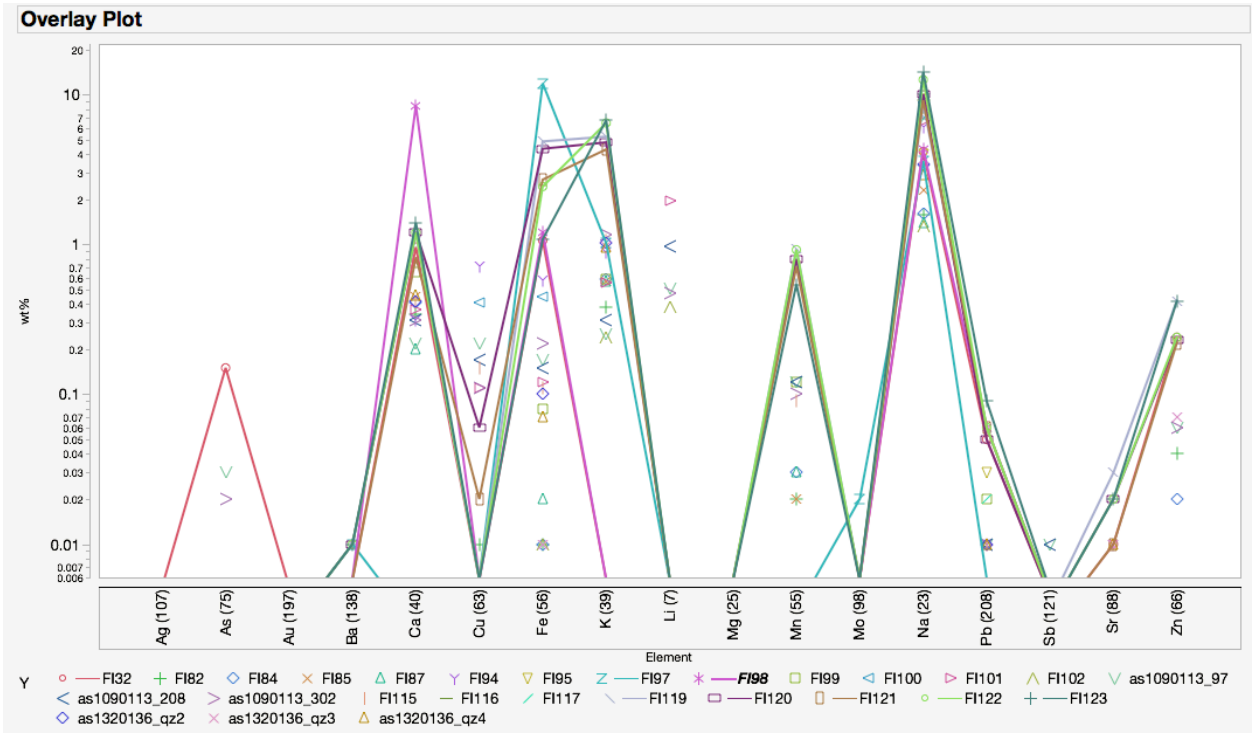

Figure 32: Type 3 signature for inclusions with high Fe content.

Type 3 inclusions have high Fe content and also have high the highest Na, K, and Ca, and Mn as well as the base metal cations Zn and Pb. Notably, these inclusions also have no lithium, in contrast to lithium values of approximately 1wt% in several Cu-rich type 3 inclusions.

Table 7: Cu-bearing fluid inclusion assemblages from microthermometry

Type	Assemblage	Number of Inclusions	Th (◦C)	% NaCl equiv.
1	1, 3	6	332-387	2.2-5.1
2a	7, 10	5	319-390	33.1-35.4
2b	16	2	370-380	10.6-10.9
3	23, 28	6	331-385	9.9-13.3

Constraints on the Cu-bearing fluid inclusion assemblages measured with microthermometry. Two assemblages consisting of at least two inclusions each were measured from type 1, 2a, and 3. Only one assemblage was measured for type 2b because type 2b inclusions are notoriously difficult to measure accurately and typically not dealt with. This data provides a greater constraint on the temperatures and salinities associated with Cu-bearing fluids, removing some of the noise in the data that is an inherent challenge in such a complex ore system.

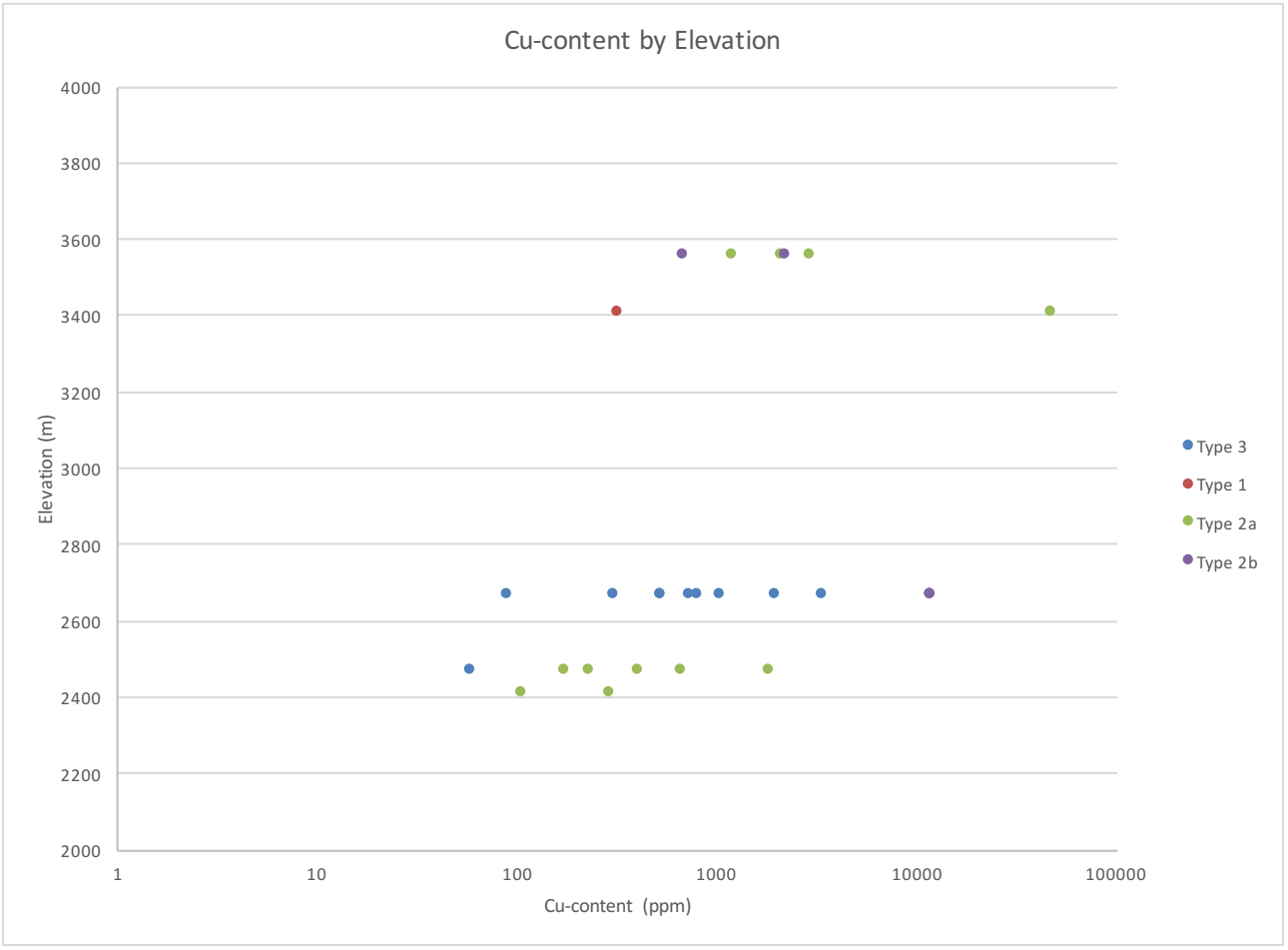

Figure 33: Fluid inclusion Cu-content variation by elevation.

29 inclusions in total had measurable Cu and at least one inclusion of each type had measurable Cu. Cu-content does not show a strongly increasing or decreasing trend by elevation. More samples are needed to accurately depict Cu-content variation by type and space. Many opaque minerals in inclusions were Fe-oxides, and many inclusions without visible daughter crystals had measurable Cu content. The lack of a strong spatial trend for Cu-content may support a mineralization model in which the phase-separation zone moved during the mineralization system evolution.

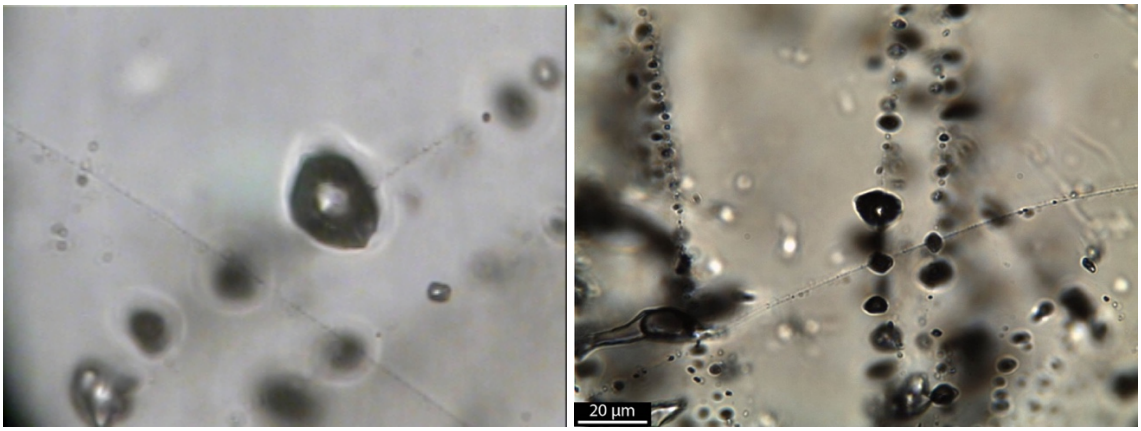

Figure 34a: Images of CO_2-bearing type 2b fluid inclusion assemblage

LEFT: Type 2b inclusion 143. **RIGHT**: Assemblage of type 2b inclusion including inclusion 143.

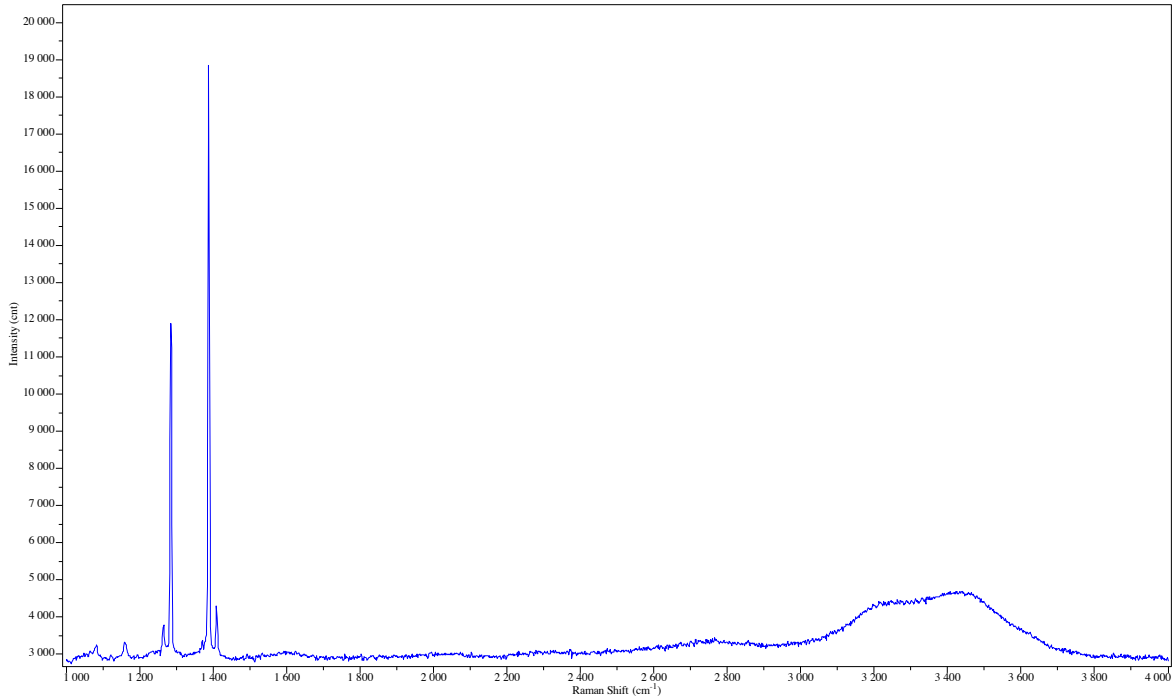

Figure 34b: RAMAN spectrum for CO_2-bearing type 2b fluid inclusion assemblage

Sample TEW09-05-789 inclusion 143 RAMAN signal from vapor bubble. CO2 peaks at 1280 and 1390cm^{-1} are larger than the broad H_2O peak from 3200-3700 cm^{-1} indicating that CO2 is present in the sample in significant enough quantities that it must be accounted for when considering fluid geochemistry.

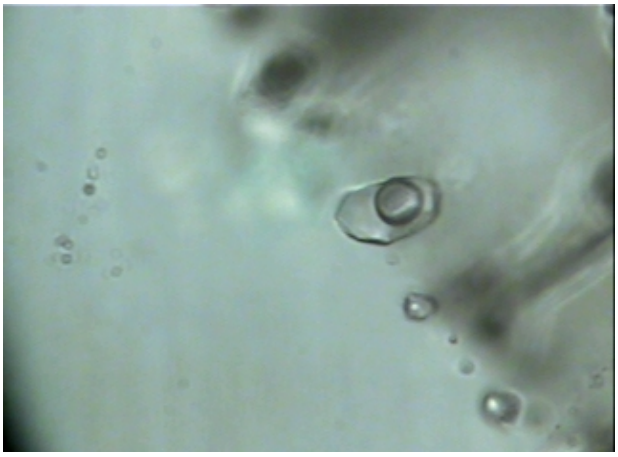

Figure 35a: **CO_2-bearing Type 1 fluid inclusion #1.**

Sample TEW09-05-789 inclusion 144, Type 3 inclusion.

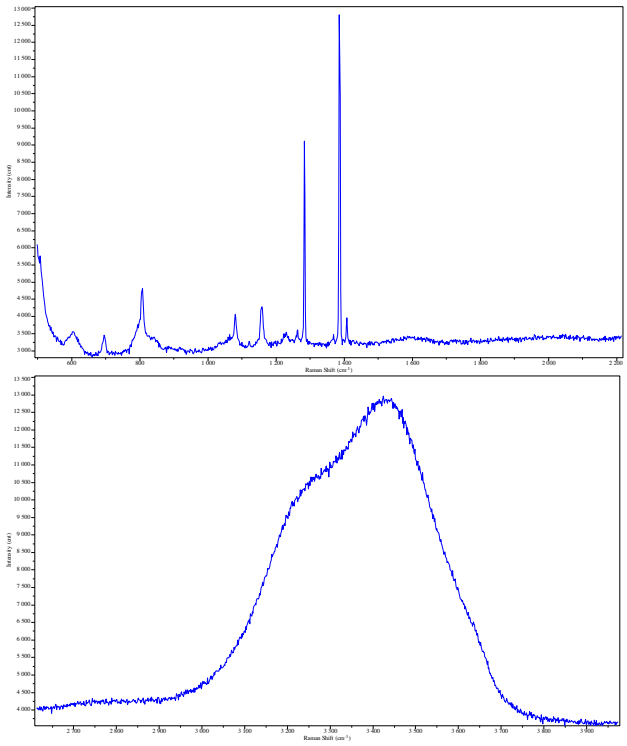

Figure 35b: RAMAN Spectrum for CO_2-bearing Type 1 fluid inclusion #1

Sample TEW09-05-789 inclusion 144 RAMAN. Top: signal from vapor bubble and Bottom: signal from liquid. CO_2 peaks are present at 1275 and 1380cm^{-1} are larger than the broad H_2O peak from 3200-3700 cm^{-1} indicating that CO_2 is present in the sample in significant enough quantities that it must be accounted for when considering fluid geochemistry.

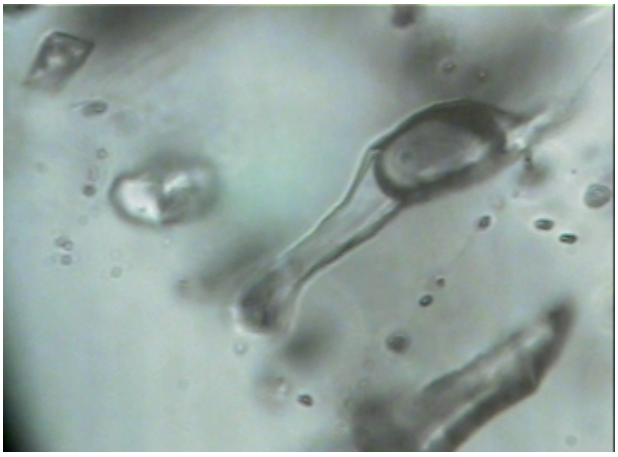

Figure 36a: **CO_2-bearing Type 1 fluid inclusion #2**

Sample TEW09-05-789 inclusion 145, Type 3 inclusion in same assemblage as inclusion 144. Inclusion in same assemblage as figure 36a.

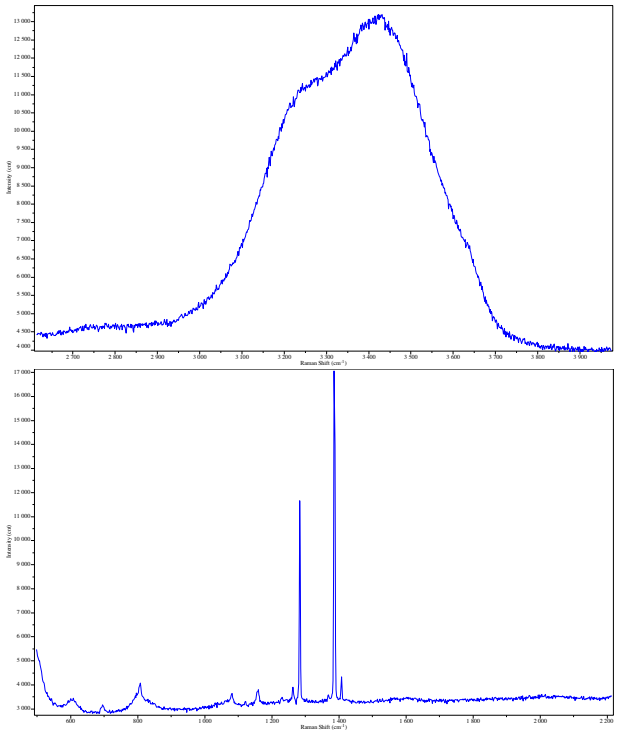

Figure 36b: RAMAN Spectrum of CO_2-bearing Type 1 fluid inclusion #2

Sample TEW09-05-789 inclusion 145 RAMAN signal from vapor bubble. CO_2 peaks at 1280 and 1390cm^{-1} are larger than the broad H_2O peak from 3200-3700 cm^{-1} indicating that CO_2 is present in the sample in significant enough quantities that it must be accounted for when considering fluid geochemistry.

Chapter 5: Conclusion

5.1 Introduction

Major conclusions of this project:

1. Porphyry- and skarn-hosted ore-stage veins in the EESS are analogous to veins in Cu-Au-porphyry systems.
2. There is evidence for many episodes of fracturing and mineralization at all scales.
3. A limit for type 1 fluid inclusions associated with EESS mineralization is defined at ~2500 m.

5.2 Analogue to porphyry veins

5.2.1 A-Veins in Brittle Host Lithologies

Ore-stage veins have a mineralogy that resembles classic porphyry A-veins and a geometry similar to B-veins that are believed to occur in cooler, more brittle host lithology suggests two things. First, the diorite (and skarn) were brittle enough for planar extension fractures to maintain their shape. A-veins commonly are described as curvi-linear and warped, which is attributable to the pluton being warm and somewhat ductile during mineralization. Secondly, the source of the fluids is below the EESS and fluids do not appear to be locally sourced from the Ertsberg Diorite that is being mineralized. Instead, the Ertsberg Diorite and adjacent skarn simply serve as hosts to mineralization. Although there are clear differences in chemistry and rheology of the diorite and skarn, they both host significant volumes of vein-hosted Cu-mineralization, thus suggesting that composition of the host lithology is not the primary control on the distribution of EESS Cu-mineralization. The most important factor determining if a host lithology will contain ore-stage veins is the rock's ability to fracture and maintain open spaces. This may

explain the empirical observation that vein size and density decreases from brittle skarn towards marble, where EESS ore-stage quartz veins are not observed.

5.2.2 CL evidence for similar vein quartz textures across host lithologies

Although veins hosted in skarn and quartzite are mineralogically different from diorite-hosted veins, comparison of SEM-CL images of vein quartz from skarn-hosted, quartzite-hosted and diorite-hosted samples reveal only minor textural differences. The primary distinction between skarn-, quartzite-, and diorite- hosted samples is that samples hosted in a sedimentary protolith contained micro-breccias. The majority of textures observed in diorite-hosted quartz veins were also seen in skarn-hosted samples, and the transition of Euhedral Banded Quartz followed by Sulfide-Associated Dark CL followed by CL-black micro-fractures held true in samples regardless of protolith. The lack of differentiation of SEM-CL veining styles by host lithology is further evidence that lithology is not the most important control on vein characteristics.

5.3 IMPLICATIONS OF FRACTURING

5.3.1Microscopic

Changes in temperature, pressure and composition during EESS mineralization are recorded in fluid inclusions in vein quartz. However, the inclusions analyzed are almost all secondary inclusions trapped along fractures, so these inclusions are records of fluid conditions at approximately the time of a fracturing event and subsequent healing of the fracture in quartz. However the use of fluid inclusions assemblages, combined with textural relationships that indicate Cu-bearing sulfides occur along these late fractures in pre-existing quartz, yields information relative to the Cu-Au mineralization. Although the

exact conditions under which vein quartz formed may not be known, it is clear that individual veins were being fractured and reopened under a wide range of fluid conditions. This observation is consistent with the observation that some veins are comprised of minerals from multiple different stages of fluid input. It is possible that fracturing occurs over a large portion of the EESS with mineralization occurring in one part of that fractured zone, while aliquots of that fluid are trapped along micro-fractures in quartz in places where no mineralization occurs.

5.3.2 Vein scale

The majority of veins in the EESS were not mineralized in a single event or under one set of fluid temperature, pressure, and salinity conditions. Rather, individual EESS veins can contain many minerals which have been deposited under different conditions and at different times. Two factors contribute to the mineralogical complexity of veining in the EESS: repeated fracturing and re-opening of veins in the system, infilling of open spaces with later mineralization which juxtaposes minerals deposited at different times, and dynamic or changing pressure, temperature, and salinity conditions as ore-forming processes progressed.

Up to 5 episodes of fracturing and mineralization of veins is demonstrated with quartz CL images that display complex cross-cutting relationships of quartz. It follows that reopening of veins and infilling with mineralization that post-dates the original vein minerals is not restricted to quartz mineralization. Pyrite-dominated veins are observed to cross-cut quartz and quartz-chalcopyrite veins. Anhydrite veins cross-cut quartz- and sulfide-bearing veins, but anhydrite is also a late phase within those same sulfide-bearing veins. Notably, there is little textural distinction between diorite- and skarn-hosted veins,

but only skarn samples contained breccias. This may suggest that a zone of shear fracturing is near these skarn samples, while only evidence of extensional fracturing has been observed in the diorite.

5.3.3 System scale

A zone of high intensity sub-parallel quartz veins has been delineated in the EESS (Young et al., 2016). The high number of individual veins present in this zone suggests that many episodes of fracturing and mineralization must have occurred. This sheeted vein system is described to follow district fault trends and may record a major early structural pathway for fluids in the EESS. The sheeting structures indicate multiple re-openings are present in the EESS, an observation that has not been made regarding the Grasberg system according to Penniston-Dorland (2001).

5.4 Defining the Phase Separation Zone

The evidence gathered in this report reveals a discrete phase separation zone with a top at ~2500 m. There is little evidence for T_h or %NaCl variation by elevation when examining all inclusions or by individual type. The absence of these physical and chemical trends may suggest that EESS mineralization occurred under conditions which varied only moderately, but in which overprinting was common. Oxidized sulfur in the form of SO_2 reacts with H_20 to form H_2SO_4 and H_2S. The H_2S0_4 reacts with wall-rock and H_2S gas controls the solubility of CuFe-sulfides. Therefore, the vertical extent of mineralzation is the result of H_2S generation within the system. Phase separation begins to occur at least as deep at 1748 m and H_2S may react causing CuFe-sulfides to precipitate anywhere above that zone. The reaction $SO_2 + H_2O = H_2SO_4 + H_2S$ occurs below 500 °C, so all EESS Fluid inclusion assemblages measured in this study fall below

this range, with the temperature range of ~320-380 °C measured. These fluids have cooled substantially from magmatic temperatures (800±°C)

5.5 FLUID INCLUSION MODEL

Four types of fluid inclusions are present based on salinities, daughter crystals, vapor bubble size, and homogenization behavior. All four types of fluids appear to be the product of unmixing of a primary magmatic fluid (*Figure 29*). Type 1 are vapor-rich and copper—bearing (based on ablation analysis). Type 2a and 2b are telated as unmixed brine and vapor. Type 3 may be unmixed brine and vapor.

The only clear observation about temporal distribution of fluid inclusions is that some Texture Group 2 quartz crystals contains only type 3 inclusions along fractures that extend beyond the edges of the quartz crystal and truncate on sulfide grains. This suggests that type three inclusions may record a fluid associated with sulfide mineralization or more likely, a fluid that is left over after ore deposition or post-dates input of high salinity ore fluid into the system. Type 3 inclusions, at least some of them, may be explained as the result of phase separation that did not result in a halite-saturated solution at ambient conditions. One explanation that explains why type 3 inclusions can occur later than type 1, 2a, and 2b is that type 3 inclusions are a remnant fluid of the ore deposition process. These depleted ore fluids may be condensed vapors which post-date ore deposition.

One factor that may account for the extensive fluid inclusion record recorded in the EESS may be attributed to the extensive degree of fracturing in the EESS. This extensive fracturing would provide a multitude of opportunities for fluids to be trapped and likely coincides with fluid movement through the system.

This study set out to understand the hydrothermal processes that drove Cu-Au mineralization in the EESS. It appears that fracture-mediated fluid flow along a NW-SE structural trend is connected to a deep magmatic source of a fluid analogous to porphyry Cu fluids. This deep magmatic fluid unmixes below ~2500 m elevation. As the present surface is near 4200 m, it appears that there was 2 km or less rock cover over the EESS when these veins were formed. Mineralization of EESS occurs where abundant H_2S causes CuFe-sulfides to precipitate and vein-hosted Cu-Au mineralization does not appear to be lithology dependent.

Appendices

APPENDIX A. SAMPLE LOCATIONS:

SEM-CL Sample Locations			
Sample (Image)	**Coordinates**		
	Y	X	Z
GBT-91R-1A	9,548,804	736,919	3,581
GBT-91R-4	9,548,877	736,869	3,571
GBT-90R-1B	9,548,827	736,896	3,566
DZ07-07-180.8	9,549,043	736,784	3,559
TE01-16-310	9,549,295	737,099	2,743
TEW-09-05-465.8	9,549,545	736,728	2,742
TE13-13-468	9,549,055	737,708	2,684
TE14-01_934.9	9,548,836	737,456	2,668
TE-13-13-494	9,549,069	737,720	2,665
TE01-16-180.5	9,549,165	737,261	2,586
TE01-16-585.2	9,549,421	737,197	2,519
TE01-16-748.7	9,549,503	737,273	2,400
TE01-16-786.8	9,549,522	737,293	2,374
TE01-16-870	9,549,565	737,339	2,320
TEW09-05-1039.7	9,549,333	736,598	2,108
TEW09-05-1421.5	9,549,948	737,152	1,988
TEW09-01-1399.5	9,549,319	736,602	1,748

Petrography Sample Locations			
Sample (Image)	**Coordinates**		
	Y	X	Z
GBT-90R-1B	9,548,827	736,896	3,566
DZ07-07-180.8	9,549,043	736,784	3,559
TE01-16-310	9,549,295	737,099	2,743
TE01-16-748.7	9,549,503	737,273	2,400
TE01-16-870	9,549,565	737,339	2,320
TE05-16-180.5	9,549,165	737,261	2,586
TE13-13-468	9,549,055	737,708	2,684
TE-13-13-494	9,549,069	737,720	2,665
TE14-01_934.9	9,548,836	737,456	2,668
TEW-09-05-465.8	9,549,545	736,728	2,742
TEW09-05-1039.7	9,549,333	736,598	2,108
TEW09-05-1421.5	9,549,948	737,152	1,988
TEW09-01-1399.5	9,549,319	736,602	1,748
TEW09-01-1266	9,549,324	736,600	1,882
DZ07-04-377.7	9,548,634	736,474	3,409
TEW09-05-789	9,549,677	736,850	2,472
TE01-16-730.4	9,549,493	737,264	2,413

APPENDIX B. DIGITIZED CORE SELECTION LOG:

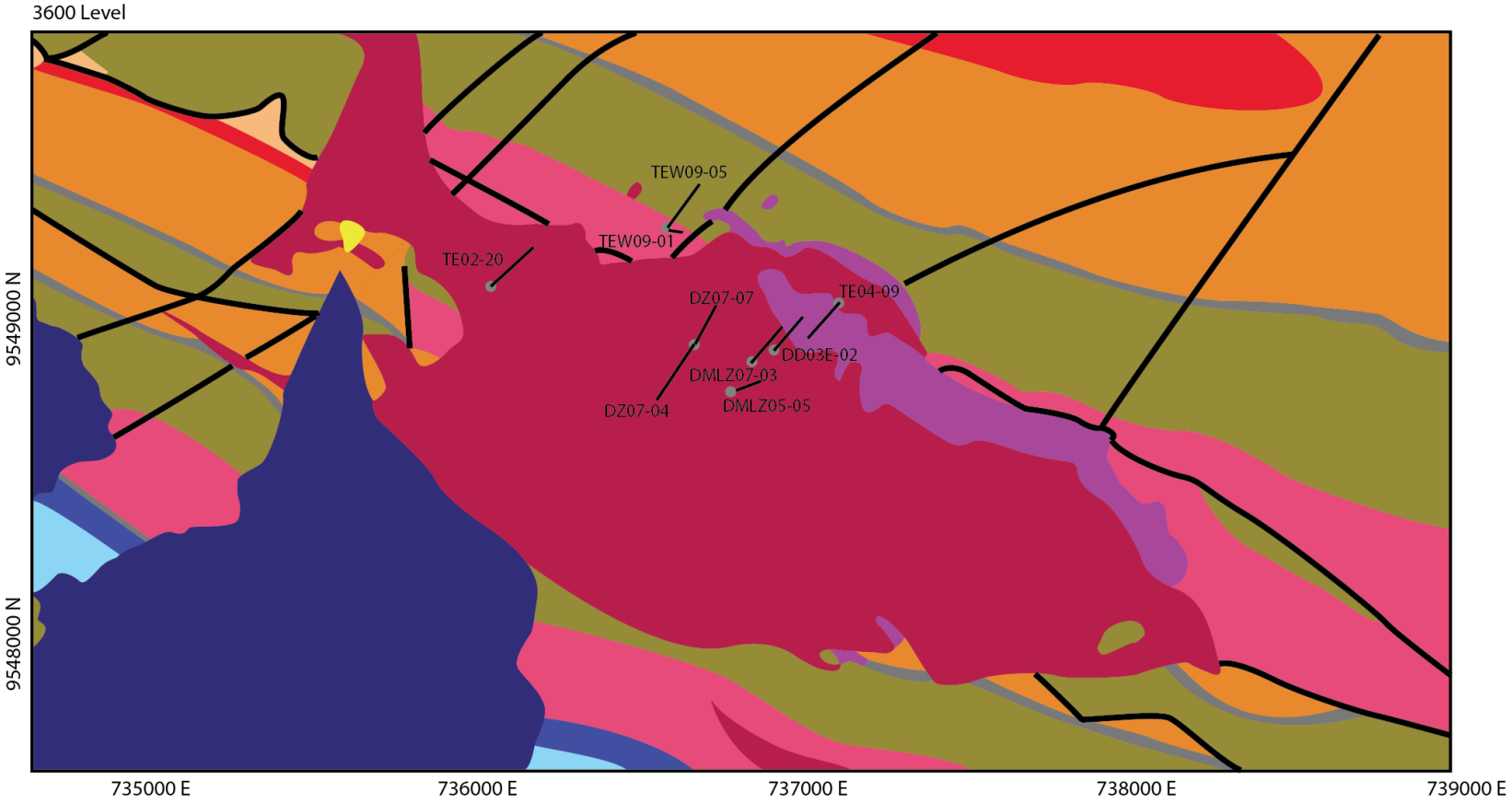

Map of the location and azimuth of drill holes sampled for this study. Samples are plotted onto the 3600 m level map.

Hole ID	Depth (m)	Lithology/Alteration	Vein Type 1	Vein Type 2	Vein Type 3	Sampling Notes	Purpose	Interval Description from PTFI log	Assays		
									Interval (m)	Cu %	Au ppm
DZ07-07						Skeleton:1.20-62.80; 110.90-411.30. Split: none.*Anhydrite in DZ07-07 is inferred from voids in veins attributed to weathering.					
DZ07-07	11	Diorite	qz			1cm main vein and veinlets.	CL & Fl (qz)	8-16.7 m - Te3, diorite. Light gray to pinkish, porhyritic texture, with biotite and	8-12 m	0.4693	0.45
DZ07-07	37.55	Diorite	qz-py				CL & Fl (qz)	16.7-69 m - Te1, diorite. Mid-pinkish gray, bch-frac equigranular, weak-mid cp. Vein	36-39	0.6045	0.93
DZ07-07	52.4	Diorite	qz-py			coarse qz-py vein and veinlets. Sample may degrade due to fractures.	CL & Fl (qz)	16.7-69 m - Te1, diorite. Mid-pinkish gray, bch-frac equigranular, weak-mid cp. Vein	51-54	0.2928	0.47
DZ07-07	113.95	Diorite	an	qz-cp		Sample tag difficult to read, sample depth may be off by a couple meters. Anhydrite veins x-cut and offset by qz-cp vein.	CL & Fl (qz)	109.2-175.2 m - Te1, diorite, pinkish gray, mid-coarse grained biot., good cp until	112.2-115.2	0.2681	1.73
DZ07-07	138.3	Diorite	qz-cp-bn			May be useful to consider the creation of porosity in Diorite - however, these pore spaces may be anhydrite lost to wethering	Review/Revise Gibbins Vein Classification	109.2-175.2 m - Te1, diorite, pinkish gray, mid-coarse grained biot., good cp until	136.2-139.2	0.7269	2.08
DZ07-07	143.05	Diorite	qz-py-cp			Offshooting sulfide vein may be source of sulfide in the quartz vein (ie. later generation and separate vein hijacking earlier	CL & Fl (qz)	109.2-175.2 m - Te1, diorite, pinkish gray, mid-coarse grained biot., good cp until	142.2-145.2	0.387	0.9
DZ07-07	158	Diorite	qz-py-an*			Much anhydrite weathered out. Depth is estimate - label was washed off.	CL & Fl (qz)	109.2-175.2 m - Te1, diorite, pinkish gray, mid-coarse grained biot., good cp until	157.2-160.2	0.2754	0.28
DZ07-07	180	Diorite	qz-py				Give context to other Samples	175.2-241.2 m - Te1, diorite, pinkish gray, mid grained equigranular, abundant	178.2-181.2	0.2706	0.27
DZ07-07	182.4	Diorite	qz-py-bn			Selected for cu-sulfide vein.	CL & Fl (qz)	175.2-241.2 m - Te1, diorite, pinkish gray, mid grained equigranular, abundant	181.2-184.2	0.7921	0.3
DZ07-07	219.7	Diorite	qz-py-an*				Give context to other Samples	175.2-241.2 m - Te1, diorite, pinkish gray, mid grained equigranular, abundant	217.2-220.2	0.8714	0.23
DZ07-07	257.2	Diorite	qz-py			Cu-carbonates in selvage?	CL & Fl (qz + calc sil?)	241.2-286.2 m - Te1, diorite, pinkish gray, brk, equigranular-diss biotie primary &	256.2-259.2	0.2063	0.15
DZ07-07	294.5	Diorite	qz-py-an*			Very milky euh-subh qz may yield excellent Fl data.	CL & Fl (qz)	286.2-307.2 m - Te1, diorite, light gray, brk-frac, equigranular, weak cp phyllic alt.	293.2-295.2	0.1837	0.93
DZ07-07	304	Diorite	qz-cp/py				CL & Fl (qz)	286.2-307.2 m - Te1, diorite, light gray, brk-frac, equigranular, weak cp phyllic alt.	301.2-304.2	0.18	0.97
DZ07-07	352.7	Hornfels	qz			dark (rusty?) selvage	Veining in Hornfels	329.3-352.9 m - Tw, forsterite diopside hornfels greenish to whiteish, brk, strong	349.2-352.9	0.3252	0.97
DZ07-07	394.1	Hornfels (marble?)	qz?			very dark selvage.	Veining in Hornfels (marble?)	352.9-411.4 m - Tw?, greenish to dark gray. Loc epidote, trace of bedding 45	391.2-394.2	0.2687	<0.01
DZ07-04						Skeleton: 94.0-166.20. Split: 378-383; 391-395.4; 402.5-407.5; 414-420; 426-443; 451-497.5.					
DZ07-04	145.2	Diorite	qz-py			145.20-148.20.	FL (qz)	71.6-236.7 m - Te1, diorite, gray, hb 8%, bi 5%. [???]-chl-epi-bio-mag?-act,.	145.2-148.2	0.5121	0.12
DZ07-04	377.7	Diorite	qz-an-py-bn?			Euhedral quartz may field good CL zonation.	CL (qz)	320.2 to 602 m - Te1, med-coarse grained hb diorite, chl-mag atlered w/ bio alt halo	377-380	0.115	0.08
DZ07-04	393.5	Diorite	qz-an-cp			Intact 1 cm anh veins. Vein may be a qz-cp and an-cp vein right next to each other.	CL & Fl (qz+anh?)	320.2 to 602 m - Te1, med-coarse grained hb diorite, chl-mag atlered w/ bio alt halo	392-395	<0.1	0.07
DZ07-04	404.5	Diorite	qz-an			Euhedral qz - good Fl candidate or for a cut across c-axis of qz.	Fl & c-axis cut (qz)	320.2 to 602 m - Te1, med-coarse grained hb diorite, chl-mag atlered w/ bio alt halo	404-407	<0.1	0.03
DZ07-04	416.5	Diorite	qz-cp-bn			Qz at good orientation for a cut perpendicular to c-axis.	perpendicular qz cut	320.2 to 602 m - Te1, med-coarse grained hb diorite, chl-mag atlered w/ bio alt halo	416-419	0.207	0.07
DZ07-04	430.7	Diorite	qz-py			Euhedral qtz, potential perpendicular cut.	perpendicular qz cut	320.2 to 602 m - Te1, med-coarse grained hb diorite, chl-mag atlered w/ bio alt halo	428-431	<0.1	0.07
DZ07-04	436.3	Diorite	qz-py			Euhedral qz, appears to have early band of qz at vein boundary w/ qz-py center.	Give context to other Samples	320.2 to 602 m - Te1, med-coarse grained hb diorite, chl-mag atlered w/ bio alt halo	434-437	<0.1	0.1
DZ07-04	438.5	Diorite	qz-py?			Sampled because may be a calc-silicate in vein.	Give context to other Samples	320.2 to 602 m - Te1, med-coarse grained hb diorite, chl-mag atlered w/ bio alt halo	437-440	<0.1	0.08
DZ07-04	440.5	Diorite	qz-py-cp?			Large 1 cm vein good for Fl.	FL (qz)	320.2 to 602 m - Te1, med-coarse grained hb diorite, chl-mag atlered w/ bio alt halo	440-443	0.165	0.05
DZ07-04	454.9	Diorite	qz-an-py			Large euhedral crystals and very clean anhydrite. V good for CL+Fl, though may fall apart.	CL & Fl (qz)	320.2 to 602 m - Te1, med-coarse grained hb diorite, chl-mag atlered w/ bio alt halo	452-455	<0.1	0.05
DZ07-04	458.8	Diorite	qz-py				Give context to other Samples	320.2 to 602 m - Te1, med-coarse grained hb diorite, chl-mag atlered w/ bio alt halo	458-461	0.197	0.05
DZ07-04	463	Diorite	an-py-bn			Sampled for future anhydrite work	anhydrite work	320.2 to 602 m - Te1, med-coarse grained hb diorite, chl-mag atlered w/ bio alt halo	461-464	<0.1	0.05
DZ07-04	465	Diorite	qz-py			Might be good for c-axis cut and Fl work.	FL & c-axis cut (qz)	320.2 to 602 m - Te1, med-coarse grained hb diorite, chl-mag atlered w/ bio alt halo	464-467	0.11	0.05
DZ07-04	476.6	Diorite	cp-qz-py			Interval sample of ch(?) qz.	Give context to other Samples	320.2 to 602 m - Te1, med-coarse grained hb diorite, chl-mag atlered w/ bio alt halo	476-479	<0.1	0.09
DZ07-04	483	Diorite	qtz-py			Large selvage-check mineralogy and CL.	Selvage mineralogy & CL	320.2 to 602 m - Te1, med-coarse grained hb diorite, chl-mag atlered w/ bio alt halo	482-485	<0.1	0.05

Hole ID	Depth (m)	Lithology/Alteration	Vein Type 1	Vein Type 2	Vein Type 3	Sampling Notes	Purpose	Interval Description from PTFI log	Assays		
									Interval (m)	Cu %	Au ppm
DZ07-04	489	Diorite	qz-py			Very cloudy qz, multigenerational veins good for paragenesis. Great for FI.	FL (qz), paragenesis	320.2 to 602 m - Te1, med-coarse grained hb diorite, chl-mag atlered w/ bio alt halo	488-491	<0.1	0.09
DZ07-04	489.1	Diorite	qz-py			Coarse qz-py vein, sampled to have additional material like 489.0.	FL (qz)	320.2 to 602 m - Te1, med-coarse grained hb diorite, chl-mag atlered w/ bio alt halo	488-491	<0.1	0.09
DZ07-04	494.5	Diorite	py-qz			Interval sample.	Give context to other Samples	320.2 to 602 m - Te1, med-coarse grained hb diorite, chl-mag atlered w/ bio alt halo	494-497	0.3397	0.18
TEW09-05						Split: 0-TD					
TEW09-05	9.5	diorite	qz-an-py-cp			largest qz vein among many an veins. Good comb quartz.		0.3-26.7 m - Te, Diorite, green-grey, medium grain, equigranular, biotite-	9-12 m	0.236	0.12
TEW09-05	14	diorite	an-qz-cp-py			disseminated cp selvage study. Vein CL & FI work.		0.3-26.7 m - Te, Diorite, green-grey, medium grain, equigranular, biotite-	12-15 m	0.103	0.07
TEW09-05	17	endoskarn	an	cp		Paragenesis. (endoskarn block?)		0.3-26.7 m - Te, Diorite, green-grey, medium grain, equigranular, biotite-	15-18	0.312	0.18
TEW09-05	33.5	diorite	an-mo	an-cp		an-cp-x-cuts an-mo vein. Paragenesis and FI in moly vein?		31.5-35.5 m - Te, Diorite, greenish grey, medium grain, equigranular, strong	33-36	0.221	0.15
TEW09-05	35	hornfels	an	qz		hornfels block. Anhydrite and quartz cross-cut eachother. Paragenesis CL/FI		31.5-35.5 m - Te, Diorite, greenish grey, medium grain, equigranular, strong	33-36	0.221	0.15
TEW09-05	58	diorite	qz			Good quartz vein to cut perpendicular to c-axis. CL/FI		52.8-90.4 m - Te, Diorite, greenish grey, medium grain, equigranular, biotite-	56.3-59.3	0.122	0.11
TEW09-05	60	diorite	bt-an-py			Diorite contact with hornfels block. Shreddy biotite veins merg with an veins. Minor sulfides. Paragenesis.		52.8-90.4 m - Te, Diorite, greenish grey, medium grain, equigranular, biotite-	59.3-63	0.541	0.65
TEW09-05	63	diorite						52.8-90.4 m - Te, Diorite, greenish grey, medium grain, equigranular, biotite-	63-66	0.245	0.14
TEW09-05	69	endoskarn	qz-ank?-py	an		Paragenesis. What is significance of ankerite?		52.8-90.4 m - Te, Diorite, greenish grey, medium grain, equigranular, biotite-	69-72	0.472	0.24
TEW09-05	82	endoskarn				no vein. Quartz and cp in endoskarn. FI on endoskarn quartz.		52.8-90.4 m - Te, Diorite, greenish grey, medium grain, equigranular, biotite-	81-84	0.144	0.13
TEW09-05	77	skarn	qz-cp-an-mo			Paragenesis. Chunky, Cloudy quartz for FI.		52.8-90.4 m - Te, Diorite, greenish grey, medium grain, equigranular, biotite-	75-78	0.296	0.16
TEW09-05	94	endoskarn	qz-cp-an-mo			Paragenesis		93.2-111.2 m - Te, Diorite, greenish grey, medium grain, equigranular, strong	93.2-96	0.159	0.16
TEW09-05	94.2	endoskarn	an			A&B. An vein with complex selvage including FeC03. Selvage identitify and FeC03 story.		93.2-111.2 m - Te, Diorite, greenish grey, medium grain, equigranular, strong	93.2-96	0.159	0.16
TEW09-05	113.5	skarn	qz-cp vein			Chunky vein good for CL/FI	CL & FI (qz)	111.2-127 m - Tw, Exoskarn-endoskarn, brown-green, fine grain diopside-garnet-	111.2-114	0.455	0.49
TEW09-05	119.5	endoskarn	qz-an-mo				Paragenesis, CL & FI (qz)	111.2-127 m - Tw, Exoskarn-endoskarn, brown-green, fine grain diopside-garnet-	117-120	0.564	0.46
TEW09-05	138	skarn	an-ank-mo			selected for the mo or mt in the vein edge	Mineralogy	127-140.4 m - Te, Endoskarn, brown-green, garnet-diopside-epidote chlorite-	138-141.5	0.216	0.45
TEW09-05	141	skarn	an			Yellow selvage.	Mineralogy	140.4-144.9 m - Tw, Exoskarn, brownish pale green-green, diopside-forsterite-	138-141.5	0.216	0.45
TEW09-05	151.5	skarn	an	cp		cp vein x-cuts anhydrite vein	Paragenesis	144.9-183 m - Te, Diorite, greyish green, medium grain, equigranular, chlorite-	150-153	0.288	0.14
TEW09-05	156	endoskarn	qz-an	mafic		endoskarn qz-an vein x-cut by mafic vein	Paragenesis, CL & FI (qz)	144.9-183 m - Te, Diorite, greyish green, medium grain, equigranular, chlorite-	156-159	0.105	0.09
TEW09-05	173	skarn	qz-cp				CL & FI (qz)	144.9-183 m - Te, Diorite, greyish green, medium grain, equigranular, chlorite-	171-174	0.22	0.15
TEW09-05	181	diorite	qz-py				CL & FI (qz)	144.9-183 m - Te, Diorite, greyish green, medium grain, equigranular, chlorite-	180-183	0.025	0.04
TEW09-05	188	skarn	an-qz-cp-mo			Messy, but great paragenesis sample	Paragenesis	183-199.3 m - Tw, Exoskarn, darkish green-greenish brown, garnet-diopside-	186-189	0.257	0.18
TEW09-05	194.5	skarn				mont + an skarn example	FI (mont?)	183-199.3 m - Tw, Exoskarn, darkish green-greenish brown, garnet-diopside-	192.3-195.8	0.138	0.12
TEW09-05	197	skarn	an-qz-cp-mo				Paragenesis, CL & FI (qz)	183-199.3 m - Tw, Exoskarn, darkish green-greenish brown, garnet-diopside-	195.8-199.3	0.526	0.31
TEW09-05	198	skarn				unknown vein: an + fe-carb?		183-199.3 m - Tw, Exoskarn, darkish green-greenish brown, garnet-diopside-	195.8-199.3	0.526	0.31
TEW09-05	205	diorite	qz-an			very large qz-an vein. To big for CL	FI (qz)	199.3-212.4 m - Te, Diorite, greenish grey, fine-medium grain, equigranular, scattered	204.3-207	0.074	0.08
TEW09-05	211	diorite				vein of skarn minerals		199.3-212.4 m - Te, Diorite, greenish grey, fine-medium grain, equigranular, scattered	209.9-212.4	0.1515	0.09
TEW09-05	212.85	diorite	an-cp			Huge vein for fluid inclusions	FI (qz)	212.4-239.5 m - Tw, Exoskarn, pale green-brown-darkish grey, fine-medium grain,	212.4-215.9	0.233	0.13
TEW09-05	222	skarn	ep-chl-px			similar to 211		212.4-239.5 m - Tw, Exoskarn, pale green-brown-darkish grey, fine-medium grain,	222-225	0.441	0.17
TEW09-05	244.3	diorite	qz-an-mo				Paragenesis, CL & FI (qz)	239.5-276.4 m - Te, Diorite-endoskarn, greyish-brownish green, fine-medium	243-246	0.144	0.12
TEW09-05	244.4	diorite	qz-an-cp			vein assemblages cross-cutting eachother	Paragenesis, FI (qz)	239.5-276.4 m - Te, Diorite-endoskarn, greyish-brownish green, fine-medium	243-246	0.144	0.12

Hole ID	Depth (m)	Lithology/Alteration	Vein Type 1	Vein Type 2	Vein Type 3	Sampling Notes	Purpose	Interval Description from PTFI log	Assays		
									Interval (m)	Cu %	Au ppm
TEW09-05	250	diorite	qz-an				Paragenesis, CL & FI (qz)	239.5-276.4 m - Te, Diorite-endoskarn, greyish-brownish green, fine-medium	249-252	0.314	0.25
TEW09-05	257.5	Diorite	qz-cp				CL & FI (qz)	239.5-276.4 m - Te, Diorite-endoskarn, greyish-brownish green, fine-medium	255-258	0.137	0.12
TEW09-05	261	diorite	fe-carb-py			poorly understood vein type	Petrography	239.5-276.4 m - Te, Diorite-endoskarn, greyish-brownish green, fine-medium	261-264	0.246	0.11
TEW09-05	268	diorite	an-mo				FI (an)	239.5-276.4 m - Te, Diorite-endoskarn, greyish-brownish green, fine-medium	267-270	0.316	0.26
TEW09-05	273.5	endoskarn	an-qz-cp-py			thin veins, many cross-cutting relationships	Paragenesis	239.5-276.4 m - Te, Diorite-endoskarn, greyish-brownish green, fine-medium	273-276	0.353	0.29
TEW09-05	274.5	hornfels	qz-fo-mafic			No veins, but blebby quartz.	FI (skarn minerals)	239.5-276.4 m - Te, Diorite-endoskarn, greyish-brownish green, fine-medium	273-276	0.353	0.29
TEW09-05	277	hornfels	qz-cp-py			veins cross-cut	Paragenesis	276.4-278.8 m - Tw, Quartz sandstone, brown, medium grain, equigranular, silica-	276-278.8	0.26	0.15
TEW09-05	278	hornfels	qz-cp-py			A&B		276.4-278.8 m - Tw, Quartz sandstone, brown, medium grain, equigranular, silica-	276-278.8	0.26	0.15
TEW09-05	283	hornfels	qz-calcsilicate					278.8-284 m - Te, Diorite, greyish green, fine-medium grain, hornblende-biotite	281.4-284	0.238	0.18
TEW09-05	306.5	endoskarn	qz-py			qz-rich matrix. Selvage/skarn qz good for FI analysis and CL.	CL & FI (qz)	305.5-320.5 m - Te, Diorite-endoskarn, greyish-brownish dark green, fine-medium	305.5-309	0.374	0.19
TEW09-05	309	skarn	an-cp	qz-cp		Paragenesis compared to qz-cp veins in skarn	Paragenesis	305.5-320.5 m - Te, Diorite-endoskarn, greyish-brownish dark green, fine-medium	309-312	0.288	0.25
TEW09-05	313	skarn	qz-calcsilicate	cp		CL & FI on qz and calcsilicate	CL & FI (qz + calc sil?)	305.5-320.5 m - Te, Diorite-endoskarn, greyish-brownish dark green, fine-medium	312-315	0.547	0.45
TEW09-05	315.5	skarn	an-cp			mt-skarn	Paragenesis	305.5-320.5 m - Te, Diorite-endoskarn, greyish-brownish dark green, fine-medium	315-318	0.476	0.33
TEW09-05	327.5	skarn	qz			irregular quartz vein. Calc-silicate and qz FI examination		320.5-338.5 m - Tw, Exoskarn, brownish pale green-dark green, fine-medium grain,	327-330	0.234	0.17
TEW09-05	341.5	endoskarn	qz-an-py-cp			Large vein good for apragenesis and coarse crystals for CL/FI	CL & FI (qz + calc sil?)	338.5-363.5 m - Te, Diorite, whitish-brownish grey, medium grain,	338.5-342	1.155	0.46
TEW09-05	345.5	diorite	qz	qz-an-py-cp		qz vein cross-cutting a vein like 341.5	CL & FI (qz)	338.5-363.5 m - Te, Diorite, whitish-brownish grey, medium grain,	345-348	0.398	0.16
TEW09-05	347.5	diorite	qz	qz-mafic		good cross-cutting relationships. Veins might be co-eval.	CL & FI (qz)	338.5-363.5 m - Te, Diorite, whitish-brownish grey, medium grain,	345-348	0.398	0.16
TEW09-05	351.5	diorite	py-qz	qz-mafic		veins cross-cut eachother	CL & FI (qz)	338.5-363.5 m - Te, Diorite, whitish-brownish grey, medium grain,	351-354	0.454	0.43
TEW09-05	356.5	endoskarn				massive qz-py vein. C-axis perpendicular cut for CL/FI.	CL & FI (qz)	338.5-363.5 m - Te, Diorite, whitish-brownish grey, medium grain,	354-357	0.824	0.26
TEW09-05	360.3	diorite	qz			cross-cutting quartz veins	Paragenesis, CL & FI (qz)	338.5-363.5 m - Te, Diorite, whitish-brownish grey, medium grain,	360-363.5	0.298	0.19
TEW09-05	364.5	hornfels	qz-an-py-mo			very milky quartz for CL/FI	CL & FI (qz)	363.5-382 m - Tw, Silicified Exoskarn, greenish-brownish grey, fine grain, silica-	363.5-366	0.65	0.33
TEW09-05	366	hornfels	qz-sulfide			many generations of cross-cutting veins	Paragenesis	363.5-382 m - Tw, Silicified Exoskarn, greenish-brownish grey, fine grain, silica-	366-369	0.56	0.74
TEW09-05	373.5	endoskarn						363.5-382 m - Tw, Silicified Exoskarn, greenish-brownish grey, fine grain, silica-	372-375	0.52	0.18
TEW09-05	375	exoskarn	qz-py	qz		exoskarn (garnet) qz-py veins, but several qz generations are apparent. Good for quartz paragenesis with CL	CL & FI (qz)	363.5-382 m - Tw, Silicified Exoskarn, greenish-brownish grey, fine grain, silica-	375-378.5	0.729	0.44
TEW09-05	381.5	skarn	qz-py			skarn? Milky qz-py vein. CL the quartz with lost of FI. May be able to get FI/CL of qz in wall rock	CL & FI (qz)	363.5-382 m - Tw, Silicified Exoskarn, greenish-brownish grey, fine grain, silica-	378.5-382	0.727	0.54
TEW09-05	389.5	diorite	qz-py			multigenerational qz-py good for CL/FI	CL & FI (qz)	382-444.6 m - Te, Diorite, whitish greenish grey, medium grain, equigranular, mafic	387-390	0.69	0.61
TEW09-05	391.5	diorite	qz-py			multigenerational qz-py good for CL/FI. Good cross-cutting veins.	CL & FI (qz)	382-444.6 m - Te, Diorite, whitish greenish grey, medium grain, equigranular, mafic	390-393	1.031	0.49
TEW09-05	400	diorite	qz-py			multigenerational qz-py good for CL/FI.	CL & FI (qz)	382-444.6 m - Te, Diorite, whitish greenish grey, medium grain, equigranular, mafic	399-402	0.489	3.88
TEW09-05	410	diorite	qz-py			multigenerational qz-py good for CL/FI.	CL & FI (qz)	382-444.6 m - Te, Diorite, whitish greenish grey, medium grain, equigranular, mafic	408-411	0.281	0.2
TEW09-05	420.5	diorite	qz-py	an			CL & FI (qz)	382-444.6 m - Te, Diorite, whitish greenish grey, medium grain, equigranular, mafic	420-423	0.386	0.25
TEW09-05	424	diorite	qz-py	an		The preceeding 150 m might be a good place to compare textures between multiple similar veins.	CL & FI (qz)	382-444.6 m - Te, Diorite, whitish greenish grey, medium grain, equigranular, mafic	423-426	0.34	0.33
TEW09-05	429	diorite	qz-mafic			Sampled because this vein may be different than the preceeding qz-sulfide veins.	CL & FI (qz)	382-444.6 m - Te, Diorite, whitish greenish grey, medium grain, equigranular, mafic	429-432	0.316	0.48
TEW09-05	441	diorite	qz-py				CL & FI (qz)	382-444.6 m - Te, Diorite, whitish greenish grey, medium grain, equigranular, mafic	438.1-441.1	0.164	0.12
TEW09-05	456.75	diorite	qz-py-mo			Paragenesis with Mo. May have anhydrite.	Paragenesis, CL & FI (qz)	451.5-509.3 m - Te, Diorite, whitish-greenish grey, medium grain,	456.5-459	0.52	1.14
TEW09-05	459.5	diorite	py-qz			One of last veins with qz before they get really skinny and hard to	CL & FI (qz)	451.5-509.3 m - Te, Diorite, whitish-greenish grey, medium grain,	459-462	0.42	0.51

Hole ID	Depth (m)	Lithology/Alteration	Vein Type 1	Vein Type 2	Vein Type 3	Sampling Notes	Purpose	Interval Description from PTFI log	Assays		
									Interval (m)	Cu %	Au ppm
TEW09-05	463.5	endoskarn	py-qz			unknown green mineral in the vein. Cross-cutting relationships between veins. Last quartz vein for a while.	CL & FI (qz)	451.5-509.3 m - Te, Diorite, whitish-greenish grey, medium grain,	462-465	0.367	0.47
TEW09-05	465.85	endoskarn	mo	py		molybdenite and quartz veins cross-cut - paragenesis	Paragenesis	451.5-509.3 m - Te, Diorite, whitish-greenish grey, medium grain,	465-468	0.484	0.71
TEW09-05	477	diorite	an			the selvage is much less extensive and altered than the pyrite veins	Paragenesis	451.5-509.3 m - Te, Diorite, whitish-greenish grey, medium grain,	477-480	0.437	0.51
TEW09-05	478.9	diorite	qz-py	py		diorite vein x-cuts qz-diorite vein. Sample may be evidence for telescoping of the system, overpriting qz with py and more py.	Paragenesis, CL & FI (qz)	451.5-509.3 m - Te, Diorite, whitish-greenish grey, medium grain,	477-480	0.437	0.51
TEW09-05	497.25	diorite	an-sulfide			contrast to pyrite vein in character	Paragenesis	451.5-509.3 m - Te, Diorite, whitish-greenish grey, medium grain,	495-498	0.687	0.94
TEW09-05	502	diorite	qz	sulfide		qz vein x-cut by vein thin sulfide veins. Multiple generations of qz visible in veins.	Qz Paragenesis.	451.5-509.3 m - Te, Diorite, whitish-greenish grey, medium grain,	501-504	0.447	0.63
TEW09-05	506.5	endoskarn	an-py			paragenesis with qz veins	Paragenesis	451.5-509.3 m - Te, Diorite, whitish-greenish grey, medium grain,	506.6-509.3	0.572	1.45
TEW09-05	509.5	diorite	qz-cp-py-mo			Milky quartz for FI analysis	Paragenesis, CL & FI (qz)	509.3-520.3 m - Tw, Exoskarn, brownish-greyish green, forsterite-magnetite-garnet-	509.3-512.4	0.358	0.44
TEW09-05	510	diorite				Late qz-py vein x-cutting earlier mineralization?	Paragenesis, CL & FI (qz)	509.3-520.3 m - Tw, Exoskarn, brownish-greyish green, forsterite-magnetite-garnet-	509.3-512.4	0.358	0.44
TEW09-05	518	hornfels	an			selected for disseminated Cu-sulfides	Paragenesis	509.3-520.3 m - Tw, Exoskarn, brownish-greyish green, forsterite-magnetite-garnet-	517.8-520.3	1.801	2.23
TEW09-05	518.1	hornfels	an-mafic				Paragenesis of hornfels formation	509.3-520.3 m - Tw, Exoskarn, brownish-greyish green, forsterite-magnetite-garnet-	517.8-520.3	1.801	2.23
TEW09-05	520	diorite	qz	an		Great x-cutting relationships.	Paragenesis	509.3-520.3 m - Tw, Exoskarn, brownish-greyish green, forsterite-magnetite-garnet-	517.8-520.3	1.801	2.23
TEW09-05	522	endoskarn	py	qz-py		More evidence for telescoping?	Paragenesis, CL & FI (qz)	520.3-689.9 m - Te, Diorite, whitish-greenish grey, medium grain,	520.3-522.8	0.71	1.61
TEW09-05	525	diorite	qz-py			Most substantial qz for 60m	Paragenesis, CL & FI (qz)	520.3-689.9 m - Te, Diorite, whitish-greenish grey, medium grain,	522.8-525.3	0.499	3.54
TEW09-05	533	diorite	py-qz	py			Paragenesis	520.3-689.9 m - Te, Diorite, whitish-greenish grey, medium grain,	532-534	0.353	1.27
TEW09-05	539.5	endoskarn	qz-py			Massive vein, good for CL/FI.	CL & FI (qz)	520.3-689.9 m - Te, Diorite, whitish-greenish grey, medium grain,	537-540	0.536	1.85
TEW09-05	547.5	endoskarn	qz-py			Cross-cutting veins with different selvages.	Paragenesis, CL & FI (qz)	520.3-689.9 m - Te, Diorite, whitish-greenish grey, medium grain,	546-549	0.528	2.37
TEW09-05	551.5	endoskarn	cp-qz-an	py			Paragenesis, CL & FI (qz)	520.3-689.9 m - Te, Diorite, whitish-greenish grey, medium grain,	549-552	0.632	1.4
TEW09-05	554.9	endoskarn	qz-py	an-mt		Timing of mt. Skarn related mt or similar to mt in grasberg veins?	Paragenesis	520.3-689.9 m - Te, Diorite, whitish-greenish grey, medium grain,	552-555	0.567	2.59
TEW09-05	560.5	endoskarn	qz-py-cp-an			very milky quartz for FI	CL & FI (qz)	520.3-689.9 m - Te, Diorite, whitish-greenish grey, medium grain,	558-561	0.881	1.8
TEW09-05	567	endoskarn	qz-cp-py			Endo/stockwork.	CL & FI (qz)	520.3-689.9 m - Te, Diorite, whitish-greenish grey, medium grain,	567-570	0.795	1.22
TEW09-05	574	endoskarn	qz-cp?-py-an				c-axis cut (qz)	520.3-689.9 m - Te, Diorite, whitish-greenish grey, medium grain,	573-576	0.749	1.04
TEW09-05	575	endoskarn	qz-cp?-py-an				Paragenesis, CL & FI (qz)	520.3-689.9 m - Te, Diorite, whitish-greenish grey, medium grain,	573-576	0.749	1.04
TEW09-05	591	stockwork	qz-py-bn?			Good size for CL, cloudy w/inclusions.	CL & FI (qz)	520.3-689.9 m - Te, Diorite, whitish-greenish grey, medium grain,	591-594	0.764	1.7
TEW09-05	601	stockwork	qz-py-cp			Multiple veins. Complex sample paragenesis, much FI potential.	Paragenesis, FI (qz)	520.3-689.9 m - Te, Diorite, whitish-greenish grey, medium grain,	600-603	1.131	1.6
TEW09-05	605	stockwork	qz-py			Good size for CL.	CL (qz)	520.3-689.9 m - Te, Diorite, whitish-greenish grey, medium grain,	603-606	0.802	1.12
TEW09-05	629.5	diorite	qz-py	an		Notable lack of selvage, looks like late anh veins.	CL & FI (qz)	520.3-689.9 m - Te, Diorite, whitish-greenish grey, medium grain,	627-630	0.947	0.89
TEW09-05	657	diorite	qz-py	qz		Crosscut paragenesis	paragenesis	520.3-689.9 m - Te, Diorite, whitish-greenish grey, medium grain,	657-659.8	1.027	1.35
TEW09-05	671	diorite	qz-py			Multiple qz generations? Compare qz to sample at 30 m. Are the qz different generations separated by same py?	paragenesis	520.3-689.9 m - Te, Diorite, whitish-greenish grey, medium grain,	668.3-671.3	0.514	0.55
TEW09-05	682	diorite	qz-py-an				paragenesis	520.3-689.9 m - Te, Diorite, whitish-greenish grey, medium grain,	680.3-683.3	0.567	0.46
TEW09-05	690	diorite	py-qz			Compare FI paragenesis of qz to previous samples.	paragenesis, FI (qz)	520.3-689.9 m - Te, Diorite, whitish-greenish grey, medium grain,	689.9-693	0.769	0.41
TEW09-05	687.5	diorite	qz-py-mo			Sampled to look at qz associated with mo. Mo may be late x-cutting stage.	paragenesis	520.3-689.9 m - Te, Diorite, whitish-greenish grey, medium grain,	686.5-689.9	0.972	0.9
TEW09-05	692.5	diorite	qz-py-unknown			Could be mo? Could be mt but not likely.	paragenesis	689.9-714.5 m - Te, Diorite, greenish locally whitish gray, equigranular mafic	689.9-693	0.769	0.41
TEW09-05	703.5	diorite	qz-py-cp-mo			Crazy catch-all vein.	paragenesis	689.9-714.5 m - Te, Diorite, greenish locally whitish gray, equigranular mafic	702-705	1.203	1.29
TEW09-05	703.6	diorite	-py-bn-cu sulfide?			Good x-cutting relationships.	paragenesis	689.9-714.5 m - Te, Diorite, greenish locally whitish gray, equigranular mafic	702-705	1.203	1.29

Hole ID	Depth (m)	Lithology/Alteration	Vein Type 1	Vein Type 2	Vein Type 3	Sampling Notes	Purpose	Interval Description from PTFI log	Assays		
									Interval (m)	Cu %	Au ppm
TEW09-05	710	diorite	qz-py-mo			Nice vein for CL-FI of qtz.	CL & FI (qz)	689.9-714.5 m - Te, Diorite, greenish locally whitish gray, equigranular mafic	708-711	0.822	0.94
TEW09-05	718.5	diorite	qz-py-cp			Good euhedral qz for perpendicular c-axis cut.	CL & FI (qz), perpendicular c-axis cut	714.5-721.3 m - Te, Diorite, whitish gray, strong sericite altered groundmass locally	717.8-721.3	1.081	0.67
TEW09-05	728	diorite	qtz			No selvage. Late qz vein? Do FI.	FI (qz)	721.3-786 m - Te, Diorite, greenish gray, equigranular mafic phenocryst strong	726.3-729	0.596	1.48
TEW09-05	747.5	diorite	qz-py-an			Clearly anh-filled vein following a shearing event, based on openeing in the vein bevel.	paragenesis, CL & FI (qz)	721.3-786 m - Te, Diorite, greenish gray, equigranular mafic phenocryst strong	747-750	0.364	0.2
TEW09-05	753.8	diorite	an-py-qz			Last good qz for 40m.	Give context to other samples	721.3-786 m - Te, Diorite, greenish gray, equigranular mafic phenocryst strong	753-756	0.209	0.14
TEW09-05	783.5	diorite	qz-py	qz-an		Bonanza of cross-cutting relationships.	paragenesis	721.3-786 m - Te, Diorite, greenish gray, equigranular mafic phenocryst strong	783-786	0.424	0.33
TEW09-05	789	diorite	qz-py-an			Awesome comb quartz texture and sequential gens of qz-py-qz-py-an.	paragenesis	786-795.5 m - Te, Diorite, whitish-greenish gray, same as above but sericite	789-792	1.433	0.87
TEW09-05	792	diorite	qz-py-cp				paragenesis, CL & FI (qz)	786-795.5 m - Te, Diorite, whitish-greenish gray, same as above but sericite	792-795.5	1.863	1.79
TEW09-05	796	diorite	qz-cp-py-an?			FI+CL and paragenesis of qz associated w/ sulfide phase.	paragenesis, CL & FI (qz)	795.5-815.6 m - Te, Diorite, greenish gray, equigranular mafic phenocryst strong	795.5-798	0.31	0.2
TEW09-05	804.5	diorite	qz-py				CL & FI (qz)	795.5-815.6 m - Te, Diorite, greenish gray, equigranular mafic phenocryst strong	804-807	0.287	0.18
TEW09-05	818	hornfels	qz-py-an				CL & FI (qz)	815.6-840.9 m - Te, Diorite, greenish gray, mostly unclear protolith texture as	815.5-819	0.357	2.45
TEW09-05	829	diorite	qz-py-mt-an				CL & FI (qz)	815.6-840.9 m - Te, Diorite, greenish gray, mostly unclear protolith texture as	828-831	0.438	0.27
TEW09-05	839.5	diorite	mt+others			If there is qz, CL/FI.	CL & FI (qz)	815.6-840.9 m - Te, Diorite, greenish gray, mostly unclear protolith texture as	837.5-840.9	0.824	0.41
TEW09-05	847.5	diorite	qz-py			Big qz for CL and FI.	CL & FI (qz)	840.9-852 m - Te, Diorite, whitish brown-greenish gray, moderate sericite selvage	847-849.5	0.551	0.25
TEW09-05	854.8	diorite	qz-py-cp			Have not seen a Cu-bearing vein in a while.	Give context to other samples	852-868.5 m - Te, Diorite, greenish gray, back to fine grained protolith texture	852-855	0.41	0.15
TEW09-05	864	diorite	an-py-qz-cp			May yield some CL after prep w/saline water wash for An removal.	CL (qz)	852-868.5 m - Te, Diorite, greenish gray, back to fine grained protolith texture	863.5-866	0.581	0.25
TEW09-05	887.5	diorite	qz-py-cp			Much x-cutting.	paragenesis	877.9-918 m - Te, Diorite, greenish gray, fine grained protolith texture destroyed by	887.4-890.4	0.405	0.2
TEW09-05	897.5	diorite	py-qz			Complex w/stringers.	paragenesis	877.9-918 m - Te, Diorite, greenish gray, fine grained protolith texture destroyed by	896.4-899.4	0.365	0.98
TEW09-05	905.4	diorite	qz-py-bn?				Give context to other samples	877.9-918 m - Te, Diorite, greenish gray, fine grained protolith texture destroyed by	905.4-908.4	0.421	0.25
TEW09-05	916	diorite	qz-py-cp			CL/FI on cu-bearing veins.	CL & FI (qz)	877.9-918 m - Te, Diorite, greenish gray, fine grained protolith texture destroyed by	914.5-918	0.542	0.18
TEW09-05	918.5	endoskarn	py-qz-an				CL & FI (qz)	918-949.8 m - Te, Diorite, greenish gray, equigranular mafic phenocryst strong	918-921	0.829	0.37
TEW09-05	926.5	endoskarn	qz-cp/py			cp and py are in different parts of vein.	Paragenesis, FI (qz)	918-949.8 m - Te, Diorite, greenish gray, equigranular mafic phenocryst strong	924-927	0.23	0.13
TEW09-05	950.5	hornfels	qz-py				CL & FI (qz)	949.8-981.8 m - Te, Diorite, dark gray, fine grained locally previous equigranular	948-951	0.354	0.28
TEW09-05	957.5	endoskarn	qz-py-cp				CL & FI (qz)	949.8-981.8 m - Te, Diorite, dark gray, fine grained locally previous equigranular	957.2-959.7	0.419	0.13
TEW09-05	961.5	endoskarn	qz-py-cp				CL & FI (qz)	949.8-981.8 m - Te, Diorite, dark gray, fine grained locally previous equigranular	959.7-962.8	0.32	0.11
TEW09-05	981.5	diorite	qz-an-sulfide				Paragenesis, CL & FI (qz)	949.8-981.8 m - Te, Diorite, dark gray, fine grained locally previous equigranular	978.4-981.8	1.008	0.47
TEW09-05	982	diorite	qz-sulfide			Might be good for c-axis cut.	CL & FI (qz), c-axis cut (qz)	981.8-985.6 m - Te, Endoskarn, green, massive epidote locally magnetite-chlorite	981.8-984.4	2.56	0.79
TEW09-05	986	diorite	qz-py			x-cutting veins, cl/fi if different generations.	CL & FI (qz)	985.6-1000.1 m - Te, Diorite, greenish gray, back to equigranular mafic	984.4-987	0.816	0.3
TEW09-05	996	diorite	qz-py-cp			Very clean vein, but appears to have multiple generations of qz.	CL & FI (qz)	985.6-1000.1 m - Te, Diorite, greenish gray, back to equigranular mafic	993.25-996.6	0.377	0.18
TEW09-05	1000.5	skarn	blebby an-qz?				Give context to other samples	1000.1-1031.4 m - Te, Endoskarn, green, massive epidote locally magnetite-brown	1000.1-1002.6	0.873	1.09
TEW09-05	1002.5	skarn	qz-py	blebby cu-qz-??			CL & FI (qz)	1000.1-1031.4 m - Te, Endoskarn, green, massive epidote locally magnetite-brown	1000.1-1002.6	0.873	1.09
TEW09-05	1011.5	skarn	an-py			skarn sample	Give context to other samples	1000.1-1031.4 m - Te, Endoskarn, green, massive epidote locally magnetite-brown	1011-1014	1.166	0.45
TEW09-05	1017	skarn	an-py			Nice x-cutting offsetting veins.	Give context to other samples	1000.1-1031.4 m - Te, Endoskarn, green, massive epidote locally magnetite-brown	1017-1020	1.16	0.45
TEW09-05	1024.05	skarn	an-sulfide			An fluid inclusions	FI (an)?	1000.1-1031.4 m - Te, Endoskarn, green, massive epidote locally magnetite-brown	1023-1026	0.955	0.56
TEW09-05	1024.5	skarn	an-sulfide			Skarn minerals	FI (skarn mins)	1000.1-1031.4 m - Te, Endoskarn, green, massive epidote locally magnetite-brown	1023-1026	0.955	0.56

Hole ID	Depth (m)	Lithology/Alteration	Vein Type 1	Vein Type 2	Vein Type 3	Sampling Notes	Purpose	Interval Description from PTFI log	Assays		
									Interval (m)	Cu %	Au ppm
TEW09-05	1039.7	diorite	qz-bn-cp-py-an			CL/FI on bn vein!	CL & FI (qz & bn?)	1031.4-1083 m - Te, Diorite, greenish gray, equigranular medium grain of mafic	1037.6-1040.7	0.364	0.17
TEW09-05	1040.5	diorite	qz-cp-py				CL & FI (qz)	1031.4-1083 m - Te, Diorite, greenish gray, equigranular medium grain of mafic	1037.6-1040.7	0.364	0.17
TEW09-05	1047	diorite	nknown(actinolite?	py		Good paragenesis info	paragenesis	1031.4-1083 m - Te, Diorite, greenish gray, equigranular medium grain of mafic	1046.9-1050	0.266	0.23
TEW09-05	1053.5	diorite	qz-an-py-cp				CL & FI (qz)	1031.4-1083 m - Te, Diorite, greenish gray, equigranular medium grain of mafic	1053-1056	0.256	0.1
TEW09-05	1065	diorite	qz-an-cp-py			Large euhedral qz and an.	CL & FI (qz)	1031.4-1083 m - Te, Diorite, greenish gray, equigranular medium grain of mafic	1065-1068	0.577	0.41
TEW09-05	1085	skarn	z-an-calc silicate			Good for FI work comparing qz and calc silicate as they appear to be somewhat contemporaneous.	FI (qz)	1083-1094.2 m - Te, Endoskarn, green, strong epidote -magnetite-brown garnet-	1083-1086	0.51	0.29
TEW09-05	1090	endoskarn	qz-an-py			Good for CL/FI on qz.	CL & FI (qz)	1083-1094.2 m - Te, Endoskarn, green, strong epidote -magnetite-brown garnet-	1089-1091.5	0.736	0.3
TEW09-05	1113.5	diorite	an-cp-qz			Some endo mins in diorite.	Give context to other samples	1100.5-1118.9 m - Te, Endoskarn, brownish-greenish grey, green-brown	1113-1116	0.673	0.31
TEW09-05	1120	endoskarn	qz-cp			Great camb qz for CL/FI.	CL & FI (qz)	1118.9-1128.8 m - Tw, Exoskarn, dark grey-brown-green, fine-medium grain,	1118.9-1122	0.74	0.3
TEW09-05	1136	hornfels/skarn	qz-an-cp-py				CL & FI (qz)	1132.3-1146.3 m - Tw, Exoskarn-hornfels, green,	1135.8-1139.3	0.192	0.07
TEW09-05	1167	hornfels/skarn	qz-an-cp-py				CL & FI (qz)	1160.5-1178.1 m - Te, Diorite, greenish grey, medium-coarse grain, equigranular,	1167-1170	0.781	0.31
TEW09-05	1171	endoskarn/diorite	qz-an				CL & FI (qz)	1160.5-1178.1 m - Te, Diorite, greenish grey, medium-coarse grain, equigranular,	1170-1173	0.099	0.06
TEW09-05	1177	endoskarn/diorite	cp-an			Paragenesis with skarn fmn?	paragenesis	1160.5-1178.1 m - Te, Diorite, greenish grey, medium-coarse grain, equigranular,	1175.5-1178.1	0.086	0.04
TEW09-05	1189	skarn	qz-calcsilicate?			Vei between two skarn min types.	CL & FI (qz & calc silicate)	1178.1-1209.2 m - Kkel, Exoskarn-hornfels, green, fine grain, hard, diopside	1188-1191	0.398	0.12
TEW09-05	1202.5	skarn	an-qz	py		Veins x-cut, py post-dates an?!	paragenesis	1178.1-1209.2 m - Kkel, Exoskarn-hornfels, green, fine grain, hard, diopside	1200-1203	1.029	0.34
TEW09-05	1228	diorite				Rich picked very thin vein, maybe for calc-silicates?	calc-silicate CL & FI?	1209.2-1332.2 m - Te, Diorite, greenish grey, medium grain locally fine grain,	1227-1230	0.379	0.14
TEW09-05	1224.5	diorite	az-cp-py-an?			Big enough euhedral qz for general CL/FI.	CL & FI (qz)	1209.2-1332.2 m - Te, Diorite, greenish grey, medium grain locally fine grain,	1224-1227	0.515	0.22
TEW09-05	1240	diorite	qz-cp-py-an?			Similar in appearance to 1224.5, but w/selvage like 1228.	Give context to other samples	1209.2-1332.2 m - Te, Diorite, greenish grey, medium grain locally fine grain,	1239-1242	0.191	0.1
TEW09-05	1247	diorite	qz-cp-py-an?			Similar to 1224.5, no selvage.	Give context to other samples	1209.2-1332.2 m - Te, Diorite, greenish grey, medium grain locally fine grain,	1245-1248	0.158	0.06
TEW09-05	1269	diorite	an-py			diorite an-py veins in largely fresh diorite.	Give context to other samples	1209.2-1332.2 m - Te, Diorite, greenish grey, medium grain locally fine grain,	1269-1272	0.023	0.02
TEW09-05	1291	diorite	py-act?-qz?			Largely barren rock.	Give context to other samples	1209.2-1332.2 m - Te, Diorite, greenish grey, medium grain locally fine grain,	1290-1293	0.051	0.04
TEW09-05	1305.5	diorite	qz-py-cp			only significant qz for 60 m up.	Give context to other samples	1209.2-1332.2 m - Te, Diorite, greenish grey, medium grain locally fine grain,	1305-1308	0.268	0.11
TEW09-05	1321	diorite	py-qz			Compare with 1325, which is much lighter, possibly intrusive diorite.	Give context to other samples	1209.2-1332.2 m - Te, Diorite, greenish grey, medium grain locally fine grain,	1320-1323	0.43	0.16
TEW09-05	1325	diorite	mt-py-qz			Compare with 1321, different looking diorite.	Give context to other samples	1209.2-1332.2 m - Te, Diorite, greenish grey, medium grain locally fine grain,	1323-1326	0.219	0.09
TEW09-05	1331	diorite	qz-py			Vein in the first diorite phase with some calc-silicate mins in diorite.	Give context to other samples	1209.2-1332.2 m - Te, Diorite, greenish grey, medium grain locally fine grain,	1329-1332.2	0.097	0.06
TEW09-05	1342.5	diorite	py-qz	py-cp	calc-sil	paragenesis from x-cuts, calc-sil inclusion data	paragenesis, CL& FI (calc-sil)	1336.7-1390.7 m - Te, Diorite, greenish grey, fine-medium grain, equigranular	1341-1344	0.229	0.11
TEW09-05	1361.5	diorite	py-FcCarb(?)			Uncommon vein.	Give context to other samples	1336.7-1390.7 m - Te, Diorite, greenish grey, fine-medium grain, equigranular	1359-1362	0.042	0.03
TEW09-05	1365.5A	diorite	an-py-mt				paragenesis	1336.7-1390.7 m - Te, Diorite, greenish grey, fine-medium grain, equigranular	1365-1368	0.045	0.04
TEW09-05	1365.5B	diorite	an-py-mt				paragenesis	1336.7-1390.7 m - Te, Diorite, greenish grey, fine-medium grain, equigranular	1365-1368	0.045	0.04
TEW09-05	1377	diorite	py-mt	py-qz			paragenesis	1336.7-1390.7 m - Te, Diorite, greenish grey, fine-medium grain, equigranular	1377-1380	0.205	0.07
TEW09-05	1387	diorite	qz-py-cp				CL & FI (qz)	1336.7-1390.7 m - Te, Diorite, greenish grey, fine-medium grain, equigranular	1385.7-1388	0.205	0.07
TEW09-05	1398A	hornfels/skarn	mt	qz		Great x-cutting relationships.	paragenesis	1390.7-1431 m - Kkes, Exoskarn, greyish green, fine-medium grain, epidote-chlorite	1397.4-1400.4	0.043	0.08
TEW09-05	1398B	hornfels/skarn	mt	qz		Great x-cutting relationships.	paragenesis	1390.7-1431 m - Kkes, Exoskarn, greyish green, fine-medium grain, epidote-chlorite	1397.4-1400.4	0.043	0.08
TEW09-05	1413	skarn	qz-py	py		May be able to get FI data.	FI (qz)	1390.7-1431 m - Kkes, Exoskarn, greyish green, fine-medium grain, epidote-chlorite	1413-1416	0.066	0.1
TEW09-05	1421.4	skarn	py-qz-cp			Pray for FI/CL.	CL & FI (qz?)	1390.7-1431 m - Kkes, Exoskarn, greyish green, fine-medium grain, epidote-chlorite	1419-1422	0.154	0.06

Hole ID	Depth (m)	Lithology/Alteration	Vein Type 1	Vein Type 2	Vein Type 3	Sampling Notes	Purpose	Interval Description from PTFI log	Assays		
									Interval (m)	Cu %	Au ppm
TEW09-05	1421.5	skarn	py-qz-cp			Pray for FI/CL.	CL & FI (qz?)	1390.7-1431 m - Kkes, Exoskarn, greyish green, fine-medium grain, epidote-chlorite	1419-1422	0.154	0.06
TEW09-05	1429.5	skarn	py-qz-cp			Pray for FI/CL.	CL & FI (qz?)	1390.7-1431 m - Kkes, Exoskarn, greyish green, fine-medium grain, epidote-chlorite	1428-1431	0.053	0.03
TEW09-01						Split: 1-1400.19? Laid out: 498.20-650.55; 1210.30-1400.19					
TEW09-01	505	diorite	qz-sulfide	py		Qz-sulfide x-cuts py.	Paragenesis, CL & FI (qz)	420.6-534.1 m - Te, Diorite, dark purplish-greenish gray, equigranular, potassic-	504.1-507.1	0.362	0.17
TEW09-01	514.5	diorite	qz-mo-an-cp				paragenesis	420.6-534.1 m - Te, Diorite, dark purplish-greenish gray, equigranular, potassic-	513.1-516.1	0.573	0.42
TEW09-01	530.5	diorite	py-qz			Coarse vein cross-cutting other veins	CL & FI (qz), perpendicular c-axis cut	420.6-534.1 m - Te, Diorite, dark purplish-greenish gray, equigranular, potassic-	528.1-531.1	0.19	0.2
TEW09-01	545.5	diorite	qz			several qz vein generations, may be good study of FI in silicified diorite.	FI (qz)	534.1-598.3 m - Te, Diorite, dark grey, medium-coarse grain,	543.1-546.1	0.35	0.33
TEW09-01	553.5	diorite	qz	qz-py-mo		Excellent paragenesis sampkle.	paragenesis	534.1-598.3 m - Te, Diorite, dark grey, medium-coarse grain,	552.1-555.1	0.162	0.12
TEW09-01	565.75	diorite	qz-py	qz?		qz x-cuts qz-py	Paragenesis, CL & FI (qz)	534.1-598.3 m - Te, Diorite, dark grey, medium-coarse grain,	564.1-567.1	0.395	0.32
TEW09-01	580.5	diorite	py-qz	qz		Excellent comb qz for CL/FI	CL & FI (qz)	534.1-598.3 m - Te, Diorite, dark grey, medium-coarse grain,	579.1-582.1	0.282	0.65
TEW09-01	596	diorite	qz-py			Vein has mo or mt verneer. Big cloudy qz for FI.	CL & FI (qz)	534.1-598.3 m - Te, Diorite, dark grey, medium-coarse grain,	594.1-597.1	0.388	0.33
TEW09-01	600	diorite	qz-an-py	sulfide		qz-py x-cut by sulfide	paragenesis	598.3-753.1 m - Te, Diorite Intrusion, greenish gray, porphyry, medium to	597.1-600.1	0.358	0.38
TEW09-01	608.6	diorite	qz-py			Many x-cutting veinlets	paragenesis	598.3-753.1 m - Te, Diorite Intrusion, greenish gray, porphyry, medium to	606.1-609.1	0.416	0.29
TEW09-01	623.8	diorite	qz-sulfide			Hoping that there may be some cu-sulfides underneath oxidation.	CL & FI (qz)	598.3-753.1 m - Te, Diorite Intrusion, greenish gray, porphyry, medium to	621.1-624.1	0.283	0.5
TEW09-01	632.3	diorite	qz-py-mo			paragenesis w/in vein.	paragenesis	598.3-753.1 m - Te, Diorite Intrusion, greenish gray, porphyry, medium to	630.1-633.1	0.236	0.24
TEW09-01	637.5	diorite	qz-py			silicified selvage	CL & FI (qz)	598.3-753.1 m - Te, Diorite Intrusion, greenish gray, porphyry, medium to	636.1-639.1	0.284	0.16
TEW09-01	644	diorite	qz-cp-py				CL & FI (cu-bearing veins)	598.3-753.1 m - Te, Diorite Intrusion, greenish gray, porphyry, medium to	642.1-645.1	0.309	0.19
TEW09-01	1205.5	diorite	qz-an	sulfide-qz		qz-an x-cuts sulfide vein, may have some mo in it as well.	CL & FI (qz)	1186.1-1354.8 m - Te, Diorite, Propylitic alteration, same as previously with locally	1203.1-1206.1	0.231	0.06
TEW09-01	1219.5	diorite	qz	qz-py	an	Great for paragenesis, many veins in many fractures.	paragenesis	1186.1-1354.8 m - Te, Diorite, Propylitic alteration, same as previously with locally	1218.1-1221.1	0.135	0.03
TEW09-01	1239.5	diorite	qz-an			Mafic frags. Interval sample.	Give context to other samples	1186.1-1354.8 m - Te, Diorite, Propylitic alteration, same as previously with locally	1239.1-1242.1	0.151	0.07
TEW09-01	1255.5	diorite	qz-mt-py				paragenesis	1186.1-1354.8 m - Te, Diorite, Propylitic alteration, same as previously with locally	1254.1-1257.1	0.104	0.08
TEW09-01	1266	diorite	qz-an-mt/mo?			Good comb qz for CL/FI, we can remove An with saline H2O to avoid CL issues.	paragenesis, CL & FI (qz)	1186.1-1354.8 m - Te, Diorite, Propylitic alteration, same as previously with locally	1263.1-1266.1	0.083	0.03
TEW09-01	1269.5	diorite	qz-py			Coarse vein.	CL & FI (qz)	1186.1-1354.8 m - Te, Diorite, Propylitic alteration, same as previously with locally	1269.1-1272.1	0.068	0.03
TEW09-01	1277	diorite	qz-py-an			Maybe cu sulfides if lucky. Good cutting angle for II c-axis cut on qz.	II c-axis cut (qz)	1186.1-1354.8 m - Te, Diorite, Propylitic alteration, same as previously with locally	1276.1-1278.1	0.096	0.04
TEW09-01	1279.5	diorite	qz	qz-an		Good x-cutting relationships.	paragenesis?	1186.1-1354.8 m - Te, Diorite, Propylitic alteration, same as previously with locally	1278.1-1281.1	0.068	0.04
TEW09-01	1287.5	diorite	qz	an		Representative sample of veins locally.		1186.1-1354.8 m - Te, Diorite, Propylitic alteration, same as previously with locally	1287.1-1290.1	0.093	0.05
TEW09-01	1297.5	diorite	qz	qz-an	qz-calc sil-py	Good x-cuts and maybe FI in calc-sil.	paragenesis (x-cuts), FI (calc sil)	1186.1-1354.8 m - Te, Diorite, Propylitic alteration, same as previously with locally	1296.1-1299.1	0.161	0.06
TEW09-01	1303.5	diorite	qz-an	qz-mt		Paragenesis of qz CL/FI. Qz-an hijacking the qz-mt vein fracture.	CL & FI (qz)	1186.1-1354.8 m - Te, Diorite, Propylitic alteration, same as previously with locally	1302.1-1305.1	0.093	0.03
TEW09-01	1315	diorite	qz-an	sulfide-bt		Veins x-cut.	paragenesis	1186.1-1354.8 m - Te, Diorite, Propylitic alteration, same as previously with locally	1314.1-1317.1	0.118	0.05
TEW09-01	1351.5	diorite	qz	qz-py	calc sil	Paragenesis of qz CL/FI, but smaller qz.	Paragenesis, CL & FI (qz)	1186.1-1354.8 m - Te, Diorite, Propylitic alteration, same as previously with locally	1349.6-1352.1	0.064	0.04
TEW09-01	1357.5	exoskarn w/diorite dike				This and the next few samples seem to grade from diorite to qz vein. Maybe an interesting FI story here.	FI (qz)	1354.8-1367.4 m - Tw, Limestone, fine grains, green-dirty gray, exoskarn to	1354.8-1358.3	0.027	0.11
TEW09-01	1360.5	exoskarn				Silicified diorite or qz vein-like structure.	mini-study?	1354.8-1367.4 m - Tw, Limestone, fine grains, green-dirty gray, exoskarn to	1358.3-1361.4	0.066	0.07
TEW09-01	1361.5	exoskarn				W/ blebby qz that does not resemble diorite at all.	mini-study?	1354.8-1367.4 m - Tw, Limestone, fine grains, green-dirty gray, exoskarn to	1361.4-1364.4	0.077	0.05
TEW09-01	1364.5	exoskarn				anhydrite dispersed throughout sample.	mini-study?	1354.8-1367.4 m - Tw, Limestone, fine grains, green-dirty gray, exoskarn to	1364.4-1367.4	0.048	0.08
TEW09-01	1370.5	diorite	qz	py-qz		Coarse qz with later py(cu-sulfide?)-qz x-cutting.	mini-study?	1367.4-1397.1 m - Te, Diorite, Propylitic to potassic, same as previous diorite but less	1367.4-1370.9	0.139	0.07

Hole ID	Depth (m)	Lithology/Alteration	Vein Type 1	Vein Type 2	Vein Type 3	Sampling Notes	Purpose	Interval Description from PTFI log	Assays		
									Interval (m)	Cu %	Au ppm
TEW09-01	1366	skarn	an			An veins lined w/calc silicate. 1357.5-1366 may serve as a mini-study.	mini-study?	1354.8-1367.4 m - Tw, Limestone, fine grains, green-dirty gray, exoskarn to	1364.4-1367.4	0.048	0.08
TEW09-01	1382	diorite	qz-an			Coarse qz good for CL study and FI work for decent part of hole.	CL & FI (qz)	1367.4-1397.1 m - Te, Diorite, Propylitic to potassic, same as previous diorite but less	1380.1-1383.1	0.063	0.03
TEW09-01	1388	diorite	bt-an-qz			Has enough qz for CL/FI, sampled for paragenesis.	Paragenesis, CL & FI (qz)	1367.4-1397.1 m - Te, Diorite, Propylitic to potassic, same as previous diorite but less	1386.1-1389.1	0.133	0.1
TEW09-01	1397	diorite	qz	py		Qz vein has qz-py sliver. Py x-cuts qz. FI/CL of deep qz.	Paragenesis, CL & FI (qz)	1367.4-1397.1 m - Te, Diorite, Propylitic to potassic, same as previous diorite but less	1394.6-1397	0.085	0.04
TEW09-01	1399.5	diorite	py-an/cu-sulfide			Excellent vein at end of hole!	Give context to other samples	1397.1-1400.1 m - Te, Diorite, greenish-pale brown-gray, Phyllic-Propylitic	1397.1-1400.1	0.433	0.09
DMLZ07-03						Split: 0-EOH Sampled 0-54, 186-303.15, 479.10-716.15					
DMLZ07-03	3.2	diorite	qz-an-mt-mo?				CL & FI (qz)	0-154 m - Te, Diorite, light gray, fine-medium grain, hornblende-biotite;	3.1-6.3	0.035	0.005
DMLZ07-03	7	diorite	qz-an			Very coarse crystals of qz, good FI candidate.	FI (qz)	0-154 m - Te, Diorite, light gray, fine-medium grain, hornblende-biotite;	6.3-9.3	0.044	0.005
DMLZ07-03	11.3	diorite				Pegmatite vein.	Give context to other samples	0-154 m - Te, Diorite, light gray, fine-medium grain, hornblende-biotite;	9.3-12.3	0.065	0.005
DMLZ07-03	24	diorite	qz-py			Huge vein, coarse qz. Might be able to pluck a crystal for use in c-axis parallel or perpendicular cut.	parallel or perpendicular c-axis cut (qz), CL & FI (qz)	0-154 m - Te, Diorite, light gray, fine-medium grain, hornblende-biotite;	21.3-24.3	0.062	0.01
DMLZ07-03	24.4	diorite	qz-an	qz-py		qz-py = veinlets	paragenesis	0-154 m - Te, Diorite, light gray, fine-medium grain, hornblende-biotite;	24.3-27.3	0.067	0.04
DMLZ07-03	38	diorite	qz-py	bt		Samples A&B	Paragenesis, CL & FI (qz)	0-154 m - Te, Diorite, light gray, fine-medium grain, hornblende-biotite;	36.3-39.3	0.062	0.005
DMLZ07-03	43	diorite	qz	bt		Largest bt vein I have seen.	Give context to other samples	0-154 m - Te, Diorite, light gray, fine-medium grain, hornblende-biotite;	42.3-45.3	0.058	0.005
DMLZ07-03	51.5	diorite	qz	sulfide		Sulfide = veinlets. Last qz vein of first 30 m.	Give context to other samples	0-154 m - Te, Diorite, light gray, fine-medium grain, hornblende-biotite;	51.3-54.3	0.025	0.005
DMLZ07-03	191.75	diorite	qz	sulfide		Many x-cutting sulfide veins.	CL & FI (qz)	154-195.1 m - Te, Diorite, continue light gray, hornblende-biotite (potassic altered)	189-192.1	0.04	0.03
DMLZ07-03	207	diorite	qz	an-sulfide		An-sulfide x-cuts and offsets qz veinlet.	Paragenesis, CL & FI (qz)	195.1-309.3 m - Te, Diorite, greenish gray - gray, potassic and propylitic altered, cut	204.3-207.3	0.191	0.08
DMLZ07-03	210	diorite	qz	qz-sulfide	bt	4th sulfide vein. Bonanza of x-cuts At least two qz generations present.	Paragenesis, CL & FI (qz)	195.1-309.3 m - Te, Diorite, greenish gray - gray, potassic and propylitic altered, cut	207.3-210.3	0.128	0.07
DMLZ07-03	222	diorite	qz-py-cp-an			Looks like early qz vein hijacked by late qz-an-sulfide vein.	Give context to other samples	195.1-309.3 m - Te, Diorite, greenish gray - gray, potassic and propylitic altered, cut	219.3-222.3	0.191	0.19
DMLZ07-03	223	diorite	qz			Large vein, Rich likes for c-axis cut.	c-axis cut (qz)	195.1-309.3 m - Te, Diorite, greenish gray - gray, potassic and propylitic altered, cut	222.3-225.3	0.131	0.07
DMLZ07-03	238	diorite	qz	qz-py		X-cutting qz and qz-py veins with and without selvage.	CL & FI (qz)	195.1-309.3 m - Te, Diorite, greenish gray - gray, potassic and propylitic altered, cut	237.3-240.3	0.15	0.06
DMLZ07-03	246	diorite	qz	qz-py		Veins x-cut.	Paragenesis, CL & FI (qz)	195.1-309.3 m - Te, Diorite, greenish gray - gray, potassic and propylitic altered, cut	243.3-246.3	0.072	0.03
DMLZ07-03	250.5	diorite	qz-cp-py			Series of qz-cp-py veins. Good chance to CL/FI large qz w/in confined cu-sulfides.	CL & FI (qz)	195.1-309.3 m - Te, Diorite, greenish gray - gray, potassic and propylitic altered, cut	249.3-252.3	0.364	0.16
DMLZ07-03	252	diorite	qz-py-an-cp	qz-py		First vein w/selvage.	paragenesis	195.1-309.3 m - Te, Diorite, greenish gray - gray, potassic and propylitic altered, cut	249.3-252.3	0.364	0.16
DMLZ07-03	252.5	diorite				Many x-cutting qz veins.	CL & FI (qz)	195.1-309.3 m - Te, Diorite, greenish gray - gray, potassic and propylitic altered, cut	252.3-255.3	0.149	0.05
DMLZ07-03	263	diorite	qz-py	qz		qz-py x-cut by qz.	paragenesis, CL & FI (qz)	195.1-309.3 m - Te, Diorite, greenish gray - gray, potassic and propylitic altered, cut	261.3-264.3	0.137	0.1
DMLZ07-03	268	diorite	qz-py	qz-sulfide		x-cutting bonanza	paragenesis	195.1-309.3 m - Te, Diorite, greenish gray - gray, potassic and propylitic altered, cut	267.3-270.3	0.186	0.08
DMLZ07-03	273.2	diorite	qz-an	mt		Good mt vein sample	Give context to other samples	195.1-309.3 m - Te, Diorite, greenish gray - gray, potassic and propylitic altered, cut	276.3-279.3	0.175	0.06
DMLZ07-03	285.05	diorite	qz	qz-py-mo		qz-py-mo inside of qz vein. Good time to compare CL/FI of mo qz to earlier qz generation.	CL & FI (qz)	195.1-309.3 m - Te, Diorite, greenish gray - gray, potassic and propylitic altered, cut	282.3-285.2	0.17	0.1
DMLZ07-03	300	diorite	qz	sulfide		Samples A&B. Based off vein morphologies, sulfides must have followed shortly after qz vein formation…I think?	paragenesis	195.1-309.3 m - Te, Diorite, greenish gray - gray, potassic and propylitic altered, cut	297.3-300.3	0.199	0.08
DMLZ07-03	488.2	diorite	py-an-mt-qz			Many x-cutting relationships. CL/FI if big enough qz. Context for sheeted qz veins.	Give context to sheeted qz, CL & FI (qz)	390.3-505.9 m - Te, Diorite, greenish gray - gray, equigranular, potassic –propylitic	486.3-489.3	1.378	0.44
DMLZ07-03	497.5	diorite	qz	cp-py-qz		Tricky paragenesis to work out. CL/FI of qz & context for sheeted qz veins.	Give context to sheeted qz, CL & FI (qz)	390.3-505.9 m - Te, Diorite, greenish gray - gray, equigranular, potassic –propylitic	495.3-498.3	0.295	0.11
DMLZ07-03	502.5	diorite	qz-py				Give context to sheeted qz, CL & FI (qz)	390.3-505.9 m - Te, Diorite, greenish gray - gray, equigranular, potassic –propylitic	500.8-503.3	0.245	0.09
DMLZ07-03	509.4	diorite	qz			sheeted qz veins	CL & FI (qz)	505.9-522.3 m - Te, Quartz + Diorite, purplish gray, flooding/cutted by big quartz	509.4-512.9	0.463	0.15
DMLZ07-03	512.5	diorite	qz			Samples A&B. sheeted qz veins.	CL & FI (qz)	505.9-522.3 m - Te, Quartz + Diorite, purplish gray, flooding/cutted by big quartz	509.4-512.9	0.463	0.15
DMLZ07-03	513	diorite	qz			Samples A,B,C,D, sheeted qz veins where all pieces connect.	CL & FI (qz)	505.9-522.3 m - Te, Quartz + Diorite, purplish gray, flooding/cutted by big quartz	512.9-516.3	0.329	0.43

Hole ID	Depth (m)	Lithology/Alteration	Vein Type 1	Vein Type 2	Vein Type 3	Sampling Notes	Purpose	Interval Description from PTFI log	Assays		
									nterval (m)	Cu %	Au ppm
DMLZ07-03	514.5	diorite	qz			Sheeted qz w/ enough selvage to see individual big veins.	CL & FI (qz)	505.9-522.3 m - Te, Quartz + Diorite, purplish gray, flooding/cutted by big quartz	512.9-516.3	0.329	0.43
DMLZ07-03	515.5	diorite	qz			sheeted qz veins	CL & FI (qz)	505.9-522.3 m - Te, Quartz + Diorite, purplish gray, flooding/cutted by big quartz	512.9-516.3	0.329	0.43
DMLZ07-03	519.5	diorite	qz			Sheeted qz veins with earlier offset qz veins.	Give context to other samples.	505.9-522.3 m - Te, Quartz + Diorite, purplish gray, flooding/cutted by big quartz	519.3-522.3	0.217	0.23
DMLZ07-03	520.5	diorite	qz			several qz veins that appear to have slightly different timing with sulfide vein x-cutting them.	Give context to other samples.	505.9-522.3 m - Te, Quartz + Diorite, purplish gray, flooding/cutted by big quartz	519.3-522.3	0.217	0.23
DMLZ07-03	529	diorite	qz			Appear to be out of sheeted veins at this point.	Give context to other samples.	528.3-614.6 m - Te, Diorite, dark greenish gray – dark gray, equigranular, potassic-	528.3-531.3	0.141	0.33
DMLZ07-03	530.5	diorite	qz-mt				paragenesis	528.3-614.6 m - Te, Diorite, dark greenish gray – dark gray, equigranular, potassic-	528.3-531.3	0.141	0.33
DMLZ07-03	545.5	diorite	qz				CL & FI (qz)	528.3-614.6 m - Te, Diorite, dark greenish gray – dark gray, equigranular, potassic-	543.3-546.3	0.204	0.31
DMLZ07-03	546	diorite	an-sulfide	qz		an-sulfide veins x-cutting offset qz veins.	Give context to other samples.	528.3-614.6 m - Te, Diorite, dark greenish gray – dark gray, equigranular, potassic-	543.3-546.3	0.204	0.31
DMLZ07-03	553.5	diorite	qz-mt			Amazing example of qz before mt. Could c-axis cut this sample, be sure to scratch mt in these, it sometimes looks bladed, like	CL & FI (qz)	528.3-614.6 m - Te, Diorite, dark greenish gray – dark gray, equigranular, potassic-	552.3-555.3	0.152	0.34
DMLZ07-03	564.5	diorite	qz-an	sulfide-an		Coarse qz-an vein x-cut by sulfide-an vein.	Give context to other samples.	528.3-614.6 m - Te, Diorite, dark greenish gray – dark gray, equigranular, potassic-	564.3-567.3	0.226	0.43
DMLZ07-03	579.75	diorite/endo	qz-an	py-bt?-mt?-an	cp	All veins x-cutting, roseta stone!	Give context to other samples.	528.3-614.6 m - Te, Diorite, dark greenish gray – dark gray, equigranular, potassic-	579.3-582.3	0.497	0.63
DMLZ07-03	593	diorite	qz-sulfide-mt			paragenesis cp-present. CL/FI on cp-qz vein.	Paragenesis, CL & FI (qz)	528.3-614.6 m - Te, Diorite, dark greenish gray – dark gray, equigranular, potassic-	591.3-594.3	0.495	0.37
DMLZ07-03	609	endoskarn	qz-cp-an-mo			Good chance to CL/FI the qz w/an and a cp vein.	CL & FI (qz)	528.3-614.6 m - Te, Diorite, dark greenish gray – dark gray, equigranular, potassic-	606.3-609.3	0.464	0.56
DMLZ07-03	618	endoskarn	qz-an				CL & FI (qz)	614.6-640.4 m - Tw, Exoskarn, greenish gray- gray forsterite-serpentine-garnet-	617.9-621.3	0.115	0.1
DMLZ07-03	629.5	skarn	an-cp-qz			CL/FI on anhydrite.	CL & FI (an)	614.6-640.4 m - Tw, Exoskarn, greenish gray- gray forsterite-serpentine-garnet-	627.3-630.3	0.208	0.18
DMLZ07-03	641.3	endoskarn	qz			Qz veins in skarn, maybe CL/FI.	CL & FI? (qz)	640.4-647.4 m - Te, Diorite, dark greenish purple pervasive anhydrite-chlorite-	640.4-643.9	0.293	0.23
DMLZ07-03	648	endoskarn	calc-silicate				CL & FI (calc-sil)	647.4-651.4 m - Tw, Exoskarn, blackish gray forsterite-magnetite-serpentine skarn,	647.4-650.9	1.016	0.81
DMLZ07-03	656.5	endoskarn	qz-an			CL/FI if possible.	CL & FI (qz)	651.5-664 m - Te, Endoskarn, dark greenish gray chlorite-epidote after mafic	655.9-658.4	0.626	0.52
DMLZ07-03	664	endoskarn	z-an-calc silicate			CL/FI whatever phases have inclusions.	CL & FI (possibly all)	651.5-664 m - Te, Endoskarn, dark greenish gray chlorite-epidote after mafic	664-667.3	0.318	0.49
DMLZ07-03	674.5	skarn	an?			Some veining, pulled sample to get FI of calc-sils?	FI (calc-sil)	664-680.3 m - Tw, Exoskarn, greenish-blackish gray forsterite-magnetite-	673.3-676.8	0.125	0.1
DMLZ07-03	681	skarn	qz			Qz veining in skarn	CL & FI (qz & calc-sil)	680.3-686 m - Te, Diorite, greenish gray chlorite after hornblende-biotite +	680.3-683	0.195	0.2
DMLZ07-03	693	endoskarn	qz-an			Intentionally oversampled due to the location and prevalent quartz veining.	CL & FI (qz)	686-707.6 m - Te +Tw, Mixing zone, greenish-blackish gray chlorite-forsterite-	691.5-694.3	0.48	0.58
DMLZ07-03	697	endoskarn	qz-an			Intentionally oversampled due to the location and prevalent quartz veining.	CL & FI (qz)	686-707.6 m - Te +Tw, Mixing zone, greenish-blackish gray chlorite-forsterite-	694.3-697.3	0.238	0.3
DMLZ07-03	702	endoskarn	qz	mt	an	Intentionally oversampled due to the location and prevalent quartz veining. Samples A&B. Qz vein with x-cutting mt vein	FI (qz + an?)	686-707.6 m - Te +Tw, Mixing zone, greenish-blackish gray chlorite-forsterite-	700.8-704.3	0.23	0.2
DMLZ07-03	707	skarn	sulfide			Intentionally oversampled due to the location and prevalent quartz veining.	Give context to other samples.	686-707.6 m - Te +Tw, Mixing zone, greenish-blackish gray chlorite-forsterite-	704.3-707.6	0.614	0.5
DMLZ07-03	710	skarn				quartz veining. Samples A&B. Bunch of x-cutting and offsetting qz and an veins, weird blebby qz vein good for comparison w/calc sils.	Give context to other samples, CL & FI (qz)	greenish-pinkish gray diopside-anhydrite, cut by anhydrite and minor pyrite-galena-sphalerite vein/lets.	707.6-710.1	0.197	0.11
DMLZ07-03	711	skarn	qz	an		Bunch of x-cutting and offsetting qz and an veins.	CL & FI (qz)	707.6-715.9 m - Tw, Exoskarn, light greenish-pinkish gray diopside-anhydrite,	710.1-712.6	0.259	0.19
TE04-09						Split 0-239					
TE04-09	0.5	diorite	qz				CL & FI (qz)	0-59.5 m - Te1, Diorite, greenish gray, biotite>hornblende, medium grained	0-3	0.25	0.6
TE04-09	7	diorite/endo	qz	an		Large veins	CL & FI (qz)	0-59.5 m - Te1, Diorite, greenish gray, biotite>hornblende, medium grained	6-10 m	0.4	1.1
TE04-09	16.5	diorite	qz			Veins possibly of different timing.	CL & FI (qz)	0-59.5 m - Te1, Diorite, greenish gray, biotite>hornblende, medium grained	14-17	0.4	1.25
TE04-09	21.5	diorite	qz	mt-an		An infiltrated by voids	Paragenesis, CL & FI (qz)	0-59.5 m - Te1, Diorite, greenish gray, biotite>hornblende, medium grained	19-22	0.25	1.1
TE04-09	38.6	diorite	qz			Excellent qz veins for CL/FI. Also good x-cutting among qz.	CL & FI (qz)	0-59.5 m - Te1, Diorite, greenish gray, biotite>hornblende, medium grained	38-40	0.75	0.8
TE04-09	41.5	diorite	qz-sulfide				CL & FI (qz)	0-59.5 m - Te1, Diorite, greenish gray, biotite>hornblende, medium grained	40-42	0.3	1
TE04-09	59.5	diorite	qz	qz-sulfide	sulfide		paragenesis	0-59.5 m - Te1, Diorite, greenish gray, biotite>hornblende, medium grained	58-61	2.2	3.7

Hole ID	Depth (m)	Lithology/Alteration	Vein Type 1	Vein Type 2	Vein Type 3	Sampling Notes	Purpose	Interval Description from PTFI log	Assays		
									Interval (m)	Cu %	Au ppm
TE04-09	65.5	massive pyrite/skarn	qz			qz veins in massive pyrite vein, wtf?	CL & FI (qz)	59.5-65.6 m - Tw, Quartz Sandstone, very fine grained pervasive silica alteration and	64-67	0.75	3.3
TE04-09	66	hornfels	mt	qz		Is this excessive py and qz veining at the contact?	CL & FI (qz)	65.6-97.85 m - Tw, Exoskarn, dioside-forsterite±green garnet-magnetite skarn,	64-67	0.75	3.3
TE04-09	66.5	hornfels	qz	qz-sulfide			CL & FI (qz)	65.6-97.85 m - Tw, Exoskarn, dioside-forsterite±green garnet-magnetite skarn,	64-67	0.75	3.3
TE04-09	71.5	skarn/hornfels	qz	sulfide		lots of x-cutting	CL & FI (qz)	65.6-97.85 m - Tw, Exoskarn, dioside-forsterite±green garnet-magnetite skarn,	69-72	0.25	0.7
TE04-09	83	skarn/hornfels	qz	qz-sulfiode			CL & FI (qz)	65.6-97.85 m - Tw, Exoskarn, dioside-forsterite±green garnet-magnetite skarn,	81-84	0.4	0.5
TE04-09	90	hornfels	qz	sulfide-qz		Much x-cutting.	CL & FI (qz)	65.6-97.85 m - Tw, Exoskarn, dioside-forsterite±green garnet-magnetite skarn,	88-90.5	0.8	1
TE04-09	90.5	hornfels	qz	sulfide-an		Massive qz with x-cutting sulfide-an vein.	CL & FI (qz & an)	65.6-97.85 m - Tw, Exoskarn, dioside-forsterite±green garnet-magnetite skarn,	90.5-93	1.1	1
TE04-09	91	hornfels	qz	sulfide-an		Similar to 90m.	Give context to other samples.	65.6-97.85 m - Tw, Exoskarn, dioside-forsterite±green garnet-magnetite skarn,	90.5-93	1.1	1
TE04-09	96.5	hornfels	qz	sulfide		Massive qz x-cut by sulfide veins. Right at hornfels-diorite contact.	CL & FI (qz)	65.6-97.85 m - Tw, Exoskarn, dioside-forsterite±green garnet-magnetite skarn,	95-97.5	1	0.9
TE04-09	97	hornfels	qz			Massive qz.	CL & FI (qz)	65.6-97.85 m - Tw, Exoskarn, dioside-forsterite±green garnet-magnetite skarn,	95-97.5	1	0.9
TE04-09	99.5	diorite	qz			Potassic alteration!	CL & FI (qz)	97.85-104.85 m - Te1, Diorite, lightgray-greenish gray, propylitic altered, locally	97.5-101	0.6	0.8
TE04-09	100.5	diorite	qz			Potassic alteration!	Paragenesis, CL & FI (qz)	97.85-104.85 m - Te1, Diorite, lightgray-greenish gray, propylitic altered, locally	97.5-101	0.6	0.8
TE04-09	110.5	hornfels	qz	qz-an		x-cutting relationships	CL & FI	104.85-133.1 m - Tw, Exoskarn, silicified, dominant diopside up to 111.00m, then	108-111	0.5	2.2
TE04-09	117	hornfels	qz+-sulfide				CL & FI (qz)	104.85-133.1 m - Tw, Exoskarn, silicified, dominant diopside up to 111.00m, then	114-117	0.6	1.8
TE04-09	129	hornfels	an			Not much else in this interval but calc-sils and anhydrite.	Give context to other samples.	104.85-133.1 m - Tw, Exoskarn, silicified, dominant diopside up to 111.00m, then	127-130	0.7	1
TE04-09	139.5	diorite/endo	qz-an-py			Large vein.	CL & FI (qz & an?)	133.1-EOH m - Te, Diorite, endoskarnoid, minor potassic alt from 145 m to EOH,	137.5-140	0.8	1.7
TE04-09	153.5	diorite	qz-an	qz-py			CL & FI (qz & an?)	133.1-EOH m - Te, Diorite, endoskarnoid, minor potassic alt from 145 m to EOH,	151-154	0.15	0.6
TE04-09	164.5	diorite	an-qz				CL & FI (qz & an?)	133.1-EOH m - Te, Diorite, endoskarnoid, minor potassic alt from 145 m to EOH,	163-166	0.2	0.6
TE04-09	177	diorite	an-qz			Coarse vein.	FI (an)	133.1-EOH m - Te, Diorite, endoskarnoid, minor potassic alt from 145 m to EOH,	177-180	0.1	0.3
TE04-09	197.5	diorite	qz	an		X-cutting veins.	Paragenesis, CL & FI (qz)	133.1-EOH m - Te, Diorite, endoskarnoid, minor potassic alt from 145 m to EOH,	194.5-197	0.3	0.6
TE04-09	207.5	diorite	py-qz-an				paragenesis	133.1-EOH m - Te, Diorite, endoskarnoid, minor potassic alt from 145 m to EOH,	207-210	0.7	1.4
TE04-09	221.5	diorite	qz				CL & FI (qz)	133.1-EOH m - Te, Diorite, endoskarnoid, minor potassic alt from 145 m to EOH,	219-222	0.3	1.2
TE04-09	234.5	diorite	qz-an-mt				Paragenesis, CL & FI (qz)	133.1-EOH m - Te, Diorite, endoskarnoid, minor potassic alt from 145 m to EOH,	234-237	0.6	1.7
DD03E-02						Split: 0-178					
DD03E-02	11	diorite	qz-py-an	qz-an		Veins x-cut.	CL & FI	0-62.6 m - Te1, Diorite (5b), gray-greenish gray, biotite>hornblende equigranular,	8.6-11.6	0.7467	1.72
DD03E-02	26.6	diorite	qz-py-an				CL & FI	0-62.6 m - Te1, Diorite (5b), gray-greenish gray, biotite>hornblende equigranular,	26.6-29.6	0.2871	0.91
DD03E-02	34.5	diorite	qz-py				CL & FI	0-62.6 m - Te1, Diorite (5b), gray-greenish gray, biotite>hornblende equigranular,	32.6-35.6	0.4214	0.55
DD03E-02	47	diorite	qz-py				CL & FI	0-62.6 m - Te1, Diorite (5b), gray-greenish gray, biotite>hornblende equigranular,	44.6-47.6	0.5482	1.16
DD03E-02	59.5	diorite	py-an-qz				CL & FI	0-62.6 m - Te1, Diorite (5b), gray-greenish gray, biotite>hornblende equigranular,	56.6-59.6	0.4311	0.52
DD03E-02	75.7	diorite	py-an-qz				CL & FI	62.6-113.8 m - Te2, Diorite (5b), green, hornblende>biotite, medium grained,	74.6-77.6	0.4767	0.59
DD03E-02	85.5	diorite	qz-py-mt				paragenesis	62.6-113.8 m - Te2, Diorite (5b), green, hornblende>biotite, medium grained,	83.6-86.6	0.2669	0.84
DD03E-02	87	diorite	mt-an-qz			Intergrown mt-an-qz vein? CL/FI?	Paragenesis, CL & FI (qz)	62.6-113.8 m - Te2, Diorite (5b), green, hornblende>biotite, medium grained,	86.6-89.6	0.3304	0.57
DD03E-02	99	diorite	qz+-an			Good to investigate qz paragenesis and CL/FI.	Paragenesis, CL & FI (qz)	62.6-113.8 m - Te2, Diorite (5b), green, hornblende>biotite, medium grained,	98.6-101.6	0.7839	1.97
DD03E-02	118.5	hornfels	an			Characteristic sample of an-veining.	Give context to other samples.	113.8-147.1 m - Tw, Exoskarn (1), greenish dark gray, forsterite, fine-medium	116.6-119.6	0.318	0.49
DD03E-02	132	diorite/hornfels/skarn	an			Diorite contact with hornfels/skarn. Massive an-skarn medley.	CL & FI (an)	113.8-147.1 m - Tw, Exoskarn (1), greenish dark gray, forsterite, fine-medium	132-135	<0.1	0.2

Hole ID	Depth (m)	Lithology/Alteration	Vein Type 1	Vein Type 2	Vein Type 3	Sampling Notes	Purpose	Interval Description from PTFI log	Assays		
									Interval (m)	Cu %	Au ppm
DD03E-02	155.5	endoskarn	an-calc sil			May end up investigating anhydrite up at this level to get FI data.	FI (an)	147.1-159.1 m - Te2, Diorite (5b), green, hornblende-biotite, fine-medium grained,	153.1-156.1	0.2182	0.23
DD03E-02	160	diorite	qz	qz-py-an		One of the few oppurtunities to collect qz veins at this hole.	paragenesis	159.1-164.2 m - Tw, Quartzite (8a), gray-dark gray, fine-medium grained,	159.1-161.6	0.9641	0.61
DD03E-02	164	diorite	qz-an	qz-an-py		qz-an-py x-cuts qz-an.	CL & FI (qz)	159.1-164.2 m - Tw, Quartzite (8a), gray-dark gray, fine-medium grained,	161.6-164.2	1.1	0.71
DD03E-02	171.5	diorite	qz			Excellent x-cutting qz veins for this hole.	CL & FI (qz)	164.2-180-8 m - Te2, Diorite(5b), grayish green same previous rock, propylitic with	171.1-174.1	0.4599	0.58
DD03E-02	176.6	diorite	qz-py-cu sulfide			Awesome vein for this hole.	CL & FI (qz)	164.2-180-8 m - Te2, Diorite(5b), grayish green same previous rock, propylitic with	174.1-177.6	0.4492	0.8
TE02-20											
TE02-20	19	endoskarn	qz-py-an				Paragenesis	0-346.5 m - Te1, Diorite (5b), gray, medium grain, biotite (8-10%)>-	19-22	0.25	0.8
TE02-20	39.5	endoskarn	py-qz	an			Paragenesis	0-346.5 m - Te1, Diorite (5b), gray, medium grain, biotite (8-10%)>-	38-41	0.2	0.5
TE02-20	52	diorite	qz				Paragenesis, CL & FI (qz)	0-346.5 m - Te1, Diorite (5b), gray, medium grain, biotite (8-10%)>-	52-55	0.2	0.5
TE02-20	59.5	diorite	calc-silicate	qz			Paragenesis	0-346.5 m - Te1, Diorite (5b), gray, medium grain, biotite (8-10%)>-	58-61	0.1	0.5
TE02-20	69.5	endoskarn	qz	n-py-unknown		unknown brown mineral	Paragenesis	0-346.5 m - Te1, Diorite (5b), gray, medium grain, biotite (8-10%)>-	67-70	0.2	0.6
TE02-20	87.5	endoskarn	qz	qz-py			Paragenesis	0-346.5 m - Te1, Diorite (5b), gray, medium grain, biotite (8-10%)>-	85-88	0.3	0.8
TE02-20	90.2	endoskarn	qz-py			Possibly two generations of quartz - transparent qz before py and opaque (cloudy quartz) after py.	Paragenesis, CL & FI (qz)	0-346.5 m - Te1, Diorite (5b), gray, medium grain, biotite (8-10%)>-	88-91	0.3	0.9
TE02-20	110	endoskarn	py-qz-an	qz		Good examples of larger "D-veins"	Paragenesis	0-346.5 m - Te1, Diorite (5b), gray, medium grain, biotite (8-10%)>-	109-112	0.4	5
TE02-20	169	endoskarn	qz	py-qz		sample is extremely complex, but might hold many of the x-cutting relationships in a single sample	Paragenesis	0-346.5 m - Te1, Diorite (5b), gray, medium grain, biotite (8-10%)>-	168-171	0.3	0.6
TE02-20	201	endoskarn	qz-py	py		Oversamples to study intensely quartz veined interal. Might relate sheeting seen in DMLZ07-03	Paragenesis, CL & FI (qz)	0-346.5 m - Te1, Diorite (5b), gray, medium grain, biotite (8-10%)>-	199-202	0.1	0.2
TE02-20	216.5	endoskarn	qz-py	py			Paragenesis, CL & FI (qz)	0-346.5 m - Te1, Diorite (5b), gray, medium grain, biotite (8-10%)>-	214-217	0.6	1
TE02-20	227	endoskarn	qz-cp-py			disseminated copper mineralization - green copper-oxide color in the wallrock	Paragenesis, CL & FI (qz)	0-346.5 m - Te1, Diorite (5b), gray, medium grain, biotite (8-10%)>-	226-229	1	2.9
TE02-20	241	endoskarn	qz	qz-py			Paragenesis, CL & FI (qz)	0-346.5 m - Te1, Diorite (5b), gray, medium grain, biotite (8-10%)>-	238-241	0.9	1.5
TE02-20	278	endoskarn	qz	qz-calc-silicate		qz veins lacking halos cross-cut qz-calc-silicate veins with 1cm white halos	Paragenesis, CL & FI (qz)	0-346.5 m - Te1, Diorite (5b), gray, medium grain, biotite (8-10%)>-	277-280	0.3	0.5
TE02-20	263	endoskarn	qz-an-py	py			Paragenesis, CL & FI (qz)	0-346.5 m - Te1, Diorite (5b), gray, medium grain, biotite (8-10%)>-	262-265	0.5	0.5
DMLZ05-05						Sampled 278.9-351.5. Split 0-EOH.					
DMLZ05-05	300.5	diorite	qz-py	qz-cu sulfide		This sample may be mislabled. It seems like it should come before the skarn like sample 295.5. Check the photo log to	CL & FI (qz)	296.1-310 m - Te, Endoskarn, green, tremolite-chlorite-epidote-brown garnet-	299.4-302.4	0.105	0.05
DMLZ05-05	295.5	diorite	qz-sulfide	magnetite		qz-sulfide vein x-cuts magnetite.	Paragenesis, CL & FI (qz)	296.1-310 m - Te, Endoskarn, green, tremolite-chlorite-epidote-brown garnet-	293.4-296.1	0.264	0.21
DMLZ05-05	300	skarn	qz-mafic/calc sil?				CL & FI	296.1-310 m - Te, Endoskarn, green, tremolite-chlorite-epidote-brown garnet-	299.4-302.4	0.105	0.05
DMLZ05-05	301	skarn	qz			Massive qz in breccia-like veining. Coarse crystals and cu-sulfides.	perpendicular c-axis cut (qz)	296.1-310 m - Te, Endoskarn, green, tremolite-chlorite-epidote-brown garnet-	299.4-302.4	0.105	0.05
DMLZ05-05	304.5	skarn	qz				CL & FI (qz)	296.1-310 m - Te, Endoskarn, green, tremolite-chlorite-epidote-brown garnet-	302.4-305	0.072	0.04
DMLZ05-05	310	diorite	qz			x-cutting qz veins. Over sampled to study intensely qz veined interval. Might relate to sheeting in DMLZ07-07	CL & FI (qz)	296.1-310 m - Te, Endoskarn, green, tremolite-chlorite-epidote-brown garnet-	310-312.5	0.09	0.09
DMLZ05-05	313.5	diorite	qz	sulfide		qz vein w/ x-cut sulfide. Over sampled to study intensely qz veined interval. Might relate to sheeting in DMLZ07-07	Paragenesis, CL & FI (qz)	310-458.4 m - Te, Diorite, greenish gray-whitish gray, equigranular mafic phenoryst	312.5-315	0.08	0.08
DMLZ05-05	314.5	diorite	qz			qz sheeted vein. Over sampled to study intensely qz veined interval. Might relate to sheeting in DMLZ07-07.	CL & FI (qz)	310-458.4 m - Te, Diorite, greenish gray-whitish gray, equigranular mafic phenoryst	312.5-315	0.08	0.08
DMLZ05-05	318.8	diorite	qz	cu-sulfide		Over sampled to study intensely qz veined interval. Might relate to sheeting in DMLZ07-07	Give context to other samples	310-458.4 m - Te, Diorite, greenish gray-whitish gray, equigranular mafic phenoryst	317.5-320.4	0.125	0.14
DMLZ05-05	318.9	diorite	qz			Tiny qz veins II. Big selvage. Early or distal sheeting? Over sampled to study intensely qz veined interval. Might relate to	CL & FI (qz)	310-458.4 m - Te, Diorite, greenish gray-whitish gray, equigranular mafic phenoryst	317.5-320.4	0.125	0.14
DMLZ05-05	324.5	diorite	qz	sulfide			Paragenesis, CL & FI (qz)	310-458.4 m - Te, Diorite, greenish gray-whitish gray, equigranular mafic phenoryst	323.4-326.4	0.153	1.04
DMLZ05-05	377	diorite				2 pieces. Massive qz and sulfide crystals. C-axis cut?	c-axis cut (qz)	310-458.4 m - Te, Diorite, greenish gray-whitish gray, equigranular mafic phenoryst	374.4-377.4	0.068	0.12
DMLZ05-05	342.5	diorite	qz-an	sulfide			CL & FI (qz)	310-458.4 m - Te, Diorite, greenish gray-whitish gray, equigranular mafic phenoryst	341.4-344.4	0.107	0.57
TE05-16											

Hole ID	Depth (m)	Lithology/Alteration	Vein Type 1	Vein Type 2	Vein Type 3	Sampling Notes	Purpose	Interval Description from PTFI log	Assays		
									Interval (m)	Cu %	Au ppm
TE05-16	2.5	diorite	qz-cp	biotite			Paragenesis, CL & FI (qz)	0-151.15 m - Te, Diorite, grey-dark grey locally whitish grey, medium-coarse grain,	0-3	0.136	0.06
TE05-16	20.5	diorite	qz	py-an	mt	mt stringer is earliest	Paragenesis, CL & FI (qz)	0-151.15 m - Te, Diorite, grey-dark grey locally whitish grey, medium-coarse grain,	18-21	0.064	0.02
TE05-16	26.5	diorite	qz	bt	py	bt stringer is earliest followed by quartz and finally pyrite.	Paragenesis, CL & FI (qz)	0-151.15 m - Te, Diorite, grey-dark grey locally whitish grey, medium-coarse grain,	24-27	0.192	0.07
TE05-16	30A	diorite	qz-cp	qz			Paragenesis, CL & FI (qz)	0-151.15 m - Te, Diorite, grey-dark grey locally whitish grey, medium-coarse grain,	30-33	0.241	0.12
TE05-16	30B	diorite	qz-cp	qz		The other half of sample A	Paragenesis, CL & FI (qz)	0-151.15 m - Te, Diorite, grey-dark grey locally whitish grey, medium-coarse grain,	30-33	0.241	0.12
TE05-16	40	diorite						0-151.15 m - Te, Diorite, grey-dark grey locally whitish grey, medium-coarse grain,	39-42	0.13	0.05
TE05-16	40.5	diorite	qz-cp-py	qz			Paragenesis, CL & FI (qz)	0-151.15 m - Te, Diorite, grey-dark grey locally whitish grey, medium-coarse grain,	39-42	0.13	0.05
TE05-16	49	diorite	qz-an-py	py-bn			Paragenesis, CL & FI (qz)	0-151.15 m - Te, Diorite, grey-dark grey locally whitish grey, medium-coarse grain,	48-51	0.05	0.04
TE05-16	173	diorite	qz-py	py-cp			Paragenesis, CL & FI (qz)	151.15-309.9 m - Te, Diorite,dark gray locally whitish gray-slight greenish	171-174	0.157	0.08
TE05-16	175.5	sheeted vein	qz	qz-py-cp			Sheeted Vein Study	151.15-309.9 m - Te, Diorite,dark gray locally whitish gray-slight greenish	174-177	0.343	0.11
TE05-16	177.5	sheeted vein	qz-py-an	qz-cp			Sheeted Vein Study	151.15-309.9 m - Te, Diorite,dark gray locally whitish gray-slight greenish	177-180	0.377	0.1
TE05-16	180	sheeted vein	qz-py	py		halos of these veins is potassic alteration	Sheeted Vein Study	151.15-309.9 m - Te, Diorite,dark gray locally whitish gray-slight greenish	180-183	0.179	0.07
TE05-16	180.5	sheeted vein	qz	qz-py	py-qz		Sheeted Vein Study	151.15-309.9 m - Te, Diorite,dark gray locally whitish gray-slight greenish	180-183	0.179	0.07
TE05-16	184.5	sheeted vein	qz	py			Sheeted Vein Study	151.15-309.9 m - Te, Diorite,dark gray locally whitish gray-slight greenish	183-186	0.176	0.11
TE05-16	188							151.15-309.9 m - Te, Diorite,dark gray locally whitish gray-slight greenish	186-189	0.343	0.12
TE05-16	189							151.15-309.9 m - Te, Diorite,dark gray locally whitish gray-slight greenish	189-192	0.141	0.09
TE05-16	194	sheeted vein	qz-bt	py		biotite pre-dates quartz	Sheeted Vein Study	151.15-309.9 m - Te, Diorite,dark gray locally whitish gray-slight greenish	192-195	0.101	0.09
TE05-16	198	sheeted vein	qz-py-an	qz		Two samples have this lable	Sheeted Vein Study	151.15-309.9 m - Te, Diorite,dark gray locally whitish gray-slight greenish	198-201	0.136	0.09
TE05-16	199.5	sheeted vein	qz	-(fe-carbonate)			Sheeted Vein Study	151.15-309.9 m - Te, Diorite,dark gray locally whitish gray-slight greenish	198-201	0.136	0.09
TE05-16	201.5							151.15-309.9 m - Te, Diorite,dark gray locally whitish gray-slight greenish	201-204	0.493	0.14
TE05-16	204							151.15-309.9 m - Te, Diorite,dark gray locally whitish gray-slight greenish	204-207	0.209	0.14
TE05-16	206.5	sheeted vein	qz-py-an	qz			Sheeted Vein Study	151.15-309.9 m - Te, Diorite,dark gray locally whitish gray-slight greenish	204-207	0.209	0.14
TE05-16	211.5	diorite	qz	qz-py	qz-cp		Paragenesis, CL & FI (qz)	151.15-309.9 m - Te, Diorite,dark gray locally whitish gray-slight greenish	210-213	0.257	0.09
TE05-16	227	diorite	qz-py-cp	cp-py-qz			Paragenesis, CL & FI (qz)	151.15-309.9 m - Te, Diorite,dark gray locally whitish gray-slight greenish	225-228	0.272	0.18
TE05-16	235.5	diorite						151.15-309.9 m - Te, Diorite,dark gray locally whitish gray-slight greenish	234-237	0.296	0.34
TE05-16	257	diorite	qz	qz-mo	qz-py		Paragenesis	151.15-309.9 m - Te, Diorite,dark gray locally whitish gray-slight greenish	255-258	0.153	0.3
TE05-16	265	diorite	qz	qz-cp			Paragenesis, CL & FI (qz)	151.15-309.9 m - Te, Diorite,dark gray locally whitish gray-slight greenish	264-267	0.39	0.52
TE05-16	265.5	diorite	qz-py-cp-an	qz	py-cp	sulfides lining the edges and center of the vein are good evidence for multiple fluid pulses. Py>qz>py+cp>an	Paragenesis, CL & FI (qz)	151.15-309.9 m - Te, Diorite,dark gray locally whitish gray-slight greenish	264-267	0.39	0.52
TE05-16	304.5	diorite	fe-carb?)-qz-py-mo				Paragenesis	151.15-309.9 m - Te, Diorite,dark gray locally whitish gray-slight greenish	303-306	0.683	0.39
TE05-16	312	diorite	qz-py-cp-an	qz-py-cp			Paragenesis, CL & FI (qz)	309.9-325.3 m - continue Te, diorite, greenish-dark gray equigranular	312-315	0.623	0.45
TE05-16	317	diorite	qz-an-py-cp				Paragenesis, CL & FI (qz)	309.9-325.3 m - continue Te, diorite, greenish-dark gray equigranular	315-317.5	0.633	0.42

APPENDIX C. FLUID INCLUSION MICROTHERMOMETRY DATA

Assemblage	Inclusion	Section	Type (classification 1-3)	Vapor Bubble (F=)	Size	Te (-C)	Tm ice (-C)	Th Sylvite (C)	Th halite (C)	Th bubble (C)	~ NaCl equiv	Daughters
1	11	DZ07-04-377.7	1	0.55		-9.7	2.3			373.3	3.9	chalcopyrite
1	12	DZ07-04-377.7	1	0.55			3.1			387	5.1	opaque (cp?)
2	44	TEW-09-01-1266	1	0.5	13	-13.3	3.7			395.7	6	0
2	45	TEW-09-01-1266	1	0.5	11	-11.5	2.8			383.1	4.6	0
3	63	TEW09-05-789	1	0.25	8	-12	2.1			338	3.5	opaque
3	64	TEW09-05-789	1	0.3	10					340		opaque
3	65	TEW09-05-789	1	0.3	10	-11.5	1.5			335	2.6	opaque
3	66	TEW09-05-789	1	0.3	8	-10.5	1.3			332	2.2	opaque
4	71	TEW09-05-789	1	0.45	11					398		
4	72	TEW09-05-789	1	0.55	27	19.1				394.9		
4	73	TEW09-05-789	1	0.6	10					398		
4	74	TEW09-05-789	1	0.4	15					389.1		
4	75	TEW09-05-789	3	0.5	13.75					377.7		
5	144	TEW09-05-789	1	0.6	25	52	4.1			380		none
5	145	TEW09-05-789	1	0.6	14					376		none
6	127	TEW09-01-934.9 Chip C (CL)	2a	0.7	20				88.4	420.1	27.66	
6	128	TEW09-01-934.9 Chip C (CL)	2a	0.7	16				167	389.5	30.35	
6	129	TEW09-01-934.9 Chip C (CL)	2a	0.7	16			170	200	368.3	51.29	
6	130	TEW09-01-934.9 Chip C (CL)	2a	0.75	10				318	286.7	39.6	
6	131	TEW09-01-934.9 Chip C (CL)	2a	0.7	17				179	382	30.88	
7	9	DZ07-04-377.7	2a	0.9					261	357.8	35.38	Halite, opaque (cp?)
7	10	DZ07-04-377.7	2a	0.9					224	389.3	33.14	Halite, opaque (cp?)
8	14	DZ07-04-377.7	3	0.6		-6.3	5.2			366	8.1	?
8	15	DZ07-04-377.7	2a	0.9					361.1	345	43.45	halite, opaque (mt or cp) plus very small second opaque
8	16	DZ07-04-377.7	2a	0.8					236	346.2	33.83	halite, transparent daughter
9	37	TE01-16-730.4	2a	0.7	15				137	347	29.17	Halite, transparent daughter
9	38	TE01-16-730.4	2a	0.8	8				152	371	29.74	Halite (suspect transparent daughter, but unclear)
9	39	TE01-16-730.4	2a	0.7	8				90	327	27.78	Halite
10	40	TE01-16-730.4	2a	0.7	12				243	337	34.25	Halite and opaque
10	41	TE01-16-730.4	2a	0.7	11				251	342	34.74	Halite and opaque
10	42	TE01-16-730.4	2a	0.7	6				233	319	33.65	Halite and opaque
10	43	TE01-16-730.4	2a	0.7	7				241	325	34.13	Halite and opaque
11	59	TEW09-05-789	2a	0.2	10				250	340	34.68	halite
11	60	TEW09-05-789	2a	0.2	5				214	345.8	32.6	halite
11	61	TEW09-05-789	2a	0.2	6.25				216	337.5	32.7	halite
11	62	TEW09-05-789	2a	0.2	9				220	370	32.92	halite, opaque
12	76	TEW09-05-789	2a	0.7	10				172.5	301.2	30.59	Halite, transparent daughter
12	77	TEW09-05-789	2a	0.7	11				168.8	280	30.43	Halite, opaque
13	78	TEW09-05-789	2a	0.8	16				183.6	338	31.09	Halite
13	79	TEW09-05-789	2a	0.8	12				184.4	301.7	31.12	Halite
13	80	TEW09-05-789	2a	0.7	10				182.5	312.5	31.04	Halite, transparent daughter
14	140	DZ07-07-180.8 (CL)	2a	0.75				86	284	380	45.61	Halite
14	141	DZ07-07-180.8 (CL)	2a	0.75					256	386	35	Halite
15	34	TE01-16-730.4	2b	0.3		-10.7	0.7			392	1.2	0
15	35	TE01-16-730.4	2b	0.3			1.2			365	2.1	0
15	36	TE01-16-730.4	2b	0.35			1.8			364	3.1	0
16	124	TEW09-01-934.9 Chip C (CL)	2b	0.35	12	-28	7.1			370	10.6	opaque
16	125	TEW09-01-934.9 Chip C (CL)	2b	0.3	15		7.3			380	10.9	opaque
16	126	TEW09-01-934.9 Chip C (CL)	2b	0.3	10		8			340	11.7	
17	137	DZ07-07-180.8 (CL)	2b	0.4	18	-65	3			382	5	
17	138	DZ07-07-180.8 (CL)	2b	0.35	16	-58	4.1			385	6.6	
17	139	DZ07-07-180.8 (CL)	2b	0.15	12		1.5			360		
18	143	TEW09-05-789	2b	0.1	14	52	4.5					none

19	25	TE01-16-730.4	3	0.7		-38	11.5			373.2	15.5		0
19	27	TE01-16-730.4	3	0.6		-28.8	12.8			390.5	16.7		0
19	30	TE01-16-730.4	3	0.7		-27.6	14.1			355	17.9	opaque, transparent(?)	
20	32	TE01-16-730.4	3	0.6		-29	4.9			361.4	7.7		0
20	33	TE01-16-730.4	3	0.55		-31	3.7			362.5	6		0
21	46	TEW-09-01-1266	3	0.5	10		3.2			378.8	5.3		0
21	47	TEW-09-01-1266	3	0.5	12	-14	2.4			376.1	4		0
21	48	TEW-09-01-1266	3	0.5	10		4.3			363.1	6.9		0
22	53	TEW-09-01-1266	3	0.6	12	-9.3	2.7			347.7	4.5	no daughters	
22	57	TEW-09-01-1266	3	0.6	12	-9	1.7			346.7	2.9	no daughters	
23	67	TEW09-05-789	3	0.7						384.9	13.2	cp	
23	68	TEW09-05-789	3	0.7						384	12.4	opaque?	
23	69	TEW09-05-789	3	0.6						384.2	13.3	opaque?	
24	81	TEW09-05-789 Chip A	3	0.6	11	-22	1.7			325.8	2.9		
24	82	TEW09-05-789 Chip A	3	0.6	15	-22	1.4			325.2	2.4		
24	83	TEW09-05-789 Chip A	3	0.75	13	-22.5	1.9			283.5	3.2		
24	84	TEW09-05-789 Chip A	3	0.6	9	-22	1.6			325	2.7		
24	85	TEW09-05-789 Chip A	3	0.55	19	-22	2			324	3.4		
24	86	TEW09-05-789 Chip A	3	0.6	23	-22	2.1			323.1	3.5		
24	87	TEW09-05-789 Chip A	3	0.7	25	-22	1.3			326	2.2		
25	88	TEW09-05-789 Chip A	3	0.7	9	-22	1.9			292.5	3.2		
25	89	TEW09-05-789 Chip A	3	0.85	11	-22	2.2			293.2	3.7		
25	90	TEW09-05-789 Chip A	3	0.75	7	-22	2.1			305.1	3.5		
25	91	TEW09-05-789 Chip A	3	0.8	10	-22	2.2			284.6	3.7		
26	93	TEW14-01-934.9 Chip A	3	0.7	9		6.9			340	10.4		
26	94	TEW14-01-934.9 Chip A	3	0.65	12	-27	6.6			344	10	opaque?	
26	95	TEW14-01-934.9 Chip A	3	0.65	7	-30	7.1			342	10.6		
26	96	TEW14-01-934.9 Chip A	3	0.75	9		8.5			330.4	12.3		
27	97	TEW14-01-934.9 Chip A	3	0.6	8		14.1			327	17.9		
27	98	TEW14-01-934.9 Chip A	3	0.6	6		13.9			324	17.7		
28	99	TEW14-01-934.9 Chip A	3	0.65	13	-26	6.8			332.2	10.2	opaque (cp)	
28	100	TEW14-01-934.9 Chip A	3	0.7	14		7.3			342	10.9	single opaque	
28	101	TEW14-01-934.9 Chip A	3	0.75	15		6.5			331.5	9.9	single opaque	
29	102	TEW14-01-934.9 Chip A	3	0.75	12	-5.6	1.2			351			
29	103	TEW14-01-934.9 Chip A	3	0.7	10	-50	6			356.1	9.2		
30	109	TEW09-01-934.9 Chip B (CL)	3	0.8	25	-45	7.1			320	10.1		
30	110	TEW09-01-934.9 Chip B (CL)	3	0.6	12	-56	7.1			347	10.6	opaque	
30	111	TEW09-01-934.9 Chip B (CL)	3	0.8	44	-42	6.9			322.3	10.9		
30	112	TEW09-01-934.9 Chip B (CL)	3	0.7	28	-40	7.5			322.9	11.1		
30	113	TEW09-01-934.9 Chip B (CL)	3	0.7	9		8.5			344.6	12.3		
30	114	TEW09-01-934.9 Chip B (CL)	3	0.6	8		7.3			350.8	10.9		
31	115	TEW09-01-934.9 Chip B (CL)	3	0.65	21	-60	8.1			342.4	11.8		
31	116	TEW09-01-934.9 Chip B (CL)	3	0.7	15	-61	8.1			335.5	11.8		
31	117	TEW09-01-934.9 Chip B (CL)	3	0.6	32	-40	7.6			332.1	11.2		
32	119	TEW09-01-934.9 Chip C (CL)	3	0.8	14	-61	19			360	23		
32	120	TEW09-01-934.9 Chip C (CL)	3	0.7	10	-58	19			403	23		
33	121	TEW09-01-934.9 Chip C (CL)	3	0.8	25	-45	14.3			390	18		
33	122	TEW09-01-934.9 Chip C (CL)	3	0.7	13	-48	23			390			
33	123	TEW09-01-934.9 Chip C (CL)	3	0.7	11	-38	24			373			
34	132	DZ07-07-180.8 (CL)	3	0.6	21	-24	-3			355.5	5		
34	133	DZ07-07-180.8 (CL)	3	0.5	12	-19.3	2.7			355.2	4.5		
34	134	DZ07-07-180.8 (CL)	3	0.6	10	-18.7	3.1			356.1	5.1		
34	135	DZ07-07-180.8 (CL)	3	0.6	27	-23.3	3.4			354.4	5.6		
34	136	DZ07-07-180.8 (CL)	3	0.55	20	-18.9	2.7			356.1	4.5		

APPENDIX D. LA-ICP-MS DATA

PPM:

Type1	PPM		
Assemblage	1	1	3
Element	FI11	FI12	as63-66
Li (7)	-	-	-
Na (23)	800	18182	5102
Mg (25)	782	-	-
K (39)	1006	-	3691
Ca (40)	2293	-	1129
Mn (55)	157	-	-
Fe (56)	2784	-	484
Cu (63)	318	-	-
Zn (66)	8499	-	-
As (75)	-	-	1335
Sr (88)	19	-	-
Mo (98)	-	-	-
Ag (107)	10	-	32
Sb (121)	-	-	-
Ba (138)	66	343	14
Au (197)	-	-	13
Pb (208)	302	81	114

2a	PPM																
Assemblage	8	8	9	9	9	10	10	11	11	12	12	13	13	13	14	14	14
Element	FI15	FI16	FI39	FI38	FI37	FI40	FI41	as59-62_187.5	as59-62_415	FI76	FI77	FI78	FI79	FI80	FI140	FI141	FI142
Li (7)	-	-	-	-	-	-	-	-	-	-	-	-	-	-	-	-	-
Na (23)	80655	63526	-	23171	22160	28019	20521	67305	21037	35537	18796	22729	63277	88095	48740	54308	54397
Mg (25)	-	-	-	-	-	-	-	-	-	-	-	-	-	-	329	-	-
K (39)	22270	26897	-	-	51363	29937	42917	16311	8968	37267	42770	34810	21314	16844	52615	33992	18990
Ca (40)	-	-	59361	20830	8869	36519	35313	4308	859	4883	6029	6149	3923	844	2153	1396	1944
Mn (55)	7730	-	-	-	2631	7455	7636	5757	1576	6529	10855	11060	5535	1503	5821	3906	5114
Fe (56)	30631	2755	14066	23557	44037	37726	40196	44094	13339	48362	55527	61181	35508	17337	86838	54365	63639
Cu (63)	-	47325	-	-	-	-	104	227	172	667	-	-	401	1816	2942	1199	2126
Zn (66)	13097	-	-	14614	1489	3087	1703	1123	407	1131	1573	1288	508	-	2372	2532	2923
As (75)	5052	-	-	-	-	-	-	327	125	463	1022	674	374	510	-	-	-
Sr (88)	-	-	-	308	33	438	328	75	16	90	104	119	63	28	127	96	136
Mo (98)	-	-	-	-	-	-	5	-	-	-	-	-	-	-	324	26	110
Ag (107)	-	-	-	-	-	20	5	-	7	6	-	7	9	-	11	-	9
Sb (121)	-	-	-	-	-	-	-	-	-	-	-	14	22	-	-	-	-
Ba (138)	-	-	-	614	30	63	40	27	5	24	22	27	20	13	39	26	43
Au (197)	-	-	-	-	-	-	-	-	-	2	-	-	-	-	-	-	-
Pb (208)	2422	287	545	2076	256	358	1379	753	294	743	304	348	695	428	1209	1287	1175

2b	PPM								
Assemblage	15	15	15	16	16	16	17	17	17
Element	FI34	FI35	FI36	FI124	FI125	FI126	as137-139_qz8	as137-139_qz9	FI137_qz7
Li (7)	-	-	-	-	-	-	-	-	-
Na (23)	325	784	-	8568	5508	22130	4907	9408	6363
Mg (25)	-	-	-	-	-	-	-	-	-
K (39)	972	695	-	16142	7109	7833	5933	3491	4739
Ca (40)	2802	604	8280	2658	-	-	806	1150	-
Mn (55)	-	-	-	2355	1122	-	917	870	555
Fe (56)	269	5702	954	14456	21749	7282	7283	3395	4988
Cu (63)	-	291	-	-	11768	11806	679	2213	-
Zn (66)	357	696	1247	1408	-	-	855	496	-
As (75)	-	-	-	-	-	-	-	-	-
Sr (88)	-	-	-	72	-	-	16	7	26
Mo (98)	-	-	-	-	104	97	19	51	-
Ag (107)	-	-	-	-	-	-	-	-	-
Sb (121)	-	-	121	-	-	-	-	-	-
Ba (138)	4	-	38	26	32	-	15	3	-
Au (197)	-	-	-	-	-	-	-	-	-
Pb (208)	17	-	62	58	64	181	297	150	86

Type 3	PPM												
Assemblage	20	24	24	24	24	26	26	27	27	28	28	28	29
Element	FI32	FI82	FI84	FI85	FI87	FI94	FI95	FI97	FI98	FI99	FI100	FI101	FI102
Li (7)	-	-	-	-	-	-	-	-	-	-	-	3185	616
Na (23)	16349	6220	6240	9018	5484	23710	15860	14134	16969	31575	28920	26224	5148
Mg (25)	-	-	-	-	-	-	-	-	-	-	-	-	-
K (39)	-	2001	3114	2978	3008	4645	-	5337	-	3094	-	2937	1237
Ca (40)	3458	1228	1472	1638	729	1132	-	-	30221	2336	-	1327	-
Mn (55)	-	82	119	70	125	-	-	-	-	502	-	-	-
Fe (56)	4688	34	37	-	69	2546	-	52163	5312	371	1974	514	45
Cu (63)	-	58	-	-	-	3338	-	-	-	-	1938	523	-
Zn (66)	1153	186	83	-	-	-	-	-	-	-	-	-	-
As (75)	618	-	-	-	-	-	-	-	-	-	-	-	-
Sr (88)	44	9	9	10	5	42	-	-	-	-	-	-	6
Mo (98)	-	-	-	-	-	-	-	88	-	-	-	-	-
Ag (107)	-	-	-	-	-	-	-	-	-	-	-	-	-
Sb (121)	-	18	-	-	-	-	-	-	-	-	-	-	-
Ba (138)	12	-	1	-	1	-	-	43	-	-	-	-	-
Au (197)	-	-	-	-	-	-	-	-	-	-	-	-	-
Pb (208)	408	-	31	-	24	93	226	-	444	125	-	31	22

Type 3	PPM													
Assemblage	30	30	30	31	31	31	32	32	33	33	33	34	34	34
Element	as109-113_97	as109-113_20	as109-113_30	FI115	FI116	FI117	FI119	FI120	FI121	FI122	FI123	as132-136_	as132-136_qz	as132-136_q
Li (7)	833	1584	767	-	-	-	-	-	-	-	-	-	-	-
Na (23)	37023	35047	33604	36387	36303	26952	34307	39366	35909	49323	55316	13362	12930	11320
Mg (25)	-	-	-	-	-	-	-	-	-	-	-	-	-	-
K (39)	1289	1612	6068	5595	-	-	27444	25145	22544	33802	35214	5334	5064	4987
Ca (40)	799	1102	1123	1471	3187	-	4258	4363	2964	4339	5013	1508	2764	1662
Mn (55)	513	544	427	403	-	-	4073	3506	3086	3999	2376	-	-	-
Fe (56)	740	652	959	484	-	-	21404	19128	11894	10710	4738	442	44	307
Cu (63)	1032	804	525	722	-	-	-	307	90	-	-	-	-	-
Zn (66)	282	-	267	-	-	-	2016	1115	1032	1135	1996	-	314	-
As (75)	135	-	85	-	-	-	-	-	-	-	-	-	-	-
Sr (88)	-	-	9	13	-	-	158	125	70	89	120	25	51	29
Mo (98)	-	-	-	-	-	-	-	-	9	-	-	-	-	-
Ag (107)	-	-	2	-	-	-	28	-	-	-	-	-	-	-
Sb (121)	36	36	22	-	-	-	-	-	-	-	-	-	-	-
Ba (138)	-	2	0	2	-	23	62	59	29	51	55	-	1	-
Au (197)	-	-	-	-	-	-	-	-	-	-	-	-	-	-
Pb (208)	76	70	92	59	-	141	443	397	420	478	642	68	16	45

Wt%:

Type1	Weight %		
Assemblage	1	1	3
Element	FI11	FI12	as63-66
Li (7)	-	-	-
Na (23)	0.2	4.62	1.3
Mg (25)	0.31	-	-
K (39)	0.19	-	0.7
Ca (40)	0.63	-	0.31
Mn (55)	0.04	-	-
Fe (56)	0.63	-	0.11
Cu (63)	0.07	-	-
Zn (66)	1.77	-	-
As (75)	-	-	0.32
Sr (88)	0.	-	-
Mo (98)	-	-	-
Ag (107)	0.	-	0.
Sb (121)	-	-	-
Ba (138)	0.01	0.05	0.
Au (197)	-	-	0.
Pb (208)	0.04	0.01	0.02

Type 2a	Weight %																
Assemblage	8	8	9	9	9	10	10	11	11	12	12	13	13	13	14	14	14
Element	FI15	FI16	FI39	FI38	FI37	FI40	FI41	as59-62_1	as59-62_415	FI76	FI77	FI78	FI79	FI80	FI140	FI141	FI142
Li (7)	-	-	-	-	-	-	-	-	-	-	-	-	-	-	-	-	-
Na (23)	20.5	16.15	-	5.89	5.63	7.12	5.22	17.11	5.35	9.03	4.78	5.78	16.09	22.39	12.39	13.81	13.83
Mg (25)	-	-	-	-	-	-	-	-	-	-	-	-	-	-	0.13	-	-
K (39)	4.25	5.13	-	-	9.79	5.71	8.18	3.11	1.71	7.11	8.16	6.64	4.06	3.21	10.03	6.48	3.62
Ca (40)	-	-	16.44	5.77	2.46	10.11	9.78	1.19	0.24	1.35	1.67	1.7	1.09	0.23	0.6	0.39	0.54
Mn (55)	1.77	-	-	-	0.6	1.71	1.75	1.32	0.36	1.5	2.49	2.53	1.27	0.34	1.33	0.89	1.17
Fe (56)	6.95	0.63	3.19	5.35	9.99	8.56	9.12	10.01	3.03	10.98	12.6	13.89	8.06	3.93	19.71	12.34	14.44
Cu (63)	-	10.01	-	-	-	-	0.02	0.05	0.04	0.14	-	-	0.08	0.38	0.62	0.25	0.45
Zn (66)	2.73	-	-	3.05	0.31	0.64	0.35	0.23	0.08	0.24	0.33	0.27	0.11	-	0.49	0.53	0.61
As (75)	1.22	-	-	-	-	-	-	0.08	0.03	0.11	0.25	0.16	0.09	0.12	-	-	-
Sr (88)	-	-	-	0.06	0.01	0.08	0.06	0.01	0.	0.02	0.02	0.02	0.01	0.01	0.02	0.02	0.02
Mo (98)	-	-	-	-	-	-	0.	-	-	-	-	-	-	-	0.06	0.	0.02
Ag (107)	-	-	-	-	-	0.	0.	-	0.	0.	-	0.	0.	-	0.	-	0.
Sb (121)	-	-	-	-	-	-	-	-	-	-	-	0.	0.	-	-	-	-
Ba (138)	-	-	-	0.09	0.	0.01	0.01	0.	0.	0.	0.	0.	0.	0.	0.01	0.	0.01
Au (197)	-	-	-	-	-	-	-	-	-	0.	-	-	-	-	-	-	-
Pb (208)	0.33	0.04	0.07	0.28	0.03	0.05	0.19	0.1	0.04	0.1	0.04	0.05	0.09	0.06	0.16	0.17	0.16

Type 3	**Weight %**												
Assemblage	20	24	24	24	24	26	26	27	27	28	28	28	29
Element	FI32	FI82	FI84	FI85	FI87	FI94	FI95	FI97	FI98	FI99	FI100	FI101	FI102
Li (7)	-	-	-	-	-	-	-	-	-	-	-	1.95	0.38
Na (23)	4.16	1.58	1.59	2.29	1.39	6.03	4.03	3.59	4.31	8.03	7.35	6.67	1.31
Mg (25)	-	-	-	-	-	-	-	-	-	-	-	-	-
K (39)	-	0.38	0.59	0.57	0.57	0.89	-	1.02	-	0.59	-	0.56	0.24
Ca (40)	0.96	0.34	0.41	0.45	0.2	0.31	-	-	8.37	0.65	-	0.37	-
Mn (55)	-	0.02	0.03	0.02	0.03	-	-	-	-	0.12	-	-	-
Fe (56)	1.06	0.01	0.01	-	0.02	0.58	-	11.84	1.21	0.08	0.45	0.12	0.01
Cu (63)	-	0.01	-	-	-	0.71	-	-	-	-	0.41	0.11	-
Zn (66)	0.24	0.04	0.02	-	-	-	-	-	-	-	-	-	-
As (75)	0.15	-	-	-	-	-	-	-	-	-	-	-	-
Sr (88)	0.01	0.	0.	0.	0.	0.01	-	-	-	-	-	-	0.
Mo (98)	-	-	-	-	-	-	-	0.02	-	-	-	-	-
Ag (107)	-	-	-	-	-	-	-	-	-	-	-	-	-
Sb (121)	-	0.	-	-	-	-	-	-	-	-	-	-	-
Ba (138)	0.	-	0.	-	0.	-	-	0.01	-	-	-	-	-
Au (197)	-	-	-	-	-	-	-	-	-	-	-	-	-
Pb (208)	0.05	-	0.	-	0.	0.01	0.03	-	0.06	0.02	-	0.	0.

Type 3	**Weight %**													
Assemblage	30	30	30	31	31	31	32	32	33	33	33	34	34	34
Element	as109-113_9	as109-113_22	as109-113_37	FI115	FI116	FI117	FI119	FI120	FI121	FI122	FI123	as132-136_q	as132-136_q	as132-136_q
Li (7)	0.51	0.97	0.47	-	-	-	-	-	-	-	-	-	-	-
Na (23)	9.41	8.91	8.54	9.25	9.23	6.85	8.72	10.01	9.13	12.54	14.06	3.4	3.29	2.88
Mg (25)	-	-	-	-	-	-	-	-	-	-	-	-	-	-
K (39)	0.25	0.31	1.16	1.07	-	-	5.23	4.79	4.3	6.45	6.71	1.02	0.97	0.95
Ca (40)	0.22	0.31	0.31	0.41	0.88	-	1.18	1.21	0.82	1.2	1.39	0.42	0.77	0.46
Mn (55)	0.12	0.12	0.1	0.09	-	-	0.93	0.8	0.71	0.92	0.54	-	-	-
Fe (56)	0.17	0.15	0.22	0.11	-	-	4.86	4.34	2.7	2.43	1.08	0.1	0.01	0.07
Cu (63)	0.22	0.17	0.11	0.15	-	-	-	0.06	0.02	-	-	-	-	-
Zn (66)	0.06	-	0.06	-	-	-	0.42	0.23	0.22	0.24	0.42	-	0.07	-
As (75)	0.03	-	0.02	-	-	-	-	-	-	-	-	-	-	-
Sr (88)	-	-	0.	0.	-	-	0.03	0.02	0.01	0.02	0.02	0.	0.01	0.01
Mo (98)	-	-	-	-	-	-	-	-	0.	-	-	-	-	-
Ag (107)	-	-	0.	-	-	-	0.	-	-	-	-	-	-	-
Sb (121)	0.01	0.01	0.	-	-	-	-	-	-	-	-	-	-	-
Ba (138)	-	0.	0.	0.	-	0.	0.01	0.01	0.	0.01	0.01	-	0.	-
Au (197)	-	-	-	-	-	-	-	-	-	-	-	-	-	-
Pb (208)	0.01	0.01	0.01	0.01	-	0.02	0.06	0.05	0.06	0.06	0.09	0.01	0.	0.01

APPENDIX E. LA-ICP-MS CORRELATION MATRICES COMPARISONS

ALL INCLUSIONS: IGNORING DETECTION LIMITS

	wt NaCl equiv	*Li (7)*	*Na (23)*	*Mg (25)*	*K (39)*	*Ca (40)*	*Mn (55)*	*Fe (56)*	*Cu (63)*	*Zn (66)*	*As (75)*	*Sr (88)*	*Mo (98)*	*Ag (107)*	*Sb (121)*	*Ba (138)*	*Au (197)*	*Pb (208)*
wt NaCl equiv	1.00																	
Li (7)	0.30	1.00																
Na (23)	0.76	0.13	1.00															
Mg (25)	-1.00		-1.00	1.00														
K (39)	0.85	0.00	0.49	-1.00	1.00													
Ca (40)	0.38	0.78	-0.01	1.00	0.46	1.00												
Mn (55)	0.81	0.76	0.36	-1.00	0.75	0.50	1.00											
Fe (56)	0.79	-0.01	0.38	-1.00	0.75	0.16	0.79	1.00										
Cu (63)	0.18	-0.47	0.16	-1.00	0.11	-0.22	-0.18	-0.13	1.00									
Zn (66)	0.38	1.00	0.26	1.00	0.13	0.36	0.22	0.16	0.11	1.00								
As (75)	0.46	1.00	0.34		0.16	0.31	0.38	0.11	0.45	0.99	1.00							
Sr (88)	0.63	1.00	0.19	-1.00	0.58	0.91	0.64	0.46	-0.04	0.44	0.71	1.00						
Mo (98)	0.43		0.29		0.36	-0.27	0.22	0.59	0.26	0.45		0.01	1.00					
Ag (107)	-0.26		-0.25	-1.00	-0.17	0.00	0.05	-0.27	0.57	0.21	0.90	0.40	0.92	1.00				
Sb (121)	-0.56	0.56	0.32		-0.66	0.76	-0.59	-0.40	0.93	0.64	-0.72	-0.63		-0.09	1.00			
Ba (138)	0.14	1.00	-0.01	1.00	0.50	0.39	0.35	0.09	0.11	0.89	0.31	0.50	0.36	0.31	0.72	1.00		
Au (197)	-1.00		-1.00		-1.00	-1.00		-1.00			1.00			1.00		-1.00	1.00	
Pb (208)	0.75	-0.38	0.55	-1.00	0.57	0.33	0.56	0.58	-0.19	0.75	0.88	0.61	0.15	-0.32	-0.47	0.52	-1.00	1.00
					Strong correlation 0.8 and above (+ or -)						Moderate correlation 0.5 to 0.8 (+ or -)							

All Inclusions: Ignoring Detection Limits with Elevation and T_h

	wt NaCl equiv	*Li (7)*	*Na (23)*	*Mg (25)*	*K (39)*	*Ca (40)*	*Mn (55)*	*Fe (56)*	*Cu (63)*	*Zn (66)*	*As (75)*	*Sr (88)*	*Mo (98)*	*Ag (107)*	*Sb (121)*	*Ba (138)*	*Au (197)*	*Pb (208)*	*Elevation*	*Th*
wt NaCl equiv	1.00																			
Li (7)	0.30	1.00																		
Na (23)	0.76	0.13	1.00																	
Mg (25)	-1.00		-1.00	1.00																
K (39)	0.85	0.00	0.49	-1.00	1.00															
Ca (40)	0.38	0.78	-0.01	1.00	0.46	1.00														
Mn (55)	0.81	0.76	0.36	-1.00	0.75	0.50	1.00													
Fe (56)	0.79	-0.01	0.38	-1.00	0.75	0.16	0.79	1.00												
Cu (63)	0.18	-0.47	0.16	-1.00	0.11	-0.22	-0.18	-0.13	1.00											
Zn (66)	0.38	1.00	0.26	1.00	0.13	0.36	0.22	0.16	0.11	1.00										
As (75)	0.46	1.00	0.34		0.16	0.31	0.38	0.11	0.45	0.99	1.00									
Sr (88)	0.63	1.00	0.19	-1.00	0.58	0.91	0.64	0.46	-0.04	0.44	0.71	1.00								
Mo (98)	0.43		0.29		0.36	-0.27	0.22	0.59	0.26	0.45		0.01	1.00							
Ag (107)	-0.26		-0.25	-1.00	-0.17	0.00	0.05	-0.27	0.57	0.21	0.90	0.40	0.92	1.00						
Sb (121)	-0.56	0.56	0.32		-0.66	0.76	-0.59	-0.40	0.93	0.64	-0.72	-0.63		-0.09	1.00					
Ba (138)	0.14	1.00	-0.01	1.00	0.50	0.39	0.35	0.09	0.11	0.89	0.31	0.50	0.36	0.31	0.72	1.00				
Au (197)	-1.00		-1.00		-1.00	-1.00		-1.00			1.00			1.00		-1.00	1.00			
Pb (208)	0.75	-0.38	0.55	-1.00	0.57	0.33	0.56	0.58	-0.19	0.75	0.88	0.61	0.15	-0.32	-0.47	0.52	-1.00	1.00		
Elevation	0.07		0.11	-1.00	-0.01	-0.25	-0.09	0.09	0.25	0.23	0.88	-0.22	0.24	-0.11	-0.51	0.03		0.15	1.00	
Th	-0.23	-0.40	-0.23	-1.00	-0.04	-0.13	-0.25	-0.22	0.04	0.06	0.15	0.02	-0.02	0.22	0.84	0.20	1.00	-0.06	0.23	1.00
					Strong correlation 0.8 and above (+ or -)						Moderate correlation 0.5 to 0.8 (+ or -)									

All Inclusions: 10% of Detection Limit

	wt NaCl equiv	*Li (7)*	*Na (23)*	*Mg (25)*	*K (39)*	*Ca (40)*	*Mn (55)*	*Fe (56)*	*Cu (63)*	*Zn (66)*	*As (75)*	*Sr (88)*	*Mo (98)*	*Ag (107)*	*Sb (121)*	*Ba (138)*	*Au (197)*	*Pb (208)*
wt NaCl equiv	1.00																	
Li (7)	0.23	1.00																
Na (23)	0.74	0.11	1.00															
Mg (25)	0.29	0.88	0.06	1.00														
K (39)	0.80	-0.18	0.49	-0.12	1.00													
Ca (40)	0.35	0.49	-0.10	0.57	0.16	1.00												
Mn (55)	0.76	-0.13	0.44	-0.09	0.80	0.22	1.00											
Fe (56)	0.80	-0.10	0.39	-0.02	0.76	0.17	0.79	1.00										
Cu (63)	0.17	0.17	0.20	0.20	0.09	-0.11	-0.11	-0.04	1.00									
Zn (66)	0.42	0.42	0.23	0.54	0.16	0.21	0.27	0.26	-0.07	1.00								
As (75)	0.37	0.41	0.36	0.44	0.13	0.03	0.37	0.17	-0.02	0.56	1.00							
Sr (88)	0.58	-0.03	0.22	0.03	0.55	0.52	0.60	0.51	-0.12	0.41	-0.03	1.00						
Mo (98)	0.36	0.10	0.12	0.20	0.24	0.03	0.10	0.50	0.26	0.12	0.01	0.06	1.00					
Ag (107)	0.38	0.73	0.11	0.85	0.03	0.59	0.09	0.11	0.15	0.51	0.48	0.24	0.20	1.00				
Sb (121)	0.19	0.80	0.03	0.85	-0.19	0.50	-0.10	-0.09	0.15	0.46	0.46	-0.05	0.09	0.71	1.00			
Ba (138)	0.18	0.28	0.02	0.35	-0.01	0.19	0.01	0.11	-0.06	0.60	0.01	0.46	0.08	0.32	0.29	1.00		
Au (197)	0.24	0.82	0.04	0.91	-0.14	0.52	-0.10	-0.06	0.19	0.45	0.51	0.01	0.13	0.90	0.80	0.33	1.00	
Pb (208)	0.76	0.36	0.55	0.45	0.48	0.29	0.54	0.56	-0.03	0.78	0.57	0.53	0.31	0.48	0.37	0.44	0.40	1.00
				Strong correlation 0.8 and above (+ or -)						Moderate correlation 0.5 to 0.8 (+ or -)								

All Inclusions: 10% of Detection Limit with Elevation and T_h

	wt NaCl equiv	Li (7)	Na (23)	Mg (25)	K (39)	Ca (40)	Mn (55)	Fe (56)	Cu (63)	Zn (66)	As (75)	Sr (88)	Mo (98)	Ag (107)	Sb (121)	Ba (138)	Au (197)	Pb (208)	Elevation	Th
wt NaCl equiv	1.00																			
Li (7)	0.23	1.00																		
Na (23)	0.74	0.11	1.00																	
Mg (25)	0.29	0.88	0.06	1.00																
K (39)	0.80	-0.18	0.49	-0.12	1.00															
Ca (40)	0.35	0.49	-0.10	0.57	0.16	1.00														
Mn (55)	0.76	-0.13	0.44	-0.09	0.80	0.22	1.00													
Fe (56)	0.80	-0.10	0.39	-0.02	0.76	0.17	0.79	1.00												
Cu (63)	0.17	0.17	0.20	0.20	0.09	-0.11	-0.11	-0.04	1.00											
Zn (66)	0.42	0.42	0.23	0.54	0.16	0.21	0.27	0.26	-0.07	1.00										
As (75)	0.37	0.41	0.36	0.44	0.13	0.03	0.37	0.17	-0.02	0.56	1.00									
Sr (88)	0.58	-0.03	0.22	0.03	0.55	0.52	0.60	0.51	-0.12	0.41	-0.03	1.00								
Mo (98)	0.36	0.10	0.12	0.20	0.24	0.03	0.10	0.50	0.26	0.12	0.01	0.06	1.00							
Ag (107)	0.38	0.73	0.11	0.85	0.03	0.59	0.09	0.11	0.15	0.51	0.48	0.24	0.20	1.00						
Sb (121)	0.19	0.80	0.03	0.85	-0.19	0.50	-0.10	-0.09	0.15	0.46	0.46	-0.05	0.09	0.71	1.00					
Ba (138)	0.18	0.28	0.02	0.35	-0.01	0.19	0.01	0.11	-0.06	0.60	0.01	0.46	0.08	0.32	0.29	1.00				
Au (197)	0.24	0.82	0.04	0.91	-0.14	0.52	-0.10	-0.06	0.19	0.45	0.51	0.01	0.13	0.90	0.80	0.33	1.00			
Pb (208)	0.76	0.36	0.55	0.45	0.48	0.29	0.54	0.56	-0.03	0.78	0.57	0.53	0.31	0.48	0.37	0.44	0.40	1.00		
Elevation	0.07	-0.01	0.16	0.06	0.05	-0.26	-0.03	0.08	0.20	0.15	0.09	-0.08	0.31	-0.01	-0.06	0.00	-0.02	0.19	1.00	
Th	-0.23	-0.15	-0.23	-0.07	-0.04	-0.13	-0.23	-0.20	0.02	0.11	-0.17	0.01	0.07	-0.16	-0.08	0.22	-0.11	-0.03	0.23	1.00
				Strong correlation 0.8 and above (+ or -)						Moderate correlation 0.5 to 0.8 (+ or -)										

All Inclusions: 1% of Detection Limit

	wt NaCl equiv	*Li (7)*	*Na (23)*	*Mg (25)*	*K (39)*	*Ca (40)*	*Mn (55)*	*Fe (56)*	*Cu (63)*	*Zn (66)*	*As (75)*	*Sr (88)*	*Mo (98)*	*Ag (107)*	*Sb (121)*	*Ba (138)*	*Au (197)*	*Pb (208)*
wt NaCl equiv	1.00																	
Li (7)	-0.05	1.00																
Na (23)	0.74	0.07	1.00															
Mg (25)	0.16	0.01	-0.03	1.00														
K (39)	0.79	-0.19	0.50	-0.04	1.00													
Ca (40)	0.35	0.02	-0.11	0.25	0.14	1.00												
Mn (55)	0.75	-0.16	0.44	-0.06	0.80	0.20	1.00											
Fe (56)	0.80	-0.18	0.39	0.07	0.75	0.17	0.79	1.00										
Cu (63)	0.16	-0.01	0.20	0.08	0.10	-0.13	-0.12	-0.04	1.00									
Zn (66)	0.40	-0.02	0.23	0.53	0.16	0.16	0.28	0.26	-0.11	1.00								
As (75)	0.34	0.01	0.36	0.12	0.16	-0.07	0.39	0.18	-0.06	0.53	1.00							
Sr (88)	0.57	-0.14	0.21	0.00	0.55	0.50	0.59	0.51	-0.13	0.42	-0.06	1.00						
Mo (98)	0.29	-0.10	0.10	0.20	0.26	-0.11	0.12	0.52	0.21	0.01	-0.08	0.05	1.00					
Ag (107)	0.25	-0.09	0.07	0.19	0.23	0.22	0.28	0.26	-0.05	0.18	0.17	0.39	0.10	1.00				
Sb (121)	-0.13	0.10	-0.13	-0.01	-0.20	0.11	-0.11	-0.14	-0.04	0.04	0.02	-0.14	-0.11	-0.07	1.00			
Ba (138)	0.17	-0.02	0.02	0.21	-0.02	0.18	0.00	0.11	-0.07	0.59	-0.06	0.44	-0.01	0.08	0.03	1.00		
Au (197)	0.28	0.06	0.06	0.34	-0.05	0.47	-0.02	0.04	0.14	0.35	0.38	0.00	-0.10	0.24	0.05	0.27	1.00	
Pb (208)	0.76	-0.05	0.55	0.29	0.46	0.29	0.53	0.56	-0.05	0.78	0.54	0.52	0.20	0.20	-0.05	0.43	0.41	1.00
					Strong correlation 0.8 and above (+ or -)						Moderate correlation 0.5 to 0.8 (+ or -)							

All Inclusions: 1% of Detection Limit with Elevation and T_h

	wt NaCl equiv	Li (7)	Na (23)	Mg (25)	K (39)	Ca (40)	Mn (55)	Fe (56)	Cu (63)	Zn (66)	As (75)	Sr (88)	Mo (98)	Ag (107)	Sb (121)	Ba (138)	Au (197)	Pb (208)	Elevation	Th
wt NaCl equiv	1.00																			
Li (7)	-0.05	1.00																		
Na (23)	0.74	0.07	1.00																	
Mg (25)	0.16	0.01	-0.03	1.00																
K (39)	0.79	-0.19	0.50	-0.04	1.00															
Ca (40)	0.35	0.02	-0.11	0.25	0.14	1.00														
Mn (55)	0.75	-0.16	0.44	-0.06	0.80	0.20	1.00													
Fe (56)	0.80	-0.18	0.39	0.07	0.75	0.17	0.79	1.00												
Cu (63)	0.16	-0.01	0.20	0.08	0.10	-0.13	-0.12	-0.04	1.00											
Zn (66)	0.40	-0.02	0.23	0.53	0.16	0.16	0.28	0.26	-0.11	1.00										
As (75)	0.34	0.01	0.36	0.12	0.16	-0.07	0.39	0.18	-0.06	0.53	1.00									
Sr (88)	0.57	-0.14	0.21	0.00	0.55	0.50	0.59	0.51	-0.13	0.42	-0.06	1.00								
Mo (98)	0.29	-0.10	0.10	0.20	0.26	-0.11	0.12	0.52	0.21	0.01	-0.08	0.05	1.00							
Ag (107)	0.25	-0.09	0.07	0.19	0.23	0.22	0.28	0.26	-0.05	0.18	0.17	0.39	0.10	1.00						
Sb (121)	-0.13	0.10	-0.13	-0.01	-0.20	0.11	-0.11	-0.14	-0.04	0.04	0.02	-0.14	-0.11	-0.07	1.00					
Ba (138)	0.17	-0.02	0.02	0.21	-0.02	0.18	0.00	0.11	-0.07	0.59	-0.06	0.44	-0.01	0.08	0.03	1.00				
Au (197)	0.28	0.06	0.06	0.34	-0.05	0.47	-0.02	0.04	0.14	0.35	0.38	0.00	-0.10	0.24	0.05	0.27	1.00			
Pb (208)	0.76	-0.05	0.55	0.29	0.46	0.29	0.53	0.56	-0.05	0.78	0.54	0.52	0.20	0.20	-0.05	0.43	0.41	1.00		
Elevation	0.07	-0.05	0.16	0.27	0.06	-0.27	-0.03	0.08	0.20	0.15	0.10	-0.09	0.31	-0.04	-0.19	0.00	-0.06	0.19	1.00	
Th	-0.23	-0.17	-0.23	0.10	-0.04	-0.13	-0.22	-0.20	0.02	0.12	-0.16	0.01	0.09	-0.15	-0.01	0.23	-0.20	-0.03	0.23	1.00
				Strong correlation 0.8 and above (+ or -)						Moderate correlation 0.5 to 0.8 (+ or -)										

All Inclusions: Number of Pairs

	wt NaCl equiv	*Li (7)*	*Na (23)*	*Mg (25)*	*K (39)*	*Ca (40)*	*Mn (55)*	*Fe (56)*	*Cu (63)*	*Zn (66)*	*As (75)*	*Sr (88)*	*Mo (98)*	*Ag (107)*	*Sb (121)*	*Ba (138)*	*Au (197)*	*Pb (208)*
wt NaCl equiv																		
Li (7)	5																	
Na (23)	59	5																
Mg (25)	2	0	2															
K (39)	51	5	51	2														
Ca (40)	49	4	46	2	42													
Mn (55)	36	3	36	2	36	33												
Fe (56)	57	5	54	2	50	48	35											
Cu (63)	29	4	29	2	28	23	21	29										
Zn (66)	36	2	34	2	32	35	27	36	18									
As (75)	12	2	12	0	11	11	10	12	7	10								
Sr (88)	37	2	37	2	35	36	30	36	18	28	9							
Mo (98)	12	0	12	1	12	7	9	12	11	7	0	7						
Ag (107)	12	1	12	2	12	12	11	12	8	11	6	11	3					
Sb (121)	8	3	6	0	6	8	6	8	5	7	4	4	0	3				
Ba (138)	41	2	39	2	35	36	30	39	19	31	10	30	10	12	6			
Au (197)	2	0	2	0	2	2	1	2	1	1	2	1	0	2	0	2		
Pb (208)	55	5	52	2	46	45	34	52	25	33	12	35	11	12	7	40	2	

	wt NaCl equiv	*Li (7)*	*Na (23)*	*Mg (25)*	*K (39)*	*Ca (40)*	*Mn (55)*	*Fe (56)*	*Cu (63)*	*Zn (66)*	*As (75)*	*Sr (88)*	*Mo (98)*	*Ag (107)*	*Sb (121)*	*Ba (138)*	*Au (197)*	*Pb (208)*	*Elevation*	*Th*
wt NaCl equiv																				
Li (7)	5																			
Na (23)	59	5																		
Mg (25)	2	0	2																	
K (39)	51	5	51	2																
Ca (40)	49	4	46	2	42															
Mn (55)	36	3	36	2	36	33														
Fe (56)	57	5	54	2	50	48	35													
Cu (63)	29	4	29	2	28	23	21	29												
Zn (66)	36	2	34	2	32	35	27	36	18											
As (75)	12	2	12	0	11	11	10	12	7	10										
Sr (88)	37	2	37	2	35	36	30	36	18	28	9									
Mo (98)	12	0	12	1	12	7	9	12	11	7	0	7								
Ag (107)	12	1	12	2	12	12	11	12	8	11	6	11	3							
Sb (121)	8	3	6	0	6	8	6	8	5	7	4	4	0	3						
Ba (138)	41	2	39	2	35	36	30	39	19	31	10	30	10	12	6					
Au (197)	2	0	2	0	2	2	1	2	1	1	2	1	0	2	0	2				
Pb (208)	55	5	52	2	46	45	34	52	25	33	12	35	11	12	7	40	2			
Elevation	62	5	59	2	51	49	36	57	29	36	12	37	12	12	8	41	2	55		
Th	62	5	59	2	51	49	36	57	29	36	12	37	12	12	8	41	2	55	62	

Type 1: Inclusions: Ignoring Detection Limits

	wt NaCl equiv	*Li (7)*	*Na (23)*	*Mg (25)*	*K (39)*	*Ca (40)*	*Mn (55)*	*Fe (56)*	*Cu (63)*	*Zn (66)*	*As (75)*	*Sr (88)*	*Mo (98)*	*Ag (107)*	*Sb (121)*	*Ba (138)*	*Au (197)*	*Pb (208)*
wt NaCl equiv	1.00																	
Li (7)		1.00																
Na (23)	0.74		1.00															
Mg (25)				1.00														
K (39)	-1.00		1.00		1.00													
Ca (40)	1.00		-1.00		-1.00	1.00												
Mn (55)							1.00											
Fe (56)	1.00		-1.00		-1.00	1.00		1.00										
Cu (63)									1.00									
Zn (66)										1.00								
As (75)											1.00							
Sr (88)												1.00						
Mo (98)													1.00					
Ag (107)	-1.00		1.00		1.00	-1.00		-1.00						1.00				
Sb (121)															1.00			
Ba (138)	0.94		0.93		-1.00	1.00		1.00						-1.00		1.00		
Au (197)																	1.00	
Pb (208)	-0.16		-0.79		-1.00	1.00		1.00						-1.00		-0.49		1.00

		Strong correlation 0.8 and above (+ or -)						Moderate correlation 0.5 to 0.8 (+ or -)						Low correlation 0.2 to 0.5 (+ or -)				

Type 1: Ignoring Detection Limits with Elevation and T_h

	wt NaCl equiv	*Li (7)*	*Na (23)*	*Mg (25)*	*K (39)*	*Ca (40)*	*Mn (55)*	*Fe (56)*	*Cu (63)*	*Zn (66)*	*As (75)*	*Sr (88)*	*Mo (98)*	*Ag (107)*	*Sb (121)*	*Ba (138)*	*Au (197)*	*Pb (208)*	*Elevation*	*Th*
wt NaCl eq	1.00																			
Li (7)		1.00																		
Na (23)	0.74		1.00																	
Mg (25)				1.00																
K (39)	-1.00		1.00		1.00															
Ca (40)	1.00		-1.00		-1.00	1.00														
Mn (55)							1.00													
Fe (56)	1.00		-1.00		-1.00	1.00		1.00												
Cu (63)									1.00											
Zn (66)										1.00										
As (75)											1.00									
Sr (88)												1.00								
Mo (98)													1.00							
Ag (107)	-1.00		1.00		1.00	-1.00		-1.00						1.00						
Sb (121)															1.00					
Ba (138)	0.94		0.93		-1.00	1.00		1.00						-1.00		1.00				
Au (197)																	1.00			
Pb (208)	-0.16		-0.79		-1.00	1.00		1.00						-1.00		-0.49		1.00		
Elevation	0.85		0.28		-1.00	1.00		1.00						-1.00		0.62		0.37	1.00	
Th	0.96		0.51		-1.00	1.00		1.00						-1.00		0.80		0.13	0.97	1.00
				Strong correlation 0.8 and above (+ or -)						Moderate correlation 0.5 to 0.8 (+ or -)						Low correlation 0.2 to 0.5 (+ or -)				

Type 1: 10% of Detection Limit

	wt NaCl equiv	*Li (7)*	*Na (23)*	*Mg (25)*	*K (39)*	*Ca (40)*	*Mn (55)*	*Fe (56)*	*Cu (63)*	*Zn (66)*	*As (75)*	*Sr (88)*	*Mo (98)*	*Ag (107)*	*Sb (121)*	*Ba (138)*	*Au (197)*	*Pb (208)*
wt NaCl eq	1.00																	
Li (7)	0.60	1.00																
Na (23)	0.74	0.98	1.00															
Mg (25)	0.33	-0.56	-0.39	1.00														
K (39)	-0.94	-0.28	-0.46	-0.64	1.00													
Ca (40)	-0.48	-0.99	-0.94	0.67	0.14	1.00												
Mn (55)	0.30	-0.59	-0.42	1.00	-0.61	0.70	1.00											
Fe (56)	-0.18	-0.89	-0.79	0.87	-0.17	0.95	0.89	1.00										
Cu (63)	0.20	-0.67	-0.51	0.99	-0.53	0.77	0.99	0.93	1.00									
Zn (66)	-0.01	-0.81	-0.68	0.94	-0.33	0.88	0.95	0.99	0.98	1.00								
As (75)	-0.82	-0.04	-0.23	-0.81	0.97	-0.11	-0.79	-0.41	-0.72	-0.56	1.00							
Sr (88)	1.00	0.52	0.67	0.42	-0.97	-0.39	0.39	-0.08	0.29	0.09	-0.88	1.00						
Mo (98)	0.62	1.00	0.99	-0.54	-0.30	-0.99	-0.57	-0.88	-0.65	-0.80	-0.06	0.53	1.00					
Ag (107)	-0.92	-0.23	-0.41	-0.68	1.00	0.09	-0.65	-0.23	-0.57	-0.39	0.98	-0.95	-0.25	1.00				
Sb (121)	0.67	1.00	1.00	-0.48	-0.37	-0.97	-0.51	-0.85	-0.59	-0.75	-0.13	0.59	1.00	-0.32	1.00			
Ba (138)	0.94	0.84	0.93	-0.02	-0.76	-0.75	-0.05	-0.50	-0.15	-0.36	-0.58	0.90	0.85	-0.73	0.88	1.00		
Au (197)	-0.74	0.09	-0.10	-0.88	0.93	-0.23	-0.86	-0.53	-0.80	-0.66	0.99	-0.81	0.07	0.95	0.00	-0.47	1.00	
Pb (208)	-0.16	-0.89	-0.79	0.88	-0.19	0.95	0.89	1.00	0.93	0.99	-0.42	-0.07	-0.88	-0.24	-0.84	-0.49	-0.54	1.00

Strong correlation 0.8 and above (+ or -)

Moderate correlation 0.5 to 0.8 (+ or -)

Low correlation 0.2 to 0.5 (+ or -)

Type 1: 10% of Detection Limit with Elevation and T_h

	wt NaCl equiv	*Li (7)*	*Na (23)*	*Mg (25)*	*K (39)*	*Ca (40)*	*Mn (55)*	*Fe (56)*	*Cu (63)*	*Zn (66)*	*As (75)*	*Sr (88)*	*Mo (98)*	*Ag (107)*	*Sb (121)*	*Ba (138)*	*Au (197)*	*Pb (208)*	*Elevation*	*Th*
wt NaCl eq	1.00																			
Li (7)	0.60	1.00																		
Na (23)	0.74	0.98	1.00																	
Mg (25)	0.33	-0.56	-0.39	1.00																
K (39)	-0.94	-0.28	-0.46	-0.64	1.00															
Ca (40)	-0.48	-0.99	-0.94	0.67	0.14	1.00														
Mn (55)	0.30	-0.59	-0.42	1.00	-0.61	0.70	1.00													
Fe (56)	-0.18	-0.89	-0.79	0.87	-0.17	0.95	0.89	1.00												
Cu (63)	0.20	-0.67	-0.51	0.99	-0.53	0.77	0.99	0.93	1.00											
Zn (66)	-0.01	-0.81	-0.68	0.94	-0.33	0.88	0.95	0.99	0.98	1.00										
As (75)	-0.82	-0.04	-0.23	-0.81	0.97	-0.11	-0.79	-0.41	-0.72	-0.56	1.00									
Sr (88)	1.00	0.52	0.67	0.42	-0.97	-0.39	0.39	-0.08	0.29	0.09	-0.88	1.00								
Mo (98)	0.62	1.00	0.99	-0.54	-0.30	-0.99	-0.57	-0.88	-0.65	-0.80	-0.06	0.53	1.00							
Ag (107)	-0.92	-0.23	-0.41	-0.68	1.00	0.09	-0.65	-0.23	-0.57	-0.39	0.98	-0.95	-0.25	1.00						
Sb (121)	0.67	1.00	1.00	-0.48	-0.37	-0.97	-0.51	-0.85	-0.59	-0.75	-0.13	0.59	1.00	-0.32	1.00					
Ba (138)	0.94	0.84	0.93	-0.02	-0.76	-0.75	-0.05	-0.50	-0.15	-0.36	-0.58	0.90	0.85	-0.73	0.88	1.00				
Au (197)	-0.74	0.09	-0.10	-0.88	0.93	-0.23	-0.86	-0.53	-0.80	-0.66	0.99	-0.81	0.07	0.95	0.00	-0.47	1.00			
Pb (208)	-0.16	-0.89	-0.79	0.88	-0.19	0.95	0.89	1.00	0.93	0.99	-0.42	-0.07	-0.88	-0.24	-0.84	-0.49	-0.54	1.00		
Elevation	0.85	0.09	0.28	0.77	-0.98	0.05	0.75	0.36	0.68	0.51	-1.00	0.90	0.11	-0.99	0.18	0.62	-0.98	0.37	1.00	
Th	0.96	0.34	0.51	0.59	-1.00	-0.20	0.56	0.11	0.47	0.28	-0.95	0.98	0.36	-0.99	0.43	0.80	-0.90	0.13	0.97	1.00
				Strong correlation 0.8 and above (+ or -)						Moderate correlation 0.5 to 0.8 (+ or -)				Low correlation 0.2 to 0.5 (+ or -)						

Type 1: 1% of Detection Limit

	wt NaCl equiv	*Li (7)*	*Na (23)*	*Mg (25)*	*K (39)*	*Ca (40)*	*Mn (55)*	*Fe (56)*	*Cu (63)*	*Zn (66)*	*As (75)*	*Sr (88)*	*Mo (98)*	*Ag (107)*	*Sb (121)*	*Ba (138)*	*Au (197)*	*Pb (208)*
wt NaCl equiv	1.00																	
Li (7)	0.60	1.00																
Na (23)	0.74	0.98	1.00															
Mg (25)	0.00	-0.80	-0.67	1.00														
K (39)	-0.96	-0.35	-0.52	-0.29	1.00													
Ca (40)	-0.51	-0.99	-0.96	0.86	0.24	1.00												
Mn (55)	0.00	-0.80	-0.67	1.00	-0.28	0.86	1.00											
Fe (56)	-0.19	-0.90	-0.80	0.98	-0.10	0.94	0.98	1.00										
Cu (63)	-0.01	-0.81	-0.68	1.00	-0.28	0.86	1.00	0.98	1.00									
Zn (66)	-0.02	-0.82	-0.69	1.00	-0.26	0.87	1.00	0.99	1.00	1.00								
As (75)	-0.85	-0.09	-0.27	-0.53	0.96	-0.02	-0.53	-0.36	-0.52	-0.51	1.00							
Sr (88)	0.13	-0.71	-0.57	0.99	-0.41	0.78	0.99	0.95	0.99	0.99	-0.63	1.00						
Mo (98)	0.62	1.00	0.99	-0.79	-0.37	-0.99	-0.79	-0.89	-0.79	-0.80	-0.11	-0.70	1.00					
Ag (107)	-0.97	-0.37	-0.54	-0.26	1.00	0.27	-0.26	-0.07	-0.25	-0.23	0.96	-0.38	-0.39	1.00				
Sb (121)	0.67	1.00	1.00	-0.74	-0.43	-0.98	-0.74	-0.85	-0.75	-0.76	-0.18	-0.65	1.00	-0.46	1.00			
Ba (138)	0.94	0.84	0.93	-0.34	-0.80	-0.77	-0.34	-0.51	-0.35	-0.37	-0.62	-0.22	0.85	-0.82	0.88	1.00		
Au (197)	-0.74	0.09	-0.10	-0.67	0.90	-0.20	-0.67	-0.52	-0.66	-0.65	0.98	-0.76	0.07	0.89	0.00	-0.47	1.00	
Pb (208)	-0.16	-0.89	-0.79	0.99	-0.12	0.93	0.99	1.00	0.99	0.99	-0.38	0.96	-0.88	-0.09	-0.84	-0.49	-0.54	1.00

Strong correlation 0.8 and above (+ or -)

Moderate correlation 0.5 to 0.8 (+ or -)

Low correlation 0.2 to 0.5 (+ or -)

Type 1: 1% of Detection Limit with Elevation and T_h

	wt NaCl equiv	Li (7)	Na (23)	Mg (25)	K (39)	Ca (40)	Mn (55)	Fe (56)	Cu (63)	Zn (66)	As (75)	Sr (88)	Mo (98)	Ag (107)	Sb (121)	Ba (138)	Au (197)	Pb (208)	Elevation	Th
wt NaCl eq	1.00																			
Li (7)	0.60	1.00																		
Na (23)	0.74	0.98	1.00																	
Mg (25)	0.00	-0.80	-0.67	1.00																
K (39)	-0.96	-0.35	-0.52	-0.29	1.00															
Ca (40)	-0.51	-0.99	-0.96	0.86	0.24	1.00														
Mn (55)	0.00	-0.80	-0.67	1.00	-0.28	0.86	1.00													
Fe (56)	-0.19	-0.90	-0.80	0.98	-0.10	0.94	0.98	1.00												
Cu (63)	-0.01	-0.81	-0.68	1.00	-0.28	0.86	1.00	0.98	1.00											
Zn (66)	-0.02	-0.82	-0.69	1.00	-0.26	0.87	1.00	0.99	1.00	1.00										
As (75)	-0.85	-0.09	-0.27	-0.53	0.96	-0.02	-0.53	-0.36	-0.52	-0.51	1.00									
Sr (88)	0.13	-0.71	-0.57	0.99	-0.41	0.78	0.99	0.95	0.99	0.99	-0.63	1.00								
Mo (98)	0.62	1.00	0.99	-0.79	-0.37	-0.99	-0.79	-0.89	-0.79	-0.80	-0.11	-0.70	1.00							
Ag (107)	-0.97	-0.37	-0.54	-0.26	1.00	0.27	-0.26	-0.07	-0.25	-0.23	0.96	-0.38	-0.39	1.00						
Sb (121)	0.67	1.00	1.00	-0.74	-0.43	-0.98	-0.74	-0.85	-0.75	-0.76	-0.18	-0.65	1.00	-0.46	1.00					
Ba (138)	0.94	0.84	0.93	-0.34	-0.80	-0.77	-0.34	-0.51	-0.35	-0.37	-0.62	-0.22	0.85	-0.82	0.88	1.00				
Au (197)	-0.74	0.09	-0.10	-0.67	0.90	-0.20	-0.67	-0.52	-0.66	-0.65	0.98	-0.76	0.07	0.89	0.00	-0.47	1.00			
Pb (208)	-0.16	-0.89	-0.79	0.99	-0.12	0.93	0.99	1.00	0.99	0.99	-0.38	0.96	-0.88	-0.09	-0.84	-0.49	-0.54	1.00		
Elevation	0.85	0.09	0.28	0.52	-0.97	0.01	0.52	0.35	0.52	0.50	-1.00	0.63	0.11	-0.96	0.18	0.62	-0.98	0.37	1.00	
Th	0.96	0.34	0.51	0.29	-1.00	-0.24	0.29	0.10	0.28	0.26	-0.97	0.41	0.36	-1.00	0.43	0.80	-0.90	0.13	0.97	1.00
				Strong correlation 0.8 and above (+ or -)						Moderate correlation 0.5 to 0.8 (+ or -)					Low correlation 0.2 to 0.5 (+ or -)					

Type 1: Number of Pairs:

	wt NaCl equiv	*Li (7)*	*Na (23)*	*Mg (25)*	*K (39)*	*Ca (40)*	*Mn (55)*	*Fe (56)*	*Cu (63)*	*Zn (66)*	*As (75)*	*Sr (88)*	*Mo (98)*	*Ag (107)*	*Sb (121)*	*Ba (138)*	*Au (197)*	*Pb (208)*
wt NaCl equiv																		
Li (7)	0																	
Na (23)	3	0																
Mg (25)	1	0	1															
K (39)	2	0	2	1														
Ca (40)	2	0	2	1	2													
Mn (55)	1	0	1	1	1	1												
Fe (56)	2	0	2	1	2	2	1											
Cu (63)	1	0	1	1	1	1	1	1										
Zn (66)	1	0	1	1	1	1	1	1	1									
As (75)	1	0	1	0	1	1	0	1	0	0								
Sr (88)	1	0	1	1	1	1	1	1	1	1	0							
Mo (98)	0	0	0	0	0	0	0	0	0	0	0	0						
Ag (107)	2	0	2	1	2	2	1	2	1	1	1	1	0					
Sb (121)	0	0	0	0	0	0	0	0	0	0	0	0	0	0				
Ba (138)	3	0	3	1	2	2	1	2	1	1	1	1	0	2	0			
Au (197)	1	0	1	0	1	1	0	1	0	0	1	0	0	1	0	1		
Pb (208)	3	0	3	1	2	2	1	2	1	1	1	1	0	2	0	3	1	

	wt NaCl equiv	Li (7)	Na (23)	Mg (25)	K (39)	Ca (40)	Mn (55)	Fe (56)	Cu (63)	Zn (66)	As (75)	Sr (88)	Mo (98)	Ag (107)	Sb (121)	Ba (138)	Au (197)	Pb (208)	Elevation	Th
wt NaCl equiv																				
Li (7)	0																			
Na (23)	3	0																		
Mg (25)	1	0	1																	
K (39)	2	0	2	1																
Ca (40)	2	0	2	1	2															
Mn (55)	1	0	1	1	1	1														
Fe (56)	2	0	2	1	2	2	1													
Cu (63)	1	0	1	1	1	1	1	1												
Zn (66)	1	0	1	1	1	1	1	1	1											
As (75)	1	0	1	0	1	1	0	1	0	0										
Sr (88)	1	0	1	1	1	1	1	1	1	1	0									
Mo (98)	0	0	0	0	0	0	0	0	0	0	0	0								
Ag (107)	2	0	2	1	2	2	1	2	1	1	1	1	0							
Sb (121)	0	0	0	0	0	0	0	0	0	0	0	0	0	0						
Ba (138)	3	0	3	1	2	2	1	2	1	1	1	1	0	2	0					
Au (197)	1	0	1	0	1	1	0	1	0	0	1	0	0	1	0	1				
Pb (208)	3	0	3	1	2	2	1	2	1	1	1	1	0	2	0	3	1			
Elevation	3	0	3	1	2	2	1	2	1	1	1	1	0	2	0	3	1	3		
Th	3	0	3	1	2	2	1	2	1	1	1	1	0	2	0	3	1	3	3	

Type 2a: Inclusions: Ignoring Detection Limits

	wt NaCl equiv	*Li (7)*	*Na (23)*	*Mg (25)*	*K (39)*	*Ca (40)*	*Mn (55)*	*Fe (56)*	*Cu (63)*	*Zn (66)*	*As (75)*	*Sr (88)*	*Mo (98)*	*Ag (107)*	*Sb (121)*	*Ba (138)*	*Au (197)*	*Pb (208)*
wt NaCl equiv	1.00																	
Li (7)	0.00	1.00																
Na (23)	0.43	0.00	1.00															
Mg (25)	0.00	0.00	0.00	1.00														
K (39)	0.41	0.00	-0.50	0.00	1.00													
Ca (40)	0.00	0.00	-0.47	0.00	0.26	1.00												
Mn (55)	0.37	0.00	-0.33	0.00	0.35	0.34	1.00											
Fe (56)	0.50	0.00	-0.20	0.00	0.59	-0.41	0.44	1.00										
Cu (63)	0.11	0.00	0.22	0.00	0.01	-0.41	-0.13	-0.49	1.00									
Zn (66)	0.30	0.00	0.21	0.00	-0.13	0.32	0.18	-0.34	0.76	1.00								
As (75)	0.66	0.00	0.39	0.00	0.04	0.66	0.28	-0.07	0.74	1.00	1.00							
Sr (88)	0.31	0.00	-0.39	0.00	0.23	0.92	0.44	-0.02	-0.08	0.49	0.69	1.00						
Mo (98)	0.96	0.00	0.37	0.00	0.48	-0.50	-0.04	0.97	0.90	0.25	0.00	-0.43	1.00					
Ag (107)	0.29	0.00	0.14	0.00	0.00	0.40	0.05	0.07	0.79	0.64	-0.17	0.59	0.92	1.00				
Sb (121)	0.00	0.00	1.00	0.00	-1.00	-1.00	-1.00	-1.00	0.00	-1.00	-1.00	-1.00	0.00	1.00	1.00			
Ba (138)	-0.01	0.00	-0.24	0.00	0.37	0.32	0.37	-0.27	0.40	0.99	0.47	0.45	0.33	0.70	-1.00	1.00		
Au (197)	0.00	0.00	0.00	0.00	0.00	0.00	0.00	0.00	0.00	0.00	0.00	0.00	0.00	0.00	0.00	0.00	1.00	
Pb (208)	0.51	0.00	0.23	0.00	0.00	0.06	0.12	0.13	-0.44	0.83	0.93	0.41	-0.65	-0.28	1.00	0.69	0.00	1.00
Null			Strong correlation 0.8 and above (+ or -)						Moderate correlation 0.5 to 0.8 (+ or -)						Low correlation 0.2 to 0.5 (+ or -)			

Type 2a: Ignoring Detection Limits with Elevation and T_h

	wt NaCl equiv	*Li (7)*	*Na (23)*	*Mg (25)*	*K (39)*	*Ca (40)*	*Mn (55)*	*Fe (56)*	*Cu (63)*	*Zn (66)*	*As (75)*	*Sr (88)*	*Mo (98)*	*Ag (107)*	*Sb (121)*	*Ba (138)*	*Au (197)*	*Pb (208)*	*Elevation*	*Th*
wt NaCl equiv	1.00																			
Li (7)	0.00	1.00																		
Na (23)	0.43	0.00	1.00																	
Mg (25)	0.00	0.00	0.00	1.00																
K (39)	0.41	0.00	-0.50	0.00	1.00															
Ca (40)	0.00	0.00	-0.47	0.00	0.26	1.00														
Mn (55)	0.37	0.00	-0.33	0.00	0.35	0.34	1.00													
Fe (56)	0.50	0.00	-0.20	0.00	0.59	-0.41	0.44	1.00												
Cu (63)	0.11	0.00	0.22	0.00	0.01	-0.41	-0.13	-0.49	1.00											
Zn (66)	0.30	0.00	0.21	0.00	-0.13	0.32	0.18	-0.34	0.76	1.00										
As (75)	0.66	0.00	0.39	0.00	0.04	0.66	0.28	-0.07	0.74	1.00	1.00									
Sr (88)	0.31	0.00	-0.39	0.00	0.23	0.92	0.44	-0.02	-0.08	0.49	0.69	1.00								
Mo (98)	0.96	0.00	0.37	0.00	0.48	-0.50	-0.04	0.97	0.90	0.25	0.00	-0.43	1.00							
Ag (107)	0.29	0.00	0.14	0.00	0.00	0.40	0.05	0.07	0.79	0.64	-0.17	0.59	0.92	1.00						
Sb (121)	0.00	0.00	1.00	0.00	-1.00	-1.00	-1.00	-1.00	0.00	-1.00	-1.00	-1.00	0.00	1.00	1.00					
Ba (138)	-0.01	0.00	-0.24	0.00	0.37	0.32	0.37	-0.27	0.40	0.99	0.47	0.45	0.33	0.70	-1.00	1.00				
Au (197)	0.00	0.00	0.00	0.00	0.00	0.00	0.00	0.00	0.00	0.00	0.00	0.00	0.00	0.00	0.00	0.00	1.00			
Pb (208)	0.51	0.00	0.23	0.00	0.00	0.06	0.12	0.13	-0.44	0.83	0.93	0.41	-0.65	-0.28	1.00	0.69	0.00	1.00		
Elevation	0.58	0.00	0.47	0.00	0.03	-0.37	-0.08	0.31	0.38	0.20	0.99	-0.13	0.51	0.11	0.00	-0.15	0.00	0.41	1.00	
Th	0.17	0.00	-0.04	0.00	0.21	0.06	-0.23	0.00	0.12	0.30	0.25	0.18	0.20	0.15	-1.00	0.32	0.00	0.34	0.25	1.00

null Elevation & Th | Strong correlation 0.8 and above (+ or -) | Moderate correlation 0.5 to 0.8 (+ or -)

Type 2a: 10% of Detection Limit

	wt NaCl equiv	*Li (7)*	*Na (23)*	*Mg (25)*	*K (39)*	*Ca (40)*	*Mn (55)*	*Fe (56)*	*Cu (63)*	*Zn (66)*	*As (75)*	*Sr (88)*	*Mo (98)*	*Ag (107)*	*Sb (121)*	*Ba (138)*	*Au (197)*	*Pb (208)*
wt NaCl equiv	1.00																	
Li (7)	0.07	1.00																
Na (23)	0.45	-0.12	1.00															
Mg (25)	0.10	1.00	-0.13	1.00														
K (39)	0.43	-0.55	-0.08	-0.53	1.00													
Ca (40)	-0.08	0.46	-0.63	0.46	-0.23	1.00												
Mn (55)	0.35	-0.45	-0.07	-0.46	0.54	-0.12	1.00											
Fe (56)	0.50	-0.54	-0.04	-0.50	0.65	-0.26	0.64	1.00										
Cu (63)	0.09	0.23	0.25	0.24	0.00	-0.18	-0.37	-0.41	1.00									
Zn (66)	0.31	0.60	0.08	0.59	-0.30	0.04	-0.05	-0.09	-0.13	1.00								
As (75)	0.35	0.46	0.36	0.43	-0.12	-0.16	0.27	-0.13	-0.07	0.60	1.00							
Sr (88)	0.18	-0.13	-0.35	-0.12	0.10	0.47	0.27	0.19	-0.24	0.27	-0.28	1.00						
Mo (98)	0.53	0.07	0.08	0.14	0.24	-0.07	-0.06	0.52	0.04	0.11	-0.07	0.00	1.00					
Ag (107)	0.12	0.94	-0.18	0.95	-0.53	0.55	-0.37	-0.46	0.19	0.59	0.41	0.07	0.17	1.00				
Sb (121)	0.11	0.99	-0.06	0.98	-0.55	0.41	-0.38	-0.52	0.20	0.63	0.55	-0.16	0.05	0.94	1.00			
Ba (138)	-0.04	0.40	-0.21	0.41	-0.37	0.17	-0.30	-0.13	-0.10	0.71	-0.07	0.47	0.06	0.39	0.37	1.00		
Au (197)	0.06	1.00	-0.14	0.99	-0.55	0.47	-0.46	-0.54	0.23	0.59	0.44	-0.12	0.06	0.94	0.98	0.41	1.00	
Pb (208)	0.51	0.41	0.26	0.41	-0.16	-0.02	0.03	0.13	-0.21	0.84	0.54	0.22	0.29	0.39	0.45	0.49	0.40	1.00
10%			Strong correlation 0.8 and above (+ or -)						Moderate correlation 0.5 to 0.8 (+ or -)						Low correlation 0.2 to 0.5 (+ or -)			

Type 2a: 10% of Detection Limit with Elevation and T_h

	wt NaCl equiv	*Li (7)*	*Na (23)*	*Mg (25)*	*K (39)*	*Ca (40)*	*Mn (55)*	*Fe (56)*	*Cu (63)*	*Zn (66)*	*As (75)*	*Sr (88)*	*Mo (98)*	*Ag (107)*	*Sb (121)*	*Ba (138)*	*Au (197)*	*Pb (208)*	*Elevation*	*Th*
wt NaCl equiv	1.00																			
Li (7)	0.07	1.00																		
Na (23)	0.45	-0.12	1.00																	
Mg (25)	0.10	1.00	-0.13	1.00																
K (39)	0.43	-0.55	-0.08	-0.53	1.00															
Ca (40)	-0.08	0.46	-0.63	0.46	-0.23	1.00														
Mn (55)	0.35	-0.45	-0.07	-0.46	0.54	-0.12	1.00													
Fe (56)	0.50	-0.54	-0.04	-0.50	0.65	-0.26	0.64	1.00												
Cu (63)	0.09	0.23	0.25	0.24	0.00	-0.18	-0.37	-0.41	1.00											
Zn (66)	0.31	0.60	0.08	0.59	-0.30	0.04	-0.05	-0.09	-0.13	1.00										
As (75)	0.35	0.46	0.36	0.43	-0.12	-0.16	0.27	-0.13	-0.07	0.60	1.00									
Sr (88)	0.18	-0.13	-0.35	-0.12	0.10	0.47	0.27	0.19	-0.24	0.27	-0.28	1.00								
Mo (98)	0.53	0.07	0.08	0.14	0.24	-0.07	-0.06	0.52	0.04	0.11	-0.07	0.00	1.00							
Ag (107)	0.12	0.94	-0.18	0.95	-0.53	0.55	-0.37	-0.46	0.19	0.59	0.41	0.07	0.17	1.00						
Sb (121)	0.11	0.99	-0.06	0.98	-0.55	0.41	-0.38	-0.52	0.20	0.63	0.55	-0.16	0.05	0.94	1.00					
Ba (138)	-0.04	0.40	-0.21	0.41	-0.37	0.17	-0.30	-0.13	-0.10	0.71	-0.07	0.47	0.06	0.39	0.37	1.00				
Au (197)	0.06	1.00	-0.14	0.99	-0.55	0.47	-0.46	-0.54	0.23	0.59	0.44	-0.12	0.06	0.94	0.98	0.41	1.00			
Pb (208)	0.51	0.41	0.26	0.41	-0.16	-0.02	0.03	0.13	-0.21	0.84	0.54	0.22	0.29	0.39	0.45	0.49	0.40	1.00		
Elevation	0.58	0.06	0.49	0.09	0.18	-0.43	-0.05	0.31	0.39	0.18	0.23	-0.23	0.59	0.07	0.08	-0.18	0.04	0.41	1.00	
Th	0.17	0.19	-0.01	0.23	0.06	0.03	-0.30	0.00	0.10	0.31	-0.03	0.14	0.30	0.18	0.17	0.30	0.18	0.34	0.25	1.00
			Strong correlation 0.8 and above (+ or -)						Moderate correlation 0.5 to 0.8 (+ or -)						Low correlation 0.2 to 0.5 (+ or -)					

Type 2a: 1% of Detection Limit

	wt NaCl equiv	*Li (7)*	*Na (23)*	*Mg (25)*	*K (39)*	*Ca (40)*	*Mn (55)*	*Fe (56)*	*Cu (63)*	*Zn (66)*	*As (75)*	*Sr (88)*	*Mo (98)*	*Ag (107)*	*Sb (121)*	*Ba (138)*	*Au (197)*	*Pb (208)*
wt NaCl equiv	1.00																	
Li (7)	0.07	1.00																
Na (23)	0.45	-0.13	1.00															
Mg (25)	0.38	0.73	-0.07	1.00														
K (39)	0.42	-0.58	-0.05	-0.20	1.00													
Ca (40)	-0.09	0.45	-0.64	0.29	-0.25	1.00												
Mn (55)	0.35	-0.47	-0.05	-0.36	0.55	-0.14	1.00											
Fe (56)	0.50	-0.54	-0.04	-0.06	0.65	-0.25	0.64	1.00										
Cu (63)	0.09	0.20	0.26	0.17	0.02	-0.20	-0.36	-0.40	1.00									
Zn (66)	0.31	0.54	0.10	0.42	-0.28	0.00	-0.03	-0.06	-0.18	1.00								
As (75)	0.36	0.35	0.39	0.19	-0.04	-0.24	0.34	-0.07	-0.12	0.56	1.00							
Sr (88)	0.17	-0.16	-0.33	-0.12	0.12	0.44	0.27	0.21	-0.24	0.28	-0.28	1.00						
Mo (98)	0.51	-0.17	0.11	0.51	0.36	-0.18	0.05	0.65	-0.02	-0.01	-0.14	0.04	1.00					
Ag (107)	0.12	-0.17	-0.18	0.07	0.04	0.29	0.23	0.22	-0.13	-0.01	-0.15	0.56	0.33	1.00				
Sb (121)	0.04	0.61	0.01	0.38	-0.44	0.20	-0.10	-0.32	0.06	0.31	0.34	-0.21	-0.24	0.04	1.00			
Ba (138)	-0.05	0.38	-0.21	0.30	-0.38	0.16	-0.30	-0.12	-0.11	0.70	-0.14	0.48	-0.04	-0.01	0.20	1.00		
Au (197)	0.02	0.82	-0.16	0.57	-0.43	0.36	-0.37	-0.43	0.15	0.42	0.29	-0.17	-0.21	-0.14	0.45	0.31	1.00	
Pb (208)	0.51	0.41	0.26	0.43	-0.16	-0.03	0.02	0.13	-0.22	0.84	0.52	0.21	0.20	-0.06	0.23	0.48	0.34	1.00
1%			Strong correlation 0.8 and above (+ or -)						Moderate correlation 0.5 to 0.8 (+ or -)						Low correlation 0.2 to 0.5 (+ or -)			

Type 2a: 1% of Detection Limit with Elevation and T_h

	wt NaCl equiv	Li (7)	Na (23)	Mg (25)	K (39)	Ca (40)	Mn (55)	Fe (56)	Cu (63)	Zn (66)	As (75)	Sr (88)	Mo (98)	Ag (107)	Sb (121)	Ba (138)	Au (197)	Pb (208)	Elevation	Th
wt NaCl equiv	1.00																			
Li (7)	0.07	1.00																		
Na (23)	0.45	-0.13	1.00																	
Mg (25)	0.38	0.73	-0.07	1.00																
K (39)	0.42	-0.58	-0.05	-0.20	1.00															
Ca (40)	-0.09	0.45	-0.64	0.29	-0.25	1.00														
Mn (55)	0.35	-0.47	-0.05	-0.36	0.55	-0.14	1.00													
Fe (56)	0.50	-0.54	-0.04	-0.06	0.65	-0.25	0.64	1.00												
Cu (63)	0.09	0.20	0.26	0.17	0.02	-0.20	-0.36	-0.40	1.00											
Zn (66)	0.31	0.54	0.10	0.42	-0.28	0.00	-0.03	-0.06	-0.18	1.00										
As (75)	0.36	0.35	0.39	0.19	-0.04	-0.24	0.34	-0.07	-0.12	0.56	1.00									
Sr (88)	0.17	-0.16	-0.33	-0.12	0.12	0.44	0.27	0.21	-0.24	0.28	-0.28	1.00								
Mo (98)	0.51	-0.17	0.11	0.51	0.36	-0.18	0.05	0.65	-0.02	-0.01	-0.14	0.04	1.00							
Ag (107)	0.12	-0.17	-0.18	0.07	0.04	0.29	0.23	0.22	-0.13	-0.01	-0.15	0.56	0.33	1.00						
Sb (121)	0.04	0.61	0.01	0.38	-0.44	0.20	-0.10	-0.32	0.06	0.31	0.34	-0.21	-0.24	0.04	1.00					
Ba (138)	-0.05	0.38	-0.21	0.30	-0.38	0.16	-0.30	-0.12	-0.11	0.70	-0.14	0.48	-0.04	-0.01	0.20	1.00				
Au (197)	0.02	0.82	-0.16	0.57	-0.43	0.36	-0.37	-0.43	0.15	0.42	0.29	-0.17	-0.21	-0.14	0.45	0.31	1.00			
Pb (208)	0.51	0.41	0.26	0.43	-0.16	-0.03	0.02	0.13	-0.22	0.84	0.52	0.21	0.20	-0.06	0.23	0.48	0.34	1.00		
Elevation	0.58	0.06	0.49	0.33	0.18	-0.44	-0.05	0.31	0.39	0.18	0.24	-0.23	0.57	0.02	-0.09	-0.18	-0.04	0.41	1.00	
Th	0.17	0.19	-0.01	0.42	0.05	0.03	-0.30	0.00	0.10	0.31	-0.06	0.13	0.25	-0.05	-0.03	0.30	0.01	0.34	0.25	1.00
			Strong correlation 0.8 and above (+ or -)						Moderate correlation 0.5 to 0.8 (+ or -)						Low correlation 0.2 to 0.5 (+ or -)					

Type 2a: Number of Pairs

	wt NaCl equiv	*Li (7)*	*Na (23)*	*Mg (25)*	*K (39)*	*Ca (40)*	*Mn (55)*	*Fe (56)*	*Cu (63)*	*Zn (66)*	*As (75)*	*Sr (88)*	*Mo (98)*	*Ag (107)*	*Sb (121)*	*Ba (138)*	*Au (197)*	*Pb (208)*
wt NaCl equiv																		
Li (7)	0																	
Na (23)	21	0																
Mg (25)	1	0	1															
K (39)	20	0	20	1														
Ca (40)	19	0	17	1	16													
Mn (55)	16	0	16	1	16	14												
Fe (56)	23	0	21	1	20	19	16											
Cu (63)	13	0	13	1	13	10	10	13										
Zn (66)	18	0	17	1	16	17	14	18	9									
As (75)	8	0	8	0	8	7	8	8	5	7								
Sr (88)	15	0	15	1	14	15	14	15	9	14	7							
Mo (98)	6	0	6	1	6	4	5	6	6	4	0	4						
Ag (107)	8	0	8	1	8	8	8	8	6	8	4	8	3					
Sb (121)	3	0	2	0	2	3	2	3	1	3	2	2	0	2				
Ba (138)	18	0	17	1	16	17	15	18	9	16	7	15	5	8	3			
Au (197)	1	0	1	0	1	1	1	1	1	1	1	1	0	1	0	1		
Pb (208)	22	0	20	1	19	18	16	22	12	17	8	15	6	8	3	18	1	

	wt NaCl equiv	*Li (7)*	*Na (23)*	*Mg (25)*	*K (39)*	*Ca (40)*	*Mn (55)*	*Fe (56)*	*Cu (63)*	*Zn (66)*	*As (75)*	*Sr (88)*	*Mo (98)*	*Ag (107)*	*Sb (121)*	*Ba (138)*	*Au (197)*	*Pb (208)*	*Elevation*	*Th*
wt NaCl equiv																				
Li (7)	0																			
Na (23)	21	0																		
Mg (25)	1	0	1																	
K (39)	20	0	20	1																
Ca (40)	19	0	17	1	16															
Mn (55)	16	0	16	1	16	14														
Fe (56)	23	0	21	1	20	19	16													
Cu (63)	13	0	13	1	13	10	10	13												
Zn (66)	18	0	17	1	16	17	14	18	9											
As (75)	8	0	8	0	8	7	8	8	5	7										
Sr (88)	15	0	15	1	14	15	14	15	9	14	7									
Mo (98)	6	0	6	1	6	4	5	6	6	4	0	4								
Ag (107)	8	0	8	1	8	8	8	8	6	8	4	8	3							
Sb (121)	3	0	2	0	2	3	2	3	1	3	2	2	0	2						
Ba (138)	18	0	17	1	16	17	15	18	9	16	7	15	5	8	3					
Au (197)	1	0	1	0	1	1	1	1	1	1	1	1	0	1	0	1				
Pb (208)	22	0	20	1	19	18	16	22	12	17	8	15	6	8	3	18	1			
Elevation	23	0	21	1	20	19	16	23	13	18	8	15	6	8	3	18	1	22		
Th	23	0	21	1	20	19	16	23	13	18	8	15	6	8	3	18	1	22	23	

Type 2b: Inclusions: Ignoring Detection Limits

	wt NaCl equiv	*Li (7)*	*Na (23)*	*Mg (25)*	*K (39)*	*Ca (40)*	*Mn (55)*	*Fe (56)*	*Cu (63)*	*Zn (66)*	*As (75)*	*Sr (88)*	*Mo (98)*	*Ag (107)*	*Sb (121)*	*Ba (138)*	*Au (197)*	*Pb (208)*
wt NaCl equiv	1.00																	
Li (7)		1.00																
Na (23)	0.72		1.00															
Mg (25)				1.00														
K (39)	0.79		0.44		1.00													
Ca (40)	-0.11		0.03		0.42	1.00												
Mn (55)	0.73		0.39		0.97	0.98	1.00											
Fe (56)	0.77		0.11		0.62	-0.36	0.49	1.00										
Cu (63)	0.97		0.63		0.78	0.98	0.95	0.66	1.00									
Zn (66)	0.67		0.48		0.93	0.50	0.93	0.60	-0.80	1.00								
As (75)											1.00							
Sr (88)	0.97		0.24		0.97	0.95	0.90	0.95	-1.00	0.96		1.00						
Mo (98)	0.93		0.47		0.61	1.00	0.85	0.61	0.97	-1.00		-1.00	1.00					
Ag (107)														1.00				
Sb (121)															1.00			
Ba (138)	0.45		0.23		0.71	0.78	0.50	0.44	0.85	0.90		0.91	0.69			1.00		
Au (197)																	1.00	
Pb (208)	0.12		0.33		-0.04	-0.52	-0.37	-0.04	-0.67	-0.08		-0.61	-0.81			-0.24		1.00
			Strong correlation 0.8 and above (+ or -)						Moderate correlation 0.5 to 0.8 (+ or -)						Low correlation 0.2 to 0.5 (+ or -)			

Type 2b: Ignoring Detection Limits with Elevation and T_h

	wt NaCl equiv	*Li (7)*	*Na (23)*	*Mg (25)*	*K (39)*	*Ca (40)*	*Mn (55)*	*Fe (56)*	*Cu (63)*	*Zn (66)*	*As (75)*	*Sr (88)*	*Mo (98)*	*Ag (107)*	*Sb (121)*	*Ba (138)*	*Au (197)*	*Pb (208)*	*Elevation*	*Th*
wt NaCl equiv	1.00																			
Li (7)		1.00																		
Na (23)	0.72		1.00																	
Mg (25)				1.00																
K (39)	0.79		0.44		1.00															
Ca (40)	-0.11		0.03		0.42	1.00														
Mn (55)	0.73		0.39		0.97	0.98	1.00													
Fe (56)	0.77		0.11		0.62	-0.36	0.49	1.00												
Cu (63)	0.97		0.63		0.78	0.98	0.95	0.66	1.00											
Zn (66)	0.67		0.48		0.93	0.50	0.93	0.60	-0.80	1.00										
As (75)											1.00									
Sr (88)	0.97		0.24		0.97	0.95	0.90	0.95	-1.00	0.96		1.00								
Mo (98)	0.93		0.47		0.61	1.00	0.85	0.61	0.97	-1.00		-1.00	1.00							
Ag (107)														1.00						
Sb (121)															1.00					
Ba (138)	0.45		0.23		0.71	0.78	0.50	0.44	0.85	0.90		0.91	0.69			1.00				
Au (197)																	1.00			
Pb (208)	0.12		0.33		-0.04	-0.52	-0.37	-0.04	-0.67	-0.08		-0.61	-0.81			-0.24		1.00		
Elevation	0.01		0.10		-0.03	-0.49	-0.75	-0.06	-0.44	-0.20		-0.97	-0.94			-0.50		0.62	1.00	
Th	-0.45		-0.81		-0.28	-0.20	-0.62	0.00	-0.34	-0.63		-0.32	-0.32			-0.55		-0.42	0.18	1.00
						Strong correlation 0.8 and above (+ or -)						Moderate correlation 0.5 to 0.8 (+ or -)					Low correlation 0.2 to 0.5 (+ or -)			

Type 2b: 10% of Detection Limit

	wt NaCl equiv	*Li (7)*	*Na (23)*	*Mg (25)*	*K (39)*	*Ca (40)*	*Mn (55)*	*Fe (56)*	*Cu (63)*	*Zn (66)*	*As (75)*	*Sr (88)*	*Mo (98)*	*Ag (107)*	*Sb (121)*	*Ba (138)*	*Au (197)*	*Pb (208)*
wt NaCl equiv	1.00																	
Li (7)	0.32	1.00																
Na (23)	0.75	0.35	1.00															
Mg (25)	0.26	1.00	0.29	1.00														
K (39)	0.81	0.02	0.52	-0.03	1.00													
Ca (40)	-0.36	0.09	-0.45	0.17	-0.27	1.00												
Mn (55)	0.55	-0.24	0.13	-0.28	0.86	-0.15	1.00											
Fe (56)	0.77	0.03	0.22	-0.02	0.67	-0.41	0.66	1.00										
Cu (63)	0.74	0.34	0.65	0.29	0.24	-0.41	-0.04	0.58	1.00									
Zn (66)	-0.15	-0.27	-0.34	-0.22	0.24	0.66	0.40	-0.11	-0.60	1.00								
As (75)	0.52	0.97	0.52	0.95	0.16	-0.01	-0.17	0.19	0.54	-0.33	1.00							
Sr (88)	0.38	-0.07	0.13	-0.09	0.83	-0.01	0.85	0.33	-0.33	0.55	-0.05	1.00						
Mo (98)	0.71	0.25	0.66	0.20	0.21	-0.44	0.02	0.55	0.97	-0.61	0.44	-0.34	1.00					
Ag (107)	0.39	0.99	0.39	0.99	0.07	0.09	-0.23	0.09	0.42	-0.27	0.99	-0.07	0.31	1.00				
Sb (121)	-0.18	0.50	-0.25	0.56	-0.33	0.87	-0.31	-0.30	-0.12	0.42	0.40	-0.20	-0.16	0.49	1.00			
Ba (138)	0.26	0.13	-0.30	0.16	0.24	0.61	0.39	0.43	0.08	0.52	0.14	0.20	0.05	0.17	0.61	1.00		
Au (197)	0.28	0.99	0.31	0.99	-0.01	0.11	-0.25	0.00	0.30	-0.27	0.95	-0.06	0.21	0.98	0.50	0.10	1.00	
Pb (208)	0.26	0.02	0.47	-0.03	0.20	-0.27	0.12	0.00	0.19	-0.05	0.06	0.00	0.30	-0.02	-0.14	-0.09	-0.07	1.00
			Strong correlation 0.8 and above (+ or -)						Moderate correlation 0.5 to 0.8 (+ or -)						Low correlation 0.2 to 0.5 (+ or -)			

Type 2b: 10% of Detection Limit with Elevation and T_h

	wt NaCl equiv	*Li (7)*	*Na (23)*	*Mg (25)*	*K (39)*	*Ca (40)*	*Mn (55)*	*Fe (56)*	*Cu (63)*	*Zn (66)*	*As (75)*	*Sr (88)*	*Mo (98)*	*Ag (107)*	*Sb (121)*	*Ba (138)*	*Au (197)*	*Pb (208)*	*Elevation*	*Th*
wt NaCl equiv	1.00																			
Li (7)	0.32	1.00																		
Na (23)	0.75	0.35	1.00																	
Mg (25)	0.26	1.00	0.29	1.00																
K (39)	0.81	0.02	0.52	-0.03	1.00															
Ca (40)	-0.36	0.09	-0.45	0.17	-0.27	1.00														
Mn (55)	0.55	-0.24	0.13	-0.28	0.86	-0.15	1.00													
Fe (56)	0.77	0.03	0.22	-0.02	0.67	-0.41	0.66	1.00												
Cu (63)	0.74	0.34	0.65	0.29	0.24	-0.41	-0.04	0.58	1.00											
Zn (66)	-0.15	-0.27	-0.34	-0.22	0.24	0.66	0.40	-0.11	-0.60	1.00										
As (75)	0.52	0.97	0.52	0.95	0.16	-0.01	-0.17	0.19	0.54	-0.33	1.00									
Sr (88)	0.38	-0.07	0.13	-0.09	0.83	-0.01	0.85	0.33	-0.33	0.55	-0.05	1.00								
Mo (98)	0.71	0.25	0.66	0.20	0.21	-0.44	0.02	0.55	0.97	-0.61	0.44	-0.34	1.00							
Ag (107)	0.39	0.99	0.39	0.99	0.07	0.09	-0.23	0.09	0.42	-0.27	0.99	-0.07	0.31	1.00						
Sb (121)	-0.18	0.50	-0.25	0.56	-0.33	0.87	-0.31	-0.30	-0.12	0.42	0.40	-0.20	-0.16	0.49	1.00					
Ba (138)	0.26	0.13	-0.30	0.16	0.24	0.61	0.39	0.43	0.08	0.52	0.14	0.20	0.05	0.17	0.61	1.00				
Au (197)	0.28	0.99	0.31	0.99	-0.01	0.11	-0.25	0.00	0.30	-0.27	0.95	-0.06	0.21	0.98	0.50	0.10	1.00			
Pb (208)	0.26	0.02	0.47	-0.03	0.20	-0.27	0.12	0.00	0.19	-0.05	0.06	0.00	0.30	-0.02	-0.14	-0.09	-0.07	1.00		
Elevation	0.01	0.04	0.20	-0.01	0.10	-0.42	0.25	-0.06	-0.15	-0.18	-0.04	0.17	0.03	-0.07	-0.32	-0.31	0.01	0.67	1.00	
Th	-0.45	-0.35	-0.69	-0.34	-0.19	-0.01	0.17	0.00	-0.43	-0.10	-0.46	0.08	-0.39	-0.40	-0.24	0.05	-0.30	-0.32	0.18	1.00
				Strong correlation 0.8 and above (+ or -)						Moderate correlation 0.5 to 0.8 (+ or -)						Low correlation 0.2 to 0.5 (+ or -)				

Type 2b: 1% of Detection Limit

	wt NaCl equiv	*Li (7)*	*Na (23)*	*Mg (25)*	*K (39)*	*Ca (40)*	*Mn (55)*	*Fe (56)*	*Cu (63)*	*Zn (66)*	*As (75)*	*Sr (88)*	*Mo (98)*	*Ag (107)*	*Sb (121)*	*Ba (138)*	*Au (197)*	*Pb (208)*
wt NaCl equiv	1.00																	
Li (7)	0.32	1.00																
Na (23)	0.75	0.35	1.00															
Mg (25)	0.26	1.00	0.29	1.00														
K (39)	0.81	0.02	0.52	-0.04	1.00													
Ca (40)	-0.36	0.08	-0.45	0.16	-0.28	1.00												
Mn (55)	0.54	-0.25	0.12	-0.29	0.85	-0.15	1.00											
Fe (56)	0.77	0.03	0.22	-0.02	0.67	-0.41	0.65	1.00										
Cu (63)	0.74	0.34	0.65	0.29	0.24	-0.42	-0.05	0.58	1.00									
Zn (66)	-0.19	-0.35	-0.37	-0.30	0.19	0.67	0.38	-0.12	-0.61	1.00								
As (75)	0.52	0.97	0.51	0.95	0.16	-0.03	-0.18	0.19	0.53	-0.41	1.00							
Sr (88)	0.36	-0.08	0.11	-0.11	0.82	-0.01	0.85	0.33	-0.35	0.50	-0.07	1.00						
Mo (98)	0.71	0.22	0.65	0.17	0.22	-0.45	0.01	0.54	0.97	-0.60	0.41	-0.36	1.00					
Ag (107)	0.39	0.99	0.39	0.99	0.06	0.08	-0.24	0.09	0.42	-0.35	0.99	-0.09	0.28	1.00				
Sb (121)	-0.27	0.37	-0.34	0.44	-0.39	0.91	-0.31	-0.35	-0.21	0.47	0.26	-0.21	-0.25	0.37	1.00			
Ba (138)	0.25	0.11	-0.31	0.14	0.22	0.62	0.39	0.43	0.07	0.52	0.12	0.19	0.04	0.14	0.62	1.00		
Au (197)	0.28	0.99	0.31	0.99	-0.01	0.09	-0.26	0.00	0.29	-0.35	0.95	-0.07	0.17	0.98	0.37	0.08	1.00	
Pb (208)	0.26	0.02	0.47	-0.03	0.20	-0.27	0.12	0.00	0.19	-0.05	0.06	0.00	0.31	-0.01	-0.16	-0.09	-0.07	1.00
			Strong correlation 0.8 and above (+ or -)						Moderate correlation 0.5 to 0.8 (+ or -)					Low correlation 0.2 to 0.5 (+ or -)				

Type 2b: 1% of Detection Limit with Elevation and T_h

	wt NaCl equiv	*Li (7)*	*Na (23)*	*Mg (25)*	*K (39)*	*Ca (40)*	*Mn (55)*	*Fe (56)*	*Cu (63)*	*Zn (66)*	*As (75)*	*Sr (88)*	*Mo (98)*	*Ag (107)*	*Sb (121)*	*Ba (138)*	*Au (197)*	*Pb (208)*	*Elevation*	*Th*
wt NaCl equiv	1.00																			
Li (7)	0.32	1.00																		
Na (23)	0.75	0.35	1.00																	
Mg (25)	0.26	1.00	0.29	1.00																
K (39)	0.81	0.02	0.52	-0.04	1.00															
Ca (40)	-0.36	0.08	-0.45	0.16	-0.28	1.00														
Mn (55)	0.54	-0.25	0.12	-0.29	0.85	-0.15	1.00													
Fe (56)	0.77	0.03	0.22	-0.02	0.67	-0.41	0.65	1.00												
Cu (63)	0.74	0.34	0.65	0.29	0.24	-0.42	-0.05	0.58	1.00											
Zn (66)	-0.19	-0.35	-0.37	-0.30	0.19	0.67	0.38	-0.12	-0.61	1.00										
As (75)	0.52	0.97	0.51	0.95	0.16	-0.03	-0.18	0.19	0.53	-0.41	1.00									
Sr (88)	0.36	-0.08	0.11	-0.11	0.82	-0.01	0.85	0.33	-0.35	0.50	-0.07	1.00								
Mo (98)	0.71	0.22	0.65	0.17	0.22	-0.45	0.01	0.54	0.97	-0.60	0.41	-0.36	1.00							
Ag (107)	0.39	0.99	0.39	0.99	0.06	0.08	-0.24	0.09	0.42	-0.35	0.99	-0.09	0.28	1.00						
Sb (121)	-0.27	0.37	-0.34	0.44	-0.39	0.91	-0.31	-0.35	-0.21	0.47	0.26	-0.21	-0.25	0.37	1.00					
Ba (138)	0.25	0.11	-0.31	0.14	0.22	0.62	0.39	0.43	0.07	0.52	0.12	0.19	0.04	0.14	0.62	1.00				
Au (197)	0.28	0.99	0.31	0.99	-0.01	0.09	-0.26	0.00	0.29	-0.35	0.95	-0.07	0.17	0.98	0.37	0.08	1.00			
Pb (208)	0.26	0.02	0.47	-0.03	0.20	-0.27	0.12	0.00	0.19	-0.05	0.06	0.00	0.31	-0.01	-0.16	-0.09	-0.07	1.00		
Elevation	0.01	0.04	0.21	-0.01	0.11	-0.42	0.26	-0.06	-0.15	-0.20	-0.04	0.18	0.03	-0.07	-0.34	-0.31	0.01	0.67	1.00	
Th	-0.45	-0.35	-0.69	-0.34	-0.19	0.00	0.19	0.00	-0.43	-0.07	-0.46	0.09	-0.38	-0.40	-0.18	0.06	-0.30	-0.32	0.18	1.00
				Strong correlation 0.8 and above (+ or -)						Moderate correlation 0.5 to 0.8 (+ or -)						Low correlation 0.2 to 0.5 (+ or -)				

Type 2b: Number of Pairs:

wt NaCl equiv	Li (7)	Na (23)	Mg (25)	K (39)	Ca (40)	Mn (55)	Fe (56)	Cu (63)	Zn (66)	As (75)	Sr (88)	Mo (98)	Ag (107)	Sb (121)	Ba (138)	Au (197)	Pb (208)
wt NaCl equiv																	
Li (7)	0																
Na (23)	8	0															
Mg (25)	0	0	0														
K (39)	8	0	8	0													
Ca (40)	6	0	5	0	5												
Mn (55)	5	0	5	0	5	3											
Fe (56)	9	0	8	0	8	6	5										
Cu (63)	5	0	5	0	5	3	3	5									
Zn (66)	6	0	5	0	5	6	3	6	3								
As (75)	0	0	0	0	0	0	0	0	0	0							
Sr (88)	4	0	4	0	4	3	4	4	2	3	0						
Mo (98)	4	0	4	0	4	2	3	4	4	2	0	2					
Ag (107)	0	0	0	0	0	0	0	0	0	0	0	0	0				
Sb (121)	1	0	0	0	0	1	0	1	0	1	0	0	0	0			
Ba (138)	6	0	5	0	5	5	4	6	3	5	0	3	3	0	1		
Au (197)	0	0	0	0	0	0	0	0	0	0	0	0	0	0	0	0	
Pb (208)	8	0	7	0	7	5	5	8	4	5	0	4	4	0	1	6	0

wt NaCl equiv	Li (7)	Na (23)	Mg (25)	K (39)	Ca (40)	Mn (55)	Fe (56)	Cu (63)	Zn (66)	As (75)	Sr (88)	Mo (98)	Ag (107)	Sb (121)	Ba (138)	Au (197)	Pb (208)	Elevation	Th
wt NaCl equiv																			
Li (7)	0																		
Na (23)	8	0																	
Mg (25)	0	0	0																
K (39)	8	0	8	0															
Ca (40)	6	0	5	0	5														
Mn (55)	5	0	5	0	5	3													
Fe (56)	9	0	8	0	8	6	5												
Cu (63)	5	0	5	0	5	3	3	5											
Zn (66)	6	0	5	0	5	6	3	6	3										
As (75)	0	0	0	0	0	0	0	0	0	0									
Sr (88)	4	0	4	0	4	3	4	4	2	3	0								
Mo (98)	4	0	4	0	4	2	3	4	4	2	0	2							
Ag (107)	0	0	0	0	0	0	0	0	0	0	0	0	0						
Sb (121)	1	0	0	0	0	1	0	1	0	1	0	0	0	0					
Ba (138)	6	0	5	0	5	5	4	6	3	5	0	3	3	0	1				
Au (197)	0	0	0	0	0	0	0	0	0	0	0	0	0	0	0	0			
Pb (208)	8	0	7	0	7	5	5	8	4	5	0	4	4	0	1	6	0		
Elevation	9	0	8	0	8	6	5	9	5	6	0	4	4	0	1	6	0	8	
Th	9	0	8	0	8	6	5	9	5	6	0	4	4	0	1	6	0	8	9

Type 3: Inclusions: Ignoring Detection Limits

	wt NaCl equiv	*Li (7)*	*Na (23)*	*Mg (25)*	*K (39)*	*Ca (40)*	*Mn (55)*	*Fe (56)*	*Cu (63)*	*Zn (66)*	*As (75)*	*Sr (88)*	*Mo (98)*	*Ag (107)*	*Sb (121)*	*Ba (138)*	*Au (197)*	*Pb (208)*
wt NaCl equiv	1.00																	
Li (7)	0.30	1.00																
Na (23)	0.80	0.13	1.00															
Mg (25)				1.00														
K (39)	0.86	0.00	0.71		1.00													
Ca (40)	0.36	0.78	-0.01		0.93	1.00												
Mn (55)	0.89	0.76	0.64		0.92	0.89	1.00											
Fe (56)	0.55	-0.01	0.10		0.33	0.20	0.93	1.00										
Cu (63)	-0.16	-0.47	-0.08		-0.30	-0.35	-0.47	-0.25	1.00									
Zn (66)	0.82	1.00	0.65		0.91	0.89	0.82	0.71	-0.39	1.00								
As (75)	-1.00	1.00	-0.97		-1.00	0.98	1.00	0.99	1.00	1.00	1.00							
Sr (88)	0.87	1.00	0.71		0.89	0.90	0.92	0.88	-0.09	0.89	1.00	1.00						
Mo (98)	-1.00		-1.00		-1.00			1.00					1.00					
Ag (107)	1.00		1.00		1.00	1.00	1.00	1.00		1.00		1.00		1.00				
Sb (121)	0.69	0.56	0.75		-0.55	-0.73	0.84	0.43	0.92	0.76	1.00	-1.00			1.00			
Ba (138)	0.90	1.00	0.57		0.86	0.90	0.94	0.62	-0.71	0.85	1.00	0.95	1.00	1.00	1.00	1.00		
Au (197)																	1.00	
Pb (208)	0.86	-0.38	0.58		0.98	0.45	0.88	0.72	-0.38	0.92	0.99	0.83		1.00	-0.97	0.86		1.00
			Strong correlation 0.8 and above (+ or -)						Moderate correlation 0.5 to 0.8 (+ or -)						Low correlation 0.2 to 0.5 (+ or -)			

Type 3: Ignoring Detection Limits with Elevation and T_h

	wt NaCl equiv	Li (7)	Na (23)	Mg (25)	K (39)	Ca (40)	Mn (55)	Fe (56)	Cu (63)	Zn (66)	As (75)	Sr (88)	Mo (98)	Ag (107)	Sb (121)	Ba (138)	Au (197)	Pb (208)	Elevation	Th
wt NaCl equiv	1.00																			
Li (7)	0.30	1.00																		
Na (23)	0.80	0.13	1.00																	
Mg (25)				1.00																
K (39)	0.86	0.00	0.71		1.00															
Ca (40)	0.36	0.78	-0.01		0.93	1.00														
Mn (55)	0.89	0.76	0.64		0.92	0.89	1.00													
Fe (56)	0.55	-0.01	0.10		0.33	0.20	0.93	1.00												
Cu (63)	-0.16	-0.47	-0.08		-0.30	-0.35	-0.47	-0.25	1.00											
Zn (66)	0.82	1.00	0.65		0.91	0.89	0.82	0.71	-0.39	1.00										
As (75)	-1.00	1.00	-0.97		-1.00	0.98	1.00	0.99	1.00	1.00	1.00									
Sr (88)	0.87	1.00	0.71		0.89	0.90	0.92	0.88	-0.09	0.89	1.00	1.00								
Mo (98)	-1.00		-1.00		-1.00			1.00					1.00							
Ag (107)	1.00		1.00		1.00	1.00	1.00	1.00		1.00		1.00		1.00						
Sb (121)	0.69	0.56	0.75		-0.55	-0.73	0.84	0.43	0.92	0.76	1.00	-1.00			1.00					
Ba (138)	0.90	1.00	0.57		0.86	0.90	0.94	0.62	-0.71	0.85	1.00	0.95	1.00	1.00	1.00	1.00				
Au (197)																	1.00			
Pb (208)	0.86	-0.38	0.58		0.98	0.45	0.88	0.72	-0.38	0.92	0.99	0.83		1.00	-0.97	0.86		1.00		
Elevation	-0.16		-0.14		-0.09	-0.05	0.54	-0.14	0.31	-0.13	-1.00	-0.01			0.69	-0.10		-0.29	1.00	
Th	0.56	-0.40	0.49		0.82	-0.05	0.91	0.19	-0.21	0.64	1.00	0.74	-1.00	1.00	0.69	0.65		0.62	0.21	1.00

Strong correlation 0.8 and above (+ or -) | Moderate correlation 0.5 to 0.8 (+ or -) | Low correlation 0.2 to 0.5 (+ or -)

Type 3: 10% of Detection Limit

	wt NaCl equiv	*Li (7)*	*Na (23)*	*Mg (25)*	*K (39)*	*Ca (40)*	*Mn (55)*	*Fe (56)*	*Cu (63)*	*Zn (66)*	*As (75)*	*Sr (88)*	*Mo (98)*	*Ag (107)*	*Sb (121)*	*Ba (138)*	*Au (197)*	*Pb (208)*
wt NaCl equiv	1.00																	
Li (7)	0.12	1.00																
Na (23)	0.80	-0.01	1.00															
Mg (25)	0.23	0.68	-0.12	1.00														
K (39)	0.78	-0.28	0.65	-0.20	1.00													
Ca (40)	0.34	0.56	0.04	0.83	0.10	1.00												
Mn (55)	0.79	-0.22	0.65	-0.15	0.93	0.14	1.00											
Fe (56)	0.55	-0.05	0.11	0.07	0.37	0.04	0.38	1.00										
Cu (63)	0.03	0.18	0.14	0.14	-0.20	-0.01	-0.18	-0.11	1.00									
Zn (66)	0.77	-0.04	0.53	0.16	0.80	0.40	0.79	0.34	-0.19	1.00								
As (75)	0.07	0.38	-0.11	0.59	-0.25	0.52	-0.18	0.02	0.05	0.28	1.00							
Sr (88)	0.67	-0.31	0.49	-0.16	0.89	0.14	0.87	0.35	-0.13	0.87	-0.08	1.00						
Mo (98)	0.30	0.32	-0.16	0.53	-0.10	0.28	-0.12	0.77	-0.01	0.02	0.27	-0.17	1.00					
Ag (107)	0.37	0.54	-0.02	0.82	0.04	0.73	0.16	0.23	0.06	0.43	0.46	0.19	0.42	1.00				
Sb (121)	0.20	0.73	-0.04	0.94	-0.26	0.78	-0.18	0.02	0.20	0.10	0.56	-0.24	0.47	0.76	1.00			
Ba (138)	0.85	-0.17	0.54	0.00	0.86	0.15	0.85	0.68	-0.23	0.82	-0.04	0.83	0.26	0.25	-0.08	1.00		
Au (197)	0.23	0.67	-0.11	1.00	-0.20	0.80	-0.15	0.06	0.15	0.16	0.57	-0.15	0.52	0.82	0.93	-0.01	1.00	
Pb (208)	0.78	0.04	0.56	0.26	0.77	0.48	0.76	0.24	-0.16	0.94	0.36	0.77	0.01	0.39	0.19	0.75	0.26	1.00
			Strong correlation 0.8 and above (+ or -)						Moderate correlation 0.5 to 0.8 (+ or -)					Low correlation 0.2 to 0.5 (+ or -)				

Type 3: 10% of Detection Limit with Elevation and T_h

	wt NaCl equiv	Li (7)	Na (23)	Mg (25)	K (39)	Ca (40)	Mn (55)	Fe (56)	Cu (63)	Zn (66)	As (75)	Sr (88)	Mo (98)	Ag (107)	Sb (121)	Ba (138)	Au (197)	Pb (208)	Elevation	Th
wt NaCl equiv	1.00																			
Li (7)	0.12	1.00																		
Na (23)	0.80	-0.01	1.00																	
Mg (25)	0.23	0.68	-0.12	1.00																
K (39)	0.78	-0.28	0.65	-0.20	1.00															
Ca (40)	0.34	0.56	0.04	0.83	0.10	1.00														
Mn (55)	0.79	-0.22	0.65	-0.15	0.93	0.14	1.00													
Fe (56)	0.55	-0.05	0.11	0.07	0.37	0.04	0.38	1.00												
Cu (63)	0.03	0.18	0.14	0.14	-0.20	-0.01	-0.18	-0.11	1.00											
Zn (66)	0.77	-0.04	0.53	0.16	0.80	0.40	0.79	0.34	-0.19	1.00										
As (75)	0.07	0.38	-0.11	0.59	-0.25	0.52	-0.18	0.02	0.05	0.28	1.00									
Sr (88)	0.67	-0.31	0.49	-0.16	0.89	0.14	0.87	0.35	-0.13	0.87	-0.08	1.00								
Mo (98)	0.30	0.32	-0.16	0.53	-0.10	0.28	-0.12	0.77	-0.01	0.02	0.27	-0.17	1.00							
Ag (107)	0.37	0.54	-0.02	0.82	0.04	0.73	0.16	0.23	0.06	0.43	0.46	0.19	0.42	1.00						
Sb (121)	0.20	0.73	-0.04	0.94	-0.26	0.78	-0.18	0.02	0.20	0.10	0.56	-0.24	0.47	0.76	1.00					
Ba (138)	0.85	-0.17	0.54	0.00	0.86	0.15	0.85	0.68	-0.23	0.82	-0.04	0.83	0.26	0.25	-0.08	1.00				
Au (197)	0.23	0.67	-0.11	1.00	-0.20	0.80	-0.15	0.06	0.15	0.16	0.57	-0.15	0.52	0.82	0.93	-0.01	1.00			
Pb (208)	0.78	0.04	0.56	0.26	0.77	0.48	0.76	0.24	-0.16	0.94	0.36	0.77	0.01	0.39	0.19	0.75	0.26	1.00		
Elevation	-0.16	-0.09	-0.14	-0.07	-0.01	-0.03	-0.12	-0.10	-0.11	-0.14	-0.21	0.07	-0.07	-0.08	-0.09	-0.14	-0.05	-0.17	1.00	
Th	0.56	-0.36	0.49	-0.25	0.78	-0.01	0.77	0.22	-0.14	0.63	-0.07	0.79	-0.22	-0.15	-0.35	0.65	-0.24	0.67	0.21	1.00
			Strong correlation 0.8 and above (+ or -)						Moderate correlation 0.5 to 0.8 (+ or -)					Low correlation 0.2 to 0.5 (+ or -)						

Type 3: 1% of Detection Limit

	wt NaCl equiv	*Li (7)*	*Na (23)*	*Mg (25)*	*K (39)*	*Ca (40)*	*Mn (55)*	*Fe (56)*	*Cu (63)*	*Zn (66)*	*As (75)*	*Sr (88)*	*Mo (98)*	*Ag (107)*	*Sb (121)*	*Ba (138)*	*Au (197)*	*Pb (208)*
wt NaCl equiv	1.00																	
Li (7)	-0.06	1.00																
Na (23)	0.80	0.10	1.00															
Mg (25)	0.23	-0.02	-0.12	1.00														
K (39)	0.77	-0.20	0.65	-0.23	1.00													
Ca (40)	0.34	-0.04	0.04	0.82	0.07	1.00												
Mn (55)	0.77	-0.17	0.65	-0.20	0.93	0.09	1.00											
Fe (56)	0.55	-0.15	0.11	0.07	0.37	0.04	0.38	1.00										
Cu (63)	-0.01	0.13	0.17	-0.02	-0.16	-0.14	-0.16	-0.12	1.00									
Zn (66)	0.69	-0.21	0.56	-0.16	0.85	0.13	0.83	0.31	-0.21	1.00								
As (75)	-0.08	-0.03	-0.07	0.02	-0.18	0.06	-0.13	-0.03	-0.05	0.23	1.00							
Sr (88)	0.65	-0.27	0.49	-0.22	0.89	0.09	0.87	0.34	-0.10	0.91	0.00	1.00						
Mo (98)	0.23	-0.08	-0.14	0.13	-0.02	-0.06	-0.08	0.86	-0.10	-0.10	-0.05	-0.13	1.00					
Ag (107)	0.34	-0.07	0.13	0.08	0.33	0.16	0.47	0.30	-0.09	0.51	-0.04	0.54	-0.03	1.00				
Sb (121)	-0.03	0.37	0.15	0.07	-0.25	0.08	-0.14	-0.15	0.19	-0.17	0.09	-0.31	-0.07	-0.05	1.00			
Ba (138)	0.82	-0.23	0.54	-0.10	0.86	0.06	0.85	0.68	-0.23	0.82	-0.06	0.83	0.30	0.43	-0.26	1.00		
Au (197)	0.23	-0.04	-0.11	1.00	-0.23	0.79	-0.20	0.06	-0.01	-0.16	0.00	-0.22	0.12	0.08	0.05	-0.10	1.00	
Pb (208)	0.77	-0.20	0.56	0.26	0.76	0.48	0.74	0.23	-0.21	0.85	0.24	0.74	-0.12	0.32	-0.14	0.71	0.26	1.00
			Strong correlation 0.8 and above (+ or -)						Moderate correlation 0.5 to 0.8 (+ or -)					Low correlation 0.2 to 0.5 (+ or -)				

Type 3: 1% of Detection Limit with Elevation and T_h

	wt NaCl equiv	*Li (7)*	*Na (23)*	*Mg (25)*	*K (39)*	*Ca (40)*	*Mn (55)*	*Fe (56)*	*Cu (63)*	*Zn (66)*	*As (75)*	*Sr (88)*	*Mo (98)*	*Ag (107)*	*Sb (121)*	*Ba (138)*	*Au (197)*	*Pb (208)*	*Elevation*	*Th*
wt NaCl equiv	1.00																			
Li (7)	-0.06	1.00																		
Na (23)	0.80	0.10	1.00																	
Mg (25)	0.23	-0.02	-0.12	1.00																
K (39)	0.77	-0.20	0.65	-0.23	1.00															
Ca (40)	0.34	-0.04	0.04	0.82	0.07	1.00														
Mn (55)	0.77	-0.17	0.65	-0.20	0.93	0.09	1.00													
Fe (56)	0.55	-0.15	0.11	0.07	0.37	0.04	0.38	1.00												
Cu (63)	-0.01	0.13	0.17	-0.02	-0.16	-0.14	-0.16	-0.12	1.00											
Zn (66)	0.69	-0.21	0.56	-0.16	0.85	0.13	0.83	0.31	-0.21	1.00										
As (75)	-0.08	-0.03	-0.07	0.02	-0.18	0.06	-0.13	-0.03	-0.05	0.23	1.00									
Sr (88)	0.65	-0.27	0.49	-0.22	0.89	0.09	0.87	0.34	-0.10	0.91	0.00	1.00								
Mo (98)	0.23	-0.08	-0.14	0.13	-0.02	-0.06	-0.08	0.86	-0.10	-0.10	-0.05	-0.13	1.00							
Ag (107)	0.34	-0.07	0.13	0.08	0.33	0.16	0.47	0.30	-0.09	0.51	-0.04	0.54	-0.03	1.00						
Sb (121)	-0.03	0.37	0.15	0.07	-0.25	0.08	-0.14	-0.15	0.19	-0.17	0.09	-0.31	-0.07	-0.05	1.00					
Ba (138)	0.82	-0.23	0.54	-0.10	0.86	0.06	0.85	0.68	-0.23	0.82	-0.06	0.83	0.30	0.43	-0.26	1.00				
Au (197)	0.23	-0.04	-0.11	1.00	-0.23	0.79	-0.20	0.06	-0.01	-0.16	0.00	-0.22	0.12	0.08	0.05	-0.10	1.00			
Pb (208)	0.77	-0.20	0.56	0.26	0.76	0.48	0.74	0.23	-0.21	0.85	0.24	0.74	-0.12	0.32	-0.14	0.71	0.26	1.00		
Elevation	-0.16	-0.08	-0.14	-0.07	-0.01	-0.03	-0.12	-0.10	-0.10	-0.13	-0.22	0.07	-0.05	-0.05	-0.14	-0.13	-0.05	-0.17	1.00	
Th	0.56	-0.25	0.49	-0.25	0.78	-0.01	0.78	0.23	-0.10	0.70	0.07	0.80	-0.14	0.08	-0.36	0.67	-0.24	0.67	0.21	1.00
						Strong correlation 0.8 and above (+ or -)						Moderate correlation 0.5 to 0.8 (+ or -)					Low correlation 0.2 to 0.5 (+ or -)			

Type 3: Number of Pairs

wt NaCl equiv		*Li (7)*	*Na (23)*	*Mg (25)*	*K (39)*	*Ca (40)*	*Mn (55)*	*Fe (56)*	*Cu (63)*	*Zn (66)*	*As (75)*	*Sr (88)*	*Mo (98)*	*Ag (107)*	*Sb (121)*	*Ba (138)*	*Au (197)*	*Pb (208)*
wt NaCl equiv																		
Li (7)	5																	
Na (23)	27	5																
Mg (25)	0	0	0															
K (39)	21	5	21	0														
Ca (40)	22	4	22	0	19													
Mn (55)	14	3	14	0	14	14												
Fe (56)	23	5	23	0	20	20	13											
Cu (63)	10	4	10	0	9	9	7	10										
Zn (66)	11	2	11	0	10	11	9	11	5									
As (75)	3	2	3	0	2	3	2	3	2	3								
Sr (88)	17	2	17	0	16	16	11	16	6	10	2							
Mo (98)	2	0	2	0	2	1	1	2	1	1	0	1						
Ag (107)	2	1	2	0	2	2	2	2	1	2	1	2	0					
Sb (121)	4	3	4	0	4	4	4	4	4	3	2	2	0	1				
Ba (138)	14	2	14	0	12	13	11	13	5	9	2	11	2	2	2			
Au (197)	0	0	0	0	0	0	0	0	0	0	0	0	0	0	0	0		
Pb (208)	22	5	22	0	18	19	12	20	8	10	3	15	2	2	4	13	0	

	wt NaCl equiv	Li (7)	Na (23)	Mg (25)	K (39)	Ca (40)	Mn (55)	Fe (56)	Cu (63)	Zn (66)	As (75)	Sr (88)	Mo (98)	Ag (107)	Sb (121)	Ba (138)	Au (197)	Pb (208)	Elevation	Th
wt NaCl equiv																				
Li (7)	5																			
Na (23)	27	5																		
Mg (25)	0	0	0																	
K (39)	21	5	21	0																
Ca (40)	22	4	22	0	19															
Mn (55)	14	3	14	0	14	14														
Fe (56)	23	5	23	0	20	20	13													
Cu (63)	10	4	10	0	9	9	7	10												
Zn (66)	11	2	11	0	10	11	9	11	5											
As (75)	3	2	3	0	2	3	2	3	2	3										
Sr (88)	17	2	17	0	16	16	11	16	6	10	2									
Mo (98)	2	0	2	0	2	1	1	2	1	1	0	1								
Ag (107)	2	1	2	0	2	2	2	2	1	2	1	2	0							
Sb (121)	4	3	4	0	4	4	4	4	4	3	2	2	0	1						
Ba (138)	14	2	14	0	12	13	11	13	5	9	2	11	2	2	2					
Au (197)	0	0	0	0	0	0	0	0	0	0	0	0	0	0	0	0				
Pb (208)	22	5	22	0	18	19	12	20	8	10	3	15	2	2	4	13	0			
Elevation	27	5	27	0	21	22	14	23	10	11	3	17	2	2	4	14	0	22		
Th	27	5	27	0	21	22	14	23	10	11	3	17	2	2	4	14	0	22	27	

APPENDIX F. SUMMARY STATISTICS FOR FI ASSEMBLAGES:

T_h:

Labels	1 (2)	2 (2)	3 (4)	4 (5)	5 (5)	6 (5)	7 (2)	8 (3)	9 (3)	10 (4)	11 (4)	12 (2)	13 (3)	14 (2)	15 (3)	16 (3)	17 (2)
Min	373.3	383.1	332	377.7	376	286.7	357.8	345	327	319	337.5	280	301.7	380	364	340	360
Q1	376.725	386.25	334.25	389.1	377	368.3	365.675	345.6	337	323.5	339.375	285.3	307.1	381.5	364.5	355	371
Median	380.15	389.4	336.5	394.9	378	382	373.55	346.2	347	331	342.9	290.6	312.5	383	365	370	382
Q3	383.575	392.55	338.5	398	379	389.5	381.425	356.1	359	338.25	351.85	295.9	325.25	384.5	378.5	375	383.5
Max	387	395.7	340	398	380	420.1	389.3	366	371	342	370	301.2	338	386	392	380	385
IQR	6.85	6.3	4.25	8.9	2	21.2	15.75	10.5	22	14.75	12.475	10.6	18.15	3	14	20	12.5
Upper Outlier	0	0	0	0	0	0	0	0	0	0	0	0	0	0	0	0	0
Lower Outlier	0	0	0	0	0	1	0	0	0	0	0	0	0	0	0	0	0
For the Box (IQR and Median)																	
Q2-Q1	3.425	3.15	2.25	5.8	1	13.7	7.875	0.6	10	7.5	3.525	5.3	5.4	1.5	0.5	15	11
Q3-Q2	3.425	3.15	2	3.1	1	7.5	7.875	9.9	12	7.25	8.95	5.3	12.75	1.5	13.5	5	1.5
For the Whiskers																	
Q3+1.5*IQR	393.85	402	344.875	411.35	382	421.3	405.05	371.85	392	360.375	370.5625	311.8	352.475	389	399.5	405	402.25
Q1-1.5*IQR	366.45	376.8	327.875	375.75	374	336.5	342.05	329.85	304	301.375	320.6625	269.4	279.875	377	343.5	325	352.25
Upper Whisk	387	395.7	340	398	380	420.1	389.3	366	371	342	370	301.2	338	386	392	380	385
Lower Whisk	373.3	383.1	332	377.7	376	336.5	357.8	345	327	319	337.5	280	301.7	380	364	340	360
Wupper-Q3	3.425	3.15	1.5	0	1	30.6	7.875	9.9	12	3.75	18.15	5.3	12.75	1.5	13.5	5	1.5
Q1-Wlower	3.425	3.15	2.25	11.4	1	31.8	7.875	0.6	10	4.5	1.875	5.3	5.4	1.5	0.5	15	11
For the Outliers																	
Max	N/A	N/A	N/A	N/A	N/A	N/A	N/A	N/A	N/A	N/A	N/A	N/A	N/A	N/A	N/A	N/A	N/A
Min	N/A	N/A	N/A	N/A	N/A	286.7	N/A	N/A	N/A	N/A	N/A	N/A	N/A	N/A	N/A	N/A	N/A
Data Table	1 (2)	2 (2)	3 (4)	4 (5)	5 (5)	6 (5)	7 (2)	8 (3)	9 (3)	10 (4)	11 (4)	12 (2)	13 (3)	14 (2)	15 (3)	16 (3)	17 (2)
	373.3	395.7	338	398	380	420.1	357.8	366	347	337	340	301.2	338	380	392	370	382
	387	383.1	340	394.9	376	389.5	389.3	345	371	342	345.8	280	301.7	386	365	380	385
			335	398		368.3		346.2	327	319	337.5		312.5		364	340	360
			332	389.1		286.7				325	370						
				377.7		382											

Labels	18 (1)	19 (3)	20 (2)	21 (3)	22 (2)	23 (3)	24 (7)	25 (4)	26 (4)	27 (2)	28 (3)	29 (2)	30 (6)	31 (3)	32 (2)	33 (3)	34 (5)
Min	0	355	361.4	363.1	346.7	384	283.5	284.6	330.4	324	331.5	351	320	332.1	360	373	354.4
Q1	N/A	364.1	361.675	369.6	346.95	384.1	323.55	290.525	337.6	324.75	331.85	352.275	322.45	333.8	370.75	381.5	355.2
Median	N/A	373.2	361.95	376.1	347.2	384.2	325	292.85	341	325.5	332.2	353.55	333.75	335.5	381.5	390	355.5
Q3	N/A	381.85	362.225	377.45	347.45	384.55	325.5	296.175	342.5	326.25	337.1	354.825	346.4	338.95	392.25	390	356.1
Max	0	390.5	362.5	378.8	347.7	384.9	326	305.1	344	327	342	356.1	350.8	342.4	403	390	356.1
IQR	N/A	17.75	0.55	7.85	0.5	0.45	1.95	5.65	4.9	1.5	5.25	2.55	23.95	5.15	21.5	8.5	0.9
Upper Outlier	0	0	0	0	0	0	0	1	0	0	0	0	0	0	0	0	0
Lower Outlier	0	0	0	0	0	0	1	0	0	0	0	0	0	0	0	0	0
For the Box (IQR and Median)																	
Q2-Q1	N/A	9.1	0.275	6.5	0.25	0.1	1.45	2.325	3.4	0.75	0.35	1.275	11.3	1.7	10.75	8.5	0.3
Q3-Q2	N/A	8.65	0.275	1.35	0.25	0.35	0.5	3.325	1.5	0.75	4.9	1.275	12.65	3.45	10.75	0	0.6
For the Whiskers																	
Q3+1.5*IQR	N/A	408.475	363.05	389.225	348.2	385.225	328.425	304.65	349.85	328.5	344.975	358.65	382.325	346.675	424.5	402.75	357.45
Q1-1.5*IQR	N/A	337.475	360.85	357.825	346.2	383.425	320.625	282.05	330.25	322.5	323.975	348.45	286.525	326.075	338.5	368.75	353.85
Upper Whisk	N/A	390.5	362.5	378.8	347.7	384.9	326	304.65	344	327	342	356.1	350.8	342.4	403	390	356.1
Lower Whisk	N/A	355	361.4	363.1	346.7	384	320.625	284.6	330.4	324	331.5	351	320	332.1	360	373	354.4
Wupper-Q3	N/A	8.65	0.275	1.35	0.25	0.35	0.5	8.475	1.5	0.75	4.9	1.275	4.4	3.45	10.75	0	0
Q1-Wlower	N/A	9.1	0.275	6.5	0.25	0.1	2.925	5.925	7.2	0.75	0.35	1.275	2.45	1.7	10.75	8.5	0.8
For the Outliers																	
Max	N/A	N/A	N/A	N/A	N/A	N/A	N/A	305.1	N/A	N/A	N/A	N/A	N/A	N/A	N/A	N/A	N/A
Min	N/A	N/A	N/A	N/A	N/A	N/A	283.5	N/A	N/A	N/A	N/A	N/A	N/A	N/A	N/A	N/A	N/A
Data Table	18 (1)	19 (3)	20 (2)	21 (3)	22 (2)	23 (3)	24 (7)	25 (4)	26 (4)	27 (2)	28 (3)	29 (2)	30 (6)	31 (3)	32 (2)	33 (3)	34 (5)
		373.2	361.4	378.8	347.7	384.9	325.8	292.5	340	327	332.2	351	320	342.4	360	390	355.5
		390.5	362.5	376.1	346.7	384	325.2	293.2	344	324	342	356.1	347	335.5	403	390	355.2
		355		363.1		384.2	283.5	305.1	342		331.5		322.3	332.1		373	356.1
							325	284.6	330.4				322.9				354.4
							324						344.6				356.1
							323.1						350.8				
							326										

Salinity:

Labels	1 (2)	2 (2)	3 (4)	4 (5)	5 (5)	6 (5)	7 (2)	8 (3)	9 (3)	10 (4)	11 (4)	12 (2)	13 (3)	14 (2)	15 (3)	16 (3)	17 (2)
Min	3.9	4.6	2.2	0	0	27.66	33.14	33.83	27.78	33.65	32.6	30.43	31.04	35	1.2	10.6	5
Q1	4.2	4.95	2.4	N/A	N/A	30.35	33.7	36.235	28.475	34.01	32.675	30.47	31.065	37.6525	1.65	10.75	5.4
Median	4.5	5.3	2.6	N/A	N/A	30.88	34.26	38.64	29.17	34.19	32.81	30.51	31.09	40.305	2.1	10.9	5.8
Q3	4.8	5.65	3.05	N/A	N/A	39.6	34.82	41.045	29.455	34.3725	33.36	30.55	31.105	42.9575	2.6	11.3	6.2
Max	5.1	6	3.5	0	0	51.29	35.38	43.45	29.74	34.74	34.68	30.59	31.12	45.61	3.1	11.7	6.6
IQR	0.6	0.7	0.65	N/A	N/A	9.25	1.12	4.81	0.98	0.3625	0.685	0.08	0.04	5.305	0.95	0.55	0.8
Upper Outlie	0	0	0	0	0	0	0	0	0	0	1	0	0	0	0	0	0
Lower Outlie	0	0	0	0	0	0	0	0	0	0	0	0	0	0	0	0	0
For the Box (IQR and Median)																	
Q2-Q1	0.3	0.35	0.2	N/A	N/A	0.53	0.56	2.405	0.695	0.18	0.135	0.04	0.025	2.6525	0.45	0.15	0.4
Q3-Q2	0.3	0.35	0.45	N/A	N/A	8.72	0.56	2.405	0.285	0.1825	0.55	0.04	0.015	2.6525	0.5	0.4	0.4
For the Whiskers																	
Q3+1.5*IQR	5.7	6.7	4.025	N/A	N/A	53.475	36.5	48.26	30.925	34.91625	34.3875	30.67	31.165	50.915	4.025	12.125	7.4
Q1-1.5*IQR	3.3	3.9	1.425	N/A	N/A	16.475	32.02	29.02	27.005	33.46625	31.6475	30.35	31.005	29.695	0.225	9.925	4.2
Upper Whisk	5.1	6	3.5	N/A	N/A	51.29	35.38	43.45	29.74	34.74	34.3875	30.59	31.12	45.61	3.1	11.7	6.6
Lower Whisk	3.9	4.6	2.2	N/A	N/A	27.66	33.14	33.83	27.78	33.65	32.6	30.43	31.04	35	1.2	10.6	5
Wupper-Q3	0.3	0.35	0.45	N/A	N/A	11.69	0.56	2.405	0.285	0.3675	1.0275	0.04	0.015	2.6525	0.5	0.4	0.4
Q1-Wlower	0.3	0.35	0.2	N/A	N/A	2.69	0.56	2.405	0.695	0.36	0.075	0.04	0.025	2.6525	0.45	0.15	0.4
For the Outliers																	
Max	N/A	N/A	N/A	N/A	N/A	N/A	N/A	N/A	N/A	N/A	34.68	N/A	N/A	N/A	N/A	N/A	N/A
Min	N/A	N/A	N/A	N/A	N/A	N/A	N/A	N/A	N/A	N/A	N/A	N/A	N/A	N/A	N/A	N/A	N/A
Data Table	1 (2)	2 (2)	3 (4)	4 (5)	5 (5)	6 (5)	7 (2)	8 (3)	9 (3)	10 (4)	11 (4)	12 (2)	13 (3)	14 (2)	15 (3)	16 (3)	17 (2)
	3.9	6	3.5			27.66	35.38	43.45	29.17	34.25	34.68	30.59	31.09	45.61	1.2	10.6	5
	5.1	4.6				30.35	33.14	33.83	29.74	34.74	32.6	30.43	31.12	35	2.1	10.9	6.6
			2.6			51.29			27.78	33.65	32.7		31.04		3.1	11.7	
			2.2			39.6				34.13	32.92						
						30.88											

Labels	18 (1)	19 (3)	20 (2)	21 (3)	22 (2)	23 (3)	24 (7)	25 (4)	26 (4)	27 (2)	28 (3)	29 (2)	30 (6)	31 (3)	32 (2)	33 (3)	34 (5)
Min	0	15.5	6	4	2.9	12.4	2.2	3.2	10	17.7	9.9	9.2	10.1	11.2	23	18	4.5
Q1	N/A	16.1	6.425	4.65	3.3	12.8	2.55	3.425	10.3	17.75	10.05	9.2	10.675	11.5	23	18	4.5
Median	N/A	16.7	6.85	5.3	3.7	13.2	2.9	3.6	10.5	17.8	10.2	9.2	10.9	11.8	23	18	5
Q3	N/A	17.3	7.275	6.1	4.1	13.25	3.3	3.7	11.025	17.85	10.55	9.2	11.05	11.8	23	18	5.1
Max	0	17.9	7.7	6.9	4.5	13.3	3.5	3.7	12.3	17.9	10.9	9.2	12.3	11.8	23	18	5.6
IQR	N/A	1.2	0.85	1.45	0.8	0.45	0.75	0.275	0.725	0.1	0.5	0	0.375	0.3	0	0	0.6
Upper Outlier	0	0	0	0	0	0	0	0	1	0	0	0	1	0	0	0	0
Lower Outlier	0	0	0	0	0	0	0	0	0	0	0	0	1	0	0	0	0
For the Box (IQR and Median)																	
Q2-Q1	N/A	0.6	0.425	0.65	0.4	0.4	0.35	0.175	0.2	0.05	0.15	0	0.225	0.3	0	0	0.5
Q3-Q2	N/A	0.6	0.425	0.8	0.4	0.05	0.4	0.1	0.525	0.05	0.35	0	0.15	0	0	0	0.1
For the Whiskers																	
Q3+1.5*IQR	N/A	19.1	8.55	8.275	5.3	13.925	4.425	4.1125	12.1125	18	11.3	9.2	11.6125	12.25	23	18	6
Q1-1.5*IQR	N/A	14.3	5.15	2.475	2.1	12.125	1.425	3.0125	9.2125	17.6	9.3	9.2	10.1125	11.05	23	18	3.6
Upper Whisk	N/A	17.9	7.7	6.9	4.5	13.3	3.5	3.7	12.1125	17.9	10.9	9.2	11.6125	11.8	23	18	5.6
Lower Whisk	N/A	15.5	6	4	2.9	12.4	2.2	3.2	10	17.7	9.9	9.2	10.1125	11.2	23	18	4.5
Wupper-Q3	N/A	0.6	0.425	0.8	0.4	0.05	0.2	0	1.0875	0.05	0.35	0	0.5625	0	0	0	0.5
Q1-Wlower	N/A	0.6	0.425	0.65	0.4	0.4	0.35	0.225	0.3	0.05	0.15	0	0.5625	0.3	0	0	0
For the Outliers																	
Max	N/A	N/A	N/A	N/A	N/A	N/A	N/A	N/A	12.3	N/A	N/A	N/A	12.3	N/A	N/A	N/A	N/A
Min	N/A	N/A	N/A	N/A	N/A	N/A	N/A	N/A	N/A	N/A	N/A	N/A	10.1	N/A	N/A	N/A	N/A
Data Table	18 (1)	19 (3)	20 (2)	21 (3)	22 (2)	23 (3)	24 (7)	25 (4)	26 (4)	27 (2)	28 (3)	29 (2)	30 (6)	31 (3)	32 (2)	33 (3)	34 (5)
		15.5	7.7	5.3	4.5	13.2	2.9	3.2	10.4	17.9	10.2		10.1	11.8	23	18	5
		16.7	6	4	2.9	12.4	2.4	3.7	10	17.7	10.9	9.2	10.6	11.8	23		4.5
		17.9		6.9		13.3	3.2	3.5	10.6		9.9		10.9	11.2			5.1
							2.7	3.7	12.3				11.1				5.6
							3.4						12.3				4.5
							3.5						10.9				
							2.2										

References

Baline, L. M., 2007, Hydrothermal fluids and Cu-Au mineralization of the Deep Grasberg Porphyry Deposit, Papua, Indonesia, p. 269.

Beane, R., and Bodnar, R., 1995, Hydrothermal fluids and hydrothermal alteration in porphyry copper deposits: Porphyry copper deposits of the American Cordillera. Arizona Geol Soc Digest, v. 20, p. 83-93.

Cline, J. S., and Bodnar, R. J., 1991, Can economic porphyry copper mineralization be generated by a typical calc-alkaline melt?: Journal of Geophysical Research: Solid Earth, v. 96, p. 8113-8126.

Cline, J. S., and Bodnar, R. J., 1994, Direct evolution of brine from a crystallizing silicic melt at the Questa, New Mexico, molybdenum deposit: Economic geology, v. 89, p. 1780-1802.

Cloos, M., 2001, Bubbling magma chambers, cupolas, and porphyry copper deposits: International Geology Review, v. 43, p. 285-311.

Cloos, M., and Housh, T. B., 2008, Collisional delamination: Implications for porphyry-type Cu-Au ore formation in New Guinea: Arizona Geological Society Digest, v. 22, p. 235-244.

Diamond, L., 2014, pers. Comm.: PACROFI XII.

Dozy, J.-J., Erdman, D., Jong, W., Krol, G., and Schouten, C., 1939, Geological results of the Carstensz expedition 1936: Leidse Geologische Mededelingen, v. 11, p. 68-131.

Driesner, T., 2007, The System H2O-NaCl. II. Correlation Formulae for Phase Relations in Temperature-Pressure-Composition Space from 0 to 1000°C, 0 to 5000 bar, and 0 to 1 XNaCl: Geochimica et Cosmochimica Acta, v. 71, p. 4880-4901.

Driesner, T., and Heinrich, C. A., 2007, The System H2O-NaCl. I. Correlations for molar volume, enthalpy, and isobaric heat capacity from 0 to 1000 degrees C, 1 to 5000 bar, and 0 to 1 X-NaCl: Geochimica et Cosmochimica Acta, v. 71, p. 4902-4919.

Einaudi, M., 1981, Skarn deposits: Econ. Geol., v. 75, p. 317-391.

Friehauf, K. C., Titley, S. R., and Gibbins, S. L., 2005, Porphyry-style Mineralisation in the Ertsberg Diorite, Gunung Bijih (Ertsberg/Grasberg) Distrct, West Papua, Indonesia: Adelaide, PGC Publishing, 357-366 p.

Gandler, L. M., 2006, Calc-silicate alteration and Cu-Au mineralization of the Deep MLZ skarn, Ertsberg District, Papua, Indonesia, The University of Texas at Austin, 273 p.

Gibbins, S. L., 2006, The Magmatic and Hydrothermal Evolution of the Ertsberg Intrusion in the Gunung Bijih (Ertsberg) Mining District, West Papua, Indonesia, PhD Dissertation, The University of Arizona, p. 385.

Harrison, J., 1999, Hydrothermal alteration and fluid evolution of the Grasberg porphyry Cu-Au deposit, Irian Jaya, Indonesia: MS Thesis, University of Texas at Austin, 205 p.

Heinrich, C., Günther, D., Audétat, A., Ulrich, T., and Frischknecht, R., 1999, Metal fractionation between magmatic brine and vapor, determined by microanalysis of fluid inclusions: Geology, v. 27, p. 755-758.

Heinrich, C. A., 2005, The physical and chemical evolution of low-salinity magmatic fluids at the porphyry to epithermal transition: a thermodynamic study: Mineralium Deposita, v. 39, p. 864-889.

Heinrich, C. A., Driesner, T., Stefánsson, A., and Seward, T. M., 2004, Magmatic vapor contraction and the transport of gold from the porphyry environment to epithermal ore deposits: Geology, v. 32, p. 761-764.

Hill, K., Kendrick, R., Crowhurst, P., and Gow, P., 2002, Copper–gold mineralisation in New Guinea: tectonics, lineaments, thermochronology and structure: Australian Journal of Earth Sciences, v. 49, p. 737-752.

Landtwing, M. R., Pettke, T., Halter, W. E., Heinrich, C. A., Redmond, P. B., Einaudi, M. T., and Kunze, K., 2005, Copper deposition during quartz dissolution by cooling magmatic–hydrothermal fluids: the Bingham porphyry: Earth and Planetary Science Letters, v. 235, p. 229-243.

Leys, C. A., Cloos, M., New, B. T. E., and MacDonald, G. D., 2012, Copper-Gold ± Molybdenum Deposits of the Ertsberg-Grasberg District, Papua, Indonesia: Society of Economic Geologists, Special Publication 16, p. 215-235.

Müller, A., Herrington, R., Armstrong, R., Seltmann, R., Kirwin, D. J., Stenina, N. G., and Kronz, A., 2010, Trace elements and cathodoluminescence of quartz in stockwork veins of Mongolian porphyry-style deposits: Mineralium Deposita, v. 45, p. 707-727.

Mertig, H. J., 1995, Geology and origin of the Dom copper skarn deposit, Ertsberg (Gunung Bijih) District, Irian Jaya, Indonesia: Unpub. MS thesis, The University of Texas at Austin, p. 169.

Mertig, H. J., Rubin, J. N., and Kyle, J. R., 1994, Skarn Cu-Au orebodies of the Gunung Bijih (Ertsberg) District, Irian Jaya, Indonesia: Journal of Geochemical Exploration, v. 50, p. 179-202.

Mutchler, S. R., Fedele, L., and Bodnar, R. J., 2008, Analysis Management System (AMS) for reduction of laser ablation ICPMS data.: Laser ablation ICP-MS in the Earth sciences: Current practices and outstanding issues, v. 40, p. 51.

Nash, J. T., 1976, Fluid-inclusion petrology--data from porphyry copper deposits and applications to exploration: a summary of new and published descriptions of fluid inclusions from 36 porphyry copper deposits and discussion of possible applications to exploration for copper deposits. US Geological Survey Professional Paper, 907-D, p. 16.

Paterson, J. T., 2004, Magmatic and pervasice hydrothermal mineralogy of the Grasberg Cu-Au porphyry copper deposit (West New Guinea): Unpub. MS thesis, The University of Texas at Austin, p. 332.

Paterson, J. T., and Cloos, M. 2005a, Grasberg porphyry Cu-Au deposit, Papua, Indonesia: 2. Pervasive hydrothermal alteration, *in* Porter, T. M., ed., Super Porphyry Copper & Gold Deposits: A Global Perspective: Adelaide, PGC Publishing, p. 331-335.

Paterson, J. T., and Cloos, M., 2005b, Grasberg porphyry Cu-Au deposit, Papua, Indonesia: 1. Magmatic history, *in* Porter, T. M., ed., Super Porphyry Copper & Gold Deposits: A Global Perspective: Adelaide, PGC Publishing, p. 313-329.

Penniston-Dorland, S. C., 2001, Illumination of vein quartz textures in a porphyry copper ore deposit using scanned cathololuminescence: Grasberg Igneous Complex, Irian Jaya, Indonesia: American Mineralogist, v. 86, p. 652-666.

Proving Our Mettle, 2015 Annual Report, Freeport-McMoRan, p. 138.

Redmond, P., Einaudi, M., Inan, E., Landtwing, M., and Heinrich, C., 2004, Copper deposition by fluid cooling in intrusion-centered systems: New insights from the Bingham porphyry ore deposit, Utah: Geology, v. 32, p. 217-220.

Roedder, E., 1985, Fluid inclusions: Reviews in Mineralogy, vol. 12, 1491 p.

Quarles van Ufford, A. I., 1996, Stratigraphy, structural geology, and tectonics of a young forearc-continent collision, western Central Range, Irian Jaya (western New Guinea), Indonesia: Unpub. Diss. thesis, The University of Texas at Austin.

Rubin, J. N., 1996, Skarn Formation and Ore Deposition at the Gunung Bijih Timur (Ertsberg East) complex, Irian Jaya, Indonesia, University of Texas at Austin, 337 p.

Rusk, B., 2012, Cathodoluminescent textures and trace elements in hydrothermal quartz, Quartz: Deposits, Mineralogy and Analytics, Springer, p. 307-329.

Rusk, B., and Reed, M., 2002, Scanning electron microscope-cathodoluminescence analysis of quartz reveals complex growth histories in veins from the Butte porphyry copper deposit, Montana: Geology, v. 30, p. 727-730.

Rusk, B. G., 2006, Intensity of quartz cathodoluminescence and trace-element content in quartz from the porphyry copper deposit at Butte, Montana: American Mineralogist, v. 91, p. 1300-1312.

Rusk, B. G., Lowers, H. A., and Reed, M. H., 2008, Trace elements in hydrothermal quartz: Relationships to cathodoluminescent textures and insights into vein formation: Geology, v. 36, p. 547-550.

Rusk, B. G., Reed, M. H., Dilles, J. H., and Kent, A. J., 2006, Intensity of quartz cathodoluminescence and trace-element content in quartz from the porphyry copper deposit at Butte, Montana: American Mineralogist, v. 91, p. 1300-1312.

Rusk, B. G., Reed, M. H., Dilles, J. H., Klemm, L. M., and Heinrich, C. A., 2004, Compositions of magmatic hydrothermal fluids determined by LA-ICP-MS of fluid inclusions from the porphyry copper–molybdenum deposit at Butte, MT: Chemical Geology, v. 210, p. 173-199.

Sapiie, B., and Cloos, M., 2004, Strike-slip faulting in the core of the Central Range of west New Guinea: Ertsberg Mining District, Indonesia: Geological Society of America Bulletin, v. 116, p. 277.

Sillitoe, R. H., 2010, Porphyry copper systems: Economic Geology, v. 105, p. 3-41.

Wallier, S., Rey, R., Kouzmanov, K., Pettke, T., Heinrich, C. A., Leary, S., O'Connor, G., Tămaş, C. G., Vennemann, T., and Ullrich, T., 2006, Magmatic fluids in the breccia-hosted epithermal Au-Ag deposit of Roşia Montană, Romania: Economic Geology, v. 101, p. 923-954.

Wilson, F., 1981, The Conquest of Copper Mountain: United States, Atheneum: New York, NY, p. 244.

Young, D.J., Ledvina, M.D., and Kyle, J.R., 2016, Characterizing the structure, mineralogy, and paragenetic sequence of the sheeted quartz veins in the Ertsberg East Skarn System, Papua, Indonesia: Geological Society of America, Abstracts with Programs, v. 48